UNIVERSITY OF SOUTHAMPTON

FACULTY OF SCIENCE

DEPARTMENT OF PHYSICS

Synchronously-pumped Optical Parametric Oscillation in Barium Borate and Potassium Titanyl Phosphate.

by

Andrew Guy

A Thesis submitted for the Degree of

Doctor of Philosophy

September 1990

Table of Contents.

Appendices

UNIVERSITY OF SOUTHAMPTON

ABSTRACT

FACULTY OF SCIENCE

PHYSICS

Doctor of Philosophy

Synchronously pumped optical parametric oscillation in barium borate and potassium titanyl phosphate.

by Andrew Guy

The synchronously pumped parametric oscillator is potentially a widely tunable source of picosecond optical radiation. The aim of this project was to assess whether continuous operation of such a device would be possible with the nonlinear materials and laser sources available at the time. Singly resonant operation, though it would result in a higher threshold, was felt to be a necessary prerequisite for the stable operation of the parametric oscillator required for it to become a viable research tool.

To assess the feasibility of continuous operation, three synchronously pumped parametric oscillators were investigated. The first utilised the nonlinear medium barium borate and, as a pump source, a frequency-doubled, amplified, Q-switched, and mode-locked Nd:YAG laser. In this case a peak power, of the most energetic pulse in the Q-switched train, of $\approx$3.5MW was required; a value several orders of magnitude higher than available from a c.w. pumped mode-locked Nd:YAG laser, as would be required to continuously pump a parametric oscillator. The threshold was lowered by around a factor of four by simply replacing the barium borate crystal with one of potassium titanyl phosphate, taking advantage of the higher nonlinearity offered by this material. The last stage of the investigation was carried out utilising a frequency doubled, amplified, mode-locked pump source to provide a long train of pulses. Using a tight focusing geometry, as allowed by the quasi-noncritical phase-matching offered by KTP for near degenerate operation, the intensity threshold was reduced by nearly three orders of magnitude to $\approx$2.2kW.

Extrapolation of this result to estimate what level of power would be required from a c.w. mode-locked Nd:YAG laser pump indicated powers in excess of those available from conventional sources, but achievable through the exploitation of pulse compression. A preliminary investigation of compression was therefore performed. While the necessary power levels were achieved, the unstable behaviour of the laser output power - resulting from unavoidable feedback - posed too great a risk of damage to the nonlinear crystal, and an experimental demonstration of optical parametric oscillation pumped by these short pulses was therefore not attempted. The final conclusion of this project was that parametric oscillation threshold should now be achievable with a c.w. diode-pumped Nd:YAG laser, using the short pulse output generated via the recently introduced technique of additive mode-locking.

Acknowledgements.

I would firstly like to acknowledge the Science and Engineering Research Council, for funding both my studentship, and also the research project itself. I thank Leigh Bromley for putting up with me for a two year period on the same research project, and Prof. David Hanna for his guidance during the period of this work.

Thanks also go to the electronic and mechanical workshops, for their technical support, and to the ancillary staff, who keep the department running, and—most importantly— help us spend our research grants.

Finally a big thank you to my parents, who firstly provided me with that extra bit of financial assistance that prevented me from going (severely) overdrawn during my time as a pauper (i.e. research student). Secondly, and more importantly, for support at those times when the project was going either nowhere fast, or even backwards.

One never notices what has been done;
one can only see what remains to be done...

Marie Curie

1 Introduction.

While the investigations described in this thesis do not represent solely my own work, I did make a substantial and original contribution to the design, realization, and characterization of the three parametric devices discussed herein. The work on synchronously pumped parametric oscillation in barium borate, as described in Chapter 6, and on the Q-switched, mode-locked pumped device (using potassium titanyl phosphate), in Section 1, Chapter 7, was performed in collaboration with Leigh Bromley [1]. Whereas in the former case I was under Leigh's 'tutelage', in the latter case we made comparable contributions. The extension to operation with a long pulse, mode-locked pump source (Section 2, Chapter 7), and the investigation of pulse compression (as a means of obtaining the power required to pump the parametric oscillator from a c.w. pumped mode-locked laser, in Section 3, Chapter 7) was performed after the cessation of Leigh's involvement with the project, and therefore does represent work that is wholly my own.

This thesis describes the development and experimental demonstration of three synchronously-pumped optical parametric oscillator systems. The aim of this work was to investigate the feasibility of continuous operation of such a device, and to determine if the material potassium titanyl phosphate [2] would be a suitable choice for use as the nonlinear gain medium.

The synchronously pumped parametric oscillator is potentially a stable source of mode-locked pulses with wide tunability over the near to medium infra-red regions of the spectrum (i.e. $\lambda = 1\text{–}5\mu$m). The extremely wide bandwidth of the parametric interaction offers this broad tuning range from only one gain medium, and also the capability of generating ultra-short pulses (duration, $\tau < 1$ps).

The wide bandwidth of the parametric interaction is a result of the non-resonant nature of the process. Parametric gain arises from coherent second-order nonlinear scattering of the pump field by the electrons bound in a asymmetric crystal potential [3]. It is an elastic process, and consequently does not lead to a loss of energy from the electric field. As there is no associated atomic (nor molecular) transition, parametric devices have the potential to operate over the whole of the transparency region of the nonlinear gain medium (e.g. Bierlein and Vanherzeele [4] have demonstrated a tuning range of 0.6–4.5μm with a parametric

generator based on potassium titanyl phosphate). The gain mechanism in a laser is, conversely, stimulated emission [5], which relies on the population inversion of a given molecular or atomic transition. As a consequence, the operating bandwidth of the laser, and hence its tuning range, is limited to that of the associated transition. Materials have been recently developed that have wide gain features due to vibronic broadening, but these still typically have tuning ranges of only 200–300nm [6].

The recent resurgence of interest in parametric devices can be attributed to two factors: the first is the availability of better nonlinear materials (e.g. barium borate [7] and potassium titanyl phosphate [7]); the second the development of improved laser sources. Improvements in both the techniques used to grow crystals, and in the degree of purity of the raw materials used in these processes, has led to a general increase in quality of the available nonlinear materials. A lot of work been also done on the development of new nonlinear materials. As these improved materials have generated more interest in nonlinear optics, it has increased the demand for even better materials. Hopefully, this will lead to further developments in materials in the near future.

One of the laser sources that has attracted the most attention in the last few years is the laser-diode pumped, mode-locked, miniature solid-state laser [8]. The use of a laser-diode, as opposed to a flashlamp, to pump the solid-state gain medium has several benefits. Most importantly, these devices offer far superior output stability and beam quality. The narrow linewidth of the laser-diode means that a much greater fraction of the pump radiation is utilised in excitation of the transition, and hence there are less problems with thermal birefringence and lensing. Together, the laser-diode pumped, mode-locked, miniature solid-state laser and potassium titanyl phosphate offer the prospect of an extremely stable synchronously-pumped parametric oscillator, which should prove a useful addition to the range of existing laser sources. It is this possibility that motivated the work described in this thesis.

1.1 Methods of generating tunable short pulses.

The requirement for tunable sources of ultrashort pulses—e.g. for time-resolved spectroscopy [9]—has led to the development of several different methods of generation. The most widely exploited techniques are based around dye lasers, where the gain medium is an organic dye dissolved in a suitable solvent [9]. The characteristics of dyes are well suited to the generation of tunable ultrashort pulses: a typical laser dye has a fluorescence linewidth of

$\sim$100nm, allowing tuning over a comparable range. Furthermore, dyes generally possess a short fluorescence lifetime, which allows for the effective exploitation of passive mode-locking techniques based upon saturable absorbers [10]. Pulse durations of a few tens of femtoseconds have been provided directly from dye lasers (e.g. [11]). This does, however, necessitate a sacrifice in tunability, as a significant fraction of the dye's gain linewidth is required to support the mode-locked pulse. Generally, the operation of a dye laser becomes progressively more difficult as the wavelength increases. The longest wavelength readily generated using a dye laser is $\sim 1\mu$m, so the utility of such devices is generally restricted to the visible and 'very-near' infrared spectral regions. Aside from the limited spectral coverage, the dye laser suffers from one major practical disadvantage. Over a period of time, the exposure to intense light—as exists in the laser cavity—leads to the chemical decomposition of the laser dye. Consequently, they must be routinely replaced; a chore that can take a reasonable amount of time, and, furthermore, can necessitate exposure to harmful chemicals.

A less commonly used technique is that of the colour centre laser [12]. The gain medium in this case is generally an alkali halide crystal that has been bombarded with electrons to create defect centres (colour centres) in the crystal lattice, which then act like an atomic system, but typically with lower transition energies [13]. This means that these devices operate in the near to medium infrared regions of the spectrum (~ 0.8–4μm [14]), and therefore augment—rather than compete with—the dye laser. The tuning range of each colour centre is comparable with that of a dye (i.e. $\sim$300nm [14]). A disadvantage of these systems is that efficient operation generally requires cooling with liquid nitrogen [14], though there are exceptional cases in which this may be obtained at room temperature [14].

More recently there has been a lot of interest in vibronic lasers [15], which utilise gain media such as Ti^+:sapphire [16]. These crystals have vibronically broadened transition features which have fluorescence linewidths of $\sim$300nm; comparable with dye lasers. The advantage of these systems—over the dye and colour centre laser—is that solid-state gain media are generally more robust; can operate at room temperature; and do not suffer from chemical decomposition during prolonged use.

There has also been some work done with semiconductor platelet devices, which utilise thin sheets of materials such as CdS, CdSe, and InGaAsP. Salour [17] has used this technique to generate pulses with a duration of 4–10ps using a mode-locked Ar^+ laser (pulse duration 150ps) as the pump source. The disadvantage of this scheme, as with colour-centre

lasers, is the necessity for cooling to liquid nitrogen temperature before operation becomes efficient.

Other available methods for the generation of tunable ultra-short pulses exploit various nonlinear processes. These include stimulated Raman scattering [18] and parametric oscillation [19], which is the main subject of this thesis. Stimulated Raman scattering is an absorption-emission process in which there is a shift in wavelength between the input and output fields resulting from a loss of energy to, or from, the interacting medium [18]. All possible frequency shifts correspond to allowed transitions in the material. Initially, this led to the use of this technique to shift the output of an available tunable source—by a constant amount (frequency)—to wavelengths that are otherwise inaccessible [18]. Techniques have also been developed to 'tune' the frequency shift [20][21], so it is now possible to utilise a pump source that operates at a fixed wavelength to provide a tunable output. When a sufficient intensity is available ($\sim$MWcm^{-2} [18]) these devices can convert up to 80% of the incident pump into the output field [22].

In the picosecond regime, the most commonly used parametric technique has been—so called—'parametric generation' [19]. This exploits parametric superfluorescence, the process by which parametric noise is amplified up to a level comparable to the pump on one pass through the gain medium [19]. While the output of these devices does consist of a cone of varying wavelengths—as determined by the phase-matching conditions [23]—spatial filtering can be used to select out a given desired frequency. These devices have been thoroughly developed now (e.g. [24][25]), and can offer reasonably narrow linewidths and beam divergences that are nearly diffraction limited. As the gain on a single pass through a parametric medium is not always high enough to generate a significant output, double- and multi-pass devices have been developed [26]. The natural progression of this is the optical parametric oscillator [19], where the gain medium is put inside a resonator. The advantages of this are two-fold: firstly the threshold is greatly reduced; secondly, it allows greater control of the spectral and spatial properties of the output.

1.2 A brief history of the parametric oscillator.

The study of parametric interactions had begun some time before the laser was developed; the technique of parametric amplification being extensively used in the microwave region of the spectrum for low noise amplification of weak signals [27]. The investigation of parametric interactions in the optical region of the spectrum, however, was not possible until

the advent of the laser [28]. This is because the nonlinear response of a material—on which the optical parametric processes depend—is only significant at high applied electric field strengths ($>1\text{kVcm}^{-1}$ [3]). These high field strengths are only available—at optical frequencies—from laser sources.

The laser was first demonstrated by Maiman [28] in 1960. Only a year after, Franken *et al* [29] experimentally verified the presence of the second-order nonlinear coupling in an optical interaction, by the observation of the generation of the second-harmonic of a ruby laser using a quartz crystal. After this initial demonstration, progress was very rapid in the newly created field of nonlinear optics. The concept of phase-matching was introduced in 1962 by Giordmaine [23], and also—independently—by Maker *et al* [30], which increased the efficiency of the optical coupling considerably. In the same year the tunable optical parametric oscillator was proposed by several parties [31][32][33]. In 1964 Boyd *et al* [34] introduced the first of several 'new' nonlinear materials: lithium niobate. Then in 1965, the pulsed optical parametric oscillator was successfully operated by Giordmaine and Miller [35]. Since then a large number of such devices have been constructed, utilising a wide range of different nonlinear materials (e.g. [36][37][38]). In 1966, Boyd and Ashkin [39] showed that the parametric oscillator could, in principle, be continuously operated. Only two years later this was experimentally demonstrated by Smith *et al* [40], and independently by Byer *et al* [41].

In the late sixties and early seventies, a lot of work was done to achieve higher output powers, higher efficiencies, and also greater stability [42][19]. A lot of problems were, however, found on the materials side. As the parametric interaction requires a high intensity to be efficient, there were problems with material damage that precluded the wide use of the parametric oscillator as a research tool. The mode-locking of the parametric oscillator was one of the last problems to be investigated [43]. As mentioned in the introduction to this chapter, the parametric oscillator does not rely on an inversion process for gain, but on the coupling arising from the electronic polarizability. This process is virtually instantaneous, and consequently there is no gain storage. As a result, coupling between fields is only possible when they overlap both spatially and temporally. This means that the only efficient way to mode-lock an OPO is by synchronous pumping. The first demonstration of the synchronously-pumped OPO, with the output of a Q-switched and mode-locked laser, was by Burneika *et al* [43] in 1972. A few years later similar devices were operated by Weisman

and Rice [44] in 1976, and by Kushida *et al* [45] in 1977. Very little work on these devices was then carried out until the late eighties when new nonlinear materials became available.

While most work on parametric oscillators has involved pumping by Q-switch pulses, there is now an increasing amount of work on the synchronously pumped OPO [46][47]. This is due, in part, to improvements in materials and partly to the availability of more convenient mode-locked pump sources. Another area of current interest is in the development of very narrow linewidth c.w. devices for use as spectroscopic sources [48].

There are two recent results of great interest. The first is the demonstration of a doubly-resonant synchronously-pumped, OPO using barium sodium niobate [49] as the gain medium. This has been operated continuously [46], and also when pumped by the temporally compressed output of Q-switched, mode-locked, c.w. pumped Nd:YAG laser [50]. The second is the first demonstration of continuous operation of a singly-resonant synchronously pumped oscillator, which is also the first OPO to operate in the sub-picosecond regime [47]. These results gives further confidence in the scheme towards which the work in this thesis was directed, i.e. that operation of a singly-resonant OPO should be possible outside of a laser cavity once diode-pumped solid-state lasers have been developed which can provide sufficient output powers.

1.3 Thesis outline.

The remaining seven chapters of this thesis are as follows: Chapter 2 gives the necessary theoretical background for the discussion of the performance of a synchronously pumped optical parametric oscillator. Chapter 3 outlines the properties wanted, and found, in parametric gain media, and then goes on to review the properties of the materials barium borate [7] and potassium titanyl phosphate [2]. In Chapter 4, consideration is given to the design of practically realisable systems. Then in Chapter 5 a brief description of the pump systems used in the experimental investigations are given. Chapter 6 summarizes the preliminary experimental results obtained in an investigation of a Q-switched, mode-locked OPO based on barium borate [7]. Chapter 7 then discusses the results obtained from the work with potassium titanyl phosphate [2]. The final chapter, Chapter 8, considers the direction in which the investigation could now proceed. The thesis ends with a brief conclusion on the possibility of continuous operation of a synchronously pumped optical parametric oscillation with the material potassium titanyl phosphate [2].

References.

[1]. Leigh J. Bromley.
Ph.D. Thesis, University of Southampton (1990).

[2]. F.C. Zumsteg, J.D. Bierlein, and T.E. Gier.
J. Appl. Phys. **47**, 4980 (1976).

[3]. Y.R. Shen.
The Principles of Nonlinear Optics (Wiley 1984).

[4]. J.D. Bierlein and H. Vanherzeele.
J. Opt. Soc. Am. B **6**, 622 (1989).

[5]. A.E. Seigman.
Chapter 1, *Lasers* (University Sciences 1986)

[6]. A. Sanchez, R.E. Fahey, A.J. Strauss, and R.L. Aggarwal.
Opt. Lett. **11**, 363 (1988).

[7]. C. Chen, B. Wu, A. Jiang, and G. You.
Sci. Sinica (Ser. B) **28**, 235 (1985).

[8]. G.T. Maker and A.I. Ferguson.
Appl. Phys. Lett. **54**, 403 (1989).

[9]. S.L. Shapiro, Ed.
Ultrashort Light Pulses (Springer-Verlag 1977).

[10]. H.A. Haus.
J. Appl. Phys. **46**, 3049 (1975).

[11]. J.A. Vladmanis, R.L. Fork, and J.P. Gordon.
Opt. Lett. **19**, 131 (1985).

[12]. K.R. German.
J. Opt. Soc Am. B **3**, 149 (1985).

[13]. C.R. Pollock, J.F. Pinto, and E. Georgiou.
Appl. Phys. B **48**, 287 (1989).

[14]. T.T. Baisiev, S.B. Mirov, and V.V. Osiko.
IEEE J. Quantum Electron. **24**, 1052 (1988).

[15]. B. Henderson and G.F. Imbusch.
Contemp. Phys. **29**, 235 (1988).

[16]. P.F. Moulton.
CLEO'84 Technical digest, Abstract WA2, p77 (1984).

[17]. M.M. Salour.
p51, *Picosecond Phenomena III* (Springer-Verlag 1982, K.B. Eisenthal, R.M. Hochstrasser, W. Kaiser, and A. Laubereau, Eds.).

[18]. D.C. Hanna, M.A. Yuratich, and D. Cotter.
Chapter 5, Nonlinear optics of free atoms and molecules
(Springer-Verlag, Berlin 1979).

[19]. R.L. Byer.
Chapter 9, *Quantum Electronics: a treatise, Vol. 1*
(Academic Press 1975)

[20]. S.K. Kurtz and J.A. Giordmaine.
Phys. Rev. Lett. **22**, 192 (1969).

[21]. C.K.N. Patel and E.D. Shaw.
Phys. Rev. Lett. **24**, 451 (1970).

[22]. R. Frey and F. Praedere.
Opt. Lett. **5**, 374 (1980).

[23]. J.A. Giordmaine.
Phys. Rev. Lett. **8**, 19 (1962).

[24]. A. Seilmeier and W. Kaiser.
Appl. Phys. Lett. **23**, 113 (1980).

[25]. R. Danelyus, A. Piskarskas, and V. Sirutkaitis.
Sov. J. Quantum Electron. **12**, 1626 (1982).

[26]. A. Piskarskas, A. Stabinis, and A. Yankauskas.
Sov. J. Quantum. Electron. **14**, 1575 (1984).

[27]. W.H. Louisell.
Coupled Mode and Parametric Electronics (Wiley 1960).

[28]. T.H. Maiman.
Nature **187**, 493 (1960).

[29]. P.A. Franken, A.E. Hill, C.W. Peters, and G. Weinreich.
Phys. Rev. Lett. **7**, 118 (1961).

[30]. P.D. Maker, R.W. Terhune, M. Nisenoff, and C.M. Savage.
Phys. Rev. Lett. **8**, 21 (1962).

[31]. S.A Akhmanov and R.V. Khokhlov.
Soviet Phys. JETP **16**, 252 (1963).

[32]. R.H. Kingston.
Proc. IRE **50**, 472 (1962).

[33]. N.M. Kroll.
Phys. Rev. **127**, 1207 (1962).

[34]. G.D. Boyd, R.C. Miller, K. Nassau, W.L. Bond, and A. Savage.
Appl. Phys. Lett. **5**, 234 (1964).

[35]. J.A. Giordmaine and R.C. Miller.
Phys. Rev. Lett. **14**, 973 (1965).

[36]. G. Nath and G. Pauli.
Appl. Phys. Lett. **22**, 75 (1973).

[37]. Y.X. Fan, R.C. Eckardt, R.L. Byer, C. Chen, and A.D. Jiang.
IEEE J. Quantum Electron. **25**, 1196 (1989).

[38]. M. Ebrahimzadeh and M. Dunn.
Opt. Commun. **69**, 161 (1988).

[39]. G.D. Boyd and A. Ashkin.
Phys. Rev. **146**, 187 (1966).

[40]. R.G. Smith, J.E. Geusic, H.J. Levinstein, J.J. Rubin, S. Singh, and L.G. Van Uitert.
Appl. Phys. Lett. **12**, 308 (1968).

[41]. R.L. Byer, M.K. Oshman, J.F. Young, and S.E. Harris.
Appl. Phys. Lett. **13**, 109 (1968).

[42]. R.G. Smith.
Chapter C8, *Laser Handbook* (North Holland 1972, F.T. Arrechi and E.O. Schulz-DuBois, Eds.)

[43]. K. Burneika, M. Ignatavichyus, V. Kabelka, A. Piskarskas, and A. Stabinis.
IEEE J. Quantum Electron. **QE-8**, 574 (1972).

[44]. R.B. Weisman and S.A. Rice.
Opt. Commun. **19**, 28 (1976).

[45]. T. Kushida, Y. Tanaka, and M. Ojima.
Jap. J. Appl. Phys. **16**, 2227 (1977).

[46]. A. Piskarskas, V. Smil'gyavichyus, and A. Umbrasas.
Sov. J. Quantum Electron. **18**, 155 (1988).

[47]. D.C. Edelstein, E.S. Wachman, and C.L. Tang.
Appl. Phys. Lett. **54**, 1728 (1989).

[48]. W.J. Kozlovsky, E.K. Gustafson, R.C. Eckardt, and R.L. Byer.
Opt. Lett. **13**, 1102 (1988).

[49]. J.E. Geusic, H.J. Levinstein, J.J. Rubin, S. Singh, and L.G. Van Uitert.
Appl. Phys. Lett. **11**, 269 (1967).

[50]. A.S. Piskarskas, V.J. Smilgevičius, A.P. Umbrasas, J.P. Juodišius, A.S.L. Gomes, and J.R. Taylor.
Opt. Lett. **14**, 557 (1989).

2 Theoretical background.

A fully general analysis of the behaviour of the synchronously pumped OPO has not—so far—been made. Moreover, it is unlikely that this will ever be possible, save by computational means. The factors that would have to be accounted for in a complete model include the finite spatial and temporal extent of the interacting radiation, and the behaviour of the crystal; including dispersive and birefringent behaviour (e.g. temporal walk-off and angular acceptance). These problems are most acute in the case of low power, ultrashort pulsed operation: the low power necessitates the use of a tight focus, so diffraction effects are significant; the short pulse duration leads to limitations of the crystal length due to temporal walk-off, and also bandwidth acceptance. Furthermore, if the analysis is to be extended to deal with the case of high ($>10\%$) conversion efficiencies, then depletion of the pump will also have to be accounted for. While no treatment has yet been presented that takes into account all of the various points mentioned above, many have been investigated in isolation, or in conjunction with one or two of the others (e.g. [1][2][3]).

The purpose of this chapter is to briefly outline a few of the more important results that have been previously published, and which were found to be of use during this project. The main use of the theory was to determine how much pump power would be required for the parametric oscillator to reach threshold, and it is therefore primarily this matter that is considered.

The chapter is split into two sections: it starts by considering optical parametric amplification, the process underlying optical parametric oscillation, concentrating on the plane-wave model—with references to where this breaks down in practice; in Section 2, the ideas relevant to optical parametric oscillation are outlined, with attention being drawn to those limitations imposed on the system due to temporal and spatial localisation of the interacting fields.

2.1 Parametric amplification.

Optical parametric amplification is the $\chi^{(2)}$ mediated interaction by which power is lost from an intense, high frequency 'pump' field to an—initially—weaker, lower frequency 'signal' field [4]. To comply with energy conservation, a third field—referred to as the 'idler'—is also generated; at the frequency difference of the pump and signal.

As has been derived in many publications (e.g. [1][4][5]), the evolution of an electromagnetic field comprised of three collinearly propagating plane-wave frequency

components at ω_1, ω_2, and ω_3 (such that $\omega_1+\omega_2=\omega_3$) travelling in a medium characterised by a nonlinear coefficient 'd' (defined such the $2d=\chi^{(2)}$ [5]), can be described by the set of coupled differential equations (2.1.a)-(2.1.c),

$$\frac{dE_1}{dz} + \alpha_1 E_1 = i\kappa_1 E_3 E_2^* e^{+i\Delta kz} \qquad \textbf{(2.1.a)}$$

$$\frac{dE_2}{dz} + \alpha_2 E_2 = i\kappa_2 E_3 E_1^* e^{+i\Delta kz} \qquad \textbf{(2.1.b)}$$

$$\frac{dE_3}{dz} + \alpha_3 E_3 = i\kappa_3 E_2 E_1 e^{-i\Delta kz} \qquad \textbf{(2.1.c)}$$

where 'E_i' are the complex amplitudes of the fields, α_i are the field absorption coefficients, $\Delta k=k_3-k_2-k_1$ is the phase-velocity mismatch, and the interaction coefficient 'κ_i' is defined by

$$\kappa_i = \frac{\omega_i d}{n_i c} \qquad \textbf{(2.2)}$$

where 'n_i' is the appropriate refractive index, and 'd' is the nonlinearity (in pmV^{-1}) mentioned above (note. 'd' has been defined such that the second order polarization field is related to the electric field by $P=\epsilon_0\chi E^2$, as opposed to the alternative convention that $P=\chi E^2$).

The set of equations given in (2.1.a)-(2.1.c) describes all possible three-photon interactions, including second harmonic generation and optical parametric amplification. The actual process that occurs in a given situation is determined by the relative phasing of the incident fields, which in turn determines the direction of power flow. Defining the 'phase factor' as $\Delta\phi=\phi_3-\phi_2-\phi_1$, where ϕ_i are the arguments of the complex field amplitudes E_i at the entrance of the crystal, it can be shown that if $\Delta\phi=+\pi/2$ then power is channelled from the field components at ω_1 and ω_2 into the component at ω_3. On the other hand, if the phase-factor is $-\pi/2$, power flows in the opposite sense. For intermediate value of $\Delta\phi$, power flow occurs in both directions simultaneously: the net power flow depending on the magnitude of the different field components at the given instant. This results in a periodic redistribution of power as the fields propagate through the nonlinear medium [1]. If only two, out of the three, field components is incident on the crystal, then the third one will be generated at the phase that maximises the rate at which its power increases. This same argument also holds if one of the fields becomes totally depleted at any point: it is then possible for the direction of the interaction to reverse—the newly generated third component of the field taking the phase required for this to occur.

The phase-mismatch 'Δk' further complicates the matter by introducing a varying phase-relationship: if it takes a non-zero value, it results in a periodic change in the direction of power flow, leading to a drastic reduction in the amount of energy that can be channelled between fields. Consequently, it is generally desired that $\Delta k=0$: an interaction that satisfies this condition is referred to as being 'phase matched'.

When pump depletion can be ignored (i.e. E_3 is constant), it is possible to find an exact solution of (2.1.a)-(2.1.c). Setting the complex amplitudes of the incident 'signal' and 'idler' fields to be $E_1(0)$ and $E_2(0)$ respectively, the amplitude of the signal field at the crystal output, after traversing a distance 'ℓ' in the nonlinear medium, is given by

$$E_1(\ell)e^{\alpha_1 \ell} = E_1(0)e^{i\Delta k\ell/2}\left(\cosh g\ell - \frac{i\Delta k}{2g}\sinh g\ell\right) + \frac{i\kappa_1 E_3}{g}E_2^*(0)e^{i\Delta k\ell/2}\sinh g\ell \qquad (2.3)$$

where the parametric gain coefficient 'Γ' and total gain coefficient 'g' are defined as,

$$\Gamma^2 = \kappa_1\kappa_2|E_3|^2 \qquad g^2 = \Gamma^2 - \left(\frac{\Delta k}{2}\right)^2 \qquad (2.4)$$

The equation describing the evolution of the idler field E_2 is identical to (2.3), except for the exchange of the subscripts '1' and '2'. Also, it has been implicitly assumed that the pump does not lose significant power to the signal and idler fields, nor through absorption or other loss mechanisms.

A case of particular interest here occurs when only one of the two lower frequency fields (say ω_1) is incident on the OPA. The single-pass power gain can then be shown to be given—neglecting loss—by,

$$G_1 \equiv \left|\frac{E_1(\ell)}{E_1(0)}\right|^2 - 1 = \Gamma^2\ell^2\frac{\sinh^2 g\ell}{(g\ell)^2} \qquad (2.5)$$

It can be seen here that the gain is independent of the relative phases of the incident pump (ω_3) and signal (ω_1) fields. This is because—as mentioned above—the idler (ω_2) is free to assume whatever phase is necessary for it to see optimum gain. This coincides with the maximum transfer of energy for the pump to the signal and idler fields [5], and therefore also leads to the optimal channelling of energy into the signal field.

In the low gain limit ($\Gamma^2 \ll \Delta k^2/4$), (2.5) becomes,

$$G_1 = \Gamma^2 \ell^2 \mathrm{sinc}^2(\tfrac{1}{2}\Delta k \ell) \equiv \Gamma^2 \ell^2 \frac{\sin^2(\tfrac{1}{2}\Delta k \ell)}{(\tfrac{1}{2}\Delta k \ell)^2} \tag{2.6}$$

which shows that for a non-zero value of Δk that the gain varies sinusoidally with the length travelled. However, for $\Delta k=0$, it can be seen that the gain varies quadratically with length—corresponding to the optimum value for a given length. More exactly, if $\Delta k=0$, it can be shown from (2.5), that the signal gain is given by,

$$G_1 = \sinh^2 \Gamma \ell \tag{2.7}$$

which can, if the gain is high ($\Gamma^2 \gg 1$), but the pump depletion still small enough to be ignored (i.e. small signal case), be well approximated by the exponential form,

$$G_1(\ell) \simeq \frac{e^{2\Gamma \ell}}{4} \tag{2.8}$$

2.1.1 Phase-matching.

It was mentioned above that the maximum gain is obtained when the phase-velocity mismatch is zero ($\Delta k=k_3-k_2-k_1=0$). Generally, the inherent dispersion of the nonlinear material means that this can not be achieved, as becomes apparent when the phase-velocity matching condition is re-expressed (using $\omega/k=c/n$) as,

$$\omega_3 n_3 = n_1 \omega_1 + n_2 \omega_2 \tag{2.9}$$

One way to satisfy this condition is through the exploitation of intrinsic, or induced, crystal birefringence [7]. For birefringent materials it can be shown that, for almost any given direction through the crystal, wave propagation is only supported for two distinct orthogonal eigen-polarizations; each seeing a different value of refractive index [8] (the exception being when propagation is in the direction of the optic axes: these are defined as the directions for which the eigen-indices are degenerate. This degeneracy means that any arbitrary polarization state will be propagated unchanged). If the difference between the two eigen-indices—as seen by a given frequency field in each of the two polarization states—is larger than the difference between the values of one of the indices as seen by the two extreme frequency components, it is then possible, through a suitable selection of both the polarization states of the interacting field components, and the direction of propagation, to counter the

effects of dispersion (and hence satisfy $\Delta k=0$). There are, however, limitations to this technique for phase-matching, which will be outlined below.

2.1.2 Bandwidth and spectral acceptance.

The dispersion of the nonlinear gain medium determines the spectral behaviour of the parametric amplifier. From equation (2.6), it can be seen that for a crystal of length 'ℓ', that the signal gain is reduced to zero by a change in the phase-(mis)match, from $\Delta k=0$, to,

$$|\Delta k| = 2\sqrt{\left(\frac{\pi}{\ell}\right)^2 + \Gamma^2} \tag{2.10}$$

or in the small gain limit ($\Gamma \ll \pi/\ell$), to

$$|\Delta k| \approx \frac{2\pi}{\ell} \tag{2.11}$$

It is possible, by relating (2.10) or (2.11) to the frequency dependency of the phase-(mis)match, to ascribe a bandwidth to the parametric interaction [5].

If the phase-velocities at the frequencies corresponding to the line-centres of the three field components are assumed to be perfectly phase-matched ($\Delta k=k_3-k_2-k_1=0$), and the pump field assumed to have a negligible bandwidth, then the phase-mismatch between the pump and fields at $\omega_1 \pm \Delta\omega$ and $\omega_2 \mp \Delta\omega$ is well approximated by,

$$\Delta k \simeq \Delta\omega\left(\frac{\partial k_1}{\partial\omega} - \frac{\partial k_2}{\partial\omega}\right) + \frac{\Delta\omega^2}{2}\left(\frac{\partial^2 k_1}{\partial\omega^2} + \frac{\partial^2 k_2}{\partial\omega^2}\right) \tag{2.12}$$

From (2.12), substituting for Δk by (2.11), it can be shown that in the small signal case the bandwidth of the parametric interaction is given by,

$$\Delta\omega = \frac{2\pi}{\ell\left(\frac{\partial k_1}{\partial\omega} - \frac{\partial k_2}{\partial\omega}\right)} \tag{2.13}$$

where the expansion of (2.12) has only been taken to first order in Δk. This approximation is generally valid; the exception being in the situation of perfect—or nearly so—group velocity matching, i.e.,

$$\frac{\partial k_1}{\partial\omega} \simeq \frac{\partial k_2}{\partial\omega} \tag{2.14}$$

when the term in $\Delta\omega^2$ must also be taken into account.

From (2.10) and (2.11), it can be seen that the bandwidth broadens as the gain increases. Byer [5] has expressed this as

$$\frac{\text{BW(high)}}{\text{BW(low)}} = \sqrt{1 + \frac{\Gamma^2 \ell^2}{\pi^2}} \tag{2.15}$$

where the low gain bandwidth is that deduced using equation (2.13). For a gain of $\sim$exp(30), which is required for an appreciable output from a single-pass parametric generator (see Subsection 6), this can give rise to a bandwidth $\sim$5 times wider than in the low-gain case [5]. The approach outlined above breaks down when the bandwidth of the pump becomes appreciable (e.g. for mode-locked pulses with a duration of, say, $<$10ps). In this case, an estimation of the bandwidth also involves a consideration of dispersion at the pump wavelength, which—unfortunately—does not lead to a more generally applicable form of equation (2.13).

If the pump bandwidth is sufficiently broad, phase-matching will not be possible over the entirety of the pump bandwidth: this will result in a reduction of the available parametric gain. For near degenerate interaction, a gauge of this effect can be obtained from a consideration of second harmonic generation; even though it is not strictly valid to consider frequency doubling as degenerate parametric oscillation in reverse.

The treatment necessary to obtain the acceptance bandwidth in the case of second harmonic generation closely follows that—given above—for the OPO gain bandwidth. The two frequency components used here are the 'harmonic' (pump) ω_3 and the fundamental (degenerate) wavelength ω_0, which are related according to $2\omega_0=\omega_3$. In this case the expression obtained is,

$$\Delta\omega = \frac{\pi}{\ell\left(\frac{\partial k_3}{\partial \omega} - \frac{\partial k_0}{\partial \omega}\right)} \tag{2.16}$$

where $\Delta\omega$ is the deviation of the signal (and also idler) from the frequency at which optimal phase-matching is obtained. It has been shown that the efficiency obtained for a given acceptance bandwidth and fundamental linewidth is well approximated by [11],

$$\frac{\eta_{\Delta\omega}}{\eta_\infty} = \frac{\Delta\omega}{\sqrt{\Delta\omega^2 + \Delta\omega_f^2}} \tag{2.17}$$

where η_∞ is the doubling efficiency ignoring any bandwidth effect (i.e. assuming the interaction has an infinite bandwidth), $\eta_{\Delta\omega}$ is the efficiency when the acceptance bandwidth of the crystal is $\Delta\omega$, and $\Delta\omega_f$ is the linewidth of the incident fundamental radiation. While this value is not directly applicable, it should scale in approximately the same way, and can therefore be used to ascertain whether or not the bandwidth acceptance is going to be a problem in practice.

2.1.3 Angular acceptance.

As mentioned in Subsection 1, one of the ways in which phase-velocity matching can be achieved is through the exploitation of crystal birefringence. It can be shown that in a birefringent crystal, the values of the two indices seen by a given frequency is dependent on the direction of propagation. The direction is usually reckoned with reference to the dielectric axes, in terms of spherical polar coordinates. It is then conceptually a matter of varying the angle(s) of propagation in the crystal to achieve phase-matching. The range over which this is possible depends on the degree of birefringence of the material in relation to the magnitude of its dispersion.

How the angular dependency of the refractive indices is related to the phase-mismatch may be seen by re-writing the condition for perfect phase-match ($k_3=k_2+k_1$), using $\omega/k=c/n$, in the form,

$$\frac{n_1(\theta)}{\lambda_1}+\frac{n_2(\theta)}{\lambda_2}=\frac{n_3(\theta)}{\lambda_3} \qquad (2.18)$$

where λ_i ($i=1,2,3$) are the values of the free-space wavelengths. The method for obtaining the values of the angles needed for phase-matching from (2.18) is not given here: the solution for the case of uniaxial crystals has been published by Midwinter and Warner [9], and by Hobden [10] for the alternative biaxial case.

Though the variation of the refractive indices with direction allows a range of different wavelengths to be matched, it also leads to the concept of angular acceptance. As will be discussed later, this is important in the case of a finite beam extent. It is, however, difficult to analyse in the case of optical parametric amplification, as for any given values of pump and signal wavelength, the idler can be generated at any angle at which the phase-mismatch is small enough for adequate gain. Some gauge of this effect may, however, be obtained from a consideration of the angular acceptance for frequency doubling.

In the case of second harmonic generation, the acceptance angle is conventionally taken to be the angular deviation, from the angle which gives optimum conversion efficiency (for the plane-wave interaction), at which the efficiency falls to 50% of its optimum value [4]. The derivation of the acceptance angle closely follows that for the bandwidth acceptance, as given in Subsection 2. If the interaction os assumed to be phase-matched for propagation at some arbitrary angle θ, then the phase-velocity mismatch at an angle $\theta \pm \Delta\theta$ is well approximated by the power series,

$$\Delta k \simeq \Delta\theta \frac{\partial}{\partial\theta}\Delta k + \frac{\Delta\theta^2}{2}\frac{\partial^2}{\partial\theta^2}\Delta k \qquad (2.19)$$

where the derivatives of Δk are evaluated at θ. If the angle θ is larger than $\approx 5°$, it can be shown that this expansion is accurate to better than $\approx 1\%$; even when taken only to first order. For smaller angles, both terms must be taken into account: the exceptions being the cases of $\theta=0$ and $\theta=90°$, when the first order term vanishes. This corresponds to a stationary point in the angular variation of the refractive index, and results in a significant increase in the acceptance angle. In these cases, due to the lack of alignment sensitivity, phase-matching is designated as 'non-critical': it can be shown to occurs when propagation is parallel to one or more of the dielectric axes.

Given that the small signal parametric gain is proportional to $\mathrm{sinc}^2(\frac{1}{2}\ell\Delta k)$, and having decided the efficiency reduction factor that will define the acceptance angle, it is then possible to calculate the maximum allowed angular deviation using (2.19). If both terms of the series are used, the solution involves a quadratic equation in terms of $\Delta\theta$. If only one or other of the terms is required, it is then possible to calculate a corresponding 'angular acceptance coefficient' that can then be scaled according to the crystal length. For the usual 'critical' case, the coefficient is normally quoted in mrad • cm: to obtain the angular acceptance for a given crystal, the coefficient must be divided by the length in cm. In the non-critical case, the coefficient is given in terms of mrad • $\mathrm{cm}^{-\frac{1}{2}}$.

2.1.4 Poynting vector walk-off.

Another property of birefringent crystals is that, in general, the direction of energy flow (as defined by the Poynting vector) is not parallel to the propagation vector. Furthermore, as mentioned in Subsection 1, an arbitrary polarized beam can be decomposed into two distinct parts, that correspond to the allowed eigen-polarizations. It can be shown that the deviation between the Poynting vector and the propagation direction is different for the two polarizations. To achieve phase-matching, one of the interacting frequency components must

always be in the opposite eigen-polarization to the other (i.e. two can have the higher index, or two can have the lower index). Consequently, in the general case, the direction of power flow will not be the same for all three fields (the exception being the case of noncritical phase-matching). In the case of a finite beam extent, this can limit the distance over which beams of a given cross-section will overlap, which in turn can limit the usable gain length, as parametric amplification can only take place when there is this overlap of the fields.

2.1.5 Temporal limitations.

As explained in Subsection 1, when the bandwidths of the interacting fields exceed the acceptance bandwidth of the nonlinear interaction, the amount of power coupled into the output is reduced. When dealing with short pulses, the difference between the group velocities of the three interacting fields also manifests itself in the temporal domain by limiting the propagation length over which the pulses will overlap, as the pulses will 'walk off' each other after propagating a given distance through the crystal. This effect is known as 'temporal walk-off' [12].

The temporal walk-off can be characterized by a 'walk-off duration' $\Delta\tau$, which between pulses with centre frequencies ω_1 and ω_2, is given by,

$$\Delta\tau = \ell\left(\frac{\partial k_1}{\partial\omega} - \frac{\partial k_2}{\partial\omega}\right) \qquad (2.20)$$

In the case of a process involving three distinct values of group velocity, the two frequency components used should be those with the most disparate values (of group-velocity).

In general, the pulses propagating through a crystal of length ℓ must have a duration of at least as long as $\approx\Delta\tau$. This can be seen by considering the overlap of two Gaussian pulses of FWHM duration 'τ'. If it is assumed that the peaks of the two pulse coincide at the input of the nonlinear crystal, it can be shown that after propagating a distance $c\Delta\tau$, that their normalised Gaussian overlap has reduced from unity (when coincident) to $\approx 60\%$. In the case of the 5mm long KTP crystal phase-matched to frequency double 1.064μm, as used during the investigations described in Chapter 7, the temporal walk-off is $\approx 0.4\text{ps}\cdot\text{mm}^{-1}$, i.e. a $\approx$2ps temporal walk-off over a propagation distance of $\approx$5mm. This amount of walk-off is, however, insignificant for pulse durations of $\approx$15ps and longer: it can be shown in this case that the Gaussian overlap is only reduced by $\sim 1\%$ over the crystal transit. It was therefore ignored in the earlier stages of this project. It is, however, a matter that must be paid attention to, as it would have been necessary to do so had the implementation of pulse-

compression, as described in Section 3, Chapter 7, come to fruition. In particular, it has been found for ultrashort duration pulses ($\tau \sim$ 1ps and shorter) that too long a length of crystal can lead to a significant reduction in the available parametric gain, resulting from pulse walk-off and bandwidth limiting effects [13].

2.1.6 Optical parametric superfluorescence.

Before moving on to consider optical parametric oscillation, a brief mention of a special case of optical parametric amplification; optical parametric superfluorescence [5]. This occurs when the parametric gain is so high that it is possible to amplify up the parametric noise—on a single pass, or after several passes, through the gain medium—to a level comparable to the incident pump. The gain necessary for this is conventionally taken to be exp(20)-exp(30) (i.e. $\sim 10^9$-10^{13})[5]; the exact value being chosen with some degree of arbitrariness. The optical noise is that which is present due to spontaneous parametric scattering [16].

The process of parametric superfluorescence has been exploited as a way of generating widely tunable radiation in devices sometimes known as 'optical parametric generators' ('OPG') [14]. An alternative name for the OPG is the 'travelling wave oscillator' ('TWO'), but this nomenclature is not strictly correct, as there is no feedback utilised in such systems. The output of a OPG consists of a cone of radiation which varies in frequency across its spatial extent (due to a the variation in the phase-matching condition across the angular divergence of the pump beam). Through the use of an aperture, an output of a high spectral purity can be obtained; but only at the expense of power. To obtain both spectral purity *and* power it has become common practice to extend this technique by using a parametric amplifier to boost the output of the OPG [14]. This allows the generated radiation to be spectrally filtered quite heavily (i.e. at the expense of the majority of the available power), as an appreciable signal can be obtained from the output of the subsequent stage of amplification.

Parametric generation does suffer from other disadvantages in addition to the difficulty of affecting full spectral and spatial control. One of the problems is that to obtain the necessary gain, the crystal used must be exposed to an intensity approaching that at which damage will typically occur. In an attempt to obtain sufficient gain at lower intensities, a lot of work has been done with multi-pass schemes. The natural extension of such schemes is to place the parametric amplifier in a resonator, thereby forming a parametric oscillator.

2.2 Optical parametric oscillation.

An alternative way to reduce the threshold requirement for a parametric generator is to enclose it in a cavity, and thereby form a parametric oscillator [5]. If only one of the generated fields is resonated, the device is known as a singly resonant oscillator ('SRO'), whereas if both are resonated, it is a doubly resonant oscillator ('DRO').

The OPO has several advantages over the OPG. Firstly, as feedback is utilised, the single-pass gain required for significant amplification of the parametric noise is generally much lower than required in the case of the OPG. Consequently, the nonlinear medium need not be exposed to an intensity so close to its damage threshold. Secondly, the resonant nature of the device also acts to constrain the generated radiation both spectrally and spatially. This is because the resonator defines a unique direction of propagation; that of the cavity axis. As the gain medium is assumed to be pumped at an intensity significantly lower than that needed to provide a single-pass gain of exp(20)–exp(30), only the on-axis spectral component (as determined by phase-matching) will be fed back, and thereby experience the multi-pass amplification required to reach a significant level.

2.2.1 Single versus double resonance.

One question that must be considered is the relative virtue of the DRO and SRO schemes. The first matter of relevance is the oscillation threshold. A continuously pumped OPO reaches threshold at the point at which the parametric gain over a single pass of the nonlinear crystal more than accounts for the round trip cavity loss. Mathematically, following Byer [5], this condition may be expressed using (2.3), and assuming perfect phase-matching ($\Delta k=0$), as,

$$\begin{aligned} E_1 &= f_1(E_1 \cosh\Gamma\ell + i(\kappa_1/\Gamma)E_3E_2^* \sinh\Gamma\ell) \\ E_2 &= f_2(E_2 \cosh\Gamma\ell + i(\kappa_2/\Gamma)E_3E_1^* \sinh\Gamma\ell) \end{aligned} \qquad (2.21)$$

where all quantities are as defined for the case of (2.3), except the fractional round-trip electric field feedback f_i. If the round trip loss is small, then it follows from (2.21) that

$$\cosh\Gamma\ell = 1 + \frac{a_1 a_2}{2 + a_1 + a_2} \qquad (2.22)$$

where a_i are the round-trip losses ($a_i=1-f_i$). If both waves experience a low loss over one round trip (i.e. DRO), then (2.22) is well approximated by,

$$\Gamma^2 \ell^2 \approx a_1 a_2 \tag{2.23}$$

whereas in the case that only one of the fields is fed back (i.e. SRO), it becomes

$$\Gamma^2 \ell^2 \approx 2a_2 \tag{2.24}$$

From (2.23) and (2.24) it can be seen that the threshold of the SRO is a factor of 2/a larger than the equivalent DRO (i.e. assume that any field that is resonated will see a loss 'a'). A low, but realistically achievable, value of cavity loss is $\sim 1\%$. In this case, the SRO threshold will be around two orders of magnitude higher than that of the equivalent DRO. This is a very significant amount: particularly in the case of continuous pumping.

The disadvantage of the doubly-resonant scheme is the requirement for 'double resonance'. The OPO, being a resonant device, can only operate at frequencies that are modes of the cavity. In the case of the SRO this is no problem, as there will always be a signal mode close to the optimally phase-matched wavelength (within half the cavity mode-spacing). The idler, being non-resonant, is not required to correspond to a cavity mode and therefore automatically assumes the correct wavelength (i.e. the difference of the pump and signal). The DRO, however, can only operate at points where there is both a signal and idler wavelength that are resonator modes: a condition which is, in practice, difficult to meet. Furthermore, it is sensitively dependent on the cavity length and pump frequency—a slight variation in either of the cavity length or pump frequency can result in a significant shift in the operating point. Consequently, these devices tend to exhibit poor stability.

While it is possible to satisfy the condition for double resonance through the use of a highly stabilized pump and cavity [15], it can—in practice—only be satisfied for one mode pair at a time. In the case of multi-longitudinal mode systems, including all synchronously pumped systems, the simultaneous resonance of condition is not readily met. The use of two juxtaposed resonators has been proposed, but the tolerance to which the relative lengths of the cavity must be controlled is at the extreme limit of currently available stabilization systems. Consequently, it does not offer a practical route to a usable system (see Chapter 8, Section 2, Subsection 3 for a further discussion).

Oscillation threshold of pulsed system.

The oscillation threshold given above was for the case of a continuously pumped device. This may be denoted the 'c.w. threshold': it defines the intensity at which gain equals loss. In practice, however, as a high intensity is required for parametric gain to become significant,

it has been more usual to use Q-switched (or similar) pump sources. In these cases, as the pump is only present for a limited amount of time, the gain per pass must be sufficient that the total accumulated gain, over the number of round trips that take place within the pulse envelope, is high enough that an appreciable signal will have built up. This contrasts with the case of continuous pumping where, once the c.w. threshold had been exceeded, the signal has unlimited time to build up. (In does not, of course, build up indefinitely: it is eventually limited by gain saturation when the signal reaches a level sufficient to cause pump depletion).

The time taken for the signal to build up, from noise, to a level comparable with the pump, is known as the rise-time [5]. This quantity is of particular importance in the case of a finite duration (i.e. pulsed) pump, as it will determine whether or not the parametric oscillator reaches threshold (i.e. whether or not the signal power level approaches that of the pump).

The rise-time can be considered as an equivalent loss [5]. In the case of the SRO this has been shown to modify the threshold equation (2.24) to,

$$\Gamma^2 \ell^2 = 2a + \frac{\tau_c}{\tau_p} \ln\left(\frac{P(t)}{P(0)}\right) \tag{2.25}$$

where τ_c is the cavity round trip time, and τ_p is the duration of the pump pulse. P(0) is the parametric noise power [16], and P(t) is—generally—the power required to reach threshold. Rather than specify P(0) and P(t) explicitly, it is the ratio itself that is generally defined. As in the case of parametric generation, the gain needed to obtain a sizeable signal, from amplification of parametric noise, is usually taken to be $\sim$exp(20)–exp(30).

2.2.2 Gaussian beams.

In the discussions above, the interacting fields have been assumed to be plane wave. This section, however, gives the results—after Byer [5]—for a near-field analysis of three interacting Gaussian fields. While Byer [5] considered both the singly-resonant and doubly resonant OPO, here only the former case will be discussed. The poor stability of the doubly resonant system makes it unattractive as far as a practically usable system is concerned (see Subsection 1, Section 1), and it is therefore of little interest at this time.

If diffraction effects can be taken to be small enough that the variation in the beam radius 'w' over the length of the nonlinear crystal can be discounted, then the Gaussian beams may be adequately described by

$$E = E_0 \, e^{-\left(\frac{r}{w}\right)^2} \tag{2.26}$$

Substituting expressions of form (2.26), for each of the three interacting fields, into equations (2.1.a)–(2.1.c) in Section 1, it follows that each pair of fields generates a Gaussian polarization at the third frequency—for instance—ω_1, which has a waist '$\tilde{w}_1$' given by,

$$(\tilde{w}_1)^{-2} = (w_2)^{-2} + (w_3)^{-2} \tag{2.27}$$

Using the coupling coefficient formalism after Kogelnik [17], the coupling of the polarization at ω_i (back) into the corresponding electric field is given by,

$$g_i = \frac{1}{2}\left[1 + \left(\frac{w_i}{\tilde{w}_i}\right)^2\right] \tag{2.28}$$

The case of interest here is that of the singly resonant oscillator. As the idler field is nonresonant, and therefore not constrained in any way, it can be assumed to adopt the mode size that maximises the coupling between field and polarization: vis. it can be assumed that the idler coupling coefficient is unity (here, $g_2=1$). In this case, the coupled equations of (2.1.a)–(2.1.c) become,

$$\begin{aligned} \frac{dE_1}{dz} &= i\kappa_1 g_s E_3 E_2^* \\ \frac{dE_2}{dz} &= i\kappa_2 E_3 E_1^* \end{aligned} \tag{2.29}$$

where the 'singly resonant' coupling factor 'g_s' is defined by,

$$\frac{1}{g_s} = 1 + \left(\frac{w_1}{w_3}\right)^2 \tag{2.30}$$

From (2.30) it can be shown that the single-pass gain 'G_s' is,

$$G_s = \frac{4\omega_1\omega_2 d^2 \ell^2}{n_1 n_2 n_3 \epsilon_0 c^3} \frac{P_3}{\pi (w_1^2 + w_3^2)} \tag{2.31}$$

where the parametric gain coefficient 'Γ' and interaction coefficients κ_i have been substituted for using (2.2) and (2.4) respectively, and the pump power 'P_3' has been introduced in place of the modulus of the electric field (at the pump wavelength), according to,

$$P = \frac{I_{30}}{2} \pi w_3^2 \qquad I_{30} = \frac{1}{2} n_3 \epsilon_0 c |E_3| \tag{2.32}$$

where I_{30} is the peak pump intensity. Being a Gaussian beam, it is possible to express the power in terms of the effective area of the beam, and average intensity $\frac{1}{2}I_{30}$ ('effectively' averaged over the waist).

The dependency exhibited by (2.32) on the beam radii of the pump and signal fields suggests that the threshold can be made as small as wished by using arbitrarily tight focusing. However, the assumption was made above that the beam size did not vary significantly over the length of the nonlinear medium. This assumption breaks down for waist sizes small enough that the corresponding confocal parameters 'b'—in the medium—approach being as short as the crystal length 'ℓ'. If is assumed that $b \approx \ell$ represents the smallest usable spot-size, then it suggests that the optimal focusing involves the use of equal confocal parameters for the pump and signal. This optimum focusing condition has been shown to hold by the more formal analysis of Sushchik and Freidman [18], and coincides with the corresponding result from the analysis of the doubly resonant oscillator, after Boyd and Kleinman [2].

References.

[1]. J.A. Armstrong, N. Bloembergen, J. Ducuing, and P.S. Pershan.
Phys. Rev. **B2**, 1918 (1962).

[2]. G.D. Boyd and D.A. Kleinman.
J. Appl. Phys. **39**, 3597 (1968).

[3]. S.J. Brosnan and R.L. Byer.
IEEE J. Quantum Electron. **QE-15**, 415 (1979).

[4]. Y.R. Shen.
The Principles of Nonlinear Optics (Wiley 1984).

[5]. R.L. Byer.
Chap. 9, *Quantum Electronics: a treatise Vol. 1* (Academic Press 1975).

[6]. R.G. Smith.
Chapter C8, *Laser Handbook* (North-Holland 1972, F.T. Arecchi and E.O. Schulz-DuBois, Eds.).

[7]. J.A. Giordmaine.
Phys. Rev. Lett. **8**, 19 (1962).

[8]. M. Born and E. Wolf.
The Principles of Optics (Perganon Press 1980).

[9]. J.E. Midwinter and J. Warner.
Brit. J. Appl. Phys. **16**, 1135 (1965).

[10]. M.V. Hobden.
J. Appl. Phys. **38**, 4365 (1967).

[11]. M.A. Persaud, J.M. Tolchard, and A.I. Ferguson.
IEEE J. Quantum Electron. **26**, 1253 (1990).

[12]. S.A. Akhmanov, A.S. Chirkin, K.N. Drabovich, A.I. Kovrigin, R.V. Khokhlov, and A.P. Sukhorukov.
IEEE J. Quantum Electron. **QE-4**, 598 (1968).

[13]. D.C. Edelstein.
Ph.D. Thesis, Cornell University (1990).

[14]. A. Seilmeier and W. Kaiser.
Appl. Phys. **23**, 113 (1980).

[15]. W.J. Kozlovsky, C.D. Nabors, R.C. Eckardt, and R.L. Byer.
Opt. Lett. **14**, 66 (1988).

[16]. D.A. Kleinman.
Phys. Rev. **174**, 1027 (1968).

[17]. H. Kogelnik and T. Li.
Proc. IEEE **54**, 1312 (1966).

[18]. M.M. Sushchik and G.I. Freidman.
Radiophys. and Quant. Elec. **92**, 689 (1973).

3 The nonlinear medium.

In the past, the scarcity of suitable nonlinear materials severely hampered the development of the optical parametric oscillator (OPO) [1]. The majority of materials previously available had either a prohibitively low damage threshold, nonlinearity, or both. As parametric processes are only efficient at high pump intensities, this meant that damage was always a potential problem. Consequently, the practical exploitation of the OPO has so far been minimal. Recently, however, materials have become commercially available with greatly improved properties (e.g. barium borate [2] and potassium titanyl phosphate [3]). This is only partly due to the development of new nonlinear materials; it is also because of a general advancement in crystal growth technology. This has led to the availability of materials that not only have higher nonlinearities and damage thresholds, but also have much higher optical quality and homogeneity.

3.1 Crystal nonlinearity and symmetry.

Strictly speaking there is no separate class of 'nonlinear crystals', as all materials exhibit 'nonlinear behaviour' when exposed to an electric field of sufficient strength [4]. It is therefore more correct to refer to 'highly nonlinear crystals'. The parametric processes encountered during the investigations described in this thesis—optical parametric amplification and second harmonic generation—involve the coupling together of three fields, and are hence mediated by the second order susceptibility '$\chi^{(2)}$' of a material. Therefore, in the following discussion, 'nonlinear' will be taken to mean that the material possesses a large value of $\chi^{(2)}$.

The nonlinear properties of a crystal—as characterized by the higher order susceptibilities—are determined by its detailed electronic and molecular structure [5]. The theoretical determination of the values of the susceptibilities involves the application of quantum mechanics to determine the microscopic behaviour of the material [5]. Once this is known, it is then possible to determine the macroscopic behaviour, and hence the values of the susceptibilities. The complexity of these calculations limits the accuracy with which the susceptibilities may be determined; it is therefore more usual for their value to be experimentally obtained.

The symmetry of a material determines the number of independent, non-zero elements of the third-order tensor used to describe the $\chi^{(2)}$ susceptibility. A prerequisite for *any* of the elements to have a non-zero value is that the material must lack inversion symmetry (i.e. be

'non-centrosymmetric'). The crystal symmetry also determines the optical isotropy of the material. As a nonlinear process is only efficient if phase-matched, which involves the exploitation of crystal birefringence [6]. Consequently, a crystal is not usable as a nonlinear medium unless it also possesses a high enough birefringence.

3.2 General considerations.

When deciding which nonlinear material to use as the parametric gain medium in an optical parametric oscillator, there are two main points to consider: Firstly, can a high enough gain be obtained to reach threshold? Secondly, over how wide a range of wavelengths can the crystal be tuned?

The maximum parametric gain available from a given crystal is determined by its nonlinearity, its length, and the incident pump intensity. The usable ('effective') nonlinearity is determined by the intrinsic properties of the material, including the symmetry and the values of the principle nonlinearities, and also the birefringence, as this determines the direction of propagation through the crystal when phase-matched.

The usable length of the crystal is limited firstly by availability. Some crystals can be grown with lengths of up to 50mm and more (e.g. lithium niobate) whereas others can only be provided with lengths of up to a few millimetres (potassium titanyl phosphate is currently limited to about 12mm; some organic materials are only available with lengths of ~ 0.1mm). The usable length of medium is restricted, in the critically phase-matched case, by Poynting vector walk-off and angular acceptance, for a given focusing condition. The length is also restricted—irrespective of whether it is critically or noncritically matched—by spectral acceptance. The acceptance bandwidth of a crystal is inversely proportional to its length; if the linewidth of the pump is significant, then only a short crystal length will be efficiently utilised. In the case of transform limited mode-locked pulses, this may be alternatively treated in terms of temporal walk-off. This occurs because the group velocity at the pump and signal wavelengths differ, and hence the pulses will only overlap over a finite propagation length. The length over which the signal and pump overlap is the same as the maximum length of medium which has a wide enough spectral acceptance to couple the mode-locked radiation effectively.

Ideally a nonlinear material should be exposed to as high an intensity as is possible without severe risk of incurring damage; the actual safety margin to be allowed depending, in practice, on the stability of the laser being used. Therefore, a nonlinear material must

have a high damage threshold (ideally $\sim 1 GWcm^{-2}$ or greater). If only a limited amount of power is available, then it may not be possible to achieve an intensity of even a few percent of the damage threshold. This is particularly a problem when angular acceptance and walk-off effects restrict the usable degree of focusing.

The tuning range of a parametric oscillator is firstly determined by the transmission range of the crystal. This is ultimately limited by the ultraviolet and infrared 'cut-offs': vis. the upper and lower wavelengths where the material *stops* transmitting. This wide transmission range may, however, not be exploitable in practice. The transmission characteristics of many crystals in practice exhibit a degree of 'roll-off' at the extreme wavelengths, which will be significant enough to terminate oscillation in a low-gain OPO. An example of this is BBO: Chen *et al* [2] report the longest wavelength transmitted by BBO to be $2.7\mu m$. The graph they publish, however, suggests that a device that can only suffer a loss of 1-2% will only be able to operate out to $2.1\mu m$.

Given that the medium can transmit a wide range of wavelengths, it does not necessarily hold that the tuning range is also wide. For the crystal to be of use it must also have a birefringence that is sufficient to counter dispersion, and hence allow phase-matching. The range over which phase-matching is possible may be significantly smaller than the transmission range, or even nonexistent.

In the case of angle tuning, a wide tuning range requires a high birefringence. This high birefringence will, however, give rise to a high Poynting vector walk-off and a low angular acceptance. This will limit how tight a focusing scheme can be used with the crystal, which will limit the parametric gain available with a given pump power. It is therefore a matter of compromise; if a very wide tuning range is required from an angle tuned source, it must be accepted that the gain available will be compromised by the various angular effects. It does, however, make sense that having decided to utilise angle tuning, that the crystal used has a birefringence with a low thermal dependency, so that temperature stabilization is not needed in addition.

Alternatively, if temperature tuning is to be used, the birefringence of the material must have a high thermal dependency, and hence allow a wide range of wavelengths to be phase-matched for propagation in the same direction. There is, however, no advantage to be gained in using temperature tuning unless non-critical (or nearly so) phase-matching is possible. This allows the use of much tighter focusing, as in this situation the angular

acceptance is wide, and the Poynting vector walk-off is non-existent. If matching is only possible critically, then the attendant angular variation of birefringence—that leads to the Poynting vector walk-off and a low angular acceptance—might as well be exploited to tune the crystal.

The aim of this project was to investigate the possibility of developing a widely tunable source of mode-locked pulses, and consequently a material was desired that could be widely tuned. Alternative uses of nonlinear crystals involve a fixed triad of wavelengths, e.g. to generate the sum frequency of two lasers. In this case, a crystal which is insensitive to all the parameters normally used to tune a parametric interaction (e.g. temperature, angle) would be ideal; assuming it could actually phase-match for the desired set of wavelengths.

3.3 The 'Figure of Merit'.

To aid in choosing a nonlinear material it is common practice to define a 'figure of merit' based on the small-signal parametric gain coefficient [1]. This allows a semi-quantitative comparison to made of the gain available from different crystals, without resort to lengthy calculation. The actual form used has varied from author to author, depending on the intended application; the one most commonly used being d^2/n^3. This does not, however, take any account of angular, spectral or temporal limitations. Together, these effects determine the usable combinations of crystal length and focusing. Furthermore, it takes no account of the damage threshold of the material. Hence, when choosing a nonlinear medium for a specific usage, it is necessary to modify the figure of merit accordingly.

The small signal parametric gain [1] depends on the refractive index and nonlinearity of the nonlinear medium, the pump intensity, and the interaction length; which is not necessarily as long as the physical length of the nonlinear medium: In the case of mode-locked pulses, group velocity dispersion can limit the interaction length to only a few millimetres (e.g. in KTP, $\sim$2ps pulses at 0.532μm and 1.064μm only overlap over a propagation length of $\sim$5mm). Given these dependencies, it is possible to 'construct' figures of merit that are applicable in different circumstances.

If the available pump power is sufficiently high that the damage threshold of the material may be approached without resort to tight focusing, hence allowing walk-off and angular limitations to be neglected, and also the linewidth of the pump radiation is significantly below the acceptance bandwidth of the crystal (equivalent, in the case of transform limited mode-locked pulses, to the requirement that the temporal walk-off be

insignificant compared to the pump pulse duration) then the available parametric gain will be proportional to,

$$\mathrm{FoM_I} = \frac{d^2}{n^3}\ell^2 I_d \qquad (3.1)$$

where 'd' is the effective nonlinearity (in pmV^{-1}), for the interaction of interest,'n' is the refractive index, 'I_d' is the damage threshold of the material (in $GWcm^{-2}$), and 'ℓ' is the available length of the material (in mm). The subscript 'I' for the figure of merit is to denote that this is the 'intrinsic' value; i.e. unlimited by temporal, spectral or angular effects.

If, however, the available power *is* limited, then focusing must be taken into account. In the critically phase-matched case, the spotsize allowed is $w \sim \rho\ell$; where ρ is the Poynting vector walk-off (in radians). In this case, a suitable figure of merit can be defined as,

$$\mathrm{FoM_P} = \frac{d^2}{n^3}\frac{1}{\rho^2} \qquad (3.2)$$

where, again, the pump bandwidth has been assumed to be sufficiently narrow that bandwidth effects will be insignificant. Note that there is no length dependency; varying the length of the crystal will therefore not lead to a different parametric gain, as long as the spotsize is varied proportionally. The only limit to the reduction of the crystal length being that damage will eventually become a problem. It has, however, been assumed that the walk-off is significant enough that tight focusing is precluded, and hence diffraction effects ignored. This assumption is reasonably valid for crystal lengths of as short as $\sim$1mm, and for materials exhibiting Poynting vector walk-offs of up to $\sim$50mrad.

In the noncritically phase-matched case, however, there is no Poynting vector walk-off to determine the focusing. In this case, the optimal spotsize to use is that which corresponds to the confocal parameter—*in the medium*—being around one third of the physical length of the crystal (i.e. $3b \sim \ell$)[7]. In this case, the figure of merit $\mathrm{FoM_P}$ becomes,

$$\mathrm{FoM_P} = 18600\frac{d^2}{n^2}\frac{\ell}{\lambda_p} \qquad (3.3)$$

where λ_p is the pump wavelength in vacuo (in μm), and the scale factor of 18600 is to preserve the dimensionality of $\mathrm{FoM_P}$ when moving from the critical to noncritical case. It

arises from the substitution of $w=\rho\ell$ by $3b=\ell$ (equivalent to $w^2=\lambda\ell/6\pi n$); i.e. ρ^2 is replaced by $\lambda/6\pi n\ell$. In this case there is a length dependency, and it can hence be seen that it *is* advantageous to use a long length of crystal.

If the linewidth of the pump is large, it is necessary to take account of temporal walk-off and spectral acceptance; both of which originate because of group velocity dispersion. As mentioned in Section 3, in the case of transform limited mode-locked pulses only one of these effects need be considered for both to be accounted for. It can be shown that in the case of a pump pulse duration 'τ', that the propagation length over which the pump and signal pulses overlap is approximately $\ell \approx \tau/\alpha$ [8]; where α is the temporal walk-off coefficient (the difference between the reciprocal group velocities of the pump and signal fields). In this situation, the figures of merit given above must be altered accordingly. The first figure of merit 'FoM_I' becomes,

$$FoM_{I,T} = \frac{d^2}{n^3}\left(\frac{\tau}{\alpha}\right)^2 I_d \qquad (3.4)$$

where 'τ' is the pulse duration in picoseconds, and 'α' is the temporal walk-off in $ps \cdot mm^{-1}$. The second figure of merit 'FoM_P' is unchanged for the critically phase-matched case, but the length must be less than τ/α. In the noncritical case, the figure of merit becomes,

$$FoM_{P,T} = 18600\,\frac{d^2}{\lambda\, n^2}\,\frac{\tau}{\alpha} \qquad (3.5)$$

The first two of these figures of merit were used at the beginning of this project to compare the nonlinear materials that were available. The latter two have more recently been used when considering the ultra-short pulsed operation of the OPO. A consideration of the four different figures of merit is felt to give a better overall picture of the crystal, as together they account for a wider variety of possible applications. It must be noted here that it was not intended for the different figures of merit to be cross-correlated, but only for the values of a given figure of merit to be compared between crystals.

The values of these figures of merit, and a summary of a few of the relevant crystal properties, is given in Section 5, after a brief overview of the various nonlinear materials considered.

3.4 An overview of nonlinear materials for use in the near infrared.

In Section 2, the primary characteristics desired of a nonlinear medium were outlined; these are a high damage threshold, a high nonlinearity, a wide transmission range, *and* a birefringence that is sufficient to allow phase-matching. In addition, they must be obtainable with long enough lengths to provide sufficient parametric gain.

The optical quality of the material must be high, as inclusions will lead to a reduction in the damage threshold. This also affects the transmission of a material, as scattering from optical inhomogeneities can result in a significant loss. Furthermore, if the material is not sufficiently homogeneous, then the birefringence of the material may vary throughout the material. In this case, phase-matching can not be achieved simultaneously over the full length of the material, and hence the parametric gain available is greatly reduced. This requirement that the crystals must be available with high optical quality and homogeneity dramatically restricts the number of crystals that need be considered.

At the time that this project commenced, the only materials available that could meet the requirements of size and homogeneity were potassium dideuterium phosphate (KD_2PO_4, 'KD*P' [9]), lithium niobate ($LiNbO_3$ [10]), lithium iodate ($LiIO_3$) [12], urea [13], and barium borate (BaB_2O_4, 'BBO' [2]). During the duration of this project, however, other materials did become available; e.g. potassium niobate ($KNbO_3$ [14]) and potassium titanyl phosphate ($KTiOPO_4$, 'KTP'[3]). With the exception of KTP, a discussion of recent developments in nonlinear materials is delayed until Chapter 8.

Potassium dideuterium phosphate [9] (KD_2PO_4, 'KD*P') is a negative uniaxial crystal of point group $\bar{4}2m$. It is the deuterated analogue of potassium dihydrogen phosphate (KH_2PO_4, 'KDP'); deuterated to increase the infrared cut-off wavelength of the material from $\approx 1.0\mu m$ to $\approx 1.2\mu m$. It has found wide-spread use in the frequency doubling of ultra-high power Nd:YAG lasers (as used in plasma fusion experiments), as it is one of the few nonlinear crystal that can be grown to have a large enough aperture size that damage can be avoided. While KD*P does possess a high damage threshold ($\sim 4GWcm^{-2}$ for 10ns pulses at $1.064\mu m$), it has a nonlinearity of only $\sim 0.5pmV^{-1}$ [9](c.f. $\approx 6.3pmV^{-1}$ of lithium niobate [11]). Furthermore, as mentioned above, it can only transmit wavelengths shorter than $\approx 1.2\mu m$. Consequently the tuning range of a parametric oscillator based on this material is very limited in the near infrared part of the spectrum. This is the reason that while

parametric oscillation *has* been demonstrated using this material, its use has not been widespread.

Lithium niobate ($LiNbO_3$)[10] is a uniaxial ferroelectric crystal of point group 3m. It has a high nonlinearity ($\approx 6.3 pmV^{-1}$ [11]), and in the case of a $0.532\mu m$ pump may be temperature tuned to noncritically phase-match for parametric oscillation about degeneracy (from 0.7-$2\mu m$ for a variation of temperature of $\sim 100°C$). Unfortunately, while it does possess an intrinsically high damage threshold ($\sim 100 MWcm^{-2}$ at $1.064\mu m$ [1]), it is susceptible to reversible photorefractive damage at very low incident intensities ($\sim 1 Wcm^{-2}$ [15]) of radiation in the visible part of the spectrum. Despite this it has received wide-spread use—the majority of early work on parametric oscillation in the near infrared utilised this material [16]—but it has prevented the effective exploitation of this material. Because of its otherwise promising characteristics, much effort has been expended on eliminating the problem of optical damage. More recently, a magnesium oxide doped variant has been developed, and been found to possess superior damage resistance; this is discussed in Appendix A1.

Lithium iodate ($LiIO_3$) is a negative uniaxial crystal of point group 6. It has a high nonlinearity ($d_{15}=5.5\pm 0.3 pmV^{-1}$ [12]), and is transparent from 0.3-$5.5\mu m$ [17]. $LiIO_3$ phase-matches at 30° for the type I frequency doubling of $1.064\mu m$, where the corresponding value of effective nonlinearity is $\approx 2.8 pmV^{-1}$, about half that of lithium niobate. Parametric generation has been demonstrated—with a $0.53\mu m$ pump—to tune from 0.68–$2.4\mu m$ for an angular variation of 5° [18]. This material does have several disadvantages. Firstly, when phase-matched for operation of a $0.532\mu m$ OPO it presents a high walk-off ($\approx 75 mrad$). Secondly, it has a prohibitively low damage threshold, of only $\approx 50 MWcm^{-2}$ (for 15ns pulses at $0.532\mu m$)[19]. Thirdly, it *can* exhibit a high absorption; at $1.064\mu m$ the loss coefficient can be as high as $\approx 0.06 cm^{-1}$, corresponding to a loss over 5mm of $\sim 3\%$.

Urea is a positive uniaxial crystal of point group $\bar{4}2m$ [13]. It has a nonlinearity of $\approx 1.4 pmV^{-1}$, about 23% of that of $LiNbO_3$, and a high damage threshold of up to $2 GWcm^{-2}$ (10ns pulses at 355nm). Its use in the infrared is limited as it can only transmit wavelengths of up to $\approx 1.4\mu m$. It does, however, transmit wavelengths as short as 200nm, and is consequently of use to those requiring wavelengths in the ultraviolet (e.g. can be used to frequency quadruple the output of a Nd:YAG laser); Until barium borate became available, it was the dominant material for this use.

Barium borate [2] (BaB_2O_4, 'BBO') is a recently developed material that is of great utility in the ultraviolet, as it transmits wavelengths down to below 180nm. However, BBO is also of use in the near infrared, as it can transmit wavelengths of as long as $\sim 2.5\mu m$. While it does not have a particularly large nonlinearity ($\approx 2pmV^{-1}$) when compared to lithium niobate, it does compare well against the other materials that transmit as far into the ultraviolet (e.g. the nonlinearity of ammonium dihydrogen phosphate, 'ADP', is only $\sim 25\%$ of that of BBO). BBO possesses a very high damage thresholds, of $\sim 13.5GWcm^{-2}$; which holds even for pulses of several hundred nanoseconds. The major disadvantage with BBO is the large walk-off over the majority of its tuning range, making it unusable for low power applications.

Potassium titanyl phosphate ($KTiOPO_4$, 'KTP') is a negative biaxial crystal—of point symmetry mm2—that has only become readily available in the last few years, even though it was first developed several years ago [3]. This is because of the difficulty in scaling up the growth technique developed in the laboratory to the point at which mass production became economically viable. KTP has rapidly found wide-spread usage, as it has a high nonlinearity ($3.2pmV^{-1}$) and can quasi-noncritically phase-match for the doubling of $1.064\mu m$.

Until recently, the effective nonlinearity of KTP for the doubling of $1.064\mu m$ was believed to be $\approx 7.3pmV^{-1}$, giving this material a 'figure of merit' (d^2/n^3); twice that of lithium niobate. As it also possessed a much higher damage threshold ($\sim 2GWcm^{-2}$ for 100ps pulses), it appeared to be significantly better. More recently, as the thresholds and efficiencies calculated using the above value have proved over-generous, the effective nonlinearity has been remeasured, and found to be $\approx 3.2pmV^{-1}$; less than half the previous value! This puts the two materials on an even footing as concerns the 'figure of merit' d^2/n^3.

As far as tuning is concerned, KTP is not as well suited as lithium niobate. As mentioned above, $LiNbO_3$ can be temperature tuned; KTP can not. Consequently, quasi-noncritical matching (i.e. propagation perpendicular to the z-axis) is only achievable for a limited range of wavelengths ($0.96\text{-}1.2\mu m$, for a $0.532\mu m$ pump). If a wide tuning range is required from KTP, then a high walk-off will be incurred (as propagation departs from being perpendicular with the z-axis).

One property that has not been mentioned so far is resistance to atmospheric water vapour. KD^*P, $LiIO_3$ and urea are highly hygroscopic, and must therefore either be permanently heated, or mounted in index matching cells. BBO is slightly hygroscopic, and

therefore should not be left exposed to the atmosphere for any appreciable length of time; if this is necessary, then the crystal should be maintained at a temperature slightly above room temperature to prevent condensation forming on the crystal faces. All the other materials mentioned above are believed to be totally impervious to water vapour: there is, however, no long term data on any of the newer materials.

3.6 Selection of the OPO gain medium.

As mentioned in Section 4, the only nonlinear materials available at the time that this project commenced, that could meet the requirements of size and homogeneity, were potassium di-deuterium phosphate (KD_2PO_4, 'KD*P'), lithium niobate ($LiNbO_3$), lithium iodate ($LiIO_3$), urea, barium borate (BaB_2O_4, 'BBO'), and potassium titanyl phosphate ($KTiOPO_4$, 'KTP').

The table on the following page compares the four figures of merit—as given in Section 2—for these six crystals.

Potassium titanyl phosphate is considered for use in its quasi-noncritical (low walk-off, and tuning) and critical (high tuning, and walk-off) cases. The potential tuning ranges are also given, though at the initial stage of the project they were treated as less important than the available parametric gain.

It can be seen from the values listed in the table on the following page, that if power is not limited, then the best crystal to use is barium borate (this feature is characterized by FoM_I). BBO continues to be the clear leader, even when temporal walk-off is taken into account ($FoM_{I,t}$).

In the case where power is limited, however, BBO does not figure so prominently. It is lithium niobate, and to a lesser extent potassium titanyl phosphate—when quasi-noncritically matched—that are most strongly featured. Even though KTP did not offer as high a parametric gain as lithium niobate, it was judged to be sufficient for the planned investigation of the OPO. Consequently it was chosen in favour of the lithium niobate, by virtue of the fact that (a) it does not require heating to (quasi-) noncritically phase-match, and (b) was known to be *totally* insensitive to photo-refractive damage.

Table 3,1 Comparison of the relative merits of the nonlinear crystals that were readily available from 1986-1989.

Material	BBO	KD*P	$LiNbO_3$	urea	$LiIO_3$	KTP	KTP
Point group	3m	$\bar{4}2m$	3m	$\bar{4}2m$	6	mm2	mm2
Type	I	I	I	I	I	IIxy	IIzy
I_d/ $GWcm^{-2}$	13.5	4	0.05	3	0.05	2	2
d_{eff}/ pmV^{-1}	2.0	0.4	6.3	1.0	2.8	3.2	2.5
n	1.6	1.5	2.2	1.6	1.8	1.8	1.8
$\Delta n/n$	7.5%	2.7%	3.7%	6.6%	8.2%	0.4%	5.9%
ℓ/mm	7	30	50	12	10	5	5
ρ/mrad	50	29	0	45	74	5	32
θ/deg	23	35	90	22	30	$\phi=25$ $\theta=90$	$\theta=69$ $\phi=90$
α/ $ps\cdot mm^{-1}$	0.08	0.03	0.54	0.10	0.26	0.43	0.40
FoM_I	650	480	670	130	10	90	60
FoM_P	390	60	$4x10^8$	150	250	$7x10^4$	1100
$FoM_{I,t}$ $\tau=100ps$	$2x10^7$	$2x10^6$	6400	$9x10^5$	$1x10^4$	$2x10^5$	$2x10^5$
$FoM_{I,t}$ $\tau=1ps$	2000	200	1	90	1	20	20
$FoM_{P,t}$ $\tau=100ps$	290	60	$5x10^7$	150	250	$7x10^4$	1100
$FoM_{P,t}$ $\tau=1ps$	290	60	$5x10^5$	150	250	$7x10^4$	1100
Tuning range/μm	0.68 -2.5	0.96 -1.2	0.63 -3.2	0.86 -1.4	0.58 -3.2	0.96 -1.2	0.6 -4.0
Hygro-scopic?	yes	yes	no	yes	yes	no	no

Note.

(1) The 'figures of merit' (FoM) are as defined in Section 3. Note that the only meaningful comparisons are between values of the *same* figure of merit, for different materials.

(2) The nonlinearity used for KTP here is the value published recently by Eckardt *et al* [24]. At the time that it was decided to use KTP, its nonlinearity was taken to be $7.2pmV^{-1}$, after Zumsteg *et al* [3]. Even using the newer, lower, value of nonlinearity, KTP still compares very favourably against the other materials.

(3). The damage threshold for $LiNbO_3$ is the more optimistic value quoted after Byer [1]. However, values of as low as $\sim 1Wcm^{-2}$ have also been reported [15].

3.5 Barium Borate (BaB_2O_4).

This section summarises the properties of barium borate that are relevant to its use as the nonlinear medium in an OPO. The pump wavelength used during the investigation of the barium borate OPO—as described in Chapter 6—was 0.532μm. Consequently, all values quoted in this section, of angular acceptance, etc., pertain to this (pump) wavelength.

3.5.1 Transmission.

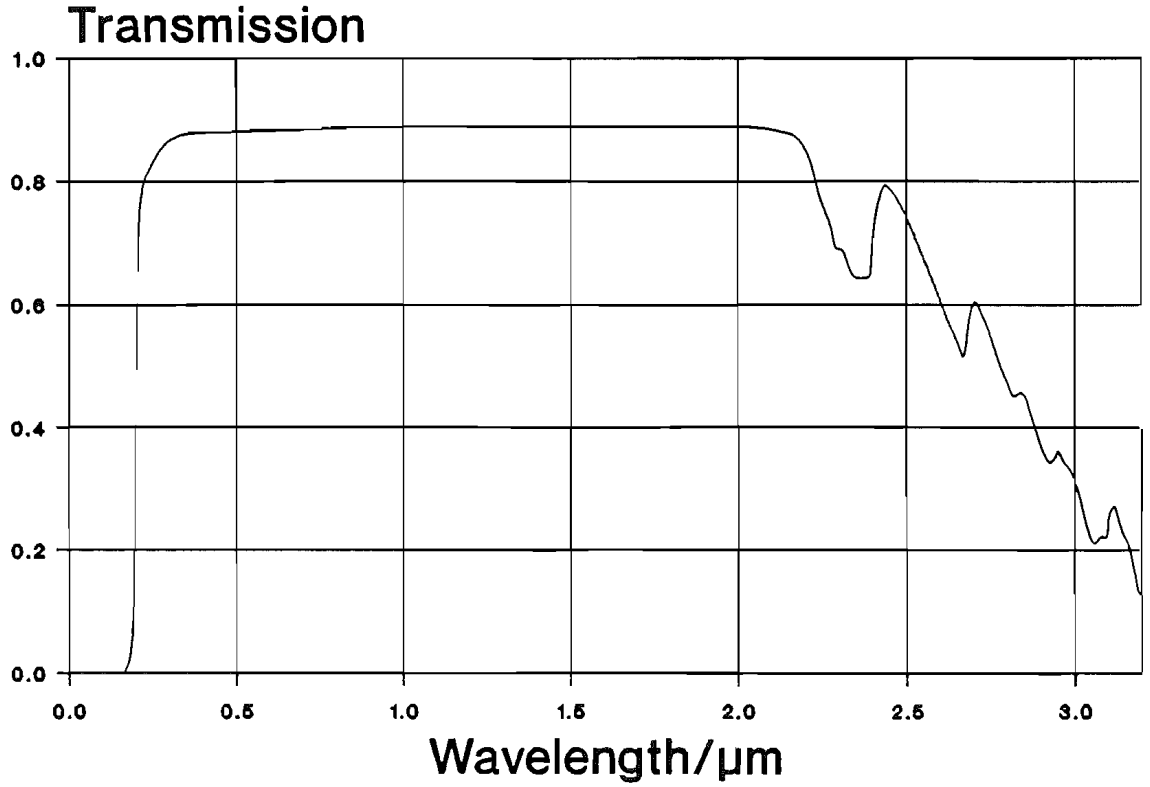

Fig. 3.1 Transmission of BBO as a function of wavelength; after Eimerl *et al* [20].

The transmission of BBO is shown as a function of wavelength in Fig. 3.1 [20]. Due to the high electronegativity of the B-O bond the transmission of BBO extends all the way down to 200nm [2], making this material of great interest to those working with wavelengths in the ultraviolet region of the spectrum. It is, however, also of interest to those working in the near infrared, as it can transmit wavelengths of up to 2.5μm (or even higher if a significant degree of loss ($\sim$20%) can be withstood). Given the upper wavelength cut-off, this means that a parametric oscillator pumped at 0.532μm can potentially tune from 0.68-2.5μm (while a parametric oscillator pumped at 266nm can potentially tune from 0.3-2.5μm; which includes the whole of the visible region of the spectrum).

3.5.2 Birefringence and dispersion.

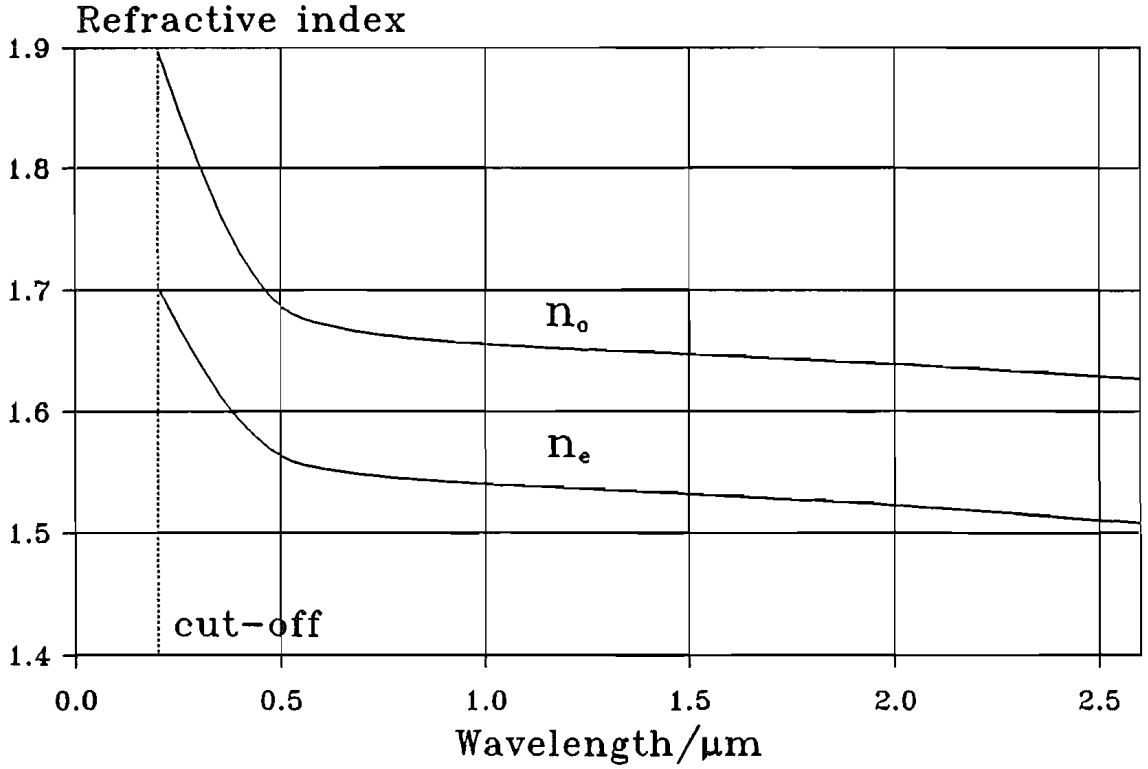

Fig. 3.2 Refractive indices of barium borate as a function of wavelength. These curves were generated using the Sellmeier's equations after Kato [18].

The refractive indices of BBO are plotted as a function of wavelength in Fig. 3.2 [21]. As it is a (negative) uniaxial crystal there are only two values of principal index, of which the extraordinary one is the smaller. The fractional birefringence of BBO is 7.0% at 1.064μm, and increases slowly with frequency up to a value of 7.5% at 355μm. The birefringence then increases more rapidly, reaching nearly 10% as the wavelength approaches the ultraviolet cut-off. This means that even in the case of pump wavelengths as short as 0.355μm, the degree of Poynting vector walk-off will be almost independent of wavelength. From the fractional birefringence, it can be seen that the maximum walk-off will be $\sim$75mrad. Few other nonlinear crystals have a walk-off this severe. Examples of those that *do* are urea ($\approx$45mrad) and lithium iodate ($\approx$75mrad).

An advantage of BBO having its ultraviolet cut-off at such a short wavelength is that the dispersion is low even at 0.532μm (i.e. $dn/d\lambda \approx -0.08\mu m^{-1}$ c.f. $dn/d\lambda \approx -0.25\mu m^{-1}$ for KTP [23]). This results in BBO having a wide spectral acceptance and a low temporal walk-off. In the case of a 0.532μm pumped, type I OPO matched at degeneracy, the corresponding

values are 550GHz·cm and 0.08ps·mm^{-1}. This means that a 5mm length BBO crystal can effectively couple light between pulses of as short as $\approx$0.4ps (c.f. $\approx$2ps in the case of KTP).

3.5.3 Angular behaviour.

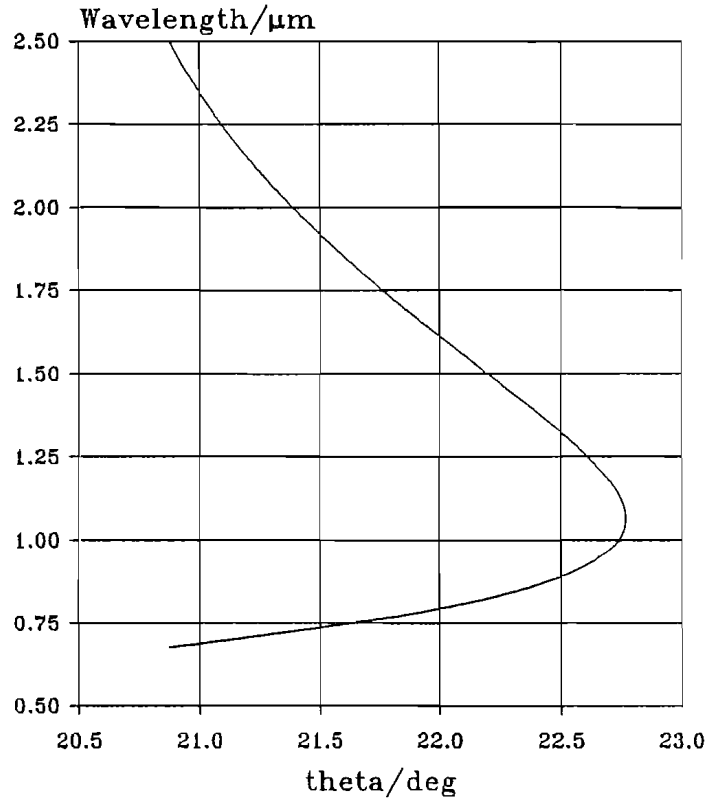

Fig. 3.3 Type I phase-matching curve for a BBO OPO pumped at 0.532μm. Calculated using Sellmeier's equations after Kato [18].

The high birefringence of BBO leads to a high Poynting vector walk-off and low angular acceptance when the phase-matching angle departs from 90°. It does mean, however, that the rate of angular tuning is also high, and consequently that even a crystal with a limited aperture can tune over a wide range of wavelengths. This is the situation when BBO is phase-matched for 0.532μm pumped parametric oscillation; in both the type I and type II cases (see Fig 3.3 and 3.4 respectively).

It can be seen from Fig. 3.3 and Fig 3.4, that the angle tuning is more rapid in the type I case, and that it also phase-matches at a smaller angle with the optic axis. This means that the degree of walk-off is smaller (52-59mrad in the type I case, c.f. 60-85mrad in the type II case). The only disadvantage of the type I case is the lower angular acceptance; at degeneracy the angular acceptances are respectively 0.57mrad·cm and 0.41mrad·cm for the type II and type I cases.

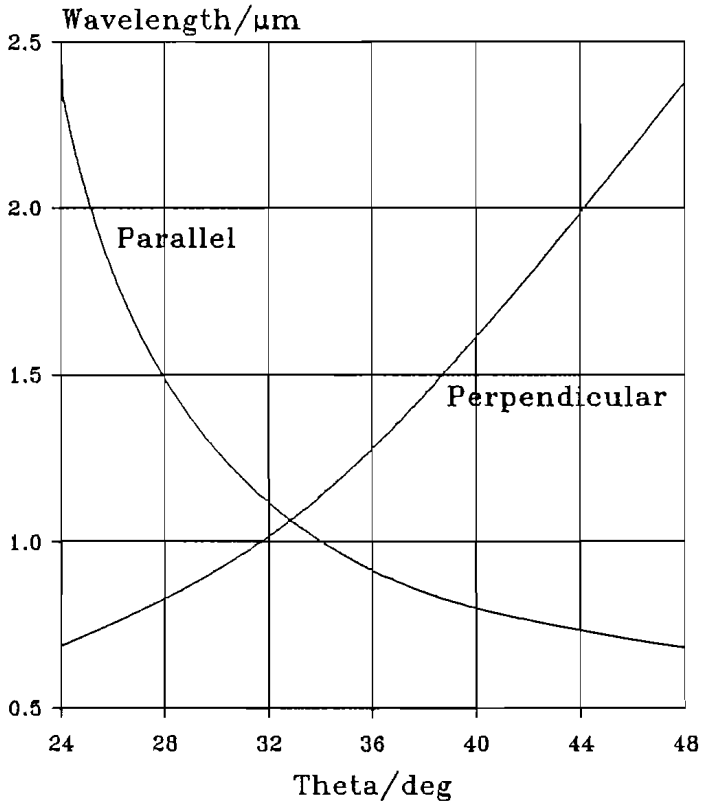

Fig. 3.4 Type II phase-matching curve for a BBO OPO pumped at 0.532μm. Calculated using the Sellmeier's equations after Kato [18].

3.5.4 Nonlinearity.

Barium borate (BBO), being of point group 3m, has five non-zero nonlinear coefficients: d_{22}, d_{11}, d_{13}, d_{14}, and d_{33}. Of these, two are very small (d_{22} and d_{14}) and one (d_{33}) makes no contribution to either the type I or type II effective nonlinearity. These are given by,

$$d_{eff}^{I} = d_{13}\sin\theta + (d_{11}\cos 3\phi - d_{22}\sin 3\phi)\cos\theta$$
$$d_{eff}^{II} = (d_{11}\sin 3\phi + d_{22}\cos 3\phi)\cos^2\theta \qquad (3.6)$$

As BBO is uniaxial only the angle θ is determined by phase-matching, and hence the angle ϕ is free to be set to maximise the effective nonlinearity. As d_{22} is small enough to be neglected [20], the optimised effective nonlinearities may be immediately written down as

$$d_{eff}^{I} = d_{13}\sin\theta + d_{11}\cos\theta$$
$$d_{eff}^{II} = d_{11}\cos^2\theta \qquad (3.7)$$

The values of the two sizeable coefficients have been determined by Chen *et al* [2] to be $d_{11}=\pm(1.6\pm0.4)pmV^{-1}$ and $d_{13}=\pm(0.11\pm0.05)pmV^{-1}$, using the Maker's fringe technique. The effective nonlinearity for the frequency doubling of $1.064\mu m$ was also determined from accurate measurements of the conversion efficiency. The value in this case was determined to be $\pm1.65pmV^{-1}$; in good agreement with the value calculated using the nonlinear coefficients determined from the Maker's fringe technique and the known phase-matching angle. The other coefficients have not been determined with any degree of accuracy, but are known to be $<0.08pmV^{-1}$ [20].

More recently, Eckardt *et al* [24] have determined the effective nonlinearity, for the same harmonic process as given above, to be $\pm2.2pmV^{-1}$. This suggests that the value of d_{11} should be taken as $\pm2.0pmV^{-1}$, about 37% higher than the earlier value. This remeasurement was made because experimentally determined thresholds were found to be consistently lower than theoretically predicted using the values of nonlinearity after Chen *et al* [2].

The effective nonlinearity for degenerate operation of an OPO is the same as that for the frequency doubling of the degenerate wavelength. Consequently, the type I OPO will see an effective nonlinearity of $\approx2.2pmV^{-1}$, as determined for the frequency doubling of $1.064\mu m$. The value in the type II case, however, is $\approx1.4pmV^{-1}$. Given the higher nonlinearity, lower walk-off and greater rapidity of tuning, the type I interaction is therefore preferred.

3.5.5 Thermal behaviour.

The birefringence of BBO has a low thermal dependency, making it insensitive to localized laser-induced heating that can be encountered in high average power applications. This does, however, preclude the possibility of temperature tuning. The temperature acceptance of BBO has been determined to be $55°C\cdot cm$, which is almost an order of magnitude higher than the corresponding value of $\approx7°C\cdot cm$ for KDP.

As mentioned in Section 3, BBO does exhibit a degree of deliquescence, and consequently must be heated if left exposed to the atmosphere for any appreciable length of time. The low temperature sensitivity of BBO means that only coarse stabilization is needed.

3.5.6 Optical damage.

The one-shot damage threshold has been found to be as high as $\approx 13.5 GWcm^{-2}$, for 1ns pulses at $1.064\mu m$ [20]. This was found to be dependent on the crystal having a high optical quality, and being free from optical inclusions. A 'not-so-perfect' crystal was also tested, and found to have a damage threshold over a factor of two down on the above result.

3.6 Potassium Titanyl Phosphate.

Potassium titanyl phosphate ($KTiOPO_4$) is a negative biaxial crystal of point symmetry mm2. It has a nonlinearity of $3.2 pmV^{-1}$—around ≈ 7.5 times that of KDP—and offers quasi-noncritical phase-matching for the doubling of wavelengths in the region of $1.064\mu m$ at room temperature. As with BBO, the birefringence of KTP has a low thermal dependence, making it insensitive to temperature gradients in the crystal caused by local heating; but it does preclude the efficient use of temperature tuning. While the damage threshold of KTP is not as high as some materials (e.g. BBO [20]), it is—however—sufficient to permit exposure to intensities high enough to give significant parametric gain.

3.6.1 Transmission.

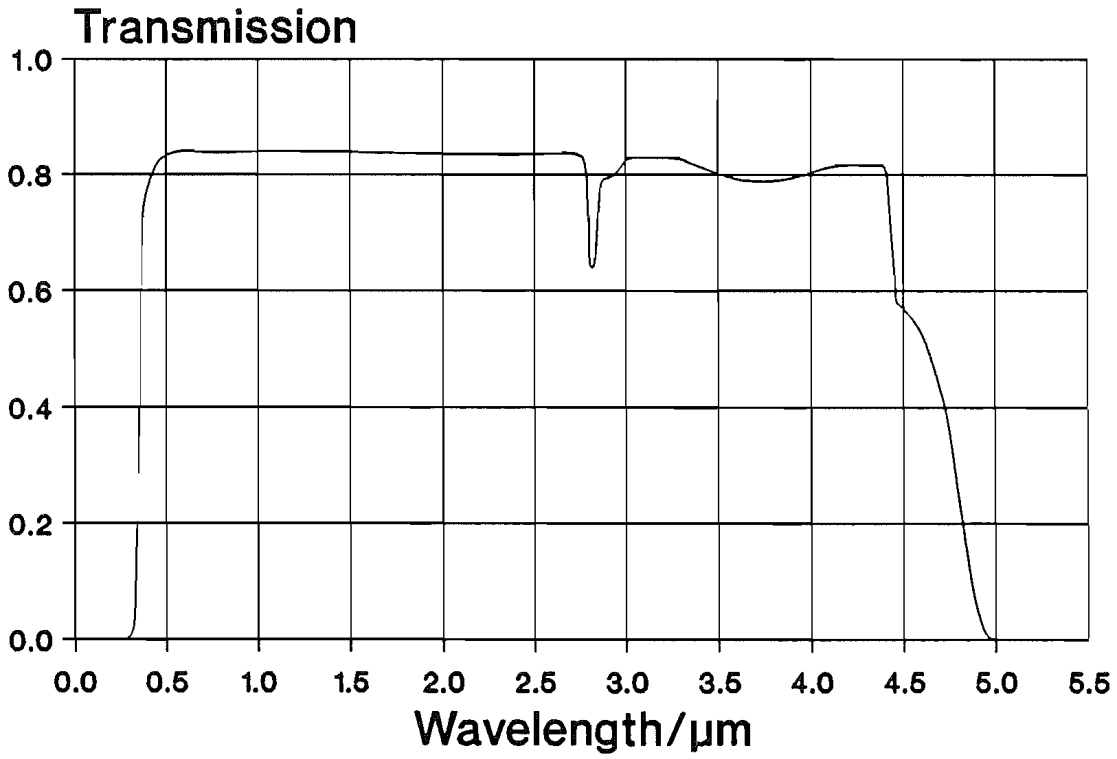

Fig. 3.5 Transmission of $KTiOPO_4$ as a function of wavelength, after Zumsteg *et al* [3]: no correction has been made for Fresnel losses.

Fig. 3.5 shows the optical transmission of KTP as a function of wavelength over the entirety of its transmission range. The curve shown is for a crystal grown by the hydrothermal technique. The absorption feature at $\approx 2.8\mu m$ most likely corresponds to an OH stretching band, and suggests that H^+ has been incorporated into the crystal lattice. This feature should be absent in the case of a flux-grown crystal, as should the broader feature centred around $3.8\mu m$. This indicates the presence of molecular H_2O as an impurity trapped in the crystal structure.

The absorption coefficients of KTP have been measured by Gettemy *et al* [22]— at 514.5nm, 660nm, $1.064\mu m$, and $1.320\mu m$—using crystals supplied by two different vendors. They were found to exhibit significantly different losses, probably as a result of different growth techniques. Unfortunately this information is not disclosed, so it does not provide a guide to selecting a crystal with the lowest loss. Of particular relevance to this work, they found the absorption at $1.064\mu m$ for one of the crystals was found to be only $4\times10^{-4}cm^{-1}$, giving a loss through a 5mm crystal of 0.02%. The loss coefficient for the other sample was over an order of magnitude higher ($\sim 5\times10^{-3}cm^{-1}$), leading to a loss of 0.25%. In a linear resonator this amounts to an extra loss of 0.5% over one round trip, which though small will be significant in the case of a low gain system.

3.6.2 Birefringence and dispersion.

While KTP is more dispersive than some materials (e.g. BBO [20], KDP [9]), it does have a high nonlinearity. Consequently the bandwidth acceptance of a crystal of a length required to achieve a sizeable efficiency is larger than average. The calculated spectral acceptance-length product for the degenerate interaction—for a $0.532\mu m$ pump—is 0.28nm·cm (or 74GHz·cm). Consequently, a 5mm long crystal has a bandwidth acceptance of 0.56nm (150GHz).

The group velocity dispersion also determines the temporal walk-of, which is—for near degenerate operation— $\approx 0.4 ps.mm^{-1}$. This limits the usable pulse duration with a 5mm length to greater than 2ps. It is assumed here that the pulse is transform limited. The bandwidth of a bandwidth limited pulse of 2ps is $\sim$250GHz, which is the same as the value determined from the consideration of the spectral acceptance.

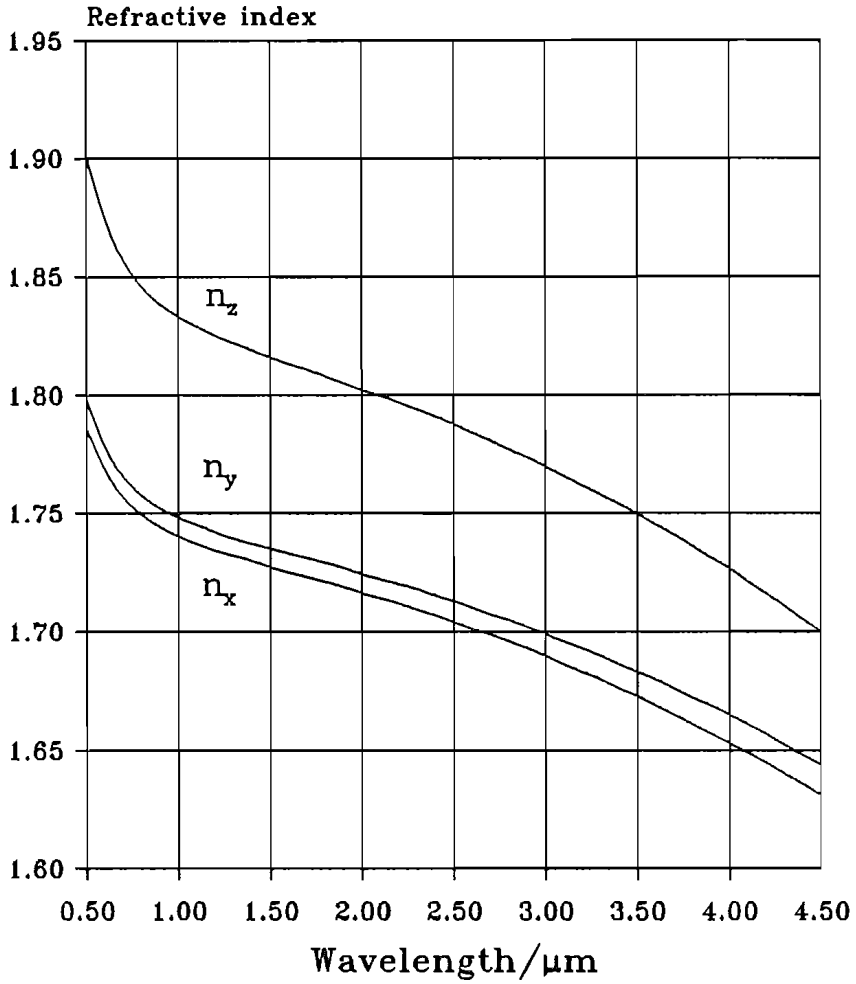

Fig. 3.6 Principle refractive indices of KTP as a function of wavelength: generated using the Sellmeier's equations after Fan *et al* [23].

3.6.3 Thermal behaviour.

The birefringence of KTP is very insensitive to temperature. Consequently, loss of uniform phase-matching due to local heating of the crystal is only a problem when the material is used in high average powers applications. The disadvantage of the small thermal dependence of the birefringence is that temperature tuning can not be exploited to provide non-critical phase-matching.

The temperature variation of the indices was briefly addressed by Zumsteg *et al* [3]. More recently Gettemy *et al* have measured the temperature dependence of the three principle indices at four wavelengths between 0.532–1.320μm [22]. The results are not of high enough precision to be used for the accurate prediction of the tuning behaviour, but can be used to estimate the rate at which tuning should occur with temperature. For the case of the temperature tuning of a crystal cut for type II doubling of 1.064μm, this rate is only $\sim$0.1nm/°C, which is not high enough to achieve any practical tuning range.

3.6.4 Angular behaviour.

As KTP is a biaxial crystal, phase-matching is dependent on both θ and ϕ. The birefringence between the x and y axes is, however, small compared to that between the x and z axes ($\approx 0.5\%$, c.f. $\approx 5\%$). Consequently, phase-matching is much more strongly dependent on θ than on ϕ. It also means that as long as the beam propagates orthogonally, or nearly so, to the z-axis that the Poynting vector walk-off will be small (< 6mrad, at 0.532μm) and the angular acceptance will be high (≈ 18mrad·cm in the critical direction (as ϕ varies), and ≈ 59mrad·cm in the noncritical direction (as θ varies). It does, however severely limit the wavelength range over which phase-matching is possible. (Second harmonic generation is only phase-matchable for fundamental wavelengths in the range 0.9–1.1μm, and an OPO pumped at 0.532μm can tune, at most, from 0.95–1.21μm. See Fig. 3.7 and Fig 3.8).

If a higher walk-off can be tolerated, angle tuning about either the x or y axis will give a much wider tuning range (see Fig. 3.9 and Fig. 3.10). In these cases the tuning range is in principle only limited by the long wave-length cut-off of the transparency of the KTP itself (i.e. $\approx 4.5\mu$m). However, as the goal of this work was to achieve continuous operation of an OPO, the wide tuning range was sacrificed to minimise problems with angular acceptance and walk-off.

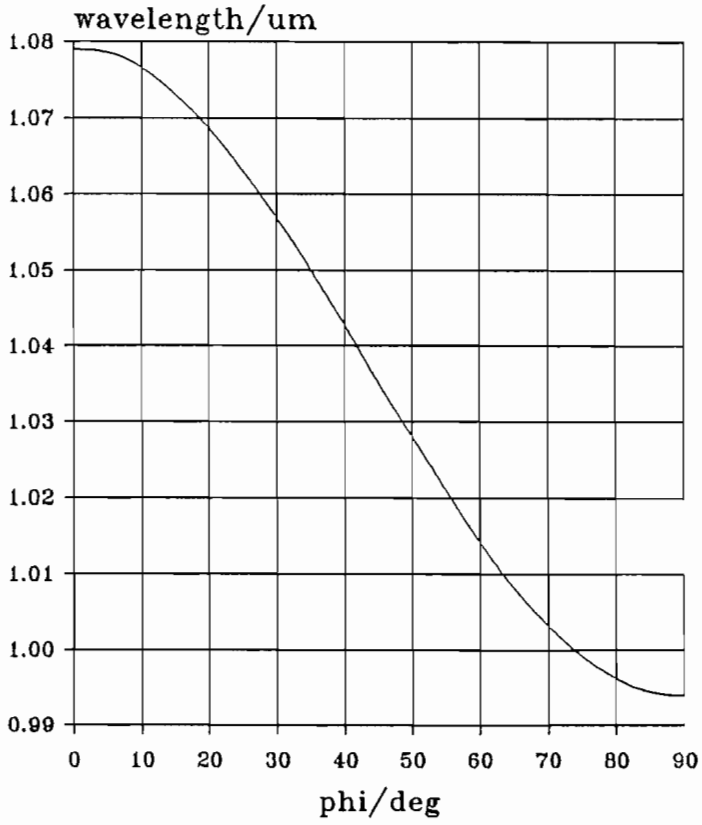

Fig. 3.7 Phase-matching curve for type II doubling in KTP. Propagation in the xy plane. Calculated using Sellmeier equations after Fan *et al.* [23]

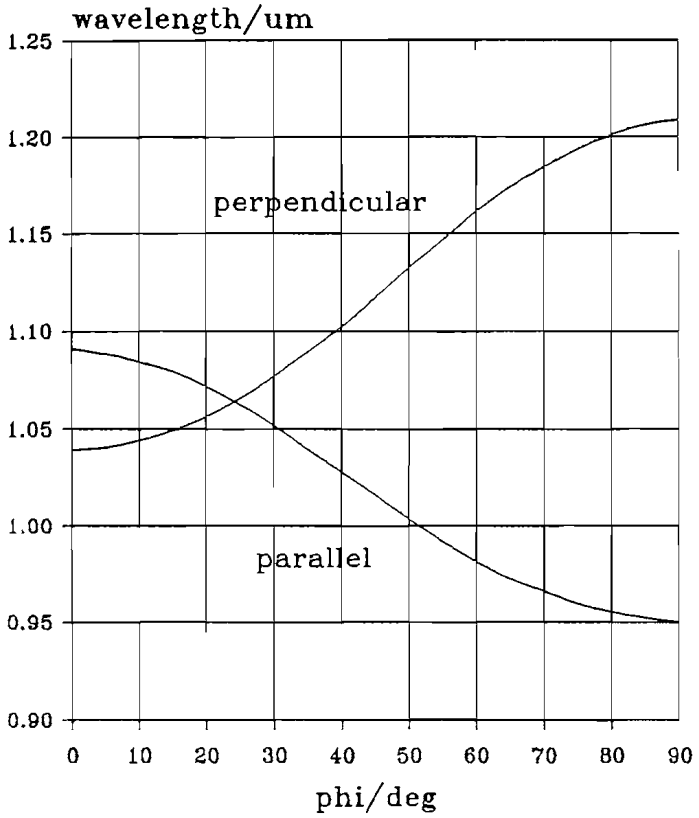

Fig. 3.8 Phase-matching curve for a 0.532μm pumped KTP OPO. Propagation in xy-plane. Indices calculated using Sellmeier's equations after Fan *et al* [19].

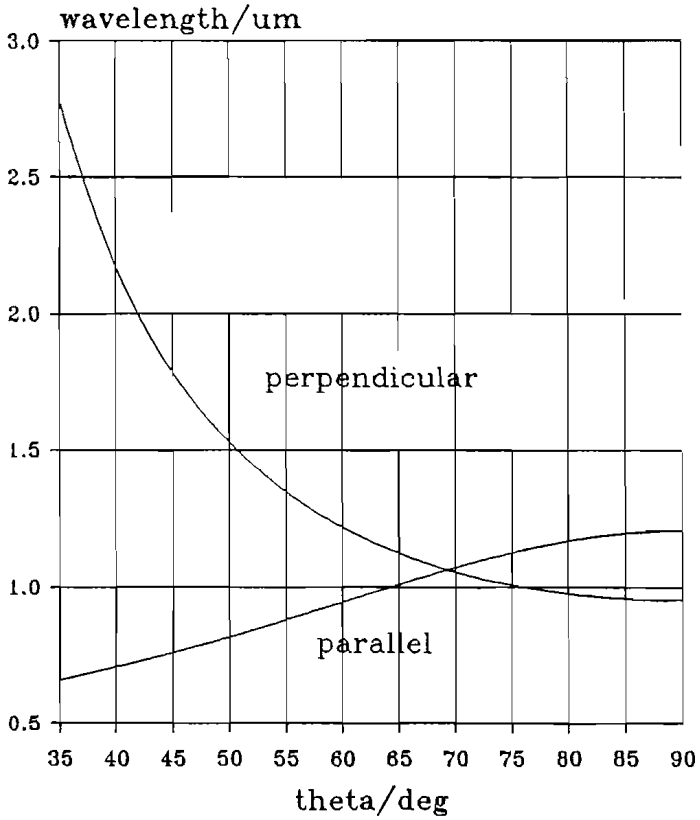

Fig. 3.9 Generated wavelengths as a function of the angle of propagation in the zy-plane (internal angle), for an OPO pumped at 0.532μm, using Sellmeier's equations after Fan *et al* [19].

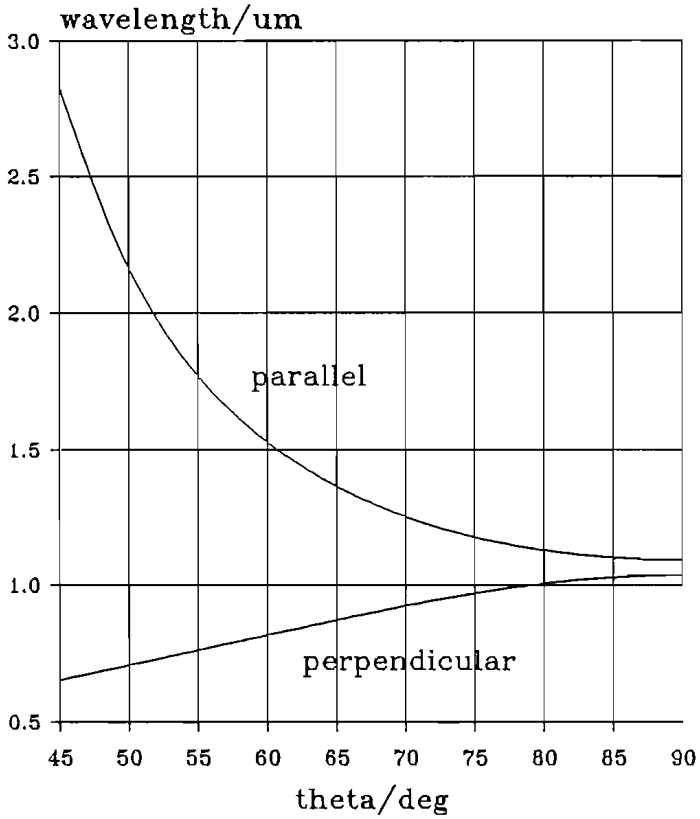

Fig. 3.10 Generated wavelengths as a function of angle of propagation in the zx-plane, for a 0.532μm pumped OPO, using Sellmeier's equations after Fan *et al* [19].

3.6.5 Nonlinearity.

Until recently, the values of the usable nonlinear coefficients have been taken to be $d_{24}=7.6\text{pmV}^{-1}$ and $d_{15}=6.1\text{pmV}^{-1}$ [3]. Fan *et al* [23] have shown that as the birefringence between the x and y axes is a lot smaller than that between either of these with the z axis, that the effective nonlinearity for KTP, in the type II case, is

$$d_{eff}^{II} \propto (d_{24}-d_{15})\sin 2\phi \sin 2\theta - (d_{15}\sin^2\phi + d_{24}\cos^2\phi)\sin\theta \qquad (3.8)$$

(the coefficient in the type I case is significantly smaller, i.e. $<1\text{pmV}^{-1}$) This predicts that the effective coefficient for the type II doubling of the fundamental wavelength of 1.064μm when phase-matched normal to the z-axis, to be 7.2pmV^{-1}. This value has been found, however, to give theoretical efficiencies that are markedly higher than those found in practice.

Recent re-measurement [24] of the small signal doubling efficiency for, this same interaction, has suggested that the effective nonlinearity should be only $3.2pmV^{-1}$; less than half the previously given value. The new value of the nonlinearity gives a 'figure of merit' d^2/n^3 of 1.8, compared with the value of 3.9 given using the old value. When compared with the value of 2.0 for Lithium Niobate, it can be seen that KTP is in fact slightly worse, and not twice as good as previously thought. KTP does, however, have the advantage in that nearly non-critical phase-matching is possible at room temperature.

3.6.6 Optical damage.

The damage information on KTP is currently rather limited. The single-shot damage threshold of KTP at $1.064\mu m$ has been experimentally determined to be as high as $15GWcm^{-2}$, for a 1ns pulse [23]. Unfortunately, this is not necessarily applicable in either the case of trains of Q-switched, or mode-locked pulses. There are, however, there are reports of intensities at which KTP has been safe operated, which are of some bearing. Perkins and Fahlen [25] report generation of 20W average power utilising intracavity doubling with a c.w. pumped, Q-switched Nd:YAG laser. Unfortunately, as they do not provide information on the focusing used, it is not possible to obtain a 'safe-to-use' intensity from this value of power.

Edelstein [26] reports that intensities of $\approx 10GWcm^{-2}$ can be safely, and routinely, used with KTP in a continuous train of ultra-short (here $\approx 200fs$) mode-locked pulses. In this case, the KTP was intracavity pumped—to obtain optical parametric oscillation—by a colliding pulse dye laser. The mode-locked pulse repetition rate being $\approx 100MHz$, the average intensity at the crystal was therefore $\sim 200kWcm^{-2}$. Care must be taken with this result, as the KTP crystal used was hydrothermally grown. It has been reported that these exhibit a single-pulse damage threshold of $\approx 30GWcm^{-2}$ at $1.064\mu m$, a factor of two higher than the value given above for flux grown material. While both these results are of use, before KTP can be effectively exploited in the case of trains of ultrashort pulses, a definitive measurement of the damage threshold for this situation is required.

References.

[1]. R.L. Byer.
Chap. 8, *Quantum Electronics: a treatise Vol 1* (Academic Press 1975).

[2]. C. Chen, B. Wu, A. Jiang, and G. You.
Sci. Sinica (Ser. B) **22**, 1013 (1986).

[3]. F.C. Zumsteg, J.D. Bierlein, and T.E. Gier.
J.Appl.Phys. **47**, 4980 (1976).

[4]. Y.R. Shen
The Principles of Nonlinear Optics (Wiley 1984)

[5]. J.A. Armstrong, N. Bloembergen, J. Ducuing, and P. Pershan.
Phys. Rev. Lett. **127**, 1918 (1962).

[6]. J.A. Giordmaine.
Phys. Rev. Lett. **8**, 19 (1962).

[7]. G.D. Boyd and D.A. Kleinman.
J. Appl. Phys. **39**, 3597 (1968).

[8]. S.A. Akhmanov, A.S. Chirkin, K.N. Drabovich, A.I. Kovrigin, R.V. Khokhlov, and A.P. Sukhorukov.
IEEE J. Quantum Electron. **QE-4**, 598 (1969).

[9]. R.S. Craxton, S.D. Jacob, J.E. Rizzo, and R. Boni.
IEEE J. Quantum Electron. **QE-17**, 1782 (1981).

[10]. G.D. Boyd, R.C. Miller, K. Nassau, W.L. Bond, and A. Savage.
Appl. Phys. Lett. **5**, 234 (1964).

[11]. R.L. Byer and S.E. Harris.
Phys. Rev. **168**, 1064 (1968).

[12]. B.F. Levine and C.G. Bethea.
Appl. Phys. Lett. **20**, 272 (1972).

[13]. C. Cassidy, J.M. Halbout, W. Donaldson, and C.L. Tang.
Opt. Commun. **29**, 243 (1979).

[14]. P. Günter.
Proc. SPIE **236**, 8 (1981).

[15]. E.P. Harris and M.L. Dakss.
IBM J. Res. Develop. **13**, 722 (1969).

[16]. J.A. Giordmaine and R.C. Miller.
Phys. Rev. Lett. **14**, 973 (1965).

[17]. G. Nath, H. Mehmanesch, and M. Gsänger.
Appl. Phys. Lett. **17**, 286 (1975).

[18]. P.G. Kryukov, Yu.A. Matveets, D.N. Nikogosyan, A.V. Sharkov, E.M. Gordeev, and S.D. Fanchenko.
Sov. J. Quantum Electron. **4**, 979 (1975).

[19]. A.P. Izrailenko, A.I. Kovrigin, and P.V. Nikles.
JETP Lett. **12**, 331 (1970).

[20]. D. Eimerl, L. Davis, S. Velsko, E.K. Graham, and A. Zalkin.
J. Appl. Phys. **62**, 1968 (1987).

[21]. K. Kato.
IEEE J. Quantum Electron. **22**, 1013 (1986).

[22]. D.J. Gettemy, W.C. Harker, G. Lindholm, and N.P. Barnes.
IEEE J. Quantum Electron. **24**, 2231 (1988).

[23]. T.Y. Fan, C.E. Huang, B.Q. Hu, R.C. Eckardt, Y.X. Fan, R.L.Byer, and R.S. Feigelson.
Appl. Opt. **26**, 2390 (1987).

[24]. R.C. Eckardt, H. Masuda, Y.X. Fan, and R.L. Byer.
IEEE J. Quantum Electron. **26**, 922 (1990).

[25]. P. Perkins and T.S. Fahlen.
J. Opt. Soc. Am. B **4**, 1066 (1987).

[26]. D.C. Edelstein.
Ph.D. Thesis, Cornell University (1990).

4 Design considerations.

This chapter discusses the problems that must be considered when designing a synchronously pumped parametric oscillator. It starts by briefly mentioning how the design is constrained by the available nonlinear crystal and pump source, including the choice of pump wavelength. The greater part of this chapter is, however, concerned with the design of the resonator for the parametric oscillator.

As was mentioned in the introduction, the aim of this project was to assess the feasibility of continuous operation of a synchronously pumped parametric oscillator [1] utilising a solid-state laser pump source [2]. It was decided that the parametric oscillator would have to be singly-resonant, even though it would require around two orders of magnitude more pump power to reach threshold than the-alternative-doubly-resonant case [3]. This was because of the fact that, in the doubly resonant case, even a slight pump frequency instability results in a large fluctuations of the OPO output [4]. As poor output stability would severely compromise the utility of the OPO as a source of radiation (e.g. for the purposes of spectroscopic investigations), the choice was made to utilise a single resonant scheme at the expense of the significantly higher pump power requirement [3].

The design of a parametric oscillator is dependent on the choice of pump source and nonlinear material. It had already been decided that the power available from a c.w. flashlamp pumped mode-locked Nd:YAG laser would not be sufficient to achieve singly resonant operation of a parametric oscillator, and that it would therefore be necessary to relax one of the design requirements: i.e. to investigate either continuous operation of a doubly-resonant OPO, or pulsed operation of a singly resonant device. The latter choice was made, as a Q-switched, mode-locked Nd:YAG laser was available for use as the pump source. With amplification, this laser was able to supply peak intensities-whilst using a relatively large pump spotsize ($\approx$0.5-1.0mm)—in excess of the damage threshold of most nonlinear materials. This allowed problems such as angular acceptance and Poynting vector walk-off to be ignored, thereby widening the choice of usable nonlinear materials. Furthermore, as the laser could be operated without Q-switching, it could also be used to provide a long train of mode-locked pulses. This would allow for the possibility of investigating quasi-continuous operation of the OPO, as an intermediate step between Q-switched and continuous operation.

4.1 The gain medium.

As mentioned in Section 5, Chapter 3, at the time that this project commenced, the most promising of the materials, that were readily available for use as the gain medium in a parametric oscillator, was barium borate [5][6]. It offered both a high nonlinearity and damage resistance. Though it also possessed a high Poynting vector walk-off, this was unimportant for the reason given in the previous section; namely, that there was sufficient power available to provide a high intensity using a spotsize of up to $\approx$0.5-1mm. In the later stages of the work, a crystal of the material potassium titanyl phosphate [7] was acquired to replace the barium borate. Though the 'merit' of this material in the high power case (as characterized by FoM_I, as defined in Section 4, Chapter 3) was significantly lower than that of barium borate, it did offer a much higher 'merit' in the situation where power was limited (as characterized by FoM_P). This makes KTP the more suitable choice of gain medium in the long term, as it offers a higher possibility of continuous operation being achievable with the existing pump sources.

4.2 The pump wavelength.

It was decided to use a pump wavelength of 0.532μm. This would, firstly, allow a wider tuning range to be accessed, as compared to that available through the direct use of the 1.064μm output of the Nd:YAG laser. Secondly, as 0.532μm is a visible wavelength, it could be readily utilised for the purpose of aligning the OPO resonator (assuming, of course, the use of a collinear pump geometry).

A shorter wavelength–that was still within the transparency region of the nonlinear medium–would have offered an even wider tuning range. The two such wavelengths that are available from Nd:YAG through the use of frequency conversion (namely, 0.355μm and 0.266μm), while they do fall outside the transmission range of KTP, could have been used in the case of BBO to provide tunability throughout both the near infrared and visible regions of the spectrum (as has already been shown for the case of an OPO pumped by a Q-switched laser source [8]). The region of interest to this project was, however, the near infrared. Furthermore, the 0.532μm could be provided from the 1.064μm using only one stage of frequency conversion: this meant that the power available at 0.532μm could be an appreciable fraction ($\approx$40-50%) of that at 1.064μm.

4.3 Resonator design.

The resonator design for a synchronously-pumped parametric oscillator must satisfy three main criteria. It must firstly have an optical length that is closely matched to that of the pump source laser. Secondly, it must have a low loss. Thirdly, it must provide a stable focus in the crystal; how tight a focus being determined by the available pump power and the nonlinear crystal (i.e. angular acceptance, damage, etc.). In this context, 'stable' refers to being insensitive to variations in the length of the resonator. In the case of high power operation, the damage threshold of the nonlinear crystal and cavity optics must also be taken into consideration. It is also not necessary to utilise a *low* loss resonator, as long as it has a *low enough* loss.

It must be noted here that the case of high *average* power is not addressed. In this situation, localized heating of the nonlinear medium would result in thermal lensing, thereby modifying the behaviour of the passive cavity. This case was ignored during this project, as firstly, a low repetition-rate pump system was used, and secondly, because neither BBO [5] nor KTP [7] are particularly susceptible to thermally induced refractive index changes.

4.3.1 Pump synchronism.

Due to the instantaneous nature of the second-order nonlinear coupling, synchronous pumping is the only efficient way to mode-lock an optical parametric oscillator [9]. A requirement for its effective utilisation is that the optical length of the OPO resonator (at the signal wavelength) must be accurately matched to that of the source laser (at the wavelength at which it operates). This ensures that every incident pump pulse will overlap with the circulating signal pulse in the nonlinear gain medium, and that as a result of this, that the circulating pulse will see a net gain on each round trip of the cavity. If the optical lengths are not accurately matched, then the overlap will lessen on each round trip, limiting the number over which appreciable gain is available. By convention, a parametric oscillator pumped by a pulsed laser source is only taken to reach threshold when the resonated signal has been amplified up by $\approx \exp(30)$ times from the parametric noise level [3]. If the number of round trips over which gain is seen is below that required for this degree of gain to be accrued, then the OPO will not reach threshold.

In practice, *perfect* synchronism is not achievable. What is required, however, is that the optical lengths are matched so that the length of the OPO cavity is within $|\Delta L| < c\tau/m$

(where L is the cavity length, m is the number of round trips needed to attain oscillation threshold, τ is the pump pulse duration, and c is the speed of light in vacuo). In practice, however, optimally efficient operation requires the cavity lengths to match within $\approx 5\%$ of ΔL, as given above.

In practice, as alignment accuracy is limited, the length of the resonator must be adjustable by some means. As mentioned above, the accuracy to which it need be adjusted is determined by the duration of the incident pump pulses, and by how far above threshold the OPO is being pumped (which determines how many round trips of the cavity are required before the signal reaches the $\approx \exp(30)$ threshold level). If only 'coarse' adjustment is required (i.e. $\Delta L > 0.01\text{mm}$), then the mounting of one of the OPO mirrors on a micrometer driven translation stage will suffice. If more sensitive adjustment is required, then a piezo adjustment must *also* be provided. Even if it *was* possible to set up the OPO with its resonator length matched accurately to that of the pump laser, adjustment of the cavity length must still be allowed for, as the variation resulting from tuning (by whatever means) can be large enough to terminate oscillation.

4.3.2 On cavity loss.

The loss of the cavity is one of the factors that determines the intensity necessary to achieve parametric threshold. The other factors being properties of the nonlinear gain medium, i.e. refractive index, effective nonlinearity, and *usable* length (i.e. as limited by angular, spectral, and temporal considerations).

In the case of a high power-pulsed-pump, where the available gain is also high, the relatively high loss can be tolerated, provided that over the number of round trips within the pump pulse, the net gain is sufficient for the OPO to reach threshold (i.e. for the signal to be amplified up, from noise, by $\approx \exp(30)$ times). For efficient exploitation of the output, however, the residual loss (i.e. not due to output coupling) must be significantly smaller than the output coupling. In the case of a low gain system it *is* of paramount importance to minimise the loss; a round trip loss of $< 1\%$ being desirable in practice. If a low round-trip loss is required, then a ring-cavity design should be considered. The main advantage of this design is that there is only one transit of the nonlinear medium per cavity round trip. This can amount to a significant reduction in the round-trip loss, especially if the crystal makes a particularly large contribution.

In the case of the parametric devices investigated so far (see Chapters 6 and 7), as there has been no shortage of pump power, the cavity loss has not been a major concern. In the case of continuous operation, however, it will be of utmost importance to reduce the loss as far as possible, and what is more, for wide tunability, it is necessary for the various coatings to perform well over a wide range of wavelengths. Dielectric mirrors utilising a multi-layer stack design can in practice provide reasonably high reflectivity ($>99.5\%$) over a reasonably wide range (several hundred nanometres).

4.3.3 Pump geometry.

By 'pump geometry' it is meant the angle between the pump and cavity axes. There are only two possible cases, those of collinear and non-collinear pumping. A collinear pump geometry has two advantages over the non-collinear alternative. Firstly, it maximises the overlap between the pump and resonated mode, and secondly, it allows the pump to be used to define the cavity axis for alignment purposes (of particular use in the case of a visible pump). The disadvantage of collinear pumping is that feedback from the OPO can be a problem in the case of a linear cavity (as opposed to the ring cavity).

A non-collinear pump geometry does lead to an unavoidable reduction in pump-signal overlap. This can, however, be minimised through the use of as small an angle as is possible between the pump and cavity axis. An advantage of the noncollinear geometry is that it offers the possibility of a loss-less pump launch. It also gives signal/idler discrimination [10], as only the signal–propagating in the direction of the cavity axis–is resonant. The idler–generally propagating off-axis–is nonresonant. It will be noted that the possibility of double resonance has been ignored in the discussion so far. Not only is this possible in principle, in fact the noncollinear geometry allows the use of independently adjustable cavities for the signal and idler. This should allow the problem of clustering to be eliminated, but in practice the tolerance to which the lengths must be matched is likely to be too demanding.

In the investigations described in this thesis, it was planned to use collinear pumping. This was found to lead to the laser exhibiting sporadic relaxation oscillations due to feedback from the OPO input mirror. Consequently, at the expense of alignment ease, a slight degree of non-collinearity was introduced. This ensured that feedback was eliminated, without resulting in significant loss of pump-signal overlap, but did require 'through-the-mirror pumping'.

4.3.4 To decouple length and spotsize.

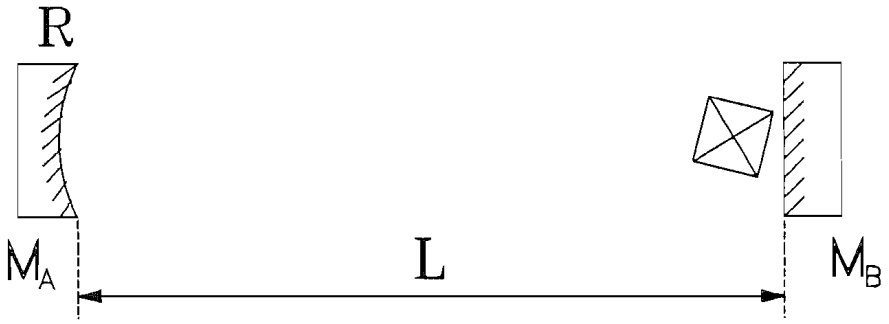

Fig. 4.1 A schematic diagram of the plane-curved resonator.

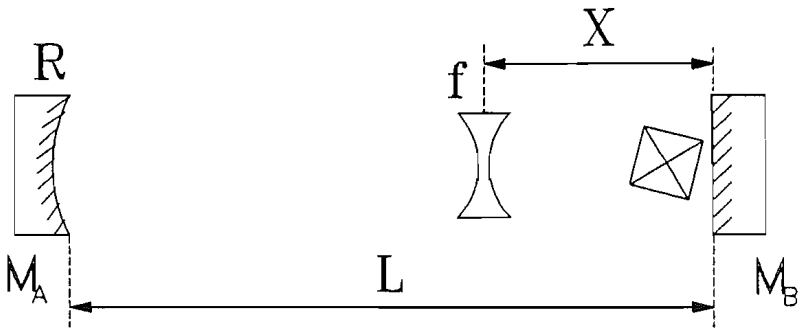

Fig. 4.2 Plane-curved cavity incorporating lens.

From the point of view of loss, stability and ease of alignment, the ideal cavity design involves the minimum possible number of components. The two designs that fit this requirement are the concave-concave and plane-concave resonator designs. The problem with both of these is the inter-dependence between the spotsize at the focus and the cavity length. As an example, consider the plane-curved resonator (see Fig. 4.1). The waist at mirror 'B' is given by,

$$w_B = \sqrt{\frac{\lambda}{\pi}}\sqrt{L(R-L)} \tag{4.1}$$

where the length 'L' and curvature 'R' are as labelled in Fig. 4.1. When a large waist size is required, the problem is not that the spotsize is too sensitive to length, but that a non-standard mirror radius of curvature might be required. e.g. for a spotsize of w_A=0.25mm with a resonator length of L=1.1m, and λ=1.064μm, a radius of curvature of $\approx$1.13m is required. A way in which the desired spotsize can be obtained from a standard mirror curvature is to use a short focal length mirror in conjunction with a negative lens (see Fig. 4.2). In this case, through a suitable choice of lens and mirror, it is possible to get a range

of possible waist-sizes without altering the length of the laser resonator. This is, of course, not the only cavity design that exhibits this property. A few of the other designs will be mentioned in the next two subsections.

4.3.5 The high power case.

In the case of pulsed, including Q-switched, laser pumped parametric oscillators, tight focusing is generally unnecessary. The high peak powers available can readily produce intensities far in excess of the damage threshold of any available nonlinear material. The damage threshold of some nonlinear materials, however, is significantly higher than that typical for dielectric thin-film coatings. It must therefore be ensured that in providing a high intensity at the crystal, none of the optical components are exposed to intensities in excess of their design limitations. One crystal that has a notably high damage threshold is barium borate [11], which was used during the initial part of the investigation of the synchronously pumped parametric oscillator as described in this thesis (see Chapter 6).

For a Q-switched pulse of a given duration and energy, the lowest possible threshold is achieved with the shortest cavity length, as this maximises the number of transits possible within the pulse envelope. As in this case the peak pump power available is high enough to allow a loose pump focus, it is common practice (in the non-mode-locked case) to use a plane-plane cavity design (e.g. [12][13]) , as the combination of a short resonator and a large spotsize results in a minimal amount of diffraction loss. In the case of a Gaussian pump, such devices have been shown to produce Gaussian signal and idler outputs [14]. This is due to the constraining action of the parametric gain profile, which–being determined by that of the pump–is also Gaussian [15].

In the case of the synchronously pumped parametric oscillator, the length is constrained by synchronism (see Subsection 1). A typical flashlamp pumped, mode-locked Nd:YAG laser, has a cavity length of $\approx$1-1.5m (both pulsed and c.w. flashlamp pumped devices). This is far too long to utilise a plane-plane resonator design, unless a *large* pump spotsize can be used (say, $>$5mm). It is therefore necessary to utilise a cavity design that supports a stable Gaussian mode [16]. As discussed in the previous section, one way of achieving any desired stable spot-size is through the use of a plane-concave cavity incorporating a negative lens. The disadvantage of this cavity design is that one of the mirrors (mirror A in this case) is exposed to the same intensity as the nonlinear crystal. Consequently, if the peak intensity required at the crystal is higher than the damage threshold

of the mirror dielectric coating, a variant of the above cavity design must be used (see Fig. 4.3). This design provides a focus in the centre, and larger spotsizes on the mirror. Note that it is not a particularly low loss design, as neither the nonlinear crystal, nor the two lenses–being exposed to the same intensity as the nonlinear crystal–can be coated.

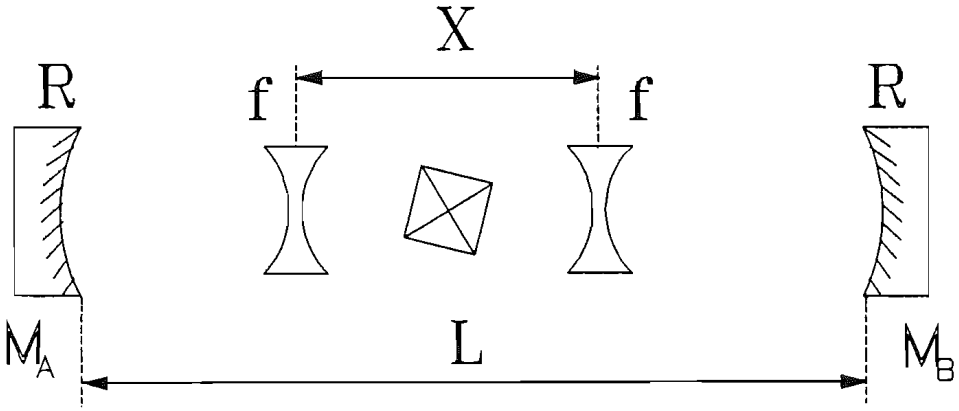

Fig. 4.3 Schematic diagram of a symmetric telescopic resonator.

4.3.6 The low power case.

In the low power case, the problem of damage to the various elements in the OPO cavity is not a cause for concern. What is required, however, is a tight focus that is unaffected by a change in cavity length. The two simplest cavity designs that fulfil this need are the plane-plane resonator incorporating a positive lens (Fig. 4.4), and the equivalent plane-concave design (Fig. 4.5).

This advantage of the plane-plane variant is that with the use of suitable dielectric coatings, the nonlinear crystal may be pumped readily through the plane mirror. The disadvantage of this design is that the waist will be on the mirror and not in the centre of the crystal. In the case of a 'large' spotsize this does not cause any problem, as the change of spotsize across the crystal is minimal (i.e. 'large' means that the confocal parameter of the beam is several times the length of the crystal). If an optimally tight focus [17][18] is required, however, the position of the waist does make a significant difference. It has been shown that when a beam is optimally focused with a waist at one end of the crystal, that the average intensity of the beam, as it propagates through the crystal, is a factor of two down compared to the equivalent case when the waist is centrally placed (note that the optimal focus is not the same in each case). The difference in average intensity leads to a factor of two difference in the oscillation thresholds [12]; the centrally focused case having the lower threshold.

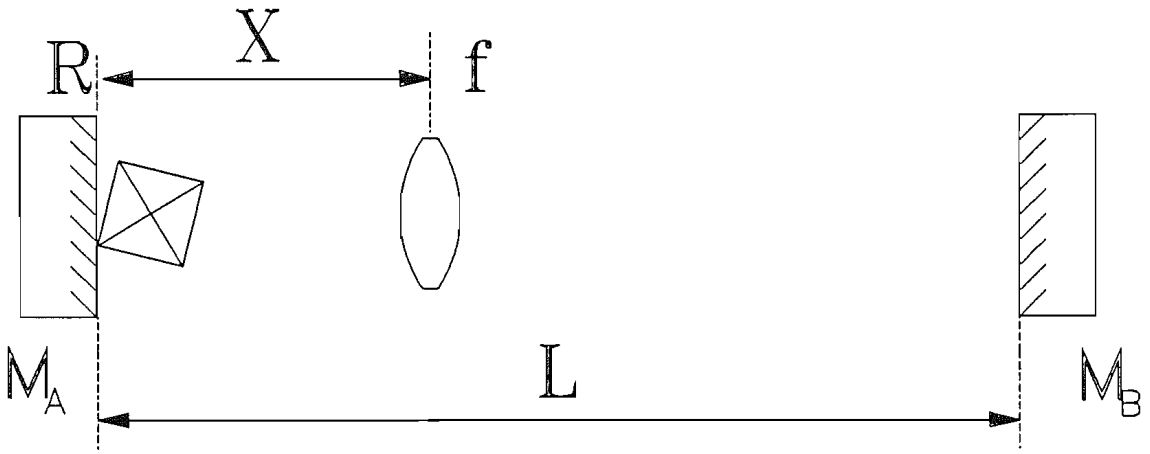

Fig. 4.4 Schematic diagram of a plane-plane resonator incorporating a positive lens.

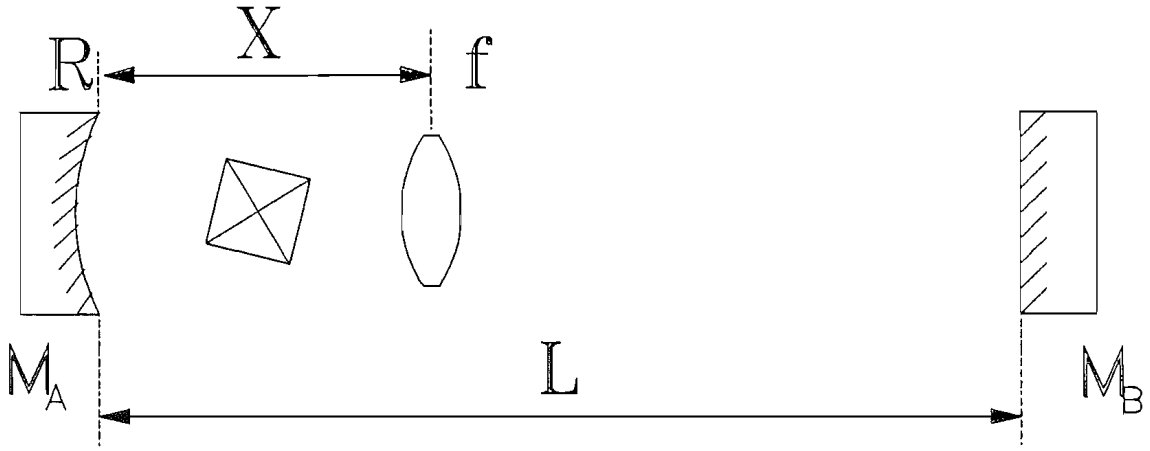

Fig. 4.5 Schematic diagram of a plane-concave resonator design incorporating a positive lens.

The concave-plane variant *does* provide a centrally placed focus. That makes this cavity the preferred choice when using a tight focus (i.e. the confocal parameter of the beam is comparable with the crystal length). The only 'disadvantage' is that to pump through the mirror, its lensing behaviour must be taken into account. This is, however, a minor inconvenience given the halving of the threshold that results from the use of a centrally placed focus (as opposed to a focus at the input face of the crystal).

4.3.7 Mirrors instead of lenses.

In the above discussion, the cavity designs utilised lenses. All may, however, be realised using mirrors instead. The advantage of using a mirror rather than a lens is loss. As the mirrors are used in reflection, whereas the lenses are used in transmission, the loss due to the imperfect behaviour of the coatings is halved. With good coating this reduction in loss

would only amount to $\approx 0.1\%$ per lens replaced, but this would be significant if the available gain was low.

A possible disadvantage of the mirror based designs is astigmatism. A mirror that replaces a lens can not direct the beam back the way it came. If a standard spherical mirror is to be used, any deviation from normal incidence results in astigmatic behaviour [19]. In general this need not be a problem, however, as the angle between the incident and reflected beams can be kept sufficiently small for the resultant astigmatism to be ignored.

References.

[1]. K. Burneika, M. Ignatavichyus, V. Kabelka, A. Piskarskas, and A. Stabinis.
IEEE J. Quantum Electron. **QE-8**, 574 (1972).

[2]. W. Koechner.
Solid State Laser Engineering 2nd Ed. (Springer-Verlag 1988).

[3]. R.L. Byer.
Chap. 9, *Quantum Electronics: a treatise, vol. 1* (Academic Press 1975).

[4]. J.E. Bjorkholm.
IEEE J. Quantum Electron. **QE-5**, 293 (1969).

[5]. C. Chen, B. Wu, A. Jiang, and G. You.
Sci. Sinica (Ser. B) **28**, 235 (1985).

[6]. T.Y. Fan, C.E. Huang, B.Q. Hu, R.C. Eckardt, Y.X. Fan, R.L. Byer, and R.S. Feigelson.
Appl. Opt. **26**, 2390 (1987).

[7]. F.C. Zumsteg, J.D. Bierlein, and T.E. Gier.
J. Appl. Phys. **11**, 4980 (1976).

[8]. W.R. Rosenberg, L.K. Cheng, and C.L. Tang.
Appl. Phys. Lett. **54**, 13 (1989).

[9]. A.E. Seigman and D.J. Kuizenga.
Opto-Electronics **6**, 43 (1974).

[10]. S.A. Akhmanov, A.G. Ershov, V.V. Fadeev, R.V. Khoklov, O.N. Chunaev, and E.M. Shvom.
JETP Lett. **2**, 285 (1965).

[11]. D. Eimerl, L. Davis, S. Velsko, E.K. Graham, and G. You.
J. Appl. Phys. **62**, 1968 (1987).

[12]. Y.X. Fan, R.C. Eckardt, R.L. Byer, C. Chen, and A.D. Jiang.
IEEE J. Quantum Electron. **25**, 1196 (1989).

[13]. M. Ebrahimzadeh and M.H. Dunn.
Opt. Commun. **69**, 161 (1988).

[14]. S.J. Brosnan and R.L. Byer.
IEEE J. Quantum Electron. **QE-15**, 415 (1979).

[15]. L.W. Casperson and S.D. Lunnam.
Appl. Opt. **14**, 1193 (1975).

[16]. H. Kogelnik and T. Li.
Proc. IEEE **54**, 1312 (1966).

[17]. G.D. Boyd and D.A. Kleinman.
J. Appl. Phys. **39**, 3597 (1968).

[18]. E.O. Ammann and P.C. Montgomery.
J. Appl. Phys. **41**, 5270 (1970).

[19]. D.C. Hanna.
IEEE J. Quantum Electron. **10**, 483 (1969).

5 The pump system.

As the efficiency of parametric interactions is strongly dependent on the intensity of the interacting fields [1], it was decided that the preliminary investigation of synchronously pumped parametric oscillator would be made using a mode-locked and Q-switched Nd:YAG laser system as the pump source (see Chapter 4). With amplification, the high peak powers available would preclude the need for tight focusing, ensuring that any reduction in parametric gain due to walk-off and angular acceptance effects [2] would be minimal.

The experience obtained from this investigation would then be applied to the design of a quasi-continuously pumped system. This would initially be pumped with the amplified output of a mode-locked laser—with a long enough pulse envelope that steady state conditions could be reached—as this would give peak powers approaching those available from the Q-switched system. With the extension to tighter focusing, and a reduction of cavity losses, the threshold should then be reduced to a level that amplification was no longer needed. At that point, the peak power necessary for the achievement of threshold should be available from a c.w. flash-lamp pumped continuously mode-locked Nd:YAG laser. Work would then concentrate on minimising the threshold for continuous operation of the OPO, so that ultimately the power requirements could be brought in reach of a diode-pumped system [3].

5.1 The laser.

The pump source used in these investigations was a Lumonics AML 2000 Nd:YAG laser. In its standard configuration it incorporates a Pockels Cell Q-switch and an acousto-optic mode-locker in a plane-concave resonator. The laser can be operated at repetition rates of up to 10Hz, and exploits prelase Q-switching [4] to allow stable mode-locking [5]. The laser resonator had been modified to incorporate a beam expanding telescope [6], to allow it to be operated under low gain conditions to provide long duration Q-switched pulse [7], without a reduction in output energy. This modification also resulted in an improved amplitude stability and spatial beam quality.

5.1.1 Cavity configuration.

The AML 2000 laser has a plane-concave resonator; the curved mirror having a radius of curvature of 5m. The optimal output coupling, under normal operating conditions, is between 50-70%. During the earlier work with Q-switched operation, the plane mirror had

a transmission of 50% and the curved mirror 30%. The latter output was of no particular use in this investigation: the configuration was a legacy of a past project. However, as there was no shortage of power at this stage, it was decided to retain the second output as it could be used to monitor the laser behaviour.

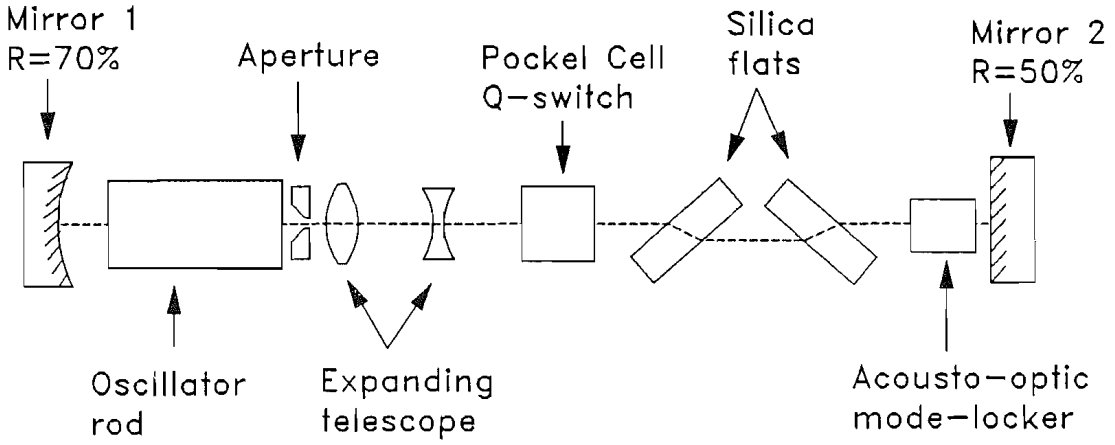

Fig. 5.1 Schematic diagram of the Lumonics AML 2000 laser cavity.

When the laser was reconfigured for long pulsed operation, the mirrors were changed so as to utilise all of the available laser output power. The plane mirror was replaced with a high-reflector and the curved mirror with a 70% transmission output coupler, giving a total output loss of a comparable value to the previous configuration. Finally, the Q-switch was removed from the cavity, and then used as a shutter for the output beam. This necessitated an increase in the physical length of the cavity in order to restore the optical length to the value determined by the fixed frequency mode-locker.

Fig. 5.1 is a schematic diagram of the laser as configured for mode-locked and Q-switched operation. The laser rod is located towards one end of the resonator, with the mode-locker at the opposite end. The Brewster plates are included to provide the fine cavity length adjustment necessary to synchronise the cavity round-trip frequency to that of the mode-locker, which was essential in this case as the mode-locker used was a fixed frequency device (see Subsection 4). The Brewster plates also perform a secondary role in that they present a high loss to electric fields polarized perpendicularly to their plane of tilt. Consequently, the resonated radiation has a well defined linear (in this case, horizontal)

polarization. To their left is the Pockels Cell used to Q-switch the laser, which will be discussed in Subsection 5.

Immediately next to the laser rod is an aperture of such a size that only the TEM_{oo} mode can resonate without incurring loss (i.e. $\phi = 3w$, where w is the 1/e radius of the E-field profile—assumed to be Gaussian—in the plane in which the aperture is located). The laser therefore runs on the lowest order spatial mode unless pumped at a lamp current approaching the maximum available. This was no problem in the Q-switched and mode-locked case, as the lamp current had to be kept low to prevent damage to the elements in the laser cavity. It was found, however, that when the laser was operated as a long pulse device that higher order modes occasionally reached threshold. This 'break through' led to sporadic relaxation oscillations and generally poorer stability.

Then there is the beam expanding telescope: This will be discussed fully in the next section.

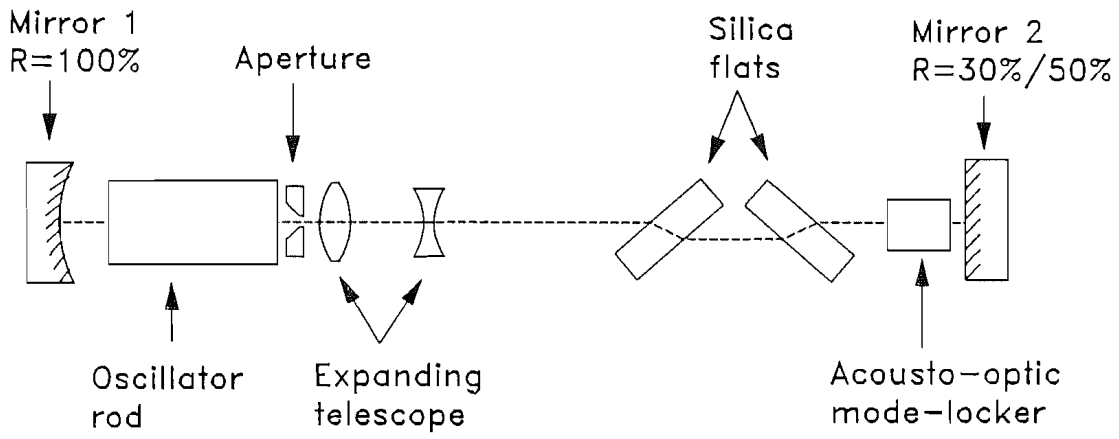

Fig. 5.2 Schematic diagram of the AML 2000 laser cavity configured for long-pulsed operation.

The cavity configuration used during the work on the long-pulse pumped parametric oscillator is shown in Fig. 5.2. As mentioned above, the Q-switch was removed from the cavity and used as an output shutter. The cavity design is otherwise the same, as can be seen from the schematic diagram.

5.1.2 The intracavity telescope.

The telescopic resonator was developed for two main reasons. Firstly, the intracavity telescope expands up the resonated TEM_{00} mode [10] in the laser rod, allowing high power single transverse mode operation. Secondly, the telescope can be adjusted off collimation to compensate for the thermal lensing of the laser rod [8]. A high TEM_{00} power is advantageous for the investigation of nonlinear mixing processes, such as parametric oscillation, as this lowest order mode has the greatest power density for a given power level [9]. The compensation for the thermal lensing also leads to an enhanced output stability [6].

The telescopic resonator achieves high TEM_{00} mode output powers by expanding the resonated mode to fill the entirety of the available gain volume [6], thereby allowing for the optimal extraction of energy. In practice, the extraction can be 'too optimal', as the spotsize at the contracted end of the cavity is no larger than in the case of a 'normal' resonator (e.g. a *stable* plane-concave cavity of the same length). In the case of the telescopic resonator, as power is being extracted from a larger gain volume, it is possible to extract more power than can be safely handled by the output coupler at the contracted end.

The surfeit of available power was of great use in the investigation of the OPO. From a consideration of losses, it can be shown that the overall Q-switched pulse energy needed for an OPO to reach threshold is lower for a shorter duration Q-switched pulse [9]. Damage does, however, limit the safely usable peak power with a given nonlinear medium. In this case it *is* advantageous to lengthen the pump pulse, as it makes available a longer build up time for oscillation. As the Q-switched pulse energy available from the AML laser exceeded the amount necessary to cause damage to the output couplers under normal conditions (i.e. a Q-switched pulse duration of 30–50ns FWHM), it was possible to operate the laser under low gain conditions, thereby broadening the Q-switched pulse duration, while still obtaining a peak powers limited by the damage threshold of the output couplers. In this case, the safely extractable energy in the Q-switched pulse, from both output couplers, was limited to around 3−4mJ—up to 2mJ being available from the 50% output coupler. Though insufficient to achieve parametric oscillation threshold of the devices investigated, it did represent a larger fraction of the required energy than would have been available from a similar laser with a conventional resonator. This reduced the requirement for amplification, thereby minimising the beam distortion that would result from this process.

As mentioned above, the intracavity telescope allows for compensation of the thermal lensing in the rod, thereby resulting in a more stable output. Expanding the TEM_{00} mode to fill the entirety of the gain medium also results in a high quality output mode profile, as little gain is available for the higher order modes to extract. In this case, the telescope was initially aligned adjusted to its collimated length (using a visible auto-collimator). The lens separation was then varied—under normal operating conditions—while both the lamp current for oscillation threshold and the shot-to-shot stability were monitored. The telescope was then adjusted to the separation that corresponded to both minimum threshold (see Fig 5.3) and maximum stability.

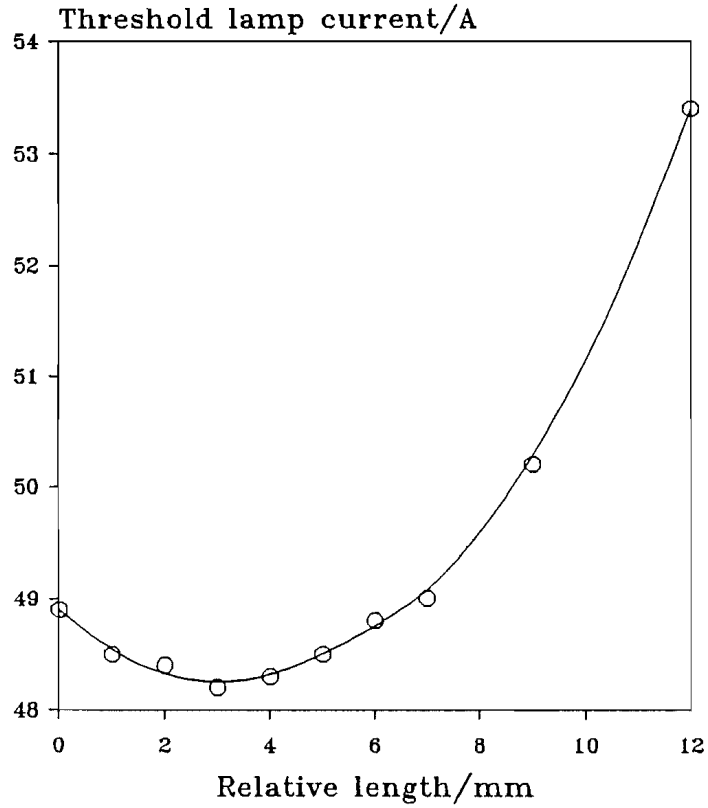

Fig. 5.3 Laser threshold as a function of the variation in the separation of the telescope lenses.

5.1.3 Output divergence.

As mentioned above, to ensure that the laser oscillated on only the lowest order transverse mode, a circular aperture was incorporated into the cavity. It has been shown [6] that its position in the cavity is unimportant, so long as the size is chosen accordingly: i.e. the aperture size 'ϕ'is chosen such that it transmits 99% of the lowest order (TEM_{00}) mode. This is given by $\phi=3w$, where 'w' is the 1/e beam radius. The aperture was placed in the expanded beam end of the cavity. This was, firstly, because the intensity at the perimeter of the aperture was lower, and therefore the likelihood of damage smaller, and secondly, as

the larger dimension allowed for greater ease of fabrication. The aperture size needed in this case was ≈ 3.3mm.

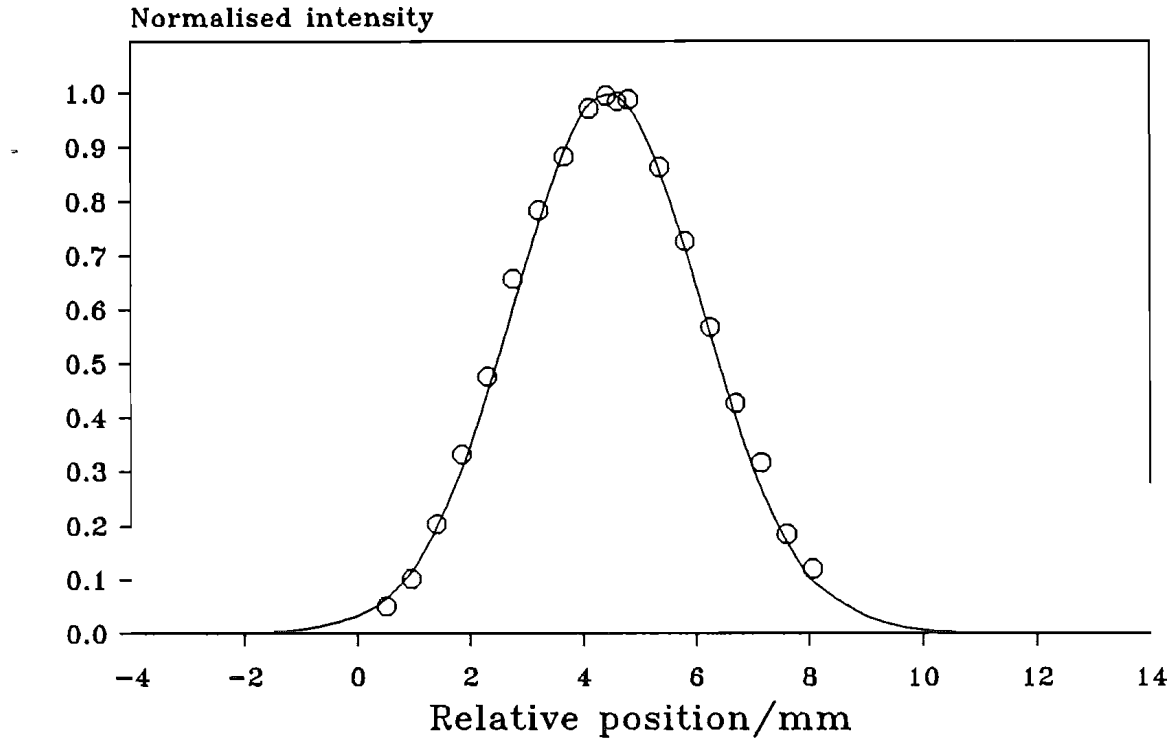

Fig. 5.4 Intensity profile of TEM_{00} output of AML 2000 laser, with Gaussian fit superposed.

To confirm that the laser was actually operating with a TEM_{00} mode, two tests were made. Firstly, the spotsize at the laser output, and at a distance of several metres away from the output (in the 'far field'), were measured with a diode-array. Knowing the far-field spotsize, and the distance at which the measurement was made, it was possible to deduce the divergence. In this case it was found to be ≈ 0.75mrad (half-angle). This agrees to within 5% of the value calculated using the measured output spotsize of 0.45mm [10]. Secondly, the beam profile was characterised using a scanning slit—after it had been expanded by a lens—and found to closely fit a superposed Gaussian (see Fig. 5.4).

5.1.4 Mode-locking.

The AML 2000 laser is actively mode-locked [5] using an acousto-optic amplitude modulator [8] located at the contracted beam end of the resonator. This was driven by a fixed frequency power oscillator, and so had to be tuned onto resonance by adjusting the temperature of the quartz block. The r.f. drive of the mode-locker was at a frequency of 67.1MHz, giving a corresponding mode-locked pulse repetition rate of 134MHz, equivalent

to a round-trip duration of 7.45ns. Acousto-optic mode-lockers amplitude modulate the cavity loss by Bragg diffracting the cavity mode into higher order diffracted beams [8]. A high diffraction efficiency is desirable to ensure reliable, stable mode-locking. The measured values for this device, of typically 45–50%, were sufficient for this purpose.

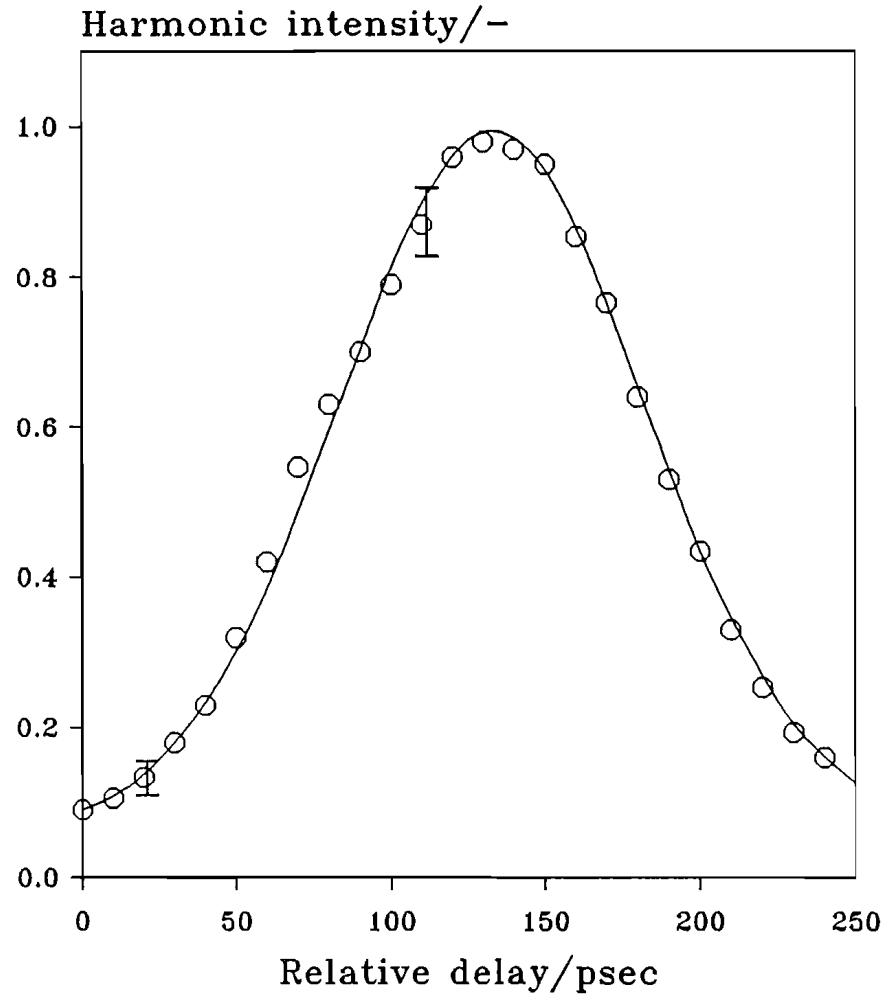

Fig. 5.5 Autocorrelation trace of mode-locked output of AML 2000 Nd:YAG laser.

The duration of the mode-locked pulses was measured by non-collinear background-free [11] second-harmonic autocorrelation [12] using a device built by Pointer and Bromley [13]. Such measurements usually represent an average over many mode-locked pulses. In this case the pulse duration obtained also represents an average over the Q-switch train. While the process of Q-switching does generally lead to broadening of the mode-locked pulses across the train, it was thought that this was unlikely to be significant in the low gain conditions used; especially as the pulse duration was given adequate time to fully stabilized before the Q-switch was opened. To confirm this, the pulse duration was also measured while the laser was running under quasi-continuous conditions. The result obtained in this

case was found to agree—within experimental error—with the result obtained when the laser was Q-switched, suggesting that any broadening that did occur was negligible.

The use of a slow detector ($\sim 1\mu s$ rise-time) meant that the harmonic pulse energy was automatically integrated over the Q-switched train. The autocorrelation was found to best fit a Gaussian envelope corresponding to a pulse duration (FWHM, I(t)) of $\approx$85ps on the various occasions that it was measured during the course of the project (see Fig. 5.5).

5.1.5 Q-switching.

The laser was Q-switched using an Electro-Optic Pockels cell [14] based on a Brewster angled KD*P crystal. The device used was trigger-synchronised to the mode-locker driver to ensure locking of the relative position of the mode-locked pulses with respect to the Q-switch envelope.

As the Q-switch was designed for use in a non-telescopic resonator, where the problem of damage was less acute (see Subsection 2), it had far too high a hold-off to be safely used as originally configured. To reduce the hold-off, modifications were made to the switching electronics, but as this alone did not lead to a sufficient reduction, the Pockels Cell was detuned slightly by tilting off axis. After adjustment, the Q-switch energy from both output couplers was measured using a cone calorimeter, and found to total $\approx$3mJ: safely below the damage limit of $\approx$4mJ. This corresponded to an energy available from the 50% output coupler of $\approx$2mJ.

Under typical operating conditions, the train had a FWHM of I(t) of 150-200ns. As the round-trip duration of the laser was 7.45ns, this meant that there were between 20-27 pulses within the FWHM; the most energetic pulse in the train having a peak power of $\approx$1.1MW. The Q-switch duration was found to be stable on the short term, but due to cavity alignment drift was found to vary over the duration of the project by around 10%. The variation in the output energy was also determined by the computer acquisition over several hundred shots. When fully optimised, the r.m.s. fluctuation in output energy was found to be $\sim$3%.

At the onset of this project the KD*P crystal in the Q-switch was both unheated and open to the atmosphere. This resulted in a gradual degradation of the optical surfaces, eventually necessitating repolishing at the half way stage of this project. Since then, the mounting has been modified to incorporate a heater, so this problem is unlikely to recur.

5.1.6 Feed-back prevention.

To prevent feedback from optical elements further on in the set-up, a second Pockels Cell shutter outside the laser was used to block the laser output during the prelase. It was designed originally to be triggered sequentially with the Q-switch Pockels cell and mode-locker so as to switch out a single pulse from the Q-switch train. For these investigations the whole of the train was required, so the circuitry responsible for the closing of the aperture was disabled. As a result of this the shutter was open long enough for the passage of the Q-switched train. This took advantage of the fact that the voltage supply to the Pockels Cell was pulsed; switching on slightly before, and off slightly after, the laser flashlamp pulse. Hence it was reset in time for the next laser shot.

During the work with the long pulsed oscillator, the Q-switch Pockels cell was used as the output shutter instead. This was because the shutter used in earlier work could only function in two ways. It could switch out just one mode-locked pulse, as it was designed to do, or it could be partially disabled such that it transmitted everything after it was triggered. The Q-switch, on the other hand, was designed to operate in such that way that a train of adjustable duration could be switched out. Unfortunately, as it was intended for use as a Q-switch, it only acted as a quarter-wave plate when switched on. Consequently, when configured to give maximum attenuation during the time it was on, it could only transmit 50% of the incident intensity when switched off.

5.1.7 Long-pulse operation.

During the last stage of this work the laser was operated without the Q-switch installed. The resultant laser output was therefore a 5ms train of mode-locked pulses.

In the long-pulsed case the laser cavity Q was not suppressed at the onset of the flashlamp pulse. This resulted in there being large output intensities during the first $\sim$0.5ms due to relaxation oscillations. Since it was intended to operate at high conversion efficiencies, and hence high intensities, during the steady state part of the pulse train, the significantly higher intensities during the relaxation oscillations posed a risk of damage. The laser output was therefore shuttered to block the first part of the output train.

The laser output was shuttered using a Pockels Cell. This necessitated the use of the laser Q-switch extra-cavity, and resulted in a 50% loss of the available laser output.

However, as this initial stage of the investigation was making use of amplification, this did not cause any problems.

A pulse train of up to $\approx 150\mu s$ was available after amplification (as limited by the amplifier flash-lamp pulse duration). As this was much longer than necessary to establish quasi-continuous operation of the OPO, it was decided to further shorten the train using the Pockels cell shutter. This was done mainly to further reduce the possibility of damage: the damage behaviour of KTP being unknown for the case of a long train of intense mode-locked pulses. The Pockels cell shutter was therefore used to reduce the duration of the pulse train by around an order of magnitude, to $20\mu s$. While somewhat shorter than the maximum available duration, it still corresponded to ~ 2500 pulses; over two orders of magnitude higher than available in the Q-switched case, and was therefore felt to be sufficient

The output extracted from this laser for this stage of the work was only ≈ 0.3mJ, in a pulse of $20\mu s$ duration, corresponding to an average power (averaged over the train) of 15W, and a peak mode-locked power of ≈ 1.25kW.

5.2 Amplification.

Up to two stages of amplification were used (see Fig. 5.6). The first stage involved a double-pass through a 3"x1/4" Nd:YAG rod, the second a single pass through a 3"x3/8" rod. Expanding telescopes were used before each stage of amplification, which not only made for efficient use of the available gain volume, but also enabled compensation of the thermal lensing in the amplifiers.

To achieve a double pass through the first amplifier stage, a quarter-wave plate isolation scheme was used (see Fig. 5.7). Thermally induced birefringence in the amplifier rod resulted in a degree of depolarization of the returning beam, which necessitated tilting the beam slightly off the amplifier axis to prevent any chance of feedback into the laser when the Pockels cell shutter was open. This tilt was not, however, sufficient to cause significant reduction in the available aperture. Fig. 5.8 shows the single- and double-pass output energies for a ≈ 2mJ input Q-switch train energy. The maximum obtainable energy in this case was limited by damage to about 65mJ, which also corresponded to the point at which unwanted effects started to occur (the amplifier gain was found to saturate at a lamp current just above that necessary to achieve this energy. It is now believed to have been due to a fault in the amplifier drivers, as opposed to the occurrence of parasitic laser oscillation, as first suspected). In the long-pulse pump case, the maximum energy extracted was ≈ 39mJ

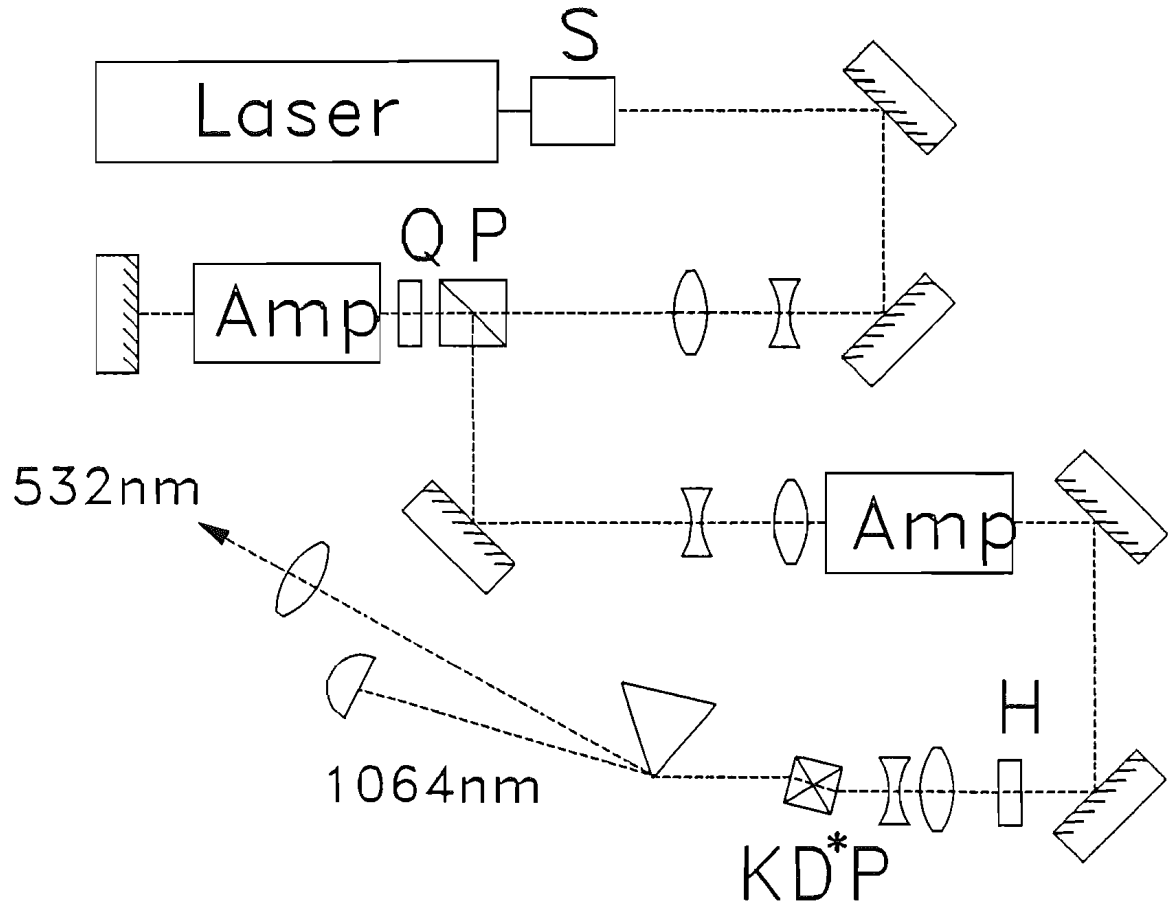

Fig. 5.6 Schematic diagram of pump scheme used during the investigation of the BBO parametric oscillator. H = half-wave plate, P = polarizing beam-splitter, Q = Quarter-wave plate, S = Pockels cell shutter.

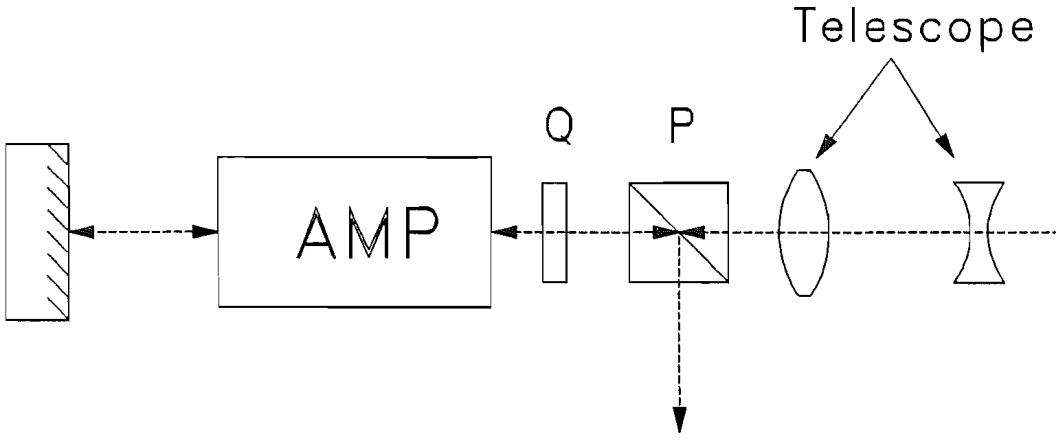

Fig. 5.7 Schematic diagram of the double-pass amplifier arrangement. Q = quarter-wave plate, P = polarizing beam-splitter.

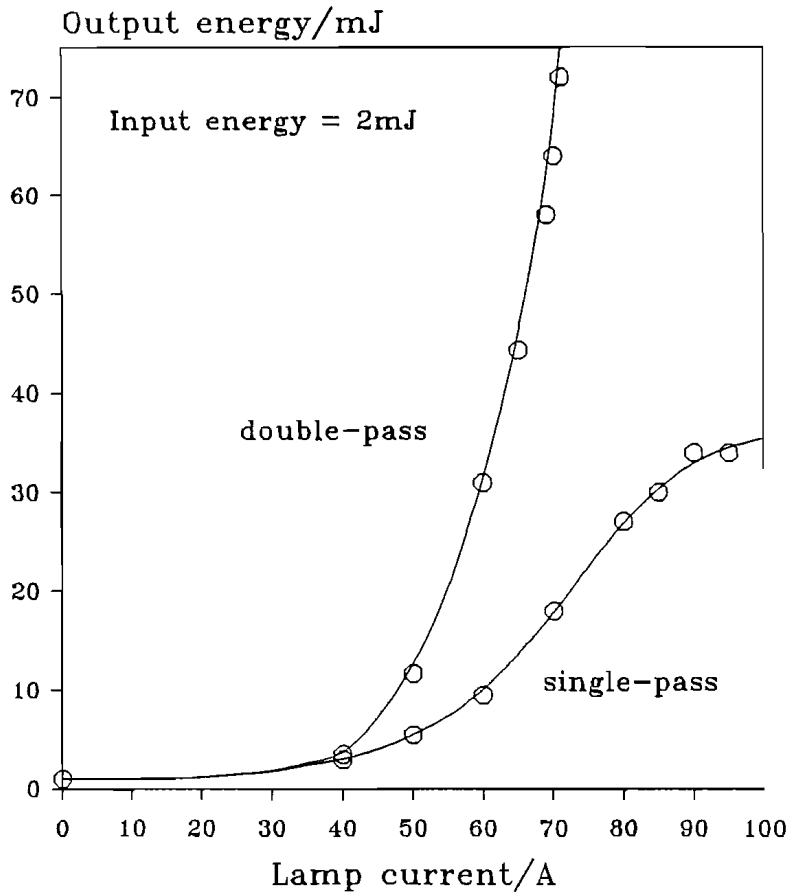

Fig. 5.8 Energy of Q-switch train after double- and single-pass amplification, as a function of lamp drive-current.

in 20μs, corresponding to an equivalent average power of $\approx$2.0kW, and a peak mode locked power of $\approx$165kW.

The second amplifier stage was only ever used with the Q-switched laser, and then only in a single-pass configuration. This is because the three-fold increase in intensity it gave was sufficient to reach the safe operating limit of the rod's anti-reflecting coatings. The energy available from this stage was 180mJ, in a Q-switched train of 160ns. The corresponding peak power of the peak mode-locked pulse was $\sim$100MW.

Between amplifier stages, and between the final stage and the frequency doubling crystal, the beam was propagated freely to allow diffraction to remove some of the higher order structure accrued from the passage through the amplifiers. There were no major features, but the beam quality was noticeably degraded relative to the output of the laser oscillator itself. This would have been caused partially by the thermal lensing and birefringence of the rod, and partially by the amplification process itself. Another cause of distortion may well have been the previously caused damage to the rod's AR coatings.

5.3 Frequency doubling.

In the earlier two stages of this work, when the laser's Q-switch was utilised, the frequency doubling was done using a 3cm long, type II potassium dihydrogen phosphate (KD^*P) crystal [15]. The high Poynting vector walk-off in KD^*P ($\approx$28mrad) limits the smallest usable spotsize—with a 3cm crystal—to $\approx$0.5mm. However, as high peak powers were readily available there were no problems in achieving the large intensity required for efficient frequency conversion.

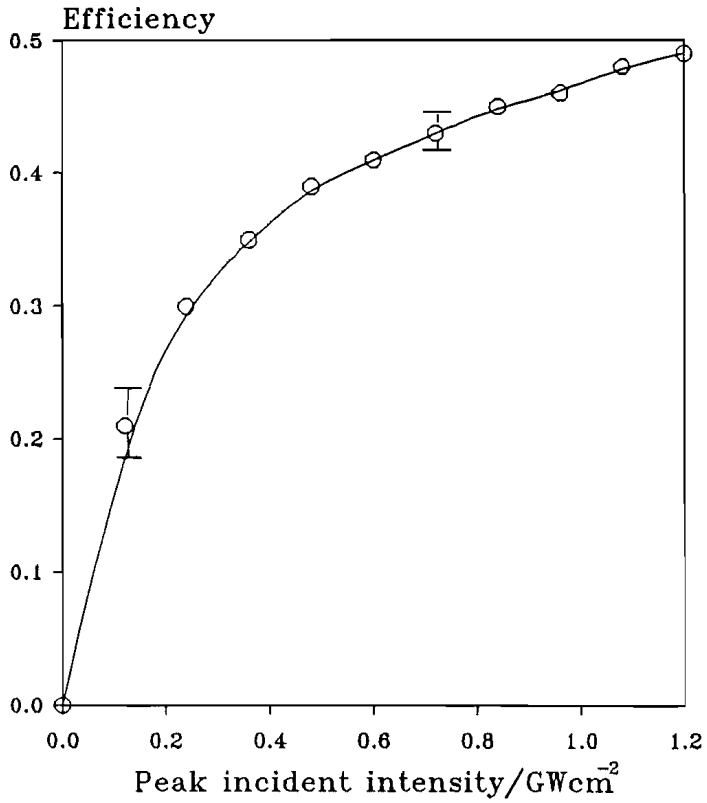

Fig. 5.9 Second harmonic efficiency (overall energy) as a function of incident energy for a train of mode-locked pulses.

The conversion efficiency was found to saturate at between 40–50% (see Fig. 5.9). This maximum value is markedly lower than the theoretically predicted value of 80%, calculated using the analysis after Sawyer [16]. The reason for this discrepancy is unknown, but most likely suggests that there is temporal substructure on the pulse which is leading to greatly reduced phase-matching. It does, however, agree with the results found by others when doubling beams of small cross-section [17]. Good agreement has been found, however, between theory and experiment when the energies used are high enough that sufficient intensity can be achieved with a spotsize of 5mm or larger [18].

In later work the doubling was done using a 5mm long uncoated, type II potassium titanyl phosphate crystal [19]. This material has two big advantages over KD*P. It exhibits a much smaller walk-off, and has a nonlinearity of nearly an order of magnitude higher. The optimal focusing for a 5mm long crystal, after the theory of Boyd and Kleinman [20], corresponds to a fundamental spotsize of $\approx 15\mu$m. With the peak powers available, the use of this focusing would have exceeded the damage threshold of the KTP by several times. In practice, focusing down to a spotsize of $\approx 50\mu$m was found to give a conversion efficiency of $\sim 20\%$, which provided sufficient power at 0.532μm for pumping the OPO whilst ensuring that the intensity that the KTP was exposed to was well below the damage threshold.

In the Q-switched case, the harmonic energy available after using one stage of amplification was 25-30mJ. After two stages, however, this was more than doubled to ≈ 70mJ. In the long pulse case, as said above, no attempt was made to optimise the doubling efficiency. A doubling efficiency of $\sim 20\%$ provided up to 7.5mJ of 0.532μm in 20μs, corresponding to an equivalent average and peak harmonic power of 375W and 30kW respectively. In practice, however, the maximum harmonic train energy used to pump the OPO was only 0.5mJ, corresponding to an average powers of 25W; peak power of ~ 2kW.

5.4 Summary.

By way of a summary, a list of the powers and energies that were available during each stage of the work carried out so far.

Q-switched, mode-locked, two stages of amplification.

After two stage of amplification, 180mJ of 1.064μm was available in a 160ns Q-switched pulse. The corresponding peak power of the peak mode-locked pulse is ~ 100MW. After doubling in KD*P, with a conversion efficiency of 40%, 75mJ of 0.532μm was available, with a peak power of ~ 38MW.

Q-switched, mode-locked, one stage of amplification.

After one stage of amplification, ≈ 65mJ of 1.064μm was available in a 150–200ns Q-switched train of pulses. The corresponding peak power of the peak mode-locked pulse in this case was ~ 33MW. After doubling in KD*P, with a conversion efficiency of 40–45%, ≈ 29mJ of 0.532μm was available, with a corresponding peak power of ~ 15MW.

Long-pulsed, mode-locked, one stage of amplification.

Note. this case, unlike the other two, is not fully optimised. At the very least higher doubling efficiencies could be achieved to increase the available power at 0.532μm.

After one stage of amplification, at least 39mJ of 1.064μm are available in a long-pulse train of 20μs. The corresponding peak power is 160kW, with an equivalent average (i.e. only over the train) of 2kW. Operating at average powers of 125W, doubling at 20% efficiency gave 0.5mJ of 0.532μm. This corresponds to peak and average powers of 2kW and 25W respectively. This last value can, in particular, be increased significantly.

References.

[1]. Y.R. Shen.
The Principles of Nonlinear Optics (Wiley 1984).

[2]. R.L. Byer.
Chap. 8, *Quantum Electronics: a treatise Vol.1* (Academic Press 1975).

[3]. G.T. Maker and A.I. Ferguson.
Appl. Phys. Lett. **54**, 403 (1989).

[4]. A.J. Berry, D.C. Hanna, and C.G. Sawyers.
Opt. Commun. **40**, 54 (1981).

[5]. A.E. Seigman and D.J. Kuizenga.
Opto-Electronics **6**, 43 (1974).

[6]. D.C. Hanna, C.G. Sawyers, and M.A. Yuratich.
Opt. Commun. **37**, 359 (1981).

[7]. A.E. Seigman.
Lasers (University Science Books 1986).

[8]. W. Koechner.
Solid State Laser Engineering 2nd Ed. (Springer-Verlag, 1988).

[9]. R.G. Smith.
Chapter C8, *Laser Handbook* (North Holland 1972, F.T. Arecchi and E.O. Schulz-duBois, Eds.).

[10]. H. Kogelnik and T. Li.
Appl. Opt. **5**, 1550 (1966).

[11]. M. Maier, W. Kaiser, and J.A. Giordmaine.
Phys. Rev. Lett. **17** 1275 (1966).

[12]. D.J. Bradley and G.C.H. New.
Proc. IEEE **62**, 313 (1974).

[13]. L.J. Bromley.
Ph.D. Thesis, University of Southampton (1990).

[14]. I.P. Kaminow and E.H. Turner.
Appl. Opt. **5**, 1612 (1966).

[15]. R.S. Craxton, S.D. Jacobs, J.E. Rizzo, and R. Boni.
IEEE J. Quantum Electron. **17**, 1782 (1981).

[16]. C.G. Sawyers.
Ph.D. Thesis, University of Southampton (1981).

[17]. R.C. Eckardt.
IEEE J. Quantum Electron. **20**, 1178 (1984).

[18]. J. Reinjtes and R.C. Eckardt.
Appl. Phys. Lett. **30**, 91 (1977).

[19]. F.C. Zumsteg, J.D. Bierlein, and T.E. Gier.
J. Appl. Phys. **47**, 4980 (1976).

[20]. G.D. Boyd and D.A. Kleinman.
J. Appl. Phys. **39**, 3597 (1968).

6 Parametric oscillation in BBO★.

This chapter describes the experimental investigation of a synchronously-pumped parametric oscillator which utilised the material barium borate ('BBO')[1] as the gain medium. At the time that this project commenced, BBO was almost unique in offering both a high damage resistance ($\approx 12.5 GWcm^{-2}$, 1ns pulses at $1.064\mu m$ [2]) and a large nonlinearity ($\approx 2pmV^{-1}$ [1][2][3], i.e. a factor of ~ 5 larger than that of KD*P [4]). The only other materials that were then readily available were deuterated potassium dihydrogen phosphate (KD*P)[4], lithium niobate [5], and urea [6]. Of these, only the latter possessed a damage threshold and nonlinearity comparable with those of BBO. Urea does, however, have a much shorter infrared cut-off wavelength than BBO ($\approx 1.4\mu m$ [6], as opposed to $\approx 2.7\mu m$ for BBO [1]), and consequently a relatively small tuning range when pumped at $0.532\mu m$. Furthermore, it is hygroscopic to such a degree that it must by necessity be permanently housed in an index matching cell [7][8], whereas BBO was believed at the time to be immune to attack from atmospheric moisture [1].

Pumping of either BBO or urea at a shorter wavelength would have offered tuning over the entirety of the visible and into the near infrared, as has been demonstrated in the case of pulsed lasers [8][9][10][11]. The additional frequency conversion processes needed to obtain such a pump wavelength from the fundamental of a Nd:YAG laser would, however, have resulted in a substantial reduction in the available pump energy. This was unacceptable at the initial stage of the investigation when, to ensure that oscillation would be readily achieved, it was desired to have at least an order of magnitude more pump power in hand than the theoretically predicted threshold [15].

The highly birefringent nature of BBO [1] results in rapid angular tuning, so even a crystal with a small angular aperture can be used to generate a wide range of wavelengths. Unfortunately, it also leads to a large value of Poynting vector walk-off for wavelengths that are critically phase-matched [2]. In this case the use of a tight pump focus is precluded, and consequently, to achieve the intensities necessary for an OPO to reach threshold, a pulsed laser must be used as the pump source. Type I parametric oscillation in BBO using a

---

★With the exception of the work on bandwidth reduction using the grating resonator (Section 4), the main results of the work described in this chapter was published in the journal *Optics Communication* (Vol. 67, pp316-320, 1988).

0.532μm pump—the interaction investigated in this case—suffers from this limitation over the entirety of its tuning range.

6.1 The pump scheme.

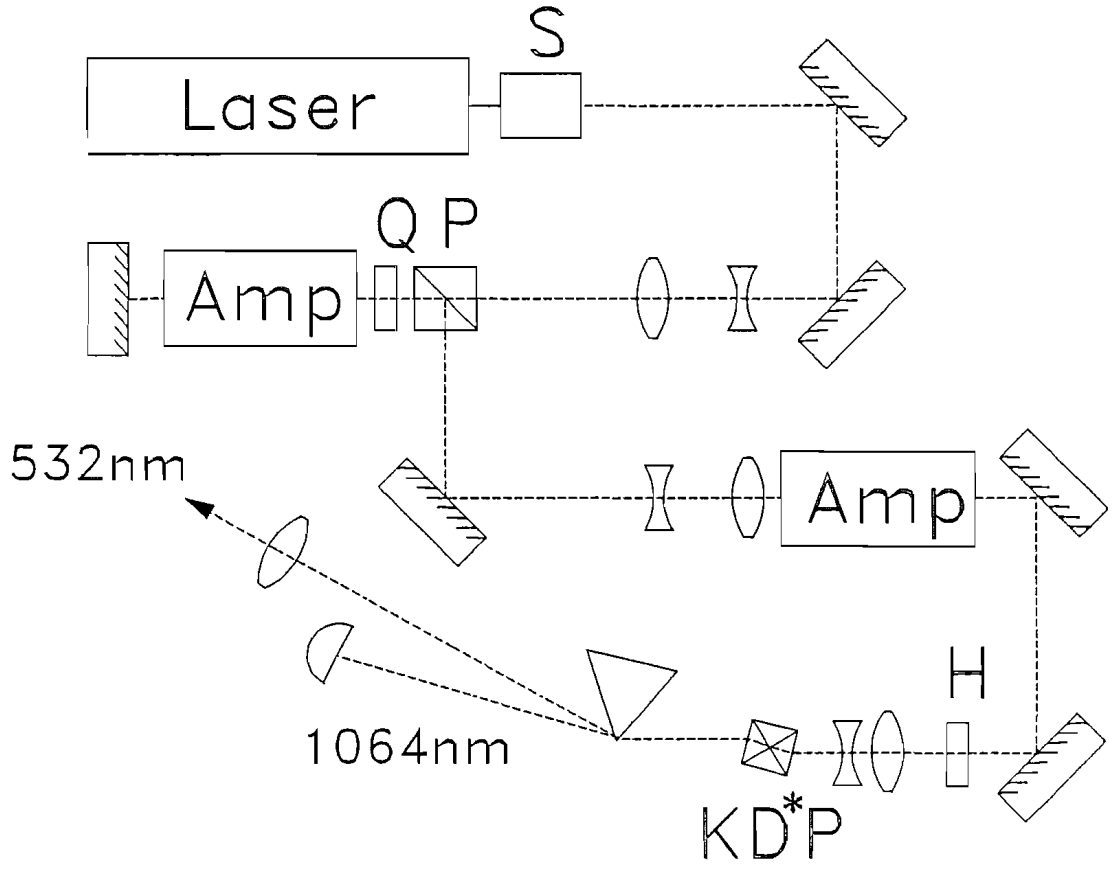

Fig. 6.1 Schematic diagram of pump system used during the investigation of the BBO parametric oscillator. S = Pockels' cell shutter, Q =quarter wave plate, P = polarizing beam splitter, H = half wave plate.

The pump scheme used for this investigation is shown in Fig. 6.1. The flash-lamp pumped Nd:YAG laser [12] was configured for prelase Q-switched [13] and mode-locked operation [14], as described in Chapter 5, Section 1. It was operated at a repetition rate of 5Hz, and produced trains of mode-locked pulses with an overall duration of 160–200ns (FWHM) and a total energy of $\approx$2mJ. The mode-locked pulses were separated by 7.45ns, and had a duration of $\approx$85ps (FWHM), which meant that there were 22-27 pulses within the Q-switch envelope, and that the corresponding peak power (of the most energetic mode-locked pulse) was $\approx$1MW. To further increase the available power, two stages of amplification were employed (see Chapter 5, Section 2). The output of the final amplifier consisted

of Q-switched trains with an overall energy of $\approx$180mJ, corresponding to a peak power of $\approx$100MW.

The resulting fundamental was frequency doubled with an energy conversion efficiency of 40–45%, using an uncoated 3cm long type II KD*P crystal [4], to give up to $\approx$75mJ of 0.532μm (see Chapter 5, Section 3). The generated harmonic was then separated from the fundamental using a dispersing prism which was orientated at minimum deviation. This ensured that, with a suitable choice of polarization for the harmonic, a minimal amount of the generated radiation was lost during this process.

As optics with high-power anti-reflection coatings for 0.532μm were not available, a power loss was incurred in focusing the light into the cavity. There were also losses of power due to the residual reflectivity of the input mirror of the OPO cavity at the pump wavelength, which had been primarily designed to provide a high reflectivity from 0.7–1.0μm, and due to Fresnel reflection from the intracavity optics (see Section 2). As a result, the maximum energy available incident on the entrance face of the BBO crystal was limited to $\approx$40mJ. This was, however, still in excess of the amount of energy required to reach threshold [15].

6.2 The cavity design.

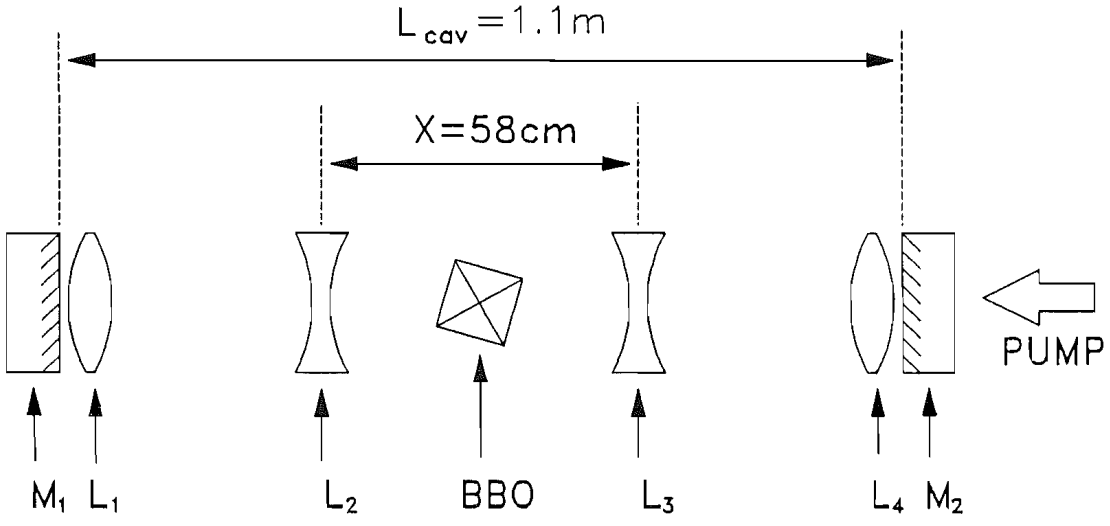

Fig. 6.2 Schematic diagram of cavity used for the preliminary investigation of the BBO parametric oscillator. M_1, M_2 = plane mirrors (HR 0.70–1.0μm, HT 0.532μm), L_1, L_4 = +50cm lenses, L_2, L_3 = −25cm lenses.

The resonator used for the BBO parametric oscillator is shown in Fig. 6.2. At the onset of the project, as the financial resources available for expenditure on optics were limited, and as the optimal cavity design was then unknown, a 'flexible' resonator was desired. Consequently, plane mirrors—with a suitable reflectivity—were acquired, and intracavity lenses used to constrain the cavity mode, as this offered easy reconfiguration of the resonator. It was planned that at a later time, when the optimal focusing and output coupling were known, that appropriate mirrors would be procured.

The mirrors used had a high reflectivity ($R \geq 99.5\%$) over the entirety of the signal region of 0.700–1.0μm, whilst having a reflectivity of only 10–20% over the corresponding idler range of 1.0–2.2μm. This meant that less than $\sim 4\%$ of the idler was fed back after one round trip, ensuring that the oscillator would operate, essentially, as singly resonant. The coatings used were designed for high power operation, but their damage threshold of $\sim 1 GWcm^{-1}$ was over an order of magnitude lower than that of the BBO crystal. Hence, they acted to constrain the design of the OPO resonator.

To maximise the probability of reaching threshold, it had been decided to operate the OPO with the BBO crystal exposed to an intensity approaching, but not exceeding, the published damage threshold ($\approx 13.5 GWcm^{-2}$ for 1ns pulses at 1.064μm [2]). Poynting vector walk-off (of $\approx$55mrad [2]) prevented focusing the pump to below $\approx$0.45mm in the BBO crystal, which corresponds to a confocal parameter of several times the length of the OPO resonator. Consequently, to avoid an excessive intensity at the mirrors, it was necessary to incorporate lenses into the cavity to expand the beam up on the mirrors. The focal lengths of the lenses used were chosen to minimise the change in spotsize as the separation of the innermost pair was varied. The accuracy with which it was necessary to position them was readily achievable during the initial alignment, and so there was no need to provide for the possibility of fine adjustment (e.g. micrometer driven translation stages).

Neither of the lenses nearest the BBO crystal nor the crystal itself could be anti-reflection coated, as the intensity they were exposed to exceeded the damage threshold of available dielectric coatings. Though this did lead to a high cavity loss, preliminary calculations did suggest that there would still be more than sufficient power available to achieve threshold even if *all* the cavity elements were uncoated. It was therefore decided to carry out a preliminary investigation of this cavity design using solely uncoated optics.

The barium borate ('BBO') crystal used was grown at the Fujian Institute of Research on the Structure of Matter, Fuzhou, People's Republic of China. It had a length of ≈ 7.2mm, uncoated faces of $\approx 4.5 \times 4.5 mm^2$, and was cut at an angle of 31° to the optic axis, to phase-match for type I tripling of 1.064μm radiation, i.e. $1.064\mu m + 0.532\mu m \rightarrow 0.355\mu m$. To facilitate angle tuning, the crystal was mounted on a rotation stage which could be set to an angular accuracy of 0.02°; equivalent to setting the angle of propagation inside the crystal to $\approx 0.013°$.

6.3 A note on the hygroscopic nature of BBO.

At the time that this project began, it was generally believed that BBO was totally impervious to attack from atmospheric moisture [1]. Unfortunately, this was found to be untrue. The first BBO crystal used suffered from slight fogging of the surface, which resulted in it incurring a significant amount of surface damage. To remove the damage 'pit-mark', it was found necessary to polish away over 2mm from the length of the crystal: this represented an unacceptably large reduction in the available gain length, and consequently it was necessary to replace the crystal.

To avoid a recurrence of this problem with the replacement crystal it was mounted in a windowless oven, and held at a constant temperature of $50 \pm 1°$. This was found to prevent surface degradation, and no further damage was incurred over the remainder of the duration of the investigation (> 300 hours). The low thermal dependence of the birefringence of BBO [2] did not necessitate the stabilization of the temperature to any greater degree of accuracy than $\pm 1°$.

6.4 Performance details.

This section gives the results of the experimental investigation of the BBO parametric oscillator described in Section 2. The main features of the device's performance were investigated, including pulse duration and spectral behaviour. The experimental results were found to be in reasonable agreement with the theory available.

Oscillation threshold.

The oscillation threshold was found by monitoring both the pump, with a vacuum photodiode (response time ≈ 0.3ns), and the generated idler, with a high gain detector (integrating time $\sim 10\mu$s). The response of the vacuum photodiode was fast enough to allow the undistorted

observation of the Q-switched envelope. It was consequently possible to detect the onset of depletion, which was taken to correspond to the point at which threshold was reached.

The lowest energy at which oscillation threshold was achieved was 12 ± 1mJ (incident on the BBO crystal) in a ≈ 160ns duration Q-switched train, which corresponded to a peak pump power, of the most energetic mode-locked pulse, of ≈ 5.6MW, and a peak intensity ($2P/\pi w^2$), again of the peak mode-locked pulse, of ≈ 1.8GWcm^{-2}. Accounting for Fresnel losses, this meant that the threshold energy internal to the crystal was ≈ 11.5mJ, which is about 20% higher than the value of ≈ 9.0mJ predicted by the theory after Brosnan and Byer [8]—where the more recent value of d_{eff} (≈ 2pmV^{-1} [3]) for BBO was employed (see Appendix A4 for details of the calculation). This was felt to be good agreement, particularly given the somewhat arbitrary way in which the experimental and theoretical thresholds were related. Following Brosnan and Byer [15], the theoretical threshold was taken to be the Q-switched train energy which led to a cumulated signal gain of $\approx \exp(30)$. In practice, the actual gain necessary for observable pump depletion was unknown. A simple consideration of the small-signal gain coefficient [16] did suggest that a pump depletion of 2–10% would require a cumulative signal gain of exp(29)–exp(31)—which leads to an uncertainty in the threshold energy of ~ 5–10%. Given additional unquantifiable effects, such a beam quality, and the error in the launched pump waistsize, etc., it is easy to account for the 20% error.

An energy threshold of ≈ 14mJ for a ≈ 200ns FWHM train was also observed. The corresponding internal energy in this case was ≈ 13mJ, which is again 20% higher than the theoretically predicted value (this time ≈ 10mJ).

Conversion efficiency.

The conversion efficiency—or more correctly, the 'pump depletion'—of the OPO was found by measuring the amount of pump energy transmitted by the cavity when oscillating, and when 'detuned' by rotating the crystal to an angle at which oscillation could not occur. As the interaction in this case was type I, oscillation only occurred when the crystal was rotated to one side of the degenerate phase-matching angle. It was therefore possible to 'detune' the OPO without causing significant misalignment, by setting the crystal at an angle just beyond degeneracy (i.e. with reference to Fig. 6.5, at a positive angular displacement from degeneracy).

The energy conversion efficiency was also deduced by measurement of the areas under the oscilloscope traces corresponding to the Q-switch envelopes of the depleted and

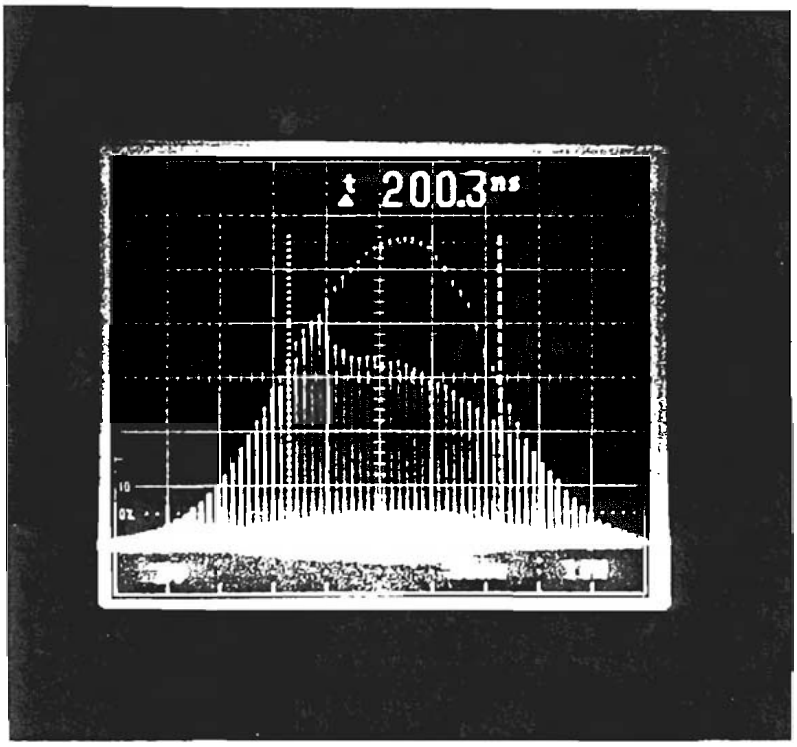

Fig. 6.3 Double exposure photograph showing the depleted pump train superimposed over the undepleted train.

undepleted pump trains (see Fig. 6.3), of which the latter was also acquired by 'detuning' the pump. In this case it was also possible, by measuring the heights of the depleted and undepleted mode-locked pulses, to make an estimate of the peak pump depletion. The overall energy conversion efficiency was found, by both techniques (within experimental error), to be around ≈ 28–32%. The corresponding peak efficiency, which occurred slightly after the peak of the Gaussian envelope of the mode-locked pump train, was found to be ≈ 37–42%.

A rigorous treatment of the mode-locked pumped parametric oscillator, as would be required to accurately estimate conversion efficiencies, has so far not been published. It would involve the consideration of saturation effects due to pump depletion, and also of the spatial and temporal behaviour of the mode-locked pulses. While the *results* of such an analysis would have been of great use, in view of its complexity, it was felt to be beyond the scope of this investigation. It would have necessitated a major numerical treatment of the problem.

To get some idea of how well the OPO was performing, the results of the one situation that has been theoretically studied in some detail were considered—that of the steady state operation of an OPO pumped by a Gaussian beam [16][17]. It must be noted that this

model makes the further assumption that the amplitude of the resonant field varies slowly through the nonlinear medium [16]. In the case of the OPO described here, this assumption is not strictly valid: The round-trip loss is significant enough that quite a high single-pass gain is required just to balance the loss.

Bjorkholm [17] predicts that in the case of a singly-resonant parametric oscillator pumped by a c.w. Gaussian beam, the pump depletion at an incident (pump) power of three times the threshold value should be $\approx 55\%$. This is not that much higher than the value of $\approx 40\%$ found for the peak depletion in practice—particularly given that the model does not account for the temporal behaviour of the pump in any way. Firstly, the fact that a mode-locked, rather than a c.w., pump was used will lead to some degree of reduction of the efficiency. Secondly, the build-up time (or rise-time) of the oscillation [18]—in conjunction with the finite duration of the experimental pump train—makes it possible that the OPO will not have had sufficient time to reach its steady-state operating condition before the termination of the pump train.

Output characteristics.

The signal spotsize was measured at the OPO output, and also in the far-field, using a photodiode array. At a signal wavelength of ≈ 680nm, the output spotsize was found to be ≈ 1.1mm, and the far-field divergence determined to be ≈ 0.20mrad. This is essentially diffraction limited, and in agreement with the value predicted using Gaussian optics [19].

The pump was launched into the cavity such that the confocal parameter at the crystal matched that of the resonated signal, this being—according to the theory after Boyd and Kleinman [20]—the situation that will give the most efficient coupling of power into an OPO. At 0.532μm, the waist at the crystal was set to be ≈ 0.45mm, which corresponded to a spot-size at the output mirror of 0.94mm. The corresponding values at 0.68μm were 0.49mm and 1.1mm respectively, giving an output divergence of 0.20mrad, agreeing well with the experimentally determined values.

The energy in the output idler train (see Fig. 6.4) was also measured. The maximum energy available, at a wavelength of $\approx 1\mu$m, was ~ 2mJ. This corresponds to the energy of the peak mode-locked pulse being $\approx 130\mu$J, and the peak power ≈ 1.6MW. The OPO output energy was sampled over several hundred laser shots and was found to fluctuate by $\sim 20\%$ (r.m.s.). This was over twice the amount of fluctuation found for the 0.532μm pump, which was, in turn, a factor of two higher than that found for the laser (generally between 3–5%).

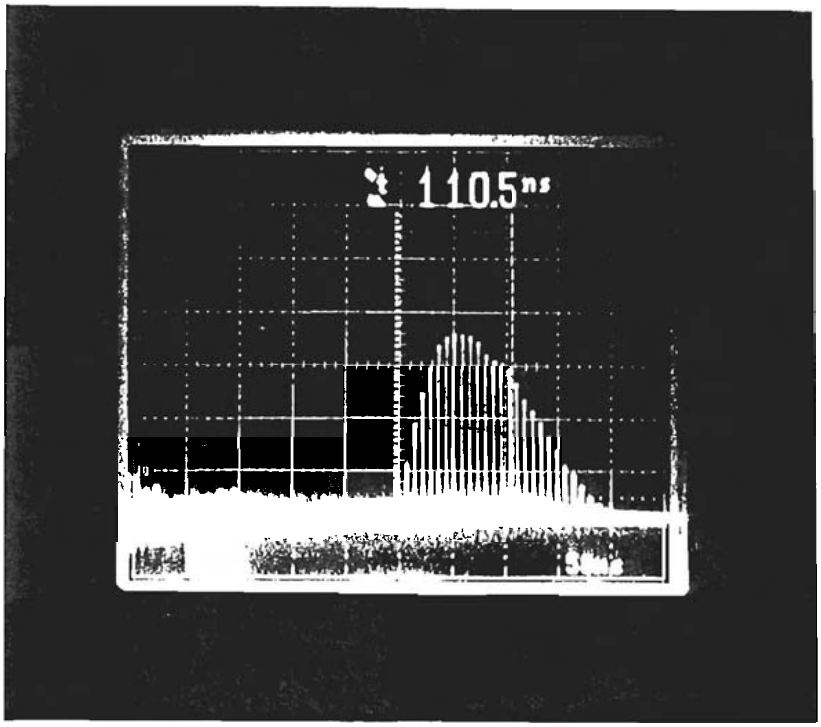

Fig. 6.4 Photograph showing output idler train.

This factor of two increase in instability due to each of the parametric processes was unexpected, as it is the behaviour predicted for operation under unsaturated conditions (i.e. when the pump is not significantly depleted). In this case, both parametric processes were definitely operating under saturated conditions—in particular the frequency doubling, which had been found to saturate at 45% efficiency—and was therefore expected to only exhibit instabilities comparable to the pump laser. The origin of this increased instability has not so far been identified. The unstable behaviour of the parametric oscillator may well be attributable to a small amount of feed-back at the idler wavelength [21], but no corresponding effect could be found to account for the increase resulting from the frequency doubling process.

Pulse duration.

The idler output pulse width was measured using background-free second-harmonic autocorrelation [22]. Assuming a Gaussian pulse shape, the duration (FWHM) of I(t) was found to be 75 ± 5ps. This is consistent with the value obtained using the analysis after Becker *et al* [23], if it is *assumed* that the pulse duration of the 0.532μm radiation is approximately the same as that of the pump source laser. The analysis of Becker *et al* [23] shows that when operating at three times the threshold pump intensity, the pulse duration of

the idler field is $\approx 90\%$ of that of the pump. In this case the pump pulse duration was taken to be ≈ 85ps, which suggested that the idler pulse duration should be ≈ 73ps—within 5% of the experimentally found value.

The assumption that the duration of the pump pulses would have broadened to a value comparable to that of the output pulses of the Nd:YAG laser source was made knowing that the frequency doubling efficiency saturated at $\sim 45\%$ for $\sim 50\%$ of the available fundamental power. This suggested that all the pulses within the FWHM of the pump train—which account for the bulk of the energy—would have broadened out to the same duration as the fundamental 1.064μm from the source laser.

A value of ≈ 75ps, for the resonated signal, is also consistent with the observed cavity length sensitivity. Oscillation was found to occur over a variation in cavity length of ~ 2mm. As it is expected that the cavity length can be mismatched by approximately one pulse-width 'τ' over the number of round-trips available to reach threshold 'm' [24], a cavity length variation of $\pm c\tau/m$ is allowed. In this case there were $m \approx 25$ pulses in the train, which had a duration of $\tau \approx 75$ps, so the cavity length was allowed to vary by approximately ± 1mm: i.e. over a range of ≈ 2mm, as found in practice.

Tuning behaviour.

The tuning behaviour of the parametric oscillator was characterized using a 1/3m grating monochromator in conjunction with a Ge detector. The response of the detector limited the longest observable wavelength to $\approx 1.8\mu$m, and consequently all longer idler wavelengths had to be inferred from the value of the corresponding signal wavelength by the application of energy conservation.

The OPO idler was found to tune all the way out to the cut-off of the Ge detector at 1.8μm. The signal, however, tuned from degeneracy—at 1.064μm—to 660nm, implying that the idler must be tuning all the way up to 2.7μm; a value well into the infrared roll-off of BBO [1]. This starts at $\approx 2.2\mu$m, and by 2.7μm around 50% of the idler will have been absorbed over a path length of ≈ 7mm. It is thought that this tuning range was only possible because: (i) it was the generated field with the lower—unabsorbed—wavelength that was resonated, and (ii) that the available parametric gain was extremely high.

Fig. 6.5 shows the experimental tuning data plotted against the theoretical curve calculated using the set of Sellmeier's equations after Kato [28], the experimental values

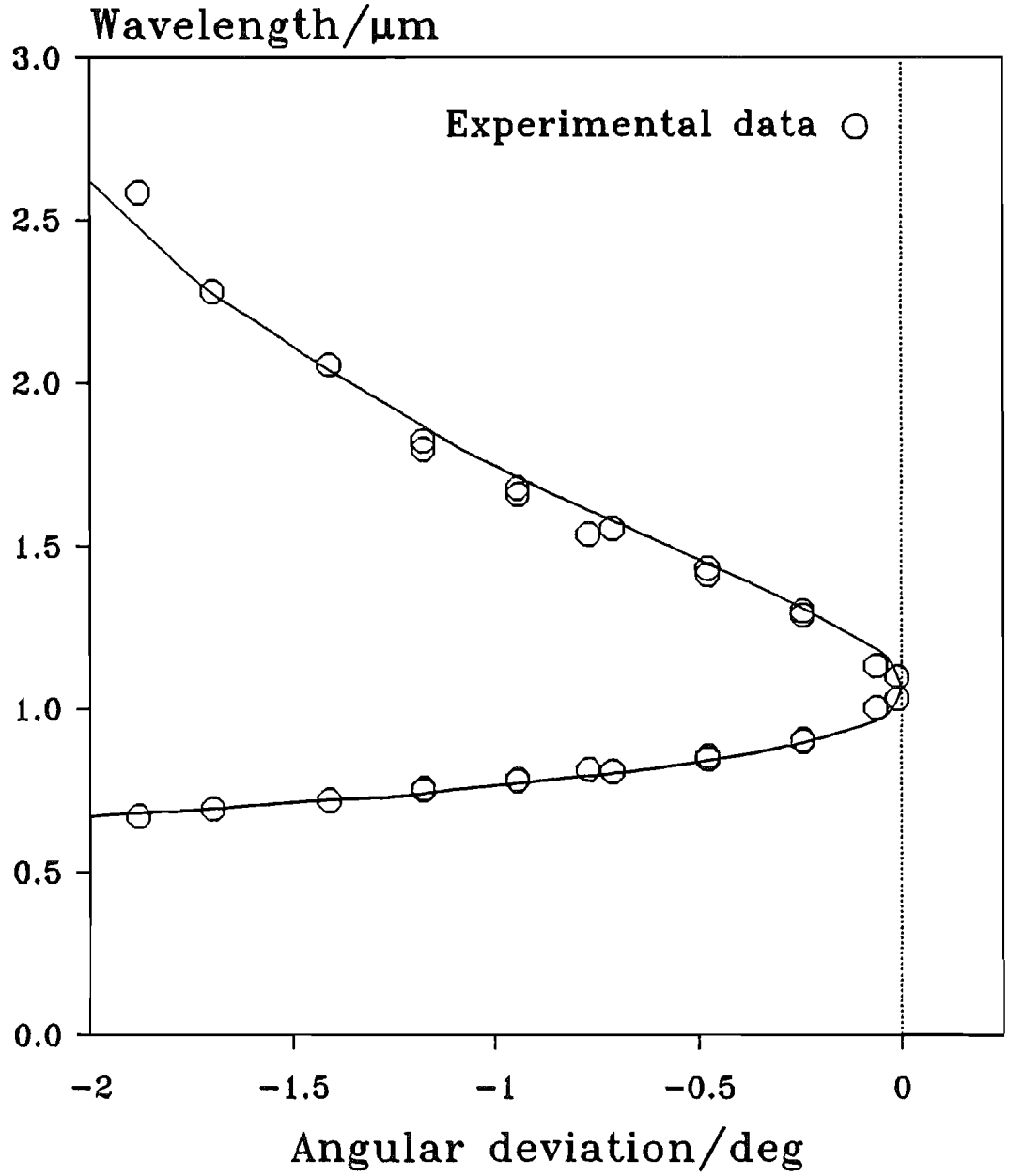

Fig. 6.5 Plot of signal and idler wavelengths as a function of angular deviation (internal) from degeneracy.

having been corrected for refraction on entering the BBO crystal. As the exact angle at which the crystal was cut was not known, it was decided to compare only the rate of tuning, and not the absolute values of angle at which a given signal-idler wavelength occurred. The graphs therefore show signal-idler wavelength as a function of angular deviation from degeneracy. The other available sets of Sellmeier's equations, after Chen *et al* [1] and Eimerl *et al* [2], were found to give noticeably poorer agreement (see Appendix A2).

To extend the range of wavelengths available from the OPO, the idler output was frequency doubled using a second type I BBO crystal. This allowed the generation of

To extend the range of wavelengths available from the OPO, the idler output was frequency doubled using a second type I BBO crystal. This allowed the generation of wavelengths in the range 0.53–0.6μm with efficiencies—with respect to the infrared OPO output—of up to $\approx 3\%$. If the signal range of wavelengths (0.7–1.0μm) had been available, this technique could have been used to extend the overall tuning range down into the ultraviolet; probably to a wavelength of $\approx$350nm.

Spectral behaviour.

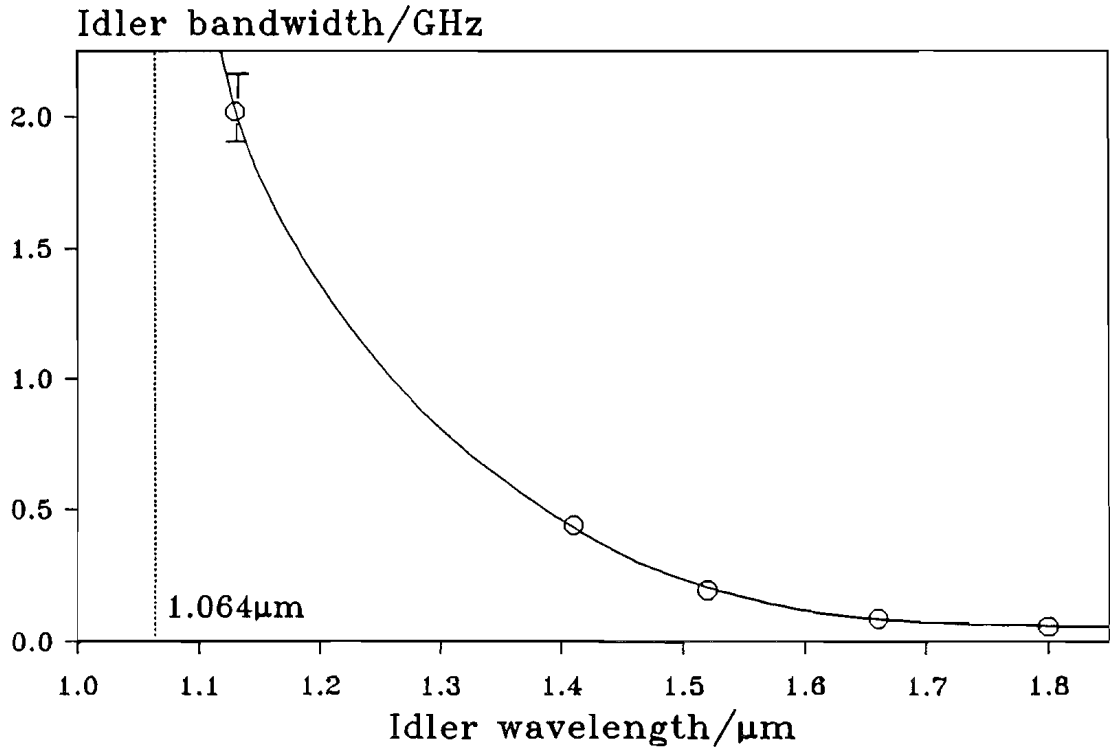

Fig. 6.6 Plot of experimentally determined idler bandwidth as a function of wavelength. The continuous line is an arbitrary fit to the data.

The bandwidth of the idler output was measured as a function of wavelength (see Fig. 6.6). As expected, the bandwidth showed a marked increase as degeneracy was approached [16]. This is due to fact that at degeneracy, as the signal and idler wavelengths are identical, there is no group velocity mismatch between the generated fields. The bandwidth at this point is therefore only constrained by the mismatch between the dispersion at the pump and signal (or idler) wavelengths. This behaviour is unique to type I interactions. The necessary disappearance of the group velocity dispersion between the signal and idler fields does not occur in the alternative type II situation. In that case the two fields are orthogonally polarized, and hence see different indices and dispersions even when they have the same wavelength.

6.5 Bandwidth control.

In an attempt to reduce the bandwidth of the OPO output to the value corresponding to the transform limit of the known mode-locked pulse duration (see Section 4), the cavity was modified to incorporate a diffraction grating (see Fig 6.7).

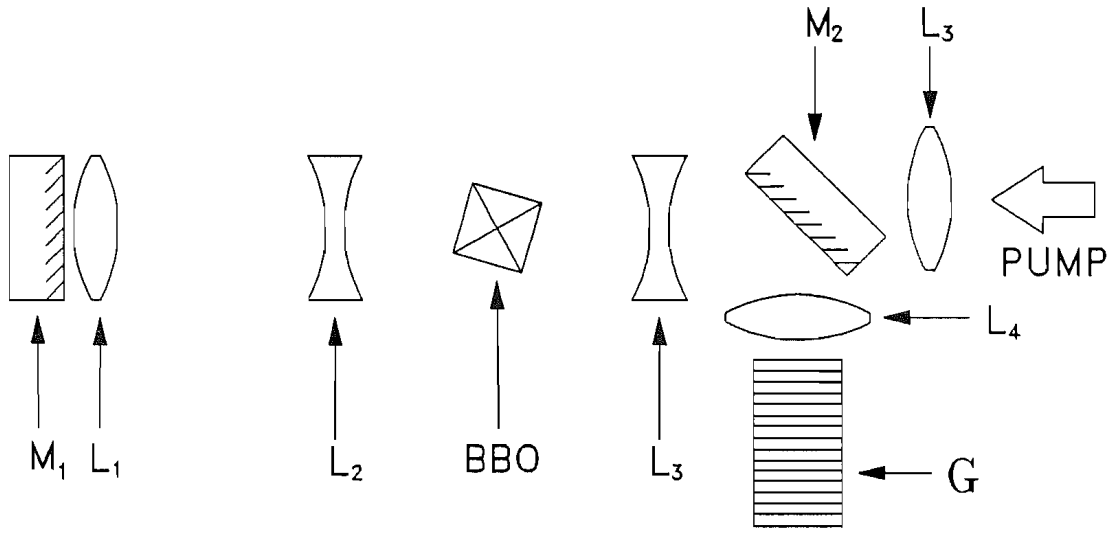

Fig 6.7 Schematic diagram of the cavity incorporating diffraction grating that was used to investigate bandwidth control of the parametric oscillator. M_1, M_2 = plane mirrors (HR 0.7–1.0μm, HT 0.532μm), L_1, L_4, L_5 = 50cm lenses, L_2, L_3 = -25cm lenses, G = 1800ℓ/mm diffraction grating.

A 1800ℓ/mm aluminium coated sinusoidal holographic grating, which had an efficiency—relative to aluminium ($\approx$90% at 0.7μm, $\approx$93% at 1.0μm)—of 85% at 0.7μm and 43% at 1.0μm, was used at Littrow orientation [29] in place of one of the resonator end mirrors. To facilitate pumping, the cavity was re-aligned with a 'dog-leg' configuration (see Fig. 6.7), using a mirror (M_2 in Fig. 6.7) that had the same reflectance characteristic as the plane mirrors referred to in Section 2 (e.g. M_1 in Fig. 6.7), but optimised for use at a 45° angle of incidence. With the grating in situ, it was found that the OPO would only operate at, or very close to, degeneracy. This implies that the singly-resonant threshold of this system was too high, whereas the doubly resonant behaviour at degeneracy made it possible to just obtain oscillation.

The pulse duration of the output idler was unaffected by the addition of the grating to the resonator (i.e. still $\approx$75ps), but the bandwidth had been reduced to $\approx$0.3nm. This corresponds to a time-bandwidth product of $\sim$6, which while still far from the transform

limited value of ≈ 0.44 (expected for an unchirped Gaussian pulse), was a factor of ~ 200 times down from the value of ≈ 60nm obtained from the resonator without spectral selection.

In principle, the signal bandwidth could have been further reduced by expanding up the beam incident on the diffraction grating—the grating resolution increasing with the number of rulings utilized [29]. This could have been accomplished by the incorporation of a prism-pair beam expander (or telescope) into the cavity. In this case, however, the additional intracavity losses would have made it impossible for the OPO to reach threshold, and consequently it was not pursued.

6.6 Conclusion.

Barium borate [1] was demonstrated to be a viable gain medium for use in a synchronously pumped optical parametric oscillator [24], but the high Poynting vector walk-off [2] in this material does limit its utility to the case of systems pumped by pulsed lasers. The use of anti-reflection coated optics within the cavity would have led to a significant reduction in the threshold, but not one that was sufficient to reduce the power requirements to a level attainable by a c.w. pumped mode-locked laser. A parametric oscillator based on BBO does offer the possibility of wide tunability across the visible and near infrared, as has been demonstrated in the case of systems pumped by pulsed (i.e. Q-switched or similar, but not mode-locked) lasers at 266nm [26] and 308nm [11]. Recently, a synchronously-pumped optical parametric oscillator based on BBO has been operated, with a 355nm pump, over the signal–idler range 0.4–3.2μm [27]—the idler wavelength range extending even further into the infrared roll-off of BBO than in the work described herein.

At the conclusion of this stage of the project, it became possible to acquire the nonlinear material potassium titanyl phosphate ('KTP')[30]. This offered both a high nonlinearity and a low walk-off, and while it was not as damage resistant as BBO [2], it did have a high enough damage threshold to allow pumping at an intensity sufficient to achieve appreciable parametric gain. It was decided that, together, these properties offered the highest probability of achieving continuously mode-locked operation in the near future, and to eventually allow parametric oscillation to be achieved using a laser-diode pumped mode-locked miniature solid-state laser [31] as the pump source.

References.

[1]. C. Chen, B. Wu, A. Jiang, and G. You.
Sci. Sinica (Ser. B) **28**, 235 (1985).

[2]. D. Eimerl, L. Davis, S. Velsko, E.K. Graham, and A. Zalkin.
J. Appl. Phys. **62**, 1968 (1987).

[3]. R.C. Eckardt, H. Masuda, Y.X. Fan, and R.L. Byer.
IEEE J. Quantum Electron. **26**, 922 (1990).

[4]. R.S. Craxton, S.D. Jacobs, J.E. Rizzo, and R. Boni.
IEEE J. Quantum Electron. **QE-17**, 1782 (1981).

[5]. R.L. Byer and S.E. Harris.
Phys. Rev. **168**, 1064 (1968).

[6]. C. Cassidy, J.M. Halbout, W. Donaldson, and C.L. Tang.
Opt. Commun. **29**, 243 (1979).

[7]. W.R. Donaldson and C.L. Tang.
Appl. Phys. Lett. **44**, 25 (1984).

[8]. M. Ebrahimzadeh and M.H. Dunn.
Opt. Commun. **69**, 161 (1988).

[9]. M.J. Rosker and C.L. Tang.
J. Opt. Soc. Am. B. **2**, 691 (1985).

[10]. H. Komine.
Opt. Lett. **13**, 643 (1988).

[11]. M. Ebrahimzadeh, A.J. Henderson, and M.H. Dunn.
IEEE J. Quantum Electron. **26**, 1241 (1990).

[12]. W. Koechner.
Solid State Laser Engineering 2nd Ed. (Springer-Verlag, 1988).

[13]. A.J. Berry, D.C. Hanna, and C.G. Sawyers.
Opt. Commun. **40**, 54 (1981).

[14]. A.E. Seigman and D.J. Kuizenga.
Opto-Electronics **6**, 43 (1974).

[15]. S.J. Brosnan and R.L. Byer.
IEEE J. Quantum Electron. **QE-15**, 415 (1979).

[16]. R.L. Byer.
Chapter 9, *Quantum Electronics: a treatise, Vol. I* (Academic Press, 1975).

[17]. J.E. Bjorkholm.
IEEE J. Quantum Electron. **7**, 109 (1971).

[18]. J.E. Pearson, U. Ganiel, and A. Yariv.
IEEE J. Quantum Electron. **QE-8**, 433 (1972).

[19]. H. Kogelnik and T. Li.
Appl. Opt. **5**, 1550 (1966).

[20]. G.D. Boyd and D.A. Kleinman.
J. Appl. Phys. **39**, 3597 (1968).

[21]. J. Falk.
IEEE J. Quantum Electron. **QE-7**, 230 (1971).

[22]. D. Bradley and G.H.C. New.
Proc. IEEE **62**, 313 (1974).

[23]. M.F. Becker, D.J. Kuizenga, D.W. Phillion, and A.E. Seigman.
J. Appl. Phys. **45**, 3996 (1974).

[24]. R.B. Weisman and S.A. Rice.
Opt. Commun. **19**, 28 (1976).

[25]. C.Chen, B. Wu, G. You, and Y. Huang.
IQEC'84 Technical Journal, Abstract **MCC5** (1984).

[26]. W.R. Rosenberg, L.K. Cheng, and C.L. Tang.
Appl. Phys. Lett. **54**, 13 (1989).

[27]. S. Burdulis, R. Grigonis, A. Piskarskas, G. Sinkevicius, and V. Sirutkaitis, A. Fix, J. Nolting, and R. Wallenstein.
Opt. Commun. **74**, 398 (1990).

[28]. K.Kato.
IEEE J. Quantum Electron. **QE-22**, 1013 (1986).

[29]. M.C. Hutley.
Diffraction Gratings (Academic Press, 1982).

[30]. F.C. Zumsteg, J.D. Bierlein, and T.E. Gier.
J. Appl. Phys. **47**, 4980 (1976).

[31]. G.T. Maker and A.I. Ferguson.
Appl. Phys. Lett. **54**, 403 (1989).

7 Parametric oscillation in KTP*.

As was mentioned in the introduction to Chapter 6, when this project began the most suitable material available for the investigation of the synchronously-pumped optical parametric oscillator ('OPO')[1] was barium borate ('BBO')[2]. BBO does, however, exhibit a large Poynting vector walk-off [3], precluding the use of a tight pump focus [4]. Consequently, the threshold power requirement for a singly-resonant OPO based on this material is beyond the current capability of c.w. flash-lamp pumped, mode-locked lasers.

The initial plan had been to optimise the performance of the 0.532μm pumped BBO parametric oscillator (see Chapter 6), and then go on to extend the tuning range over the whole of the visible part of the spectrum by exploiting a shorter wavelength pump (e.g. 0.355μm). This has since been demonstrated for both pulsed [5][6] and pulsed, mode-locked [7] BBO devices. When c.w. pumped, mode-locked lasers could supply sufficient power, or a nonlinear crystal appear with a sufficiently high nonlinearity *and* damage threshold, work could then proceed on the realization of continuous operation of a singly-resonant synchronously-pumped optical parametric oscillator. However, by the time that the initial investigation of the BBO device had been completed, it had become possible to obtain the nonlinear material potassium titanyl phosphate [8].

Potassium titanyl phosphate ('KTP') was first proposed for use as a nonlinear crystal in 1976 by Zumsteg *et al* [8], but it had then taken several years of research to develop the techniques needed to grow it in a quantity sufficient to make its production commercially viable. In the interim period, KTP had been shown to possess properties that offered a real possibility of achieving continuous operation of a synchronously pumped parametric oscillation with existing laser sources [8][9][10][11]. The decision was therefore made to pursue this possibility, and a KTP crystal acquired for use as the gain medium during the following stage of the investigation.

The main attractions of KTP are its high nonlinearity [8][10][12], and the fact that 'quasi-noncritical' phase-matching—for want of a better name—is possible for near-degenerate

---

*The work on the mode-locked and Q-switched parametric oscillator (Section 1) was published in the journal *Optics Communication* (Vol. 70, pp350-354, 1989). With the exception of the unconcluded work on the utilization of a pulse-compressed pump source (Section 3), the work in this chapter was presented at CLEO'89, Baltimore, Maryland, U.S.A., 24-28 April, 1989 (CLEO'89 Technical Digest, Abstract FK3, 1989).

operation of an OPO pumped at 0.532μm [8][9][10]. 'Quasi-noncritical' phase-matching is possible in biaxial crystals that exhibit a low birefringence between two of their principal indices, and occurs when the direction of propagation is perpendicular to the dielectric axis which corresponds to the most disparate value of refractive index. In this case, the interaction *is* noncritically phase-matched with respect to the 'disparate' axis, and hence exhibits a very wide angular acceptance and low walk-off in this direction. As the birefringence between the other two axes is small, the walk-off will be low for all directions of propagation that lie within the plane they define; it also follows that the corresponding angular acceptance will be high. This allows for the use of a tight focus, for the interacting fields, in the nonlinear medium [4]—even if the crystal used is several millimetres in length. The focusing allowed is almost, but not quite, as tight as that allowed in the case of noncritical phase-matching (e.g. in the case of KTP, when quasi-noncritically phase-matched to frequency double 1.064μm, the walk-off at 0.532μm is $\approx$5mrad—limiting the focusing to $\sim$15μm in a 5mm long crystal [4]. If even this walk-off was absent, a confocal focus of $\sim$13μm would have been allowed [4]. If this tighter focus was permitted, it would amount to a $\approx$40% increase in small-signal doubling efficiency [4]). There is, however, one major disadvantage exhibited by quasi-noncritical phase-matching; it does severely limit the tuning range.

In KTP, quasi-noncritical phase-matching is preserved only as long as the angle 'θ', between the propagation vector and the dielectric z-axis, does not depart significantly—say $\pm$3°—from 90°. The potential tuning range of a parametric oscillator pumped at 0.532μm based on KTP is 0.6–4.5μm, as has already been demonstrated in the case of parametric generation [13]—but this requires the phase-matching angle 'θ' to vary continuously over the range 45°–90° [13]. At an angle of $\approx$45° the Poynting vector walk-off is at its maximum value, which can be shown to be (in radians) roughly equal to the fractional birefringence between the appropriate pair of axes. In KTP, the fractional birefringence between the z and x (or y) axes is $\approx$5% [8][10], and so the Poynting vector walk-off at θ=45° will be $\approx$50mrad—comparable to that exhibited by BBO [2] when type I phase-matched to frequency double the same fundamental wavelength [3]. The tuning range available with a 0.532μm pump in the quasi-noncritical case is, however, a rather limited 1.00–1.12μm—much less than the total phase-matchable tuning range, as given above.

Even though the utility of the device would be initially limited, it was decided to concentrate on the quasi-noncritical case until the oscillation threshold had been reduced to a value low enough to enable continuous operation. At that time it would then be appropriate

for work to commence on the extension of the tuning range, as this, along with the implementation of bandwidth control and active stabilization, would be necessary to make the device a viable research tool. Work would also continue on reducing the power necessary to reach oscillation threshold, until it eventually reached a level that would allow pumping by a mode-locked, diode-pumped miniature Nd:YAG laser [14]. The high spatial quality, amplitude, and frequency stability of the output of these devices makes them ideally suited to this task.

The remainder of this chapter describes the experimental investigation of synchronously pumped optical parametric oscillation [1] in potassium titanyl phosphate [8]. Two devices were demonstrated; the first using a frequency doubled [15], prelase Q-switched [16], mode-locked [17] Nd:YAG laser [18] pump source (see Section 1). The second device was pumped by the same laser, but operated to generate a long-pulsed, rather than a Q-switched, mode-locked output, to achieve quasi-continuous operation of the parametric oscillator (see Section 2). In both of these cases amplification [19] of the Nd:YAG laser's 1.064μm output was required to supply—after frequency doubling—the necessary 0.532μm pump power. An attempt was made to exploit pulse compression [20] as a means of eliminating the need for amplification (see Section 3). This technique was found to enhance the peak power, available from the long-pulsed output of the laser, to a level comparable to that which had been required to achieve threshold when utilising amplification (Section 2). Unfortunately, due to the unstable behaviour of the flashlamp-pumped laser source, resulting from feedback from the fibre-grating compressor [21][22], and the necessity to operate close to the damage threshold of the KTP frequency doubling crystal [23][24] to obtain efficient harmonic generation [24], it was decided that the risk to the nonlinear medium was too great. It was therefore decided that the next stage of the investigation would have to await the development of a more stable pump source.

7.1 The mode-locked and Q-switched oscillator.

It was decided to first investigate parametric oscillation in KTP [8] using a Q-switched and mode-locked pump source [18], as this would take advantage of the experience gained during the development of the barium borate [2] device (see Chapter 6). At that time, the effective nonlinearity of KTP, for the quasi-noncritically phase-matched frequency doubling of 1.064μm radiation, was believed to be $\approx 7.2\text{pmV}^{-1}$ [8]. Preliminary calculations, using the analysis of Brosnan and Byer [25], suggested that with the available pump powers, the threshold intensity for parametric oscillation could be surpassed by well over an order of

magnitude—even if the resonator used was very lossy. It was found, however, that the experimental threshold was more than a factor of 5 times higher than the theoretically predicted value. This was far too large a discrepancy to be accounted for by the known uncertainties in the cavity loss and the pump waist size. The only factor remaining was the nonlinearity of the parametric gain medium. The higher than expected threshold was initially thought to be due to an abnormally low nonlinearity for the KTP crystal, resulting from it not being a single domain crystal [26]. This did, however, turn out to be an unnecessary, and erroneous, conjecture.

Recently, Eckardt *et al* [12] have re-measured the nonlinearity of a limited range of nonlinear crystals, including BBO [2] and KTP [8]. The results of these re-measurements were found to agree well with the values that had been previously published for the majority of the materials, the exceptions being BBO and KTP. BBO was found to have a higher nonlinearity [2][12], whereas the value for KTP was found to be less than half that of the one previously accepted (i.e. $d_{eff}=3.2pmV^{-1}$ [12] c.f. $d_{eff}=7.3pmV^{-1}$ [8]). Use of the new value of nonlinearity when calculating the threshold was found to give much better agreement with the experimental results, and was consequently utilized in all subsequent calculations.

7.1.1 The pump system.

The schematic diagram of the pump system used for this stage of the investigation is shown in Fig. 7.1. The laser used was a Q-switched and actively mode-locked flash-lamp pumped Nd:YAG laser [18], as is described in Chapter 5, Section 2. The laser was operated at 5Hz, and its output consisted of 150ns (FWHM) Q-switched trains of mode-locked pulses, with an overall energy of $\approx$1.5mJ. The mode-locked pulses had a duration of 85ps (FWHM, I(t)), and were temporally separated by 7.45ns. Consequently there were $\approx$21 mode-locked pulses within the FWHM of the Q-switched envelope, and the peak power, of the most energetic mode-locked pulse, was $\approx$770kW. The output of the laser was amplified by a double-pass through a flash-lamp pumped, 2"×¼" Nd:YAG rod [19], to give a final train energy of 65mJ, corresponding to a peak power of $\approx$33MW.

The output of the amplifier was focused into a 3cm long, type I KD^*P [27] crystal to generate the second harmonic of Nd:YAG at 0.532μm. The conversion efficiency was typically between 40–45%, which corresponded to harmonic energies of up to $\approx$29mJ. A prism was used to separate the fundamental from the harmonic, as this ensured that any 1.064μm that reached the cavity would be sufficiently non-collinear with the 0.532μm pump

that unwanted parametric interactions (e.g. parametric amplification [28] of the 1.064μm) could not take place. The low divergence of the beam through the prism, and the fact that the path-length in glass was kept minimal, limited the amount of astigmatism introduced by the prism to less than 5-10%, which corresponded to the accuracy at which the spotsizes could be determined.

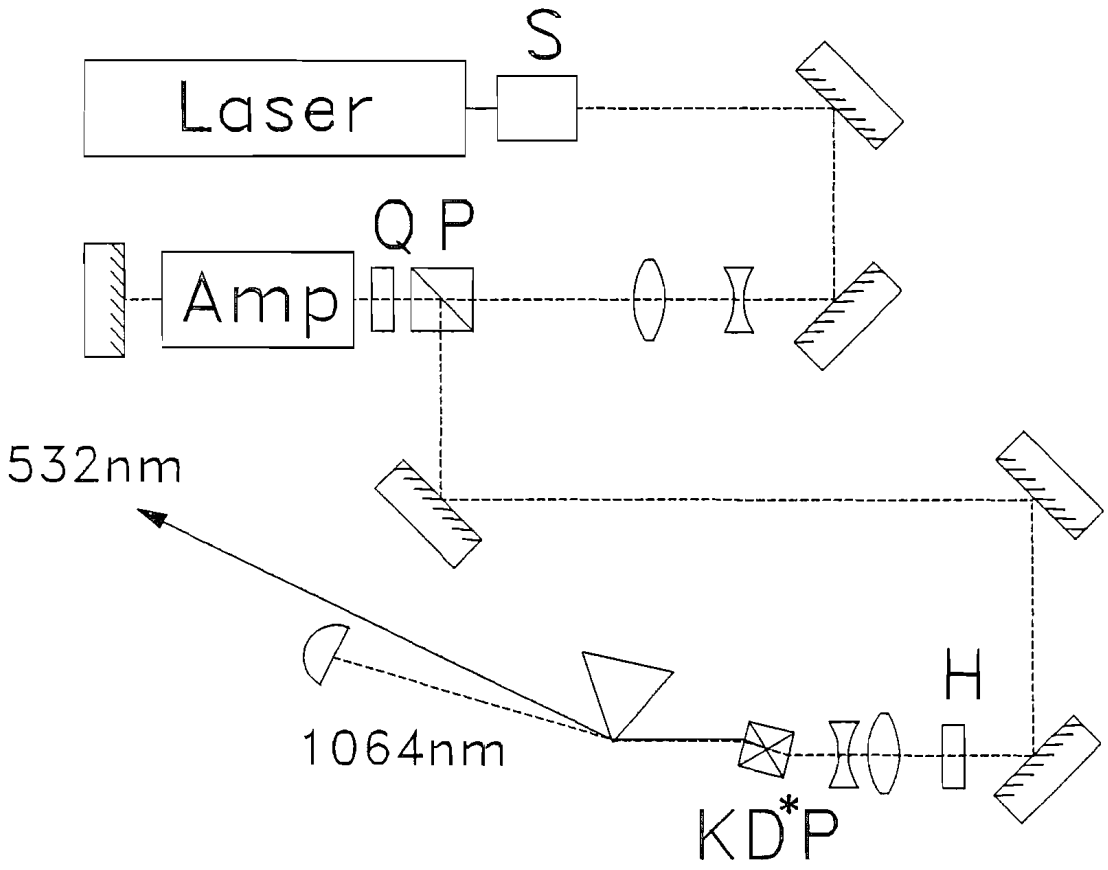

Fig. 7.1 Schematic diagram of the pump system used during the investigation of the Q-switched and mode-locked pumped KTP parametric oscillator. S = Pockels Cell shutter, Q = quarter-wave plate, H = half-wave plate, and P = polarizing beam splitter.

7.1.2 The cavity design.

The parametric oscillator was constructed using a flux-grown KTP crystal [10] from Anhui Institute of Optics and Fine Mechanics, Hefei, People's Republic of China. It was 5.8mm long, with uncoated faces of 5.1 x 5.4 mm^2, and was cut for type II phase-matching—in the xy-plane—for the quasi-noncritical frequency doubling of 1.064μm radiation (i.e. at Θ=90°, $\phi \approx 25°$ [8][9][10]).

The OPO resonator design that was used during the investigation with the Q-switched, mode-locked pump source is shown in Fig. 7.2. The cavity mirrors were the ones that had been previously used during the work with barium borate (see Section 2, Chapter 6). The mirror reflectivity was high (>99.5%) over the entirety of the signal wavelength range of 1.040–1.064μm, but fell to ~85% at the extreme of the idler tuning range (1.09μm). The mirror coating had also been designed to have a high transmission (of ≈80%) at 0.532μm, so that it would be possible to utilize a collinear pump geometry.

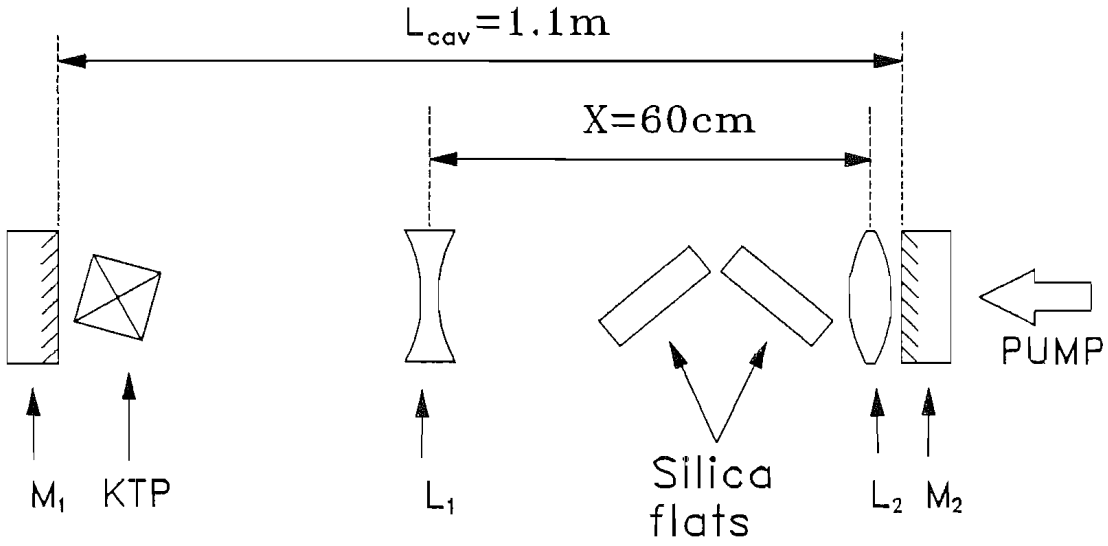

Fig. 7.2 Schematic diagram of the resonator design used during the investigation of the Q-switched and mode-locked OPO. L_1, L_2 = +1m,-1m lenses respectively, M_1, M_2 = plane mirrors (HR 0.7–1.0μm, HT 0.532μm). The silica flats, orientated at Brewster's angle, are each 1cm thick.

To ensure that the round-trip time of the circulating signal pulses accurately matched the separation of the incoming mode-locked pulses, the optical lengths of the laser and OPO had to be closely matched. The necessary length adjustment of the OPO resonator was achieved by mounting mirror M_2 on a micrometer-driven translation stage. This allowed the mirror to be positioned reproducibly to within ±10μm of the required value.

The high reflectivity at both the signal and idler wavelengths would normally have led to doubly-resonant operation of the OPO. This was undesirable as it would have led to a very poor output stability, due to the clustering effect [29][30]. Consequently, in an attempt to prevent doubly-resonant operation, two fused silica flats were introduced into the cavity at Brewster's angle. This scheme took advantage of the fact that—as it was a type II

interaction—the signal and idler were orthogonally polarized. The plates therefore presented an additional $\approx 66\%$ round trip power loss to one of the fields, but only near-negligible scattering losses to the other. This was judged to represent a high enough loss to the idler to prevent, or at least severely suppress, doubly-resonant oscillation.

To eliminate the small possibility of light generated by the OPO feeding back to the läser, which could have led to gross output fluctuations or disruption of the mode-locking [31], a slightly non-collinear pump geometry was used. The angle between the cavity axis and pump beam was $\approx 0.3°$; small enough that it could be neglected when comparing the experimental tuning behaviour with that which was theoretically predicted [32][33][34]. This simplified the phase-matching calculations as it could be assumed that the interacting fields were, in fact, collinear. It also acted to further ensure that the oscillator could not operate doubly-resonantly, as the generated idler would be slightly off-axis and consequently improperly resonated.

The inclusion of two intracavity lenses (see Fig. 7.2) allowed the diameter of the beam at the plane mirror to be varied independently of the cavity length. This contrasts with the case of the plane-concave resonator, in which the resonated spotsize is determined, for a given mirror radius of curvature, by the cavity length. In the case of the synchronously pumped OPO, the length of the cavity is constrained to match that of the pump source laser. As it had been decided to use a large spotsize in the KTP, to minimise alignment and spotsize tolerances, it was found that a non-standard mirror curvature would be required (or rather lens focal length, as a mirror/lens combination would have been used in place of a concave mirror). Given that the cavity was ~ 1.1m long, a signal spotsize of 0.25–0.35mm—as desired—would have required a 'mirror curvature' of ≈ 1.2–1.3m. The nearest values of focal length readily available were 1.5m, which would have given a spotsize of ~ 0.5mm (too large), and 1m, with which the cavity would have been unstable. The two-lens configuration allowed the desired spotsize to be attained with standard lens sizes—in this case focal lengths of +1m and a -1m were required.

As was mentioned in the introduction to this section, there was believed to be more than an order of magnitude more power available than needed to reach threshold [25], even in the case of a lossy resonator. It was therefore decided to implement the above cavity design using uncoated lenses, and an uncoated crystal. This did, of course, result in there being a high cavity loss ($\sim 50\%$ round-trip power loss), but then no attempt was made to couple out any of the generated light. If the lenses had been replaced with anti-reflection

coated equivalents, or curved mirrors, then it would have been possible to reduce the reflectivity of one of the mirrors to provide a substantial output.

7.1.3 Performance details.

This subsection summarizes the results of the investigation of the Q-switched and mode-locked pumped optical parametric oscillator. The experimental results were compared with the corresponding theoretical predictions and found to give reasonable agreement.

The operation of the parametric oscillator was observed by monitoring both the infrared output train and the transmitted pump; both a high gain detector and a vacuum photodiode were available for this purpose. The former had a slow response ($\sim 10\mu$s), and was therefore useless for observing the transient behaviour of the OPO. It was employed to detect the presence of the idler at the onset of oscillation, and hence for the determination of threshold. It was also of use during alignment as it could detect oscillation at a level slightly below that at which pump depletion became noticeable (there was less background illumination in this case, compared to during the investigation of the BBO device, and hence lower level infrared signals were observable). Conversely, the vacuum photodiode, having a ≈ 0.3ns rise-time, was fast enough to just resolve the mode-locked pulses in the pump train, and was therefore readily able to follow the temporal response of the OPO.

Oscillation threshold.

The oscillation threshold was taken to be the point at which an idler output could just be detected; this was generally found to occur at powers slightly lower than those that resulted in discernible pump depletion. It was determined by slowly reducing the output of the laser amplifier with a variable optical attenuator. This avoided the change in thermal lensing—and hence focusing into the OPO—that would have resulted had the pump energy been varied through altering the amplifier flash-lamp current. Having adjusted the pump level until parametric oscillation was just occurring on every laser pulse, the energy incident on the KTP crystal was measured using a pyro-electric calorimeter. Threshold was found to be achieved at an incident energy (in the Q-switched train) of $2.0\text{mJ} \pm 10\%$, which—accounting for Fresnel loss—is equivalent to 1.8 ± 0.2mJ actually entering into the KTP crystal. This corresponds to a peak power, of the most energetic mode-locked pulse, of 920 ± 90kW, which is equivalent to an intensity of $870 \pm 110\text{MWcm}^{-2}$—where the experimentally determined pump spotsize of 0.26 ± 0.02mm was used in the calculation of the last value.

The experimentally found threshold was compared with the value predicted using the theory after Brosnan and Byer [25] (see Appendix A4 for further details). For the purposes of the calculation, the following values were used.

(a). The round-trip duration of the cavity was 7.45ns, and the mode-locked pulse duration was 85ps. This meant that there were ≈ 21 cavity transits during the ≈ 150ns intensity FWHM, I(t) of the Q-switch train, and that the ratio of peak to average power was ≈ 82. From this, and the Q-switched and mode-locked pulse durations, it can be shown that the most energetic pulse in the Q-switched train will contain $\approx 4.7\%$ of the overall energy.

(b). The Fresnel losses due to transmission through a single surface at 1.064μm were 4.1% and 7.4% for BK7 Schott glass and KTP respectively. The fractional power feed-back over one round-trip was therefore ≈ 0.53.

(c). The pump spotsize—in the KTP crystal—was measured using a photo-diode array and found to be 0.26 ± 0.02mm.

(d). The signal spotsize was also measured, and found to be 0.37 ± 0.02mm.

(e). The more recent, and lower, value of nonlinearity for KTP, of $d_{eff} = 3.2 \text{pmV}^{-1}$ [12].

(f). The Poynting vector walk-off in KTP is ≈ 4.5mrad [9]. Note that as KTP is type II phase-matched, both the signal (or idler) and pump walk off the idler (or signal). Here it has been treated *as if* it is the pump that walks away from the other two fields—as assumed by Brosnan and Byer's model [25]. Furthermore, the pump and signal walk-off by different amounts; the largest value has been taken.

(g). That a net gain of $\approx \exp(30)$ would be required for the signal to build up to an appreciable strength [35] from the parametric noise level [36]. Assuming that the initial signal bandwidth was the same as that experimentally determined for the OPO output ($\Delta\nu \approx 250$GHz), the noise power would have been ~ 50nW [36]. This suggests that with a gain of $\exp(30) \approx 10^{13}$, the final resonated signal power would have been ~ 0.5MW, which would have been detectable outside the cavity. In addition, from an elementary consideration of the single-pass parametric equations [35], it can be shown that this signal level would lead to a pump depletion of 3–5%. This is

comparable to the pump fluctuation, and therefore corresponds roughly to the point at which depletion would have become observable.

Before commenting on the value of threshold predicted using the analysis after Brosnan and Byer [25], it must be noted the major uncertainties in this calculation were the pump and signal spotsizes in the KTP crystal. Threshold was predicted to occur at a train energy of 1.7 ± 0.1mJ, corresponding to a peak power of 880 ± 60kW, of the most energetic mode-locked pulse in the crystal, and a peak intensity ($2P/\pi w^2$) of 830 ± 60MWcm^{-2}. Comparing these values with the experimental results, given on the previous page, shows good agreement—the experimental results coming towards the tops of the ranges of the predicted values.

The earlier value of $d_{eff}=7.2$pmV^{-1} [8] had been used to estimate the oscillation threshold before the work on the KTP oscillator commenced. Using this value, the predicted threshold was at an energy of 0.35 ± 0.05mJ in the Q-switch train, equivalent to a peak power of 180 ± 20kW, and a peak intensity of ≈170MWcm^{-2}—a factor of ≈5 times smaller than the experimentally found values. As mentioned in the introduction to this section, this was far too large a discrepancy to be accounted for by the known uncertainties in the cavity loss and the pump waist size. The only factor remaining was the nonlinearity of the parametric gain medium. The higher than expected threshold could have been due to an abnormally low nonlinearity for the KTP crystal, suggesting that it was not a single domain crystal [26]. This did, however, turn out later to be an unnecessary conjecture.

With the maximum available pump energy, of 5.0 ± 0.2mJ, the OPO could be run with approaching three times the threshold intensity incident on the crystal. As the relative stability of a parametric oscillator improves the further above threshold it is operated, the majority of the measurements were taken when running at this uppermost level. The peak intensity seen by the crystal was therefore 2.4 ± 0.1GWcm^{-2}, which is well above the earlier more pessimistic damage thresholds of ≈400MWcm^{-2} ($\tau=10$ns, $\lambda=1.064\mu$m)[23] and ≈650MWcm^{-2} ($\tau=30$ns, $\lambda=1.064\mu$m)[24] quoted for KTP, but around an order of magnitude below the single-shot values found for short (i.e. ~1ns, and below) pulses of ≈15GWcm^{-2} ($\tau=1$ns, $\lambda=1.064\mu$m)[10] and ≈30GWcm^{-2} ($\tau=30$ps, $\lambda=0.532\mu$m)[13]. It was decided, however, to exercise caution. No measurement of the damage threshold of a train of mode-locked pulses has been reported at that time, but it was felt that it was likely to be somewhat lower than in the case of single mode-locked pulses. As there was no occurrence of damage even after several hundred hours of operation at ≈2.4GWcm^{-2}, it

appears that the damage threshold in this circumstance must be an appreciable fraction of the single-shot value [10][13].

Conversion efficiency.

The OPO conversion efficiency was determined indirectly by measuring the depletion of the pump. As in the case of the BBO parametric oscillator (see Chapter 6, Section 4), the depletion was measured in two ways. The first technique involved the measurement of the amount of pump energy transmitted by the OPO cavity when oscillating and when 'detuned'. In this case, the interaction being type II, the tuning is continuous through degeneracy (c.f. type I, where tuning is only in one possible direction from degeneracy), and hence one of the mirrors had to be very slightly misaligned to achieve the detuning.

The second method used was photographic. A double-exposure photograph of the intensity envelopes of the depleted and undepleted (when the OPO was detuned) pump trains was obtained (see Fig. 7.4). Care was taken to ensure that the two images were of the same relative amplitude, as can be seen by the fact that the leading edges of the trains coincide. For the lower trace this corresponds to an undepleted part of an otherwise depleted train, and was therefore adjusted to follow the equivalent portion of the upper, undepleted pump train. An estimate of the overall energy conversion efficiency could then be obtained from a measurement of the areas of the two trains—the depletion efficiency being ascertained from the difference of the two. In a similar way, it was also possible to determine the peak depletion efficiency from a measurement of the heights of overlapping pairs—one from each train—of mode-locked pulses.

In both cases the total pump depletion was found, when three times the threshold energy was incident on the KTP crystal, to be $\approx 30\%$. The peak conversion efficiency, occurring just after the peak of the Q-switched envelope, was found to be up to $\approx 45\%$. From it was deduced that the internal energy conversion efficiency to the signal, and also to the idler, was $\approx 15\%$ overall and $\approx 23\%$ peak (as the device was operating near degeneracy, the depleted pump is partitioned almost equally between the two generated fields).

As the transmission of the OPO cavity mirrors was too small to be accurately determined, it was neither possible to determine an external conversion efficiency, nor to meaningfully compare the energy of the output pulse with the value predicted from the known internal conversion efficiency and cavity loss. With suitably coated optics, however, it would have been possible to couple out a high fraction of the signal and idler fields. Given that the

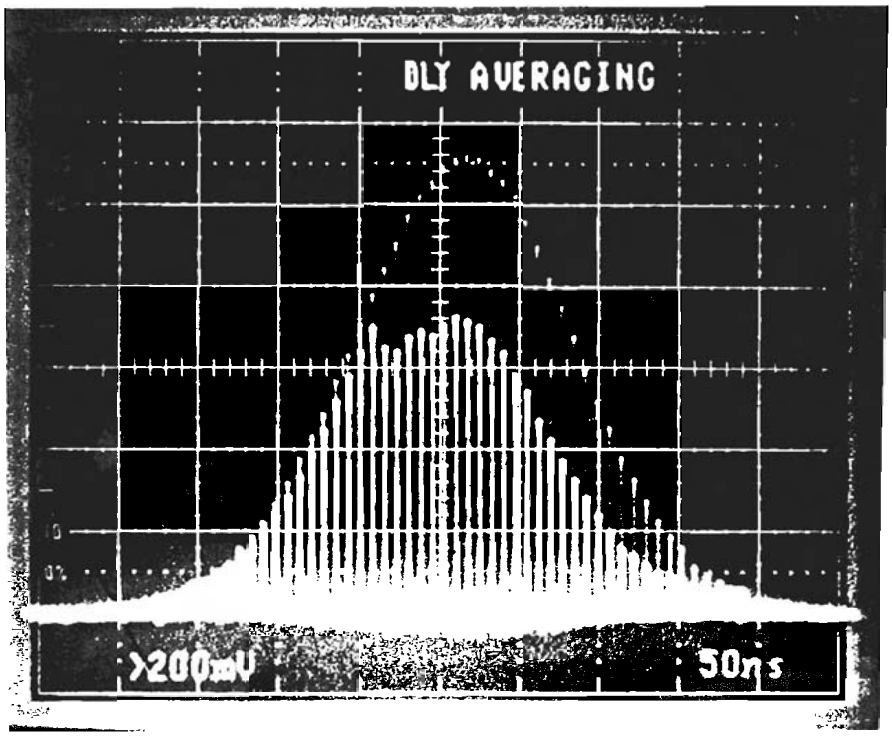

Fig. 7.3 Double exposure photograph showing the depleted 0.532μm pump train superimposed over the undepleted train, for the case of the Q-switched and mode-locked pumped KTP parametric oscillator.

round-trip cavity loss was 47%, solely due to Fresnel reflection, if all the lenses had been anti-reflection coated, or replaced with equivalent mirrors, and then one of the HR mirrors had been replaced with an output coupler of $\sim$47% at the signal wavelength, and $\sim$100% at the idler wavelength, the net round-trip loss would be virtually unchanged. In this case, the output idler pulse train would have contained $\sim$0.7mJ, which corresponds to a peak power of $\sim$500kW. In estimating the peak power, it was assumed that the idler output train would be approximately Gaussian, with a FWHM, I(t) of $\approx$110ns, as shown for the output idler in Fig. 7.4. The other information used, that the signal pulse duration was approximately equal to that of the 1.064μm output from the Nd:YAG source laser, was later confirmed by autocorrelation measurements [37] of the signal and idler outputs.

Output behaviour.

The waistsize of the pump at the cavity mirror near the KTP crystal was found, using a photodiode-array, to be 0.26$\pm$0.2mm. The waistsize of the signal/idler output was similarly measured, and found to be 0.37$\pm$0.2mm. The signal/idler spotsize was also measured in the far field, and the angular divergence of the output deduced. At a wavelength of 1.075μm, the half-angle diffraction was found to be $\approx$0.9mrad, agreeing well with the value expected

from a TEM_{00} mode [38] having a waistsize of the experimentally determined value. This suggests that the OPO output was essentially diffraction limited.

Note that the signal/idler spotsize agrees well with the value pre-selected during the cavity design stage, using Gaussian optical analysis [38], and also that the pump waistsize is a factor of $\approx\sqrt{2}$ smaller. For near degenerate operation, this is the condition that is supposed to result in optimal coupling of pump energy into the signal mode [4].

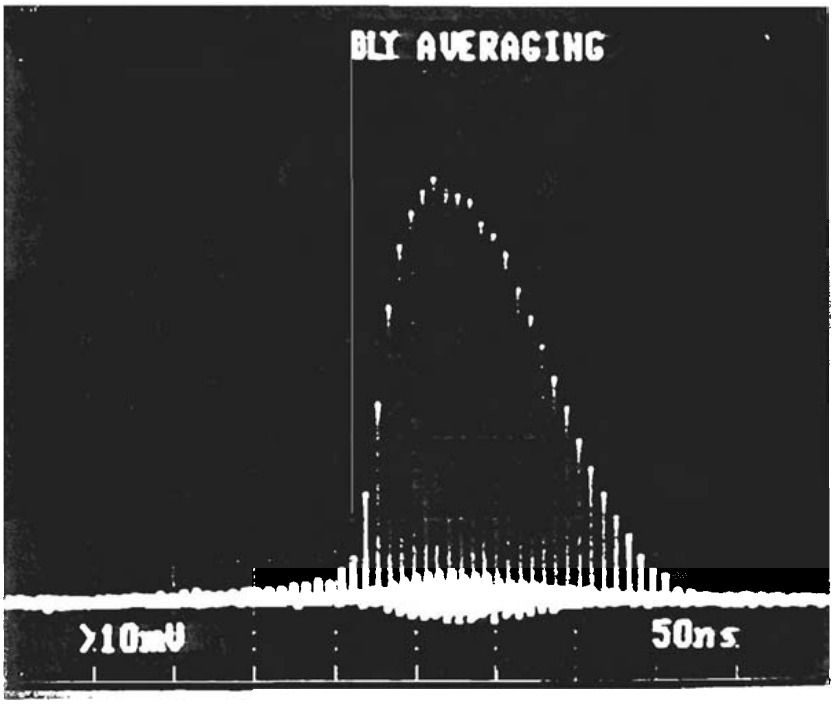

Fig. 7.4 Photograph showing idler output train from the Q-switched and mode-locked KTP parametric oscillator.

The stability of the output of this device was also measured. The energy of output signal was sampled for several hundred laser shots, and found to have an r.m.s. variation of 16%; slightly over twice the fluctuation that was exhibited by the 0.532μm pump. This effect was also noticed while working with the BBO parametric oscillator, but had not been accounted for. Unfortunately, the cause has still not been determined. The two-fold increase in fluctuations is characteristic of a parametric interaction operating in the small-signal regime, whereas with the high degree of depletion a reduction in the instability had been expected.

Pulse duration.

The signal and idler pulse durations were measured by second harmonic autocorrelation [37]. At zero cavity length detuning (corresponding to optimum amplitude stability of the output pulses), the signal and idler pulse durations were both measured to be 75 ± 10ps. Within experimental error, this value remained constant across the OPO tuning range. The pulse duration of the 0.532μm pump was not measured due to the lack of a suitable nonlinear crystal for the purpose of autocorrelation, but due to the high doubling efficiency was expected to have saturated out to a value approaching that of the pump (i.e. 80-85ps).

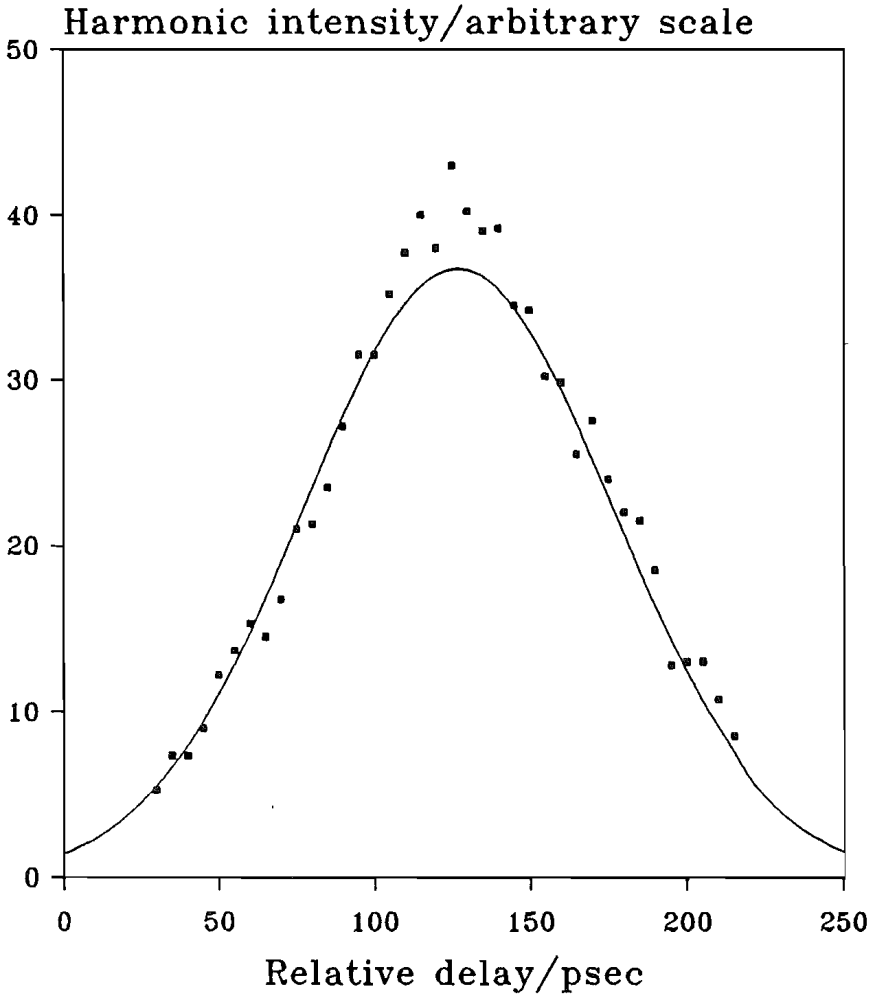

Fig. 7.5 Second-harmonic autocorrelation trace of the Q-switched and mode-locked OPO idler output. Assuming a Gaussian fit, as shown, the FWHM of I(t) is ≈ 75ps.

Becker *et al* [39] have theoretically predicted that when a parametric oscillator is operated many times (say >10) above threshold, the resonated signal pulse duration will broaden to be $\sqrt{2}$ longer than that of the pump pulse. This same model predicts that when an OPO is operated at three times the pump threshold level, the duration of the resonated

pulse will be ≈90% of that of the pump (see Fig. 7.6). If it is *assumed* that the 0.532μm pump pulses had broadened to approach the duration of the 1.064μm output from the Nd:YAG source laser (i.e. ≈85ps), Becker *et al*'s model suggests that the signal duration would have been ≈72ps, which is consistent with the experimental result.

The argument that the 0.532μm pulses would have broadened out to approach the duration of the pulses from the Nd:YAG source laser is borne out by the observed saturation of the doubling process used to generate the pump wavelength. The second harmonic conversion efficiency was found to saturate at ≈45%, at a 1.064μm intensity of less than half the operating value. This suggested that the pulses within the FWHM of the Q-switched train, which contained the bulk of its energy, would have all broadened out to the same duration as the fundamental 1.064μm input.

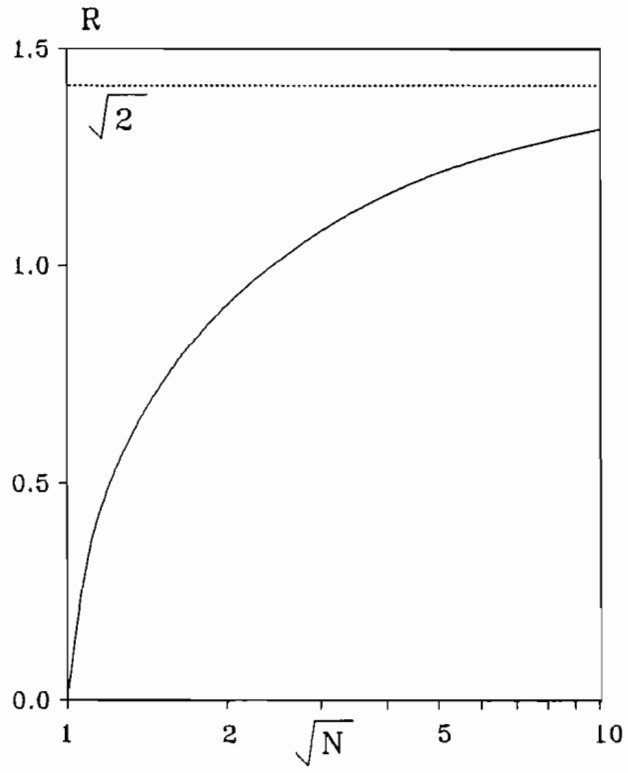

Fig. 7.6 Graph showing ratio of the signal to pump pulse duration as a function of the square-root of the number of times above threshold ($R = \tau_1/\tau_3$, $N = P_3/P_3th$; τ_1, τ_3 = signal, pump duration, P_3 (P_{3th}) = (threshold) pump power). Based on the analysis after Becker *et al* [39].

Oscillation was found to occur over a cavity length range of ≈2.5mm. As found in the case of the BBO parametric oscillator, this agrees well with the approximate value given by considering the pump pulse duration and the number of pulses available to achieve

threshold. i.e. If there are 'm' pulses in the FWHM of the Q-switch train, and each pulse has a duration of τ, then a departure of up to $\pm c\tau/m$ is allowed [40]. In this case there are ≈ 21 pulses, and the pump pulse duration is ≈ 85ps, so the operational range of cavity length is $2c\tau/m \approx 2.4$mm. As the OPO cavity length was adjusted off synchronism with the source laser, the output pulses were found to exhibit a slight decrease in duration ($\sim$5-10ps). The maladjustment of the length did, however, also lead to a reduction in OPO output stability, making an accurate determination of the magnitude of this effect impossible.

Tuning behaviour.

The signal and idler tuning range was measured with a ⅓m monochromator, using a 600ℓ/mm grating blazed at 1μm, and a silicon photo-diode at the exit slit. In this case, the tuning range was limited enough that the problem of detector cut-off—as had been encountered with the BBO device (see Chapter 6, Section 4)—would be no problem; even in the case of a silicon detector. The parametric oscillator was only tuned such that propagation was perpendicular to the z-axis—to preserve quasi-noncritical phase-matching—and so the potential tuning range was already fairly limited. In practice, it was further limited by the angular aperture of the KTP crystal, and so the tuning range achieved was only 1.04-1.09μm (see Fig. 7.7).

As the angle at which the crystal had been cut was not known to a sufficient degree of accuracy, the generated wavelengths were measured as a function of relative angle. Having determined the relative angle at which degenerate oscillation occurred, the wavelength dependency was then re-expressed as a function of the angular deviation from degeneracy. The experimental points were then fitted to the theoretical curves [34], generated using various sets of Sellmeier's equations [10][41][42][43], relative to the degenerate point.

Reasonable agreement was found between the experimental values and those calculated using four of the available sets of Sellmeier's equations [10][41][42][43]. This was not unexpected, as when used to calculate the phase-matching angles for near degenerate operation of a 0.532μm pumped OPO, they had been found to generate very similar phase-matching curves (see Appendix A2). Therefore, the choice of Sellmeier's equation used to generate the theoretical curve given in Fig.7.7 (after Fan *et al* [10]) was somewhat arbitrary.

To investigate the possibility of temperature tuning, the KTP crystal was mounted in a temperature stabilised oven. The temperature could only be adjusted over a rather limited range (25-50°C), and was accurate to $\pm$1°C. No variation in the wavelength at which the

OPO operated could be discerned over this range, which put an upper bound on the rate of tuning of $\approx$ 1nm over 25°C (i.e. $<$ 0.04nm/°C).

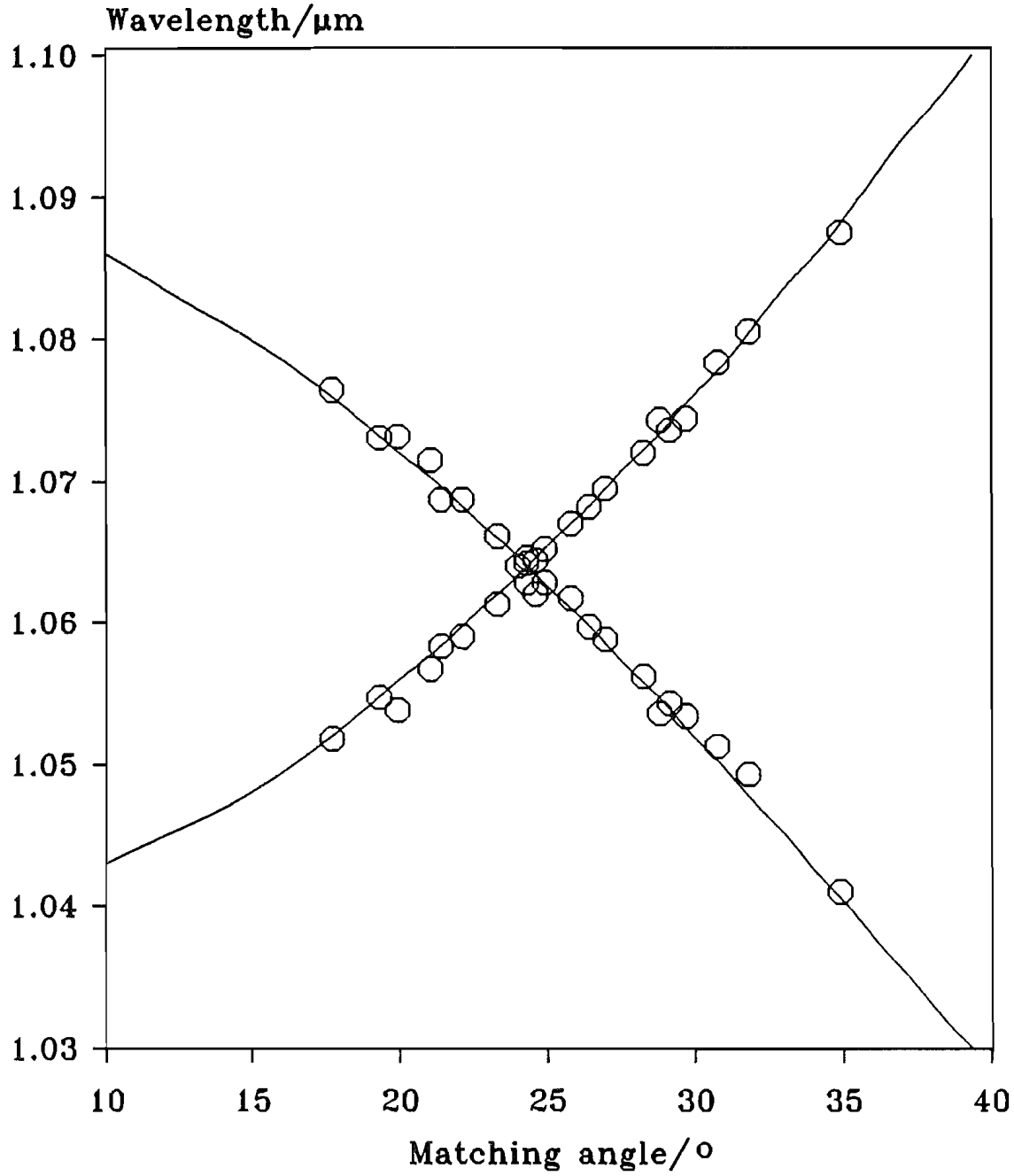

Fig. 7.7 Type II, KTP parametric tuning curve for 0.532μm pump, and propagation in the xy-plane. The experimentally determined points have been plotted against a curve calculated using the set of Sellmeier's equations after Fan *et al* [10].

At the time the work on the Q-switched and mode-locked OPO was in progress, the information necessary to predict the thermal tuning behaviour was not available. Zumsteg *et al* [8] had published a graph of refractive index variation with temperature, but only at one

(undisclosed) wavelength. The only other information then available was the fact that KTP had a high thermal acceptance ($\approx$25°Ccm [44][10]).

More recently, Gettemy *et al* [45] have published experimentally determined values of dn/dT for the principal indices at 0.532μm, 0.660μm, 1.064μm, and 1.320μm. This allowed for a theoretical estimation of the rate of tuning with temperature for near degenerate operation. The predicted value was found to be $\sim$0.1nm/°C, corresponding to a change of wavelength of $\approx$2.5nm over 25°C (see Fig. 7.8), which should have been just discernible. However, as the values of dn/dT used were only quoted to an accuracy of $\pm$20% [45], the tuning rate could lead to a change of anywhere between 0.05-0.20nm°C^{-1}. To agree with the experimentally found result, the smaller value is probably correct.

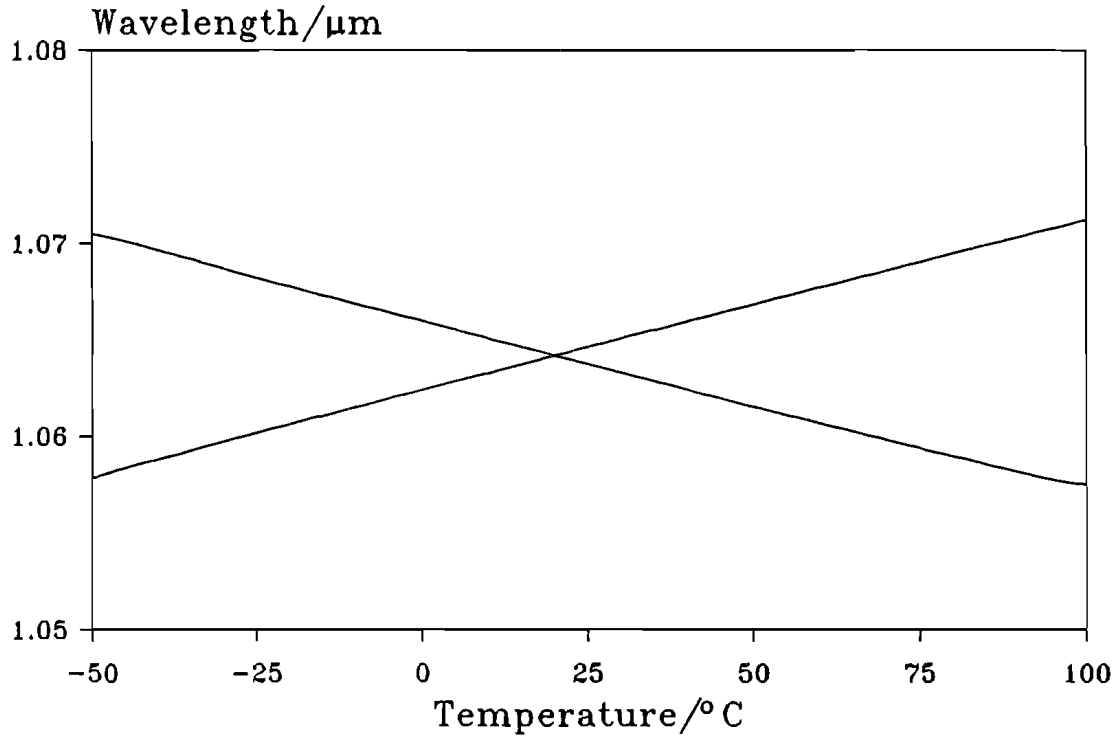

Fig. 7.8 Signal/idler wavelengths as a function of temperature for propagation at θ=90°, ϕ=25°.

Spectral behaviour.

The bandwidth of the OPO output radiation was measured using a plane-plane Fabry-Perot interferometer, and found to be $\Delta\nu$=260$\pm$40GHz (FWHM, I(ν)) for both the signal and idler outputs. It was constant, within experimental error, across the whole of the demonstrated tuning range, and is only slightly smaller than the $\approx$300GHz spectral acceptance of the (5.8mm long) KTP crystal [10]; this is the characteristic of a high gain system [25].

The linewidth of the output radiation from a parametric oscillator is determined by the acceptance bandwidth of the crystal, and how far above threshold the OPO is operating [25]. This is because the nearer to threshold the OPO is operating, the higher the number of crystal transits required for the signal to build up from parametric noise [36]. Consequently, the gain length seen by the signal field can be considerably longer than the physical length of the crystal. As the bandwidth acceptance of a parametric process is inversely proportional to its gain length [35], this results in a corresponding reduction of the bandwidth. In the high gain case, however, the number of passes needed for a sizeable signal to be built up from noise can approach unity, and hence the linewidth can broaden to that of the acceptance bandwidth of the crystal [25].

This lack of variation in the linewidth, as the OPO was tuned, is predominantly due to the limited range over which tuning was achieved. It is also due, in part, to the fact that the parametric interaction was type II. Type II interactions do not exhibit the marked broadening near degeneracy [46] as seen in the type I case (e.g. the BBO parametric oscillator described in Chapter 6). This is because the signal and idler fields are orthogonally polarized, and hence see a different value of group velocity even when they have the same wavelength. Consequently, a type II OPO can never actually be 'degenerate': this term should really be reserved for the case when the two interacting fields are identical in frequency *and* polarization. In the type II case, as there is no degeneracy to be approached, there is consequently no variation in linewidth as 'degeneracy' (i.e. $\lambda_{idler}=\lambda_{signal}$) is neared.

7.2 The long-pulse mode-locked OPO

The next stage of work involved a brief investigation of a long-pulse mode-locked pumped OPO, also based on the material KTP [8]. Unfortunately, the output stability was poor, and consequently few meaningful results were obtained. This was, however, only seen as an intermediate step between the Q-switched, mode-locked device, and the continuously mode-locked device that would be subsequently developed.

It was decided that only when continuous operation of a synchronously-pumped parametric oscillator was achieved would it be possible to carry out a proper investigation of the gain dynamics. The behaviour of the Q-switched mode-locked system is complicated by the fact that it operates under high gain, transient conditions. The continuously mode-locked system would, conversely, be operating under low gain, steady-state conditions. In this case, the temporal behaviour resulting from the synchronous pumping can more easily be studied.

Once the steady state operation of the mode-locked system was understood, it would then be possible to address the problem of the transient, Q-switched and mode-locked system having already gained some understanding of the mode-locking process.

To achieve long-pulsed, mode-locked operation of the OPO, two major modifications had to be made to the experimental set up. Firstly, the pump source laser had to be reconfigured to operate with a long pulsed, as opposed to a Q-switched, mode-locked output. Secondly, the OPO cavity had to be altered to markedly reduce the round-trip power loss, and also to provide a tighter signal focus in the KTP crystal. This was because the pump power available was significantly lower than in the Q-switched case, and consequently a tighter pump focus was required for the intensity to exceed the threshold value—even having reduced the cavity losses. To maintain efficient power coupling into the signal mode, it was therefore necessary to reduce the signal waist-size (proportionally) as well.

7.2.1 The pump system.

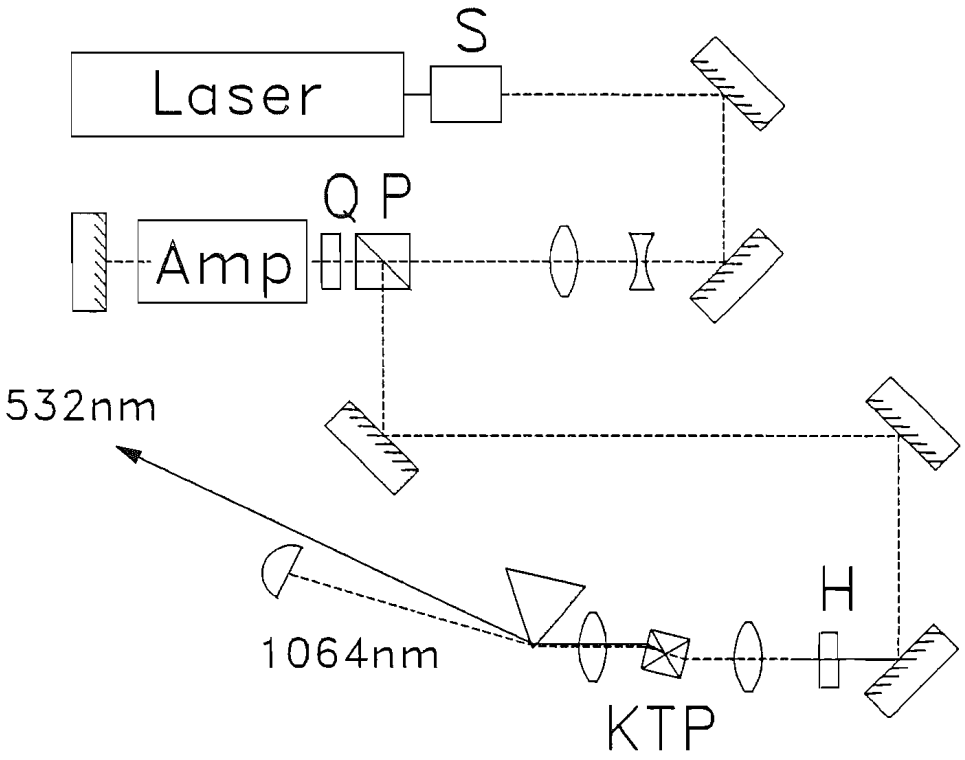

Fig. 7.9 Schematic diagram of pump layout used during the investigation of the long-pulse mode-locked laser pumped KTP parametric oscillator. S = Pockels cell shutter, Q = quarter-wave plate, P = polarizing beam splitter, H = half-wave plate.

The pump laser used during this stage of the work was the same one as had been employed in the demonstration of the two Q-switched, mode-locked pumped optical parametric oscillators (see Section 1 and Chapter 6 for the KTP and BBO devices respectively). In this case, the Nd:YAG laser was operated without Q-switching to provide an output consisting of 5ms long trains of mode-locked pulses, at a repetition rate of 5Hz. The majority of the 5ms train was not usable, however, as it took over 2ms for the stable build-up of the mode-locked pulses [47]. Also, it was found that operation of the laser without the Q-switch resulted in substantial relaxation oscillations at the onset of each laser flash-lamp pulse [48]. As a tight focus in the doubling crystal was required to achieve the necessary harmonic conversion efficiency, the exposure of the crystal to this highly energetic spikes would have probably caused it severe damage. To eliminate the chance of damage due to the relaxation oscillations, and also to give the laser mode-locking a chance to properly stabilize, a Pockels cell shutter [49] was used at the laser output. This opened towards the end of the 5ms flashlamp pulse for $\approx 20\mu s$. Though this is not that long a duration when compared to the flash-lamp pulse (of 5ms duration), it does correspond to ~ 2700 cavity round-trips. This was felt to be sufficient for quasi-c.w. operation to be achieved.

Due to problems with the Pockels cell shutter used in the previous stages of this work, it was necessary to utilize the laser's Q-switch Pockels cell as the shutter during this investigation. This resulted in a $\approx 50\%$ loss of laser power, as the Q-switch Pockels cell could only supply a quarter-wave polarization rotation, and not the half-wave available from the shutter used previously. The laser could be operated stably at 'equivalent average powers' (i.e. averaged over the duration of the pulse train only) of up to ~ 70W, which meant that output powers of ~ 35W were available. This corresponded to an energy—in the $20\mu s$ train—of ≈ 0.75mJ. As it was already known that amplification would be necessary to attain the required train energy, it was decided to reduce wear on the flash-lamps by running the laser at a level below this maximum value—the deficit being made up by using slightly higher amplification. Consequently the laser was run to give an output power of ~ 45W, leading to a usable output of ~ 22W, equivalent to a train energy of ≈ 0.3mJ.

The output of the Pockels cell shutter was amplified by a double pass through a flash-lamp pumped Nd:YAG rod, to give an energy of up to ≈ 39mJ, corresponding to an equivalent average power of ≈ 2.0kW. The output of the amplifier was then frequency doubled using an uncoated type II KTP crystal [8]. The KTP crystal utilized was the one that had been used during the investigation of the mode-locked, Q-switched device—as described in Section 1—and had a length of ≈ 6mm and uncoated apertures of $5 \times 5\text{mm}^2$.

In practice, the 1.064μm energy available after amplification was far in excess of that needed to operate the parametric oscillator. The OPO required only $\approx$0.35mJ to reach threshold, and so the amplifier was usually run at a power level that provided an output of 150-200W. With this 1.064μm power, a doubling efficiency of 15-20% was all that was needed to provide the required 0.532μm pump radiation. After separating the 0.532μm from the residual fundamental using a dispersing prism, and the losses incurred on entering the OPO cavity, an equivalent average pump power of up to $\approx$30W was available.

7.2.2 The cavity.

The mirrors used for the long-pulsed, mode-locked pumped OPO resonator were the same as used for the previous two—Q-switched, mode-locked pumped—OPO resonator designs (see Section 1 and Chapter 6 for the KTP and BBO devices respectively). To reduce the intracavity power loss, a coated KTP crystal, and coated lenses, were acquired. The round-trip power loss of this modified resonator—resulting from Fresnel reflections—was estimated to be $\sim$5%. This was an order of magnitude smaller than in the previous case (see Section 1). There was, however, still the possibility of loss due to small angle scattering by inhomogeneities in the KTP crystal. This was assumed to be less than $\sim$1%, and hence could be neglected in this case. It would, however, be a significant problem in the low loss resonator that would be needed for efficient operation of a continuously pumped OPO.

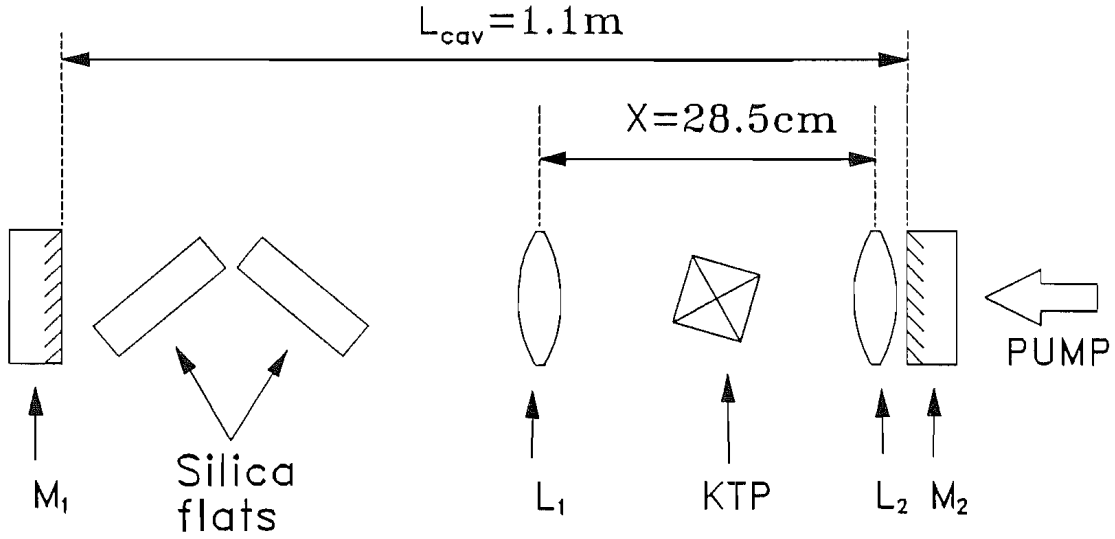

Fig. 7.10 Schematic diagram of the cavity design used during the investigation of the long-pulsed, mode-locked pumped KTP parametric oscillator. M_1, M_2 = plane mirrors (HR 0.7-1.0μm, HT 0.532μm), L_1, L_2 = +13cm lenses.

The cavity design used in this oscillator is shown in Fig. 7.10. The two +13cm lenses are positioned equidistant from the KTP crystal—which was 5.5mm long, and had an aperture of $\approx 5 \times 5 mm^2$—to give a central focus of $\approx 65 \mu m$. The large spot-size outside of the two lenses allows the cavity length to be adjusted by several millimetres without perturbing the focus in the crystal by more than $\pm 5\%$. Allowance was made for the need to adjust the cavity—to achieve synchronism with the pump laser—by mounting mirror M_1 on a micrometer driven translation stage. Finally, as with the previous KTP parametric oscillator, a pair of Brewster flats was introduced into the cavity to prevent doubly-resonant oscillation.

7.2.3 Performance details.

As mentioned in the introduction to this section, the output of the long pulse, mode-locked pumped OPO exhibited poor amplitude stability. It was therefore decided not to investigate it in any detail, other than to verify that the power levels needed to reach oscillation threshold could be reduced by the reduction of cavity losses to a level available from a c.w. flash-lamp pumped mode-locked Nd:YAG laser.

The threshold energy for this system was found to be $0.35 \pm 0.05 mJ$. This corresponded to an equivalent average power (averaged over the FWHM I(t) only) of $\approx 11.5W$, with a peak mode-locked intensity of $\approx 2.2kW$. The corresponding peak pump intensity was found to be $\approx 25 MWcm^{-2}$. Here it has been assumed that, as the harmonic conversion efficiency was low ($< 20\%$), the pump pulses would be a factor of $\sqrt{2}$ shorter in duration than the output $1.064 \mu m$ from the source laser. If this was not the case, then the threshold peak power would—in fact—be lower.

More importantly, the beam quality of the $0.532 \mu m$ pump was very poor. Therefore, to avoid the possibility of damage, resulting from too small a spotsize, the pump beam was focused more loosely than optimal [4]. The measured spotsize was estimated to be $\sim 75 \mu m$; somewhat larger than that of the resonated signal. This is almost a factor of two larger than the optimal focus of $\sim 45 \mu m$, which would have possessed the same confocal parameter as the signal [4]. However, if the optimal focusing had been used, the fractional error in the spotsize would then have been far too large—the spotsize of $45 \mu m$ having been found to be too small to accurately characterize with the diode array, or with a scanning slit on the micrometer stages available (accurate to $\pm 10 \mu m$). Furthermore, the beam quality was found to be too poor to allow the waist size to be deduced from the beam divergence.

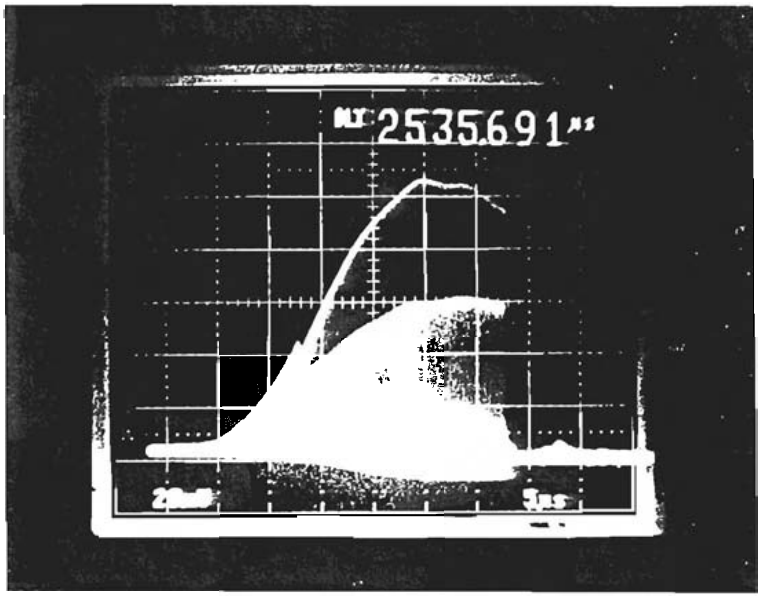

Fig. 7.11 Double exposure photograph showing the depleted 0.532μm pump train superimposed over the undepleted train, for the case of the long-pulsed and mode-locked pumped KTP parametric oscillator.

Using the estimated pump spotsize of $\sim 75\mu$m, and the design spotsize of the resonated signal of $\approx 65\mu$m, the analysis after Brosnan and Byer [25] predicted that the threshold energy would be ~ 0.15-0.20mJ. The agreement is not as good as in the previous two cases; here the experimental value is a factor of 2-2.5 times higher than the theoretical one.

The efficiency of the long-pulse, mode-locked pumped OPO was found in exactly the same way as described in the case of the Q-switched and mode-locked device. At a pump level of three times the threshold value, the overall efficiency was found to be $\approx 20\%$, while the peak efficiency was found to be $\approx 30\%$—only slightly lower than in the case of the Q-switched, mode-locked pumped device. It was found, however, to be a lot more sensitive to length adjustment than the previous devices—a cavity length mis-adjustment of 10-20μm being sufficient to terminate oscillation. This is believed to be solely due to the fact that the single-pass power gain was significantly smaller than in the Q-switched case, and that it consequently takes an order of magnitude more cavity transits until the parametric threshold is reached (From the fact that depletion had reached the same level as obtained in the Q-

switched, mode-locked case, the signal pulse duration was expected to have broadened to a width comparable with the pump).

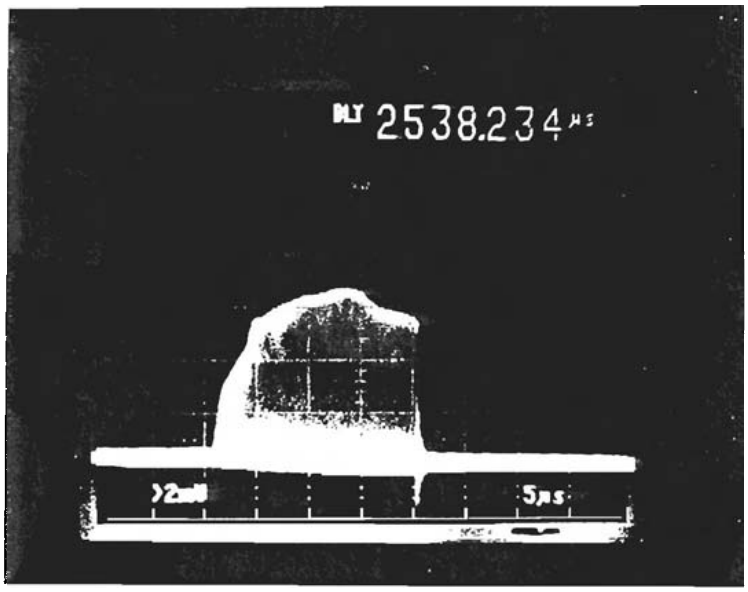

Fig. 7.12 Photograph showing idler output train from the long-pulsed and mode-locked KTP parametric oscillator.

The tuning behaviour of the oscillator was found to agree well with that measured in the case of the Q-switched and mode-locked pumped parametric oscillator (see Section 1). The use of a smaller spotsize did, however, allow the tuning range to be extended slightly (to 1.0-1.13μm), as a greater angular aperture was exploitable.

Unfortunately, neither a value of pulse duration nor bandwidth was determined for this device. An attempt was made to measure these factors, but the instability and low signal level caused severe problems. It was therefore decided that all efforts should be directed to the realization of continuous operation of a parametric oscillator in the near future. When that had been achieved, a more complete study of the synchronously-pumped parametric oscillator would then have been carried out.

7.3 Implementation of a shorter pulse duration pump.

As had been determined from the brief investigation of the long-pulse, mode-locked pumped system, the singly-resonant operation of a parametric oscillator would require a higher peak power than was currently available from c.w. flash-lamp pumped mode-locked Nd:YAG lasers. However, the use of pulse compression [20] offered the means of increasing the peak power—for the same average power—to a level above that needed for the OPO to achieve threshold. A preliminary investigation was therefore initiated using the long-pulse pumped laser, with the plan to implement the scheme with a c.w. flash-lamp pumped laser in the near future, if it was determined that sufficiently efficient pulse compression was achievable.

The technique employed to temporally compress the output pulses from the mode-locked Nd:YAG laser was self-phase modulation in a single-mode optical fibre—in the regime of positive group velocity dispersion [50][21][51]—followed by de-chirping with a diffraction-grating-pair delay line [22].

At a sufficiently high intensity, propagation through an optical fibre results in the broadening of the frequency linewidth of the mode-locked pulses [52] due to self-phase modulation [50], resulting from the optical Kerr effect [53](the intensity dependent refractive index that arises due to the third order susceptibility, $\chi^{(3)}$)[28]). The output pulses not only have a bandwidth several times wider than that of the input, but are also frequency chirped due to group velocity dispersion [51]. This chirp can be removed through the use of a diffraction-grating pair delay line [22], resulting in output pulses with a significantly shorter duration than were incident on the optical fibre (single-stage compressors have reduced pulse durations by as much as ≈ 80 times [54]). However, as the delay due to the grating pair is linear—to first approximation—with respect to frequency, it can only compensate for a linear frequency chirp [20]. If the chirp is *not* linear, it will not be fully removed, and consequently a smaller fraction of the input energy will be compressed into the output pulses. The energy that does not follow the linear chirp will, instead, appear - after the grating pair - in the form of a pedestal; a longer duration, frequency chirped pulse upon which the desired short pulse is superposed.

If the propagation length in the fibre is sufficiently long, it has been shown that the group velocity dispersion acts to almost completely 'linearize' the chirp [51]. In this case, almost all of the energy can then be compressed into the output pulse. However, if the power launched into the fibre is high enough, stimulated Raman scattering ('SRS')[55] can

lead to a significant loss of power (80–90%)[56]. As the threshold for SRS is dependent on the intensity-length product in a given case, it can therefore be avoided by using a short enough length of fibre. This does result in a lower degree of compression, but the final peak power is greater as less of the input energy is lost through SRS.

The practical set-up is shown in Fig. 7.13. M_1, M_2 are 10× microscope objectives, and P_1, P_2, P_3 are 90° prisms. P_1 and P_2 were used as roof-prism retro-reflectors, P_1 displacing the beam horizontally and P_2 displacing it vertically, so that four passes of the grating were possible. Each pair of passes did half the work of removing the chirp, while countering the frequency dependent transverse spreading of the other [54]. The Grating used had a pitch of 1700ℓ/mm, and was optimised for the Littrow reflection of 1.064μm, having an absolute efficiency [57] of 90%.

The fibre used had a large core diameter, and a high birefringence. It was chosen for the former characteristic as this would minimise the probability of damage—the output of the laser already being at quite a high peak power level—and for the latter as this would ensure that the compressor output would have a well defined linear polarization, and could therefore be used efficiently in any subsequent nonlinear processes. The relevant specifications of the fibre used [58]—which was fabricated from undoped silica—are as follows:- (i). 115μm core diameter, (ii). numerical aperture of 0.14, and (iii). cut-off wavelength of 1000nm. Using this information the effective area of the fibre, at 1.064μm, was calculated to be $\approx 2.3\times10^{-11}$m^2. The high birefringence of the fibre was achieved by the use of a 'bow-tie' construction.

The bandwidth acceptance of the KTP crystal used—having a length of $\approx$5mm—was $\Delta\nu_A \approx$ 200GHz, so the 0.532μm pump pulse was required to have a duration of greater than $\approx$2ps (assumed to be transform limited, and have a Gaussian shape). As the input pulse duration was $\approx$85ps, the largest usable compression factor was therefore $\approx$25. It was decided to operate the pulsed laser at a level that provided $\approx$1ms long pulse trains with an overall energy of $\approx$20mJ, to give an equivalent average power of $\approx$20W (averaged over the train), and a peak power of $\approx$1.65kW (pulse duration 85ps, and separation 7.45ns). This is somewhat higher than is available from most c.w. lamp-pumped Nd:YAG lasers, but it can be provided by the higher power variants such as the Coherent Antares ($\approx$25W at 1.064μm). With this peak power, the longest length of fibre that could be used before any loss was incurred from Raman scattering [56] was ~5m, depending on how efficiently the light could be launched into the fibre. Using the theory after Tomlinson *et al* [51], the predicted

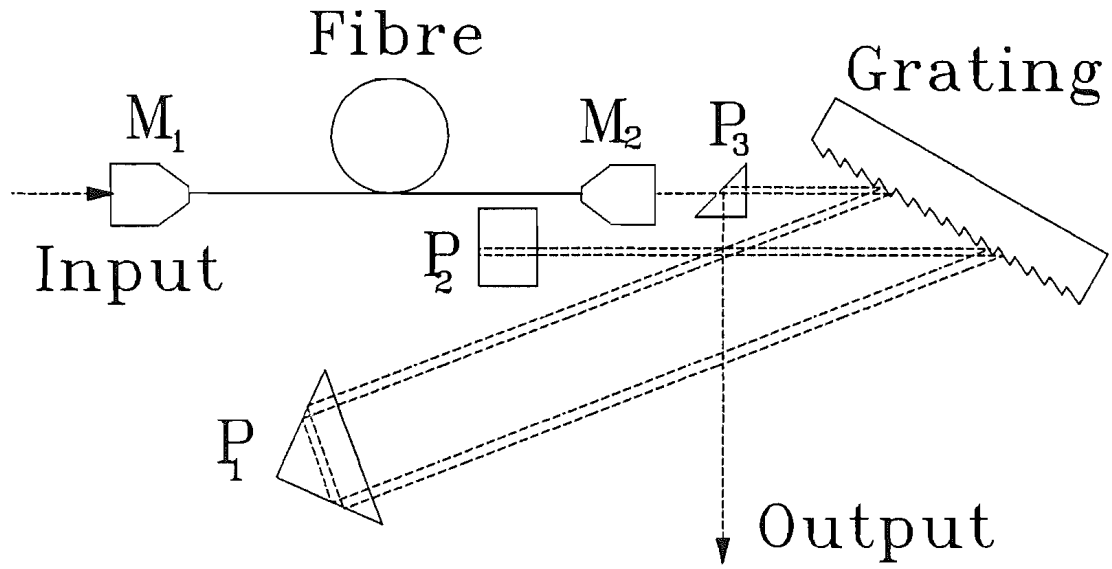

Fig. 7.13 Schematic diagram of the fibre-grating pulse compressor. M_1, M_2 = 10× microscope objectives, P_1, P_2, P_3 = 90° prisms.

compression factor was found to be 20–25, resulting in an output pulse duration of ~3.5–4.5ps. If Raman scattering had not been a problem, a fibre length of ~400m would have led to optimal linearization, and an output pulse duration of ~0.15ps [51]. This would, of course, have been too short to have been of any use with the crystal available, as the bandwidth acceptance would have been exceeded by over an order of magnitude.

The optimal performance was experimentally obtained with a fibre length of ≈7.4m, and a fibre launch efficiency of ≈55%. In this situation the Raman threshold [56] was found to be just exceeded—resulting in a loss of 5–10% of the available power—but the additional pulse compression obtained more than compensated in terms of peak power. The grating compressor was optimised by varying the position of prism P_1 with respect to the grating, while monitoring the harmonic generation efficiency obtained when frequency doubling the output pulses. The pulse duration of the compressor output was then measured using background free second-harmonic autocorrelation [37]. The resulting curve was found to show best agreement with a Gaussian fit (see Fig. 7.14) which suggests that the pulse duration is 3.0±0.3ps—FWHM, I(t).

The output 1.064μm average power was measured to be ≈5.5W. From the measurement of the areas of the pedestal and pulse on the autocorrelation, it was estimated that 50–60% of the output power was compressed into the pulses. This suggested that the

peak power, after compression, should be ≈7kW. It must be mentioned here that all the prisms used at this point of the investigation were uncoated. If anti-reflection coatings (having, say, R<0.5% at 1.064μm) had been applied, then the available average power would have been increased to ≈7.4W, corresponding to a peak power of ≈9.5kW. Assuming a modest conversion efficiency of ≈30%, this would have resulted in ≈2.2W of 0.532μm. If the harmonic pulses were as broad as the fundamental pulses, this would have been equivalent to a peak power of 5.1kW; if the harmonic pulses were a factor of $\sqrt{2}$ shorter again, however, this would have been equivalent to a peak power of 7.2kW. This means that up to 2–3 times the power needed to achieve threshold in the long-pulsed OPO could have been made available.

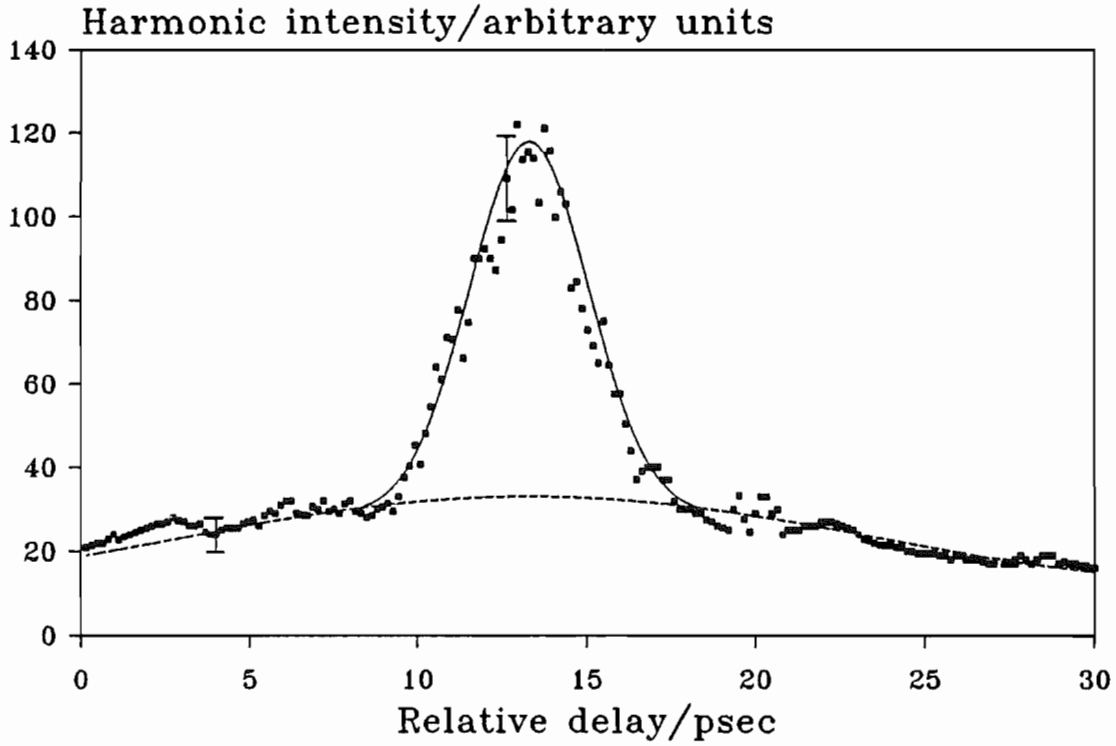

Fig. 7.14 Second-harmonic autocorrelation of compressor output train. The autocorrelation FWHM of the pulse was ≈4.3ps, corresponding to a FWHM for I(t) of ≈3.0ps.

Unfortunately, the subsequent investigation of the OPO pumped by these compressed pulses was not made, due to severe problems with feedback to the laser. When the fibre was aligned to give an efficient launch, the Fresnel reflections from both its end were found to be sufficient to upset the laser mode-locking. This resulted in the regular occurrence of noise bursts. It was felt that these noise bursts could have led to the occurrence of severe damage to the harmonic doubling crystal, given the tight focusing needed to achieve the necessary doubling efficiency.

Various attempts were made to eliminate the feedback. Misalignment of the fibre launch was found to eliminate feedback, but only when sufficient to lead to an unacceptably high reduction in the launch efficiency. Index matching fluid was used to match the fibre ends to anti-reflection coated windows, but the high average power, unfortunately, led to breakdown of the index matching fluid and this had to be abandoned. Finally, the fibre was glued into glass capillary tube with a high temperature epoxy (Epo-tek 353ND, manufactured by Epoxy technology Inc.) and polished at an angle of 30°. This complicated the launching of the laser light, but efficiencies approaching those obtained with the unwedged launch were achieved (45–50%). This did, however, also fail because of the high powers used. In this case it was the epoxy that broke down when the incident intensity approached the required power level ($\approx$20W).

The use of a polarization isolation scheme (quarter-wave plate and polarizing beam-splitter) would have been possible if the fibre used had not been birefringent. In this case, however, randomly orientated, stress induced birefringence in the fibre would have led to depolarization of the fibre output. This would, in turn, have resulted in an unacceptable reduction of the efficiencies of the later parametric processes. Furthermore, the depolarization would have rendered the isolation scheme ineffective as far as the reflection from the far end of the fibre was concerned. The only practical way of achieving isolation in this circumstance would have been through the use of a Faraday isolator [59][60]. Unfortunately, the only Faraday isolator then available was uncoated, and therefore would have introduced severe loss (possibly as much as 50%, including Fresnel and absorption losses), and hence reduced the power available to below the level needed to achieve parametric oscillation.

The continuation of this investigation would have required the acquisition of a high-power, low-loss (i.e. $<5\%$) Faraday Isolator and anti-reflection coated prisms. After demonstration with the pulsed Nd:YAG laser, it would then have required the use of a high power c.w. lamp-pumped Nd:YAG laser. At the time, however, Goodberlet *et al* [61] reported a technique for producing pulses as short as 2ps directly from Nd:YAG lasers using passive mode-locking [62]. These potentially offered the same peak powers as the high power flash-lamp pumped Nd:YAG laser system, as the inherent loss due to the compressor would be avoided. It was decided that such a source offered the optimal route toward continuous operation of a singly-resonant OPO, and further work on compression was therefore suspended.

7.4 Conclusion.

The primary aim of this work was to assess whether it would be possible to achieve continuous operation of a singly-resonant, synchronously-pumped optical parametric oscillator ('OPO') utilizing the material potassium titanyl phosphate ('KTP')[8] as the nonlinear gain medium. The longer term objective was to reduce the threshold power to a level that would allow operation with an actively mode-locked, laser-diode pumped miniature Nd:YAG laser pump source [14].

With this aim in mind, two devices were investigated: a Q-switched, mode-locked pumped, and a long-pulsed, mode-locked pumped OPO. In the case of the Q-switched and mode-locked pumped OPO, good agreement was found between the calculated and experimental values of threshold [25], bandwidth [25], and tuning behaviour [34][10]. Rotation of the KTP crystal about its dielectric z-axis, such that the propagation vector always lay within the xy-plane, gave a tuning range of 1.04–1.09μm, which was limited by the angular aperture of the crystal. The tuning behaviour of the long-pulse pumped device agreed with that found for the Q-switched, mode-locked pumped device, but the experimental threshold was found to be at variance with the theoretical prediction [25]. The threshold power was, however, three orders of magnitude lower than that for the Q-switched and mode-locked pumped OPO.

It was found that pulse compression [21][22][20] could be exploited to obtain the necessary peak powers from a high power c.w. flash-lamp pumped mode-locked Nd:YAG laser. However, to eliminate problems with feed-back, it would have been necessary to acquire a high-power low-loss Faraday isolator [59][60]. This step was not taken, as a passive mode-locking technique had just been reported that offered $\approx$2ps pulses directly from a Nd:YAG laser source [61][63]. It was decided that this offered the best route towards continuous operation of a synchronously-pumped, singly-resonant parametric oscillator, and further work on the OPO was suspended until such a laser could be constructed.

References.

[1]. K. Burneika, M. Ignatavichyus, V. Kabelka, A. Piskarskas, and A. Stabinis.
IEEE J. Quantum Electron. **QE-8**, 574 (1972).

[2]. C. Chen, B. Wu, A. Jiang, and G. You.
Sci. Sinica (Ser. B) **28**, 235 (1985).

[3]. D. Eimerl, L. Davis, S. Velsko, E.K. Graham, and A. Zalkin.
J. Appl. Phys. **62**, 1968 (1987).

[4]. G.D. Boyd and D.A. Kleinman.
J. Appl. Phys. **39**, 3597 (1968).

[5]. H. Komine.
Opt. Lett. **13**, 643 (1988).

[6]. M. Ebrahimzadeh, A.J. Henderson, and M.H. Dunn.
IEEE J. Quantum Electron. **26**, 1241 (1990).

[7]. S. Burdulis, R. Grigonis, A. Piskarskas, G. Sinkevicius, and V. Sirutkaitis, A. Fix, J. Nolting, and R. Wallenstein.
Opt. Commun. **74**, 398 (1990).

[8]. F.C. Zumsteg, J.D. Bierlein, and T.E. Gier.
J. Appl. Phys. **47**, 4980 (1976).

[9]. J.Q. Yao and T.S. Fahlen.
J. Appl. Phys. **55**, 65 (1984).

[10]. T.Y. Fan, C.E. Huang, B.Q. Hu, R.C. Eckardt, Y.X. Fan, R.L. Byer, and R.S. Feigelson.
Appl. Opt. **26**, 2390 (1987).

[11]. P.E. Perkins and T.S. Fahlen.
J. Opt. Soc. Am. B **4**, 1066 (1987).

[12]. R.C. Eckardt, H. Masuda, Y.X. Fan, and R.L. Byer.
IEEE J. Quantum Electron. **26**, 922 (1990).

[13]. H. Vanherzeele.
J. Opt. Soc. Am. A **5**, 87 (1988).

[14]. G.T. Maker and A.I. Ferguson.
Appl. Phys. Lett. **54**, 403 (1989).

[15]. P.A. Franken, A.E. Hill, C.W. Peters, and G. Weinreich.
Phys. Rev. Lett. **7**, 118 (1961).

[16]. A.J. Berry, D.C. Hanna, and C.G. Sawyers.
Opt. Commun. **40**, 54 (1981).

[17]. D.J. Kuizenga.
IEEE J. Quantum Electron. **QE-6**, 694 (1970).

[18]. D.J. Kuizenga.
Opt. Commun. **22**, 156 (1977).

[19]. N.P. Barnes, V.J. Corcoran, I.A. Crabbe, L.L. Harper, R.W. Williams, and J.W. Wragg.
IEEE J. Quantum Electron. **QE-10**, 195 (1974).

[20]. A.S.L. Gomes, A.S. Gouveia-Neto, and J.R. Taylor.
Opt. Quantum Electron. **20**, 95 (1988).

[21]. D. Grischkowsky and A.C. Balant.
Appl. Phys. Lett. **41**, 566 (1982).

[22]. E.B. Treacy.
IEEE J. Quantum Electron. **QE-5**, 454 (1969).

[23]. A.L. Aleksandrovskii, S.A. Akhmanov, V.A. D'yakov, N.I. Zheludev, and V.IO. Pryalkin.
Sov. J. Quantum Electron. **15**, 885 (1985).

[24]. T.A. Driscoll, H.J. Hoffman, R.E. Stone, and P.E. Perkins.
J. Opt. Soc. Am. B **3**, 683 (1986).

[25]. S.J. Brosnan and R.L. Byer.
IEEE J. Quantum Electron. **QE-15**, 415 (1979).

[26]. J.D. Bierlein.
private communication (1989).

[27]. R.S. Craxton, S.D. Jacobs, J.E. Rizzo, and R. Boni.
IEEE J. Quantum Electron. **QE-17**, 1782 (1981).

[28]. Y.R. Shen.
The Principles of Nonlinear Optics (Wiley, 1984).

[29]. J.A. Giordmaine and R.C. Miller.
Appl. Phys. Lett. **14**, 973 (1965).

[30]. R.G. Smith.
Chapter C8, *Laser Handbook* (North Holland, 1972).

[31]. A.E. Seigman and D.J. Kuizenga.
Opto-Electronics **6**, 43 (1974).

[32]. J.A. Giordmaine.
Phys. Rev. Lett. **8**, 19 (1962).

[33]. P.D. Maker, R.W. Terhune, R.M. Nisenoff, and C.M. Savage.
Phys. Rev. Lett. **8**, 21 (1962).

[34]. M.V. Hobden.
J. Appl. Phys. **38**, 4365 (1967).

[35]. R.L. Byer.
Chapter 9, *Quantum Electronics: a treatise, Vol. I* (Academic Press, 1975).

[36]. D.A. Kleinman.
Phys. Rev. **174**, 1027 (1968).

[37]. D. Bradley and G.H.C. New.
Proc. IEEE **62**, 313 (1974).

[38]. H. Kogelnik and T. Li.
Appl. Opt. **5**, 1550 (1966).

[39]. M.F. Becker, D.J. Kuizenga, D.W. Phillion, and A.E. Seigman.
J. Appl. Phys. **45**, 3996 (1974).

[40]. R.B. Weisman and S.A. Rice.
Opt. Commun. **19**, 28 (1976).

[41]. K.Kato.
IEEE J. Quantum Electron. **QE-24**, 3 (1988).

[42]. D.W. Anthon and C.D. Crowder.
Appl. Opt. **27**, 2650 (1988).

[43]. J.D. Bierlein and H. Vanherzeele.
J. Op. Soc. Am. B **6**, 622 (1989).

[44]. R.F. Belt, G. Gashurov, and Y.S. Liu.
Laser Focus **21**, 110 (1985).

[45]. D.J. Gettemy, W.C. Harker, G. Lindholm, and N.P. Barnes.
IEEE J. Quantum Electron. **24**, 2231 (1988).

[46]. C.L. Tang, W.R. Bosenberg, T. Ukachi, R.J. Lane, and L.K. Cheng.
Laser Focus World **26**, 107 (1990).

[47]. D.J. Kuizenga, D.W. Phillion, T. Lund, and A.E. Seigman.
Opt. Commun. **9**, 221 (1973).

[48]. W. Koechner.
Solid State Laser Engineering 2nd Ed. (Springer-Verlag, 1988).

[49]. I.P. Kaminow and E.H. Turner.
Appl. Opt. **54**, 1374 (1966).

[50]. R.H. Stolen and C. Lin.
Phys. Rev. **17A**, 1448 (1978).

[51]. W.J. Tomlinson, R.H. Stolen, and C.V. Shank.
J. Opt. Soc. Am. B **1**, 139 (1984).

[52]. R.A. Fisher, P.L. Kelly, and T.K. Gustafson.
Appl. Phys. Lett. **14**, 140 (1969).

[53]. F. Shimizu.
Phys. Rev. Lett. **19**, 1097 (1967).

[54]. A.M. Johnson, R.H. Stolen, and W.M. Simpson.
Appl. Phys. Lett. **44**, 729 (1984).

[55]. R.H. Stolen, E.P. Ippen, and A.R. Tynes.
Appl. Phys. Lett. **20**, 62 (1972).

[56]. R.G. Smith.
Appl. Opt. **11**, 2489 (1972).

[57]. M.C. Hutley.
Diffraction Gratings (Academic Press, 1982).

[58]. J.E. Townsend.
private communication (1989).

[59]. H. Iwamura, S. Hayashi, and H. Iwasaki.
Opt. Quantum Electron. **10**, 398 (1978).

[60]. D.J. Gauthier, P. Narum, and R.W. Boyd.
Opt. Lett. **11**, 623 (1986).

[61]. J. Goodberlet, J. Jacobson, J.G. Fujimoto, P.A. Schulz, and T.Y. Fan.
Opt. Lett. **15**, 504 (1990).

[62]. J. Mark, L.Y. Yiu, K.L. Hall, H.A. Haus, and E.P. Ippen.
Opt. Lett. **14**, 48 (1989).

[63]. L.Y. Liu, J.M. Huxley, E.P. Ippen, and H.A. Haus.
Opt. Lett. **15**, 553 (1990).

8 Further work.

This chapter starts by summarising the recent developments in the areas relevant to synchronously pumped parametric oscillators; namely those of nonlinear materials, laser sources, and of the parametric oscillators themselves. It then goes on to outline the general direction in which the investigation of the synchronously pumped optical parametric oscillator is currently proceeding, and—under the heading of 'Further extensions'—to consider the problems that will have to be resolved to make the OPO an exploitable source of tunable mode-locked pulse.

8.1 Recent developments.

This section discusses the recent developments of direct relevance to this project. Though only limited progress has been made in the area of nonlinear materials, major advances *have* been in the other two areas of interest; laser and parametric oscillator development.

8.1.1 The nonlinear material.

Development of nonlinear materials for use in the near infrared part of the spectrum over the last few years has been limited. Only one new material of merit has actually become available; lithium borate (LiB_3O_5 'LBO')[1]. The only other new material of interest reported—potassium titanyl arsenate ($KTiOAsO_4$, 'KTA')[2]—is not yet readily available.

LBO is related to—but not isomorphic—with the material BBO [3]. It has a slightly more limited transmission range (200nm–2.5μm [1] c.f. 180nm–2.5μm of BBO [3]), and a smaller nonlinearity ($\sim 60\%$ of that of BBO). It does, however, possess a remarkably high damage threshold for Q-switched pulses ($\approx 25 GWcm^{-2}$), and can also be quasi-noncritically phase-matched—like KTP—for the frequency doubling of a fundamental wavelength of 1.064μm at room temperature. Unlike KTP, it has a sufficient thermal variation of the birefringence to enable it to be temperature tuned to achieve noncritical phase-matching for the aforementioned process (at $\approx 150°C$ [4]). This, along with the high damage threshold, allows high conversion efficiencies to be achieved despite the small nonlinearity. As it does, like BBO, only have a limited transmission range in the infrared, the longest wavelength available from an OPO based on this material is $\approx 2.6\mu$m [5].

KTA [2] is an isomorph of KTP [6]; it has almost identical dispersive properties, transparency and, probably, damage threshold; it is, however, reported to have a nonlinearity

twice as large as that of KTP [2]. Based on the limited information so far available, it is likely that an OPO based on this material will have a potential operating range comparable to that demonstrated using KTP; i.e. wavelengths 0.6–4.5μm. Unfortunately, it is not yet commercially available, but when it does become so it is likely to completely supersede the older material: KTP.

Organic nonlinear materials, such as NNP [7], MAP [8] and MNA [9] have attracted a lot of attention due to their high nonlinearities (e.g. $d_{eff} \approx 85 pmV^{-1}$ for type I harmonic generation of a 1.5μm fundamental in NNP [7]) and damage thresholds (e.g. $\approx 3 GWcm^{-2}$ for MAP [8]). They do, however, only offer limited tuning within the near infrared, as the longest wavelength that any of them transmits is $\sim 2\mu$m. Moreover, the majority of these materials are only now becoming available in sizes large enough to provide sufficient parametric gain at safely usable intensities. One exception is that of the material urea, which has been available with crystal lengths of up to $\sim$20mm for some time [10]; it does, however, have an even more limited infrared transmission range (the longest wavelength transmitted is $\approx 1.4\mu$m). Though the limited transmission ranges of these materials does preclude their use as the gain medium in a widely tunable infrared OPO, when fully developed they will no doubt—because of their high nonlinearities—be widely exploited for use in the 'very-near infrared' and visible regions.

KTP [2] and BBO [3] are currently the most commonly used nonlinear materials for frequency conversion processes; others that find application are urea [10], KD^*P [11], and $LiNbO_3$ [12]. As BBO offers a larger nonlinearity than urea, can transmit further into the ultraviolet, and is markedly less hygroscopic by nature, urea is now used to a much smaller extent. KD^*P still finds wide application in ultra-high power applications, as it is still one of the few nonlinear materials which can be grown to a large size. This allows the fabrication of crystals with a large enough aperture size that damage free operation is possible. Lithium niobate is now being increasingly utilised due to the development of an magnessium oxide (MgO) doped variant [13](see Section 3, Appendix A1). The MgO has been found to increase the photorefractive damage threshold by up to two orders of magnitude as compared with the undoped material [13].

Another material that has recently attracted a lot of interest is potassium niobate ($KNbO_3$). This was first demonstrated to have an exceptionally high second harmonic coefficient—using the powder method—in 1969 [14]. It did, however, prove awkward to grow routinely with high optical quality, and was hence marketed at a prohibitively high

price, which led to the limited application of this material. It is attracting attention now as it noncritically phase—matches—at room temperature—for the frequency doubling of 860nm; a wavelength that is directly available for laser-diodes. This technique offers an efficient source of blue light, and is therefore of much current interest. It is hoped that the increased demand for this material will lead to the development of more efficient growth techniques, and that this will—in turn—lead to the availability of $KNbO_3$ crystals with a higher optical quality, at a lower price. Especially as, with its high nonlinearity and wide infrared transmission range, it will also be of great utility for infrared generation.

Barium sodium niobate ($Ba_2NaNb_5O_{15}$, 'BNN' or 'BSN') was, like potassium niobate, developed several years ago [15], and it, too, proved difficult to grow with a high enough optical quality for use in parametric devices. It does, however, have a nonlinearity comparable to $KNbO_3$; can also be noncritically phase-matched, through temperature tuning, for parametric oscillation with a $0.532\mu m$ pump; and is also unaffected by photorefractive damage. The 'only' disadvantage of BNN compared to $KNbO_3$ is a low surface damage threshold ($\sim 10 MWcm^{-2}$, 10ns pulses at $1.064\mu m$ [16]). Its high nonlinearity does mean that the low damage threshold does not preclude its use as the gain medium in an OPO; BNN has, in fact, been recently used as the gain medium in a continuously pumped doubly resonant optical parametric oscillator (see Subsection 4)[17]. It is, however, likely that $KNbO_3$, when more readily available, will be used in favour of this material, as not only does it match BNN in terms of nonlinearity and walk-off (or rather, lack of walk-off), does also have a higher damage threshold.

8.1.2 Laser sources.

Within the last few years, there have been three advances in the field of laser development that are of importance to this project. The first is the development of a new passive mode-locking technique, the second the application of resonant enhancement to the frequency doubling of mode-locked pulses, and the third, the demonstration of a high power diode-pumped laser source.

The new mode-locking technique developed is known as 'additive pulse mode-locking' ('APM')[18]. It is a passive mode-locking technique that achieves short pulse operation through the use of a nonlinear external cavity. When the length of the external cavity is accurately matched to that of the laser resonator (or to a multiple thereof), it has been found that stable mode-locked pulses rapidly build up from the small inherent fluctuations in the

initial c.w. lasing level. Furthermore, the pulse duration reached appears to be determined solely by the gain bandwidth of the lasing transition. Output pulses of as short as $\approx$2ps have been obtained directly from a Nd:YAG laser; the shortest duration ever obtained from a system based on this material.

In Section 4, Chapter 7, it was mentioned that while a c.w. pumped solid state laser could not directly supply the peak powers necessary to pump a singly-resonant OPO, through the use of compression it would be possible to enhance the peak power to the required level. The disadvantage of pulse compression is that it is inherently lossy, and much of the benefit of pulse compression is wasted due to this loss. What was therefore really required was a technique for providing short pulses directly from the laser, with negligible loss of the available average power.

In the case of active mode-locking using a sinusoidal loss modulation, the pulse duration is inversely proportional to the square root of the mode-locking frequency [19]. The energy per pulse, however, varies inversely to the mode-locking frequency itself, so that the net effect is that the peak power available is also inversely proportional to the square root of the mode-locking frequency. It can therefore be seen that as the pulses get shorter, the peak power available also reduces. What is needed is a technique for providing short duration pulses from a long resonator, such that the pulse duration can be reduced without affecting the pulse energy.

The method most commonly utilised for this purpose in the case of the dye-laser, that of passive mode-locking with a saturable absorber, has been applied to solid state lasers in the past; when used with a Nd:YAG laser it was demonstrated to give pulses of as short as $\approx$3ps [20]. It is, however, only generally applicable in the case of a pulsed flash-lamp pumped solid state laser as the high powers needed to saturate the dye are otherwise unavailable. Furthermore, the dyes also lead to Q-switching, so this technique can not be exploited to generate a continuous train of mode-locked pulses [21].

Additive pulse mode-locking ('APM'), however, has been demonstrated to be able to achieve short pulsed operation even with the low powers currently available from diode-pumped solid-state laser systems. This technique was derived from the use of nonlinear external cavities with mode-locked colour centre lasers, which was found to result in dramatic shortening of the circulating pulse. The technique involves the coherent addition of pulses from a nonlinear external cavity back into the laser resonator. The technique has more

recently been applied to Ti:sapphire and Nd:YAG laser systems using a fibre external cavity. A fraction of the laser output is propagated through the optical fibre, and then fed back into the laser. When the laser and external cavity lengths are accurately matched, and the power incident on the fibre sufficiently high, this technique has been demonstrated to self-start from fluctuations on the initial c.w. lasing level. As was mentioned above, the process has been found to exploit the entirety of the available gain bandwidth of the lasing transition. This has resulted, in the case of Nd:YAG, in output pulse durations of as short as $\approx$2ps. So far, the average output powers that have been obtained from these systems are quite low ($\approx$60mW [18]), as a significant amount of power is lost to the external cavity for purposes of mode-locking. With the implementation of a higher power laser-diode pump for the miniature solid-state laser, however, these systems should be able to offer sufficient peak powers to readily pump a synchronously pumped parametric oscillator (see Section 2).

As diode-pumped lasers have so far only been able to offer relatively low output powers, the harmonic conversion efficiencies achievable—via direct doubling of the output—have been limited. A way to circumvent the shortage of power is through the use of resonant doubling. Resonant optical harmonic generation was first proposed by Ashkin and Boyd in 1966 [22]. They exploited both harmonic and fundamental resonance to achieve enhancements of around an order of magnitude in the available harmonic (compared with that available from single-pass schemes). This technique has since found extensive application in the doubling of low power c.w. lasers. To achieve efficient conversion, a stable laser source, and also a low loss nonlinear material, is required. Fundamental enhancements of around $\sim$10 are now readily achievable, and lead to an enhancement in the available harmonic of around two orders of magnitude.

Recently, the technique of resonant doubling has been applied to the case of mode-locked pulses [22][23]. Efficiencies of $\approx$53% have been achieved for incident average powers of 66mW. As the incident radiation consisted of 12ps pulses at a repetition rate of 366MHz, the corresponding incident peak power was $\approx$15W. The output pulse duration was found to be down to $\approx$9.5ps, so the average output power of 35mW corresponded to a peak power of 10W. The peak conversion efficiency was therefore $\sim$70%. When this technique is applied to the output of a higher power diode-laser pumped system, (average) doubling efficiencies of as high as 80–90% could be achievable.

The final development of interest in the field of laser development concerns *average* power. While passive mode-locking techniques offer the highest peak-to-average power ratio,

their peak output power is still quite low (c.f. flash-lamp pumped systems). To achieve higher peak powers from these systems, a higher average power is going to have to be made available. To achieve a higher average power from a laser, a higher pump power is required. It is only within the few years that the 1W diode array has become widely exploited; both singly and in multiple (polarization coupled) schemes. The power available from arrays is limited by considerations of heat dissipation.

To provide higher powers still from laser-diode sources, the solution has involved the modification of the design used. Instead of trying to push up the power available from a small area device, the area has been increased commensurately with the power to form a longer structure. The resultant 'diode-bars' can provide powers of up to 10-11W, but due to their extended length can not be used efficiently with an end-pumped geometry, as is widely used in the case of the smaller diode array. These devices have, however, been used to side-pump a variety of laser devices. By far the most impressive application has been the side-pumping of tightly folded resonator ('TFR') lasers. In the TFR laser, the resonated beam is folded between two mirrors such that it makes multiple passes through a Nd:YAG slab. The diode-bar is orientated so that each of its elements effectively end-pumps the individual passes. Using this technique with a Nd:YAG slab and a 11W diode-bar, Baer *et al* [24] have achieved c.w. output powers of 3.6W at 1.064μm. Utilising APM with such a system could potentially provide peak powers of up to 18kW; consequently, when this technology becomes more readily available in the near future, the powers available from diode pumped systems will far exceed those required to pump a parametric oscillator.

8.1.3 Synchronously pumped optical parametric oscillators.

In the last few years very little work has been published on the synchronously-pumped parametric oscillator. The work that has been published, however, represents important advances towards the goal of this project; the utilisation of a laser-diode pumped miniature solid state laser to achieve continuous operation of a *singly-resonant* synchronous pumped optical parametric oscillator.

The first demonstration of continuous operation of a synchronous pumped optical parametric oscillator was reported by Piskarskas *et al* in 1989 [17]. The gain medium utilised in this device was a 1cm long barium sodium niobate crystal, and it was pumped by the frequency doubled output of a c.w. flash-lamp pumped Nd:YAG laser. To achieve threshold with the peak powers available, double resonance of the parametric oscillator had

to be exploited. This did lead to a low oscillation threshold, of 28mW average power, but also resulted in a wildly fluctuating output due to clustering and the related gain competition effects. The laser pump source was mode-locked at a repetition rate of 140MHz, and the 0.532μm pump pulse duration was determined to be 40ps. The corresponding peak power at threshold was therefore $\approx$5W. The tuning range of this device was limited, by the reflectivity of the cavity mirrors, to 0.96–1.19μm.

The first demonstration of synchronously pumped operation of an OPO using the output of a frequency-doubled diode-pumped miniature Nd:YAG laser was reported by Maker and Ferguson in 1989 [25]. To provide the necessary peak power from the actively mode-locked laser, Q-switching had to be exploited. Even then it was only possible to achieve near degenerate operation of a doubly resonant device. Oscillation threshold was reached for an incident energy (at the OPO crystal; 3mm long, MgO:$LiNbO_3$) of 7.5μJ. The Q-switched train at 0.532μm had a FWHM of 65ns, and consisted of $\approx$7.5ps pulses at a repetition rate of 360MHz. The peak power at threshold therefore corresponds to 18–19kW. The tuning range of this device, like the previous one, was limited by the cavity mirror reflectivities to 0.98–1.12μm. It also suffered from poor stability due to the fact that it was doubly resonant.

The most impressive result attained within the last few years has been the continuous operation of a *singly*-resonant synchronously pumped optical parametric oscillator [26]. It is also the first OPO to operate within the femtosecond time domain. To achieve oscillation threshold, however, advantage had to be taken of the high intracavity powers available within a colliding pulse mode-locked (CPM) dye-laser. The OPO cavity was interlinked with that of the CPM dye-laser at the position of the 1.4mm long KTP crystal. The device was pumped at 620nm, and could be tuned from 820–920nm (signal), 1.90–2.54 (idler); as limited by the cavity mirrors. With replacement mirror sets, the available tuning range should be $\approx$0.7–4.5μm. The OPO resonated in two counter propagating directions, leading to two outputs of 2mW each. The output pulse duration was found to be $\approx$220fs in the uncompensated case, and when intracavity dispersion compensation was added to the OPO cavity, the pulse duration was reduced to 105fs.

More recently Laenen *et al* [27] have managed to achieve even shorter pulses from a parametric oscillator. The parametric oscillator was based on a 6mm long BBO crystal, and pumped by the amplified and frequency doubled output of an actively mode-locked pulsed flash-lamp pumped Nd:glass laser. Pulse durations of as short as 65fs were achieved for near degenerate operation. Though this system does not represent a step towards continuous

operation with a diode-laser pump source, it did exploit one usable technique; that of double-pass pumping. This can reduce the power required to reach oscillation by ~ 2 times, and is therefore a technique that will no doubt find further usage. In this case it was also exploited to partially compensate for group velocity mismatch between the pump and signal, which allowed short pulse operation without recourse to the utilisation of a prism compensation scheme.

8.2 Future directions.

Work is now in progress towards the realization of continuous operation of a singly-resonant synchronously pumped optical parametric oscillator using a laser-diode pumped, mode-locked miniature Nd:YAG laser. The results reported in the last few years, and contained within this thesis, suggest that the stage has now almost been reached where this is a readily achievable goal.

The pump system currently under development is based on an additive pulse mode-locked Nd:YAG laser. With the exploitation of a diode-laser pump power of 2W or higher, it should be able to supply ≈ 500mW (average power) of 1.064μm output. If the cavity length used is ≈ 1.5m, and the pulse duration achieved is ≈ 2ps, then the corresponding available peak power will be ≈ 2.5kW. The exploitation of resonant doubling should be capable of converting at least 50% of the (average) power to 0.532μm. Assuming a factor of $\sqrt{2}$ due to the frequency conversion process, the available peak powers could be as high as ≈ 1.8kW. The experimentally obtained threshold, in the case of the long-pulse, mode-locked OPO as described in Section 2, Chapter 7, was a peak power of ≈ 25MWcm^{-2}. If a pump focus of $\approx 30\mu$m is used, the peak power needed to achieve this intensity is ≈ 350W. This is a factor of ~ 5 lower than the power that should be available.

8.3 Further developments.

Once continuous operation of a singly-resonant parametric oscillator has been achieved, work will then commence on improving the performance of the device to a level at which it could be usefully exploited as a research tool. The ultimate goal of this project was to produce a *widely tunable* source of mode locked pulses, and so extension of the tuning range is a major priority. The possibility of extension to ultrashort operation is also considered.

8.3.1 Extension of the tuning range.

The material potassium titanyl phosphate has one major disadvantage; to access a wide tuning range the crystal must be tilted significantly off-normal with the z-axis. As the predominant birefringence is between the z and x (or y) axes, this results in a large Poynting vector walk-off. When phase-matched for degenerate operation at $1.064\mu m$ for propagation in the zy-plane, the Poynting vector walk-off at $0.532\mu m$ is $\approx 32mrad$. This limits the minimum focusing in a 5mm long KTP crystal to $\approx 0.16mm$, which is ~ 5 times larger than the spotsize utilised in the estimation in Section 4. It therefore needs a power of ~ 25 times higher to achieve the same intensity. The required peak intensity is known to be $\approx 25MWcm^{-2}$ (Section 2, Chapter 7), which could be achieved with a $\approx 30\mu m$ spotsize through the use of a peak pump power of $\approx 350W$. In the case of a 0.18mm spot size, however, the pump power requirement is increased to $\approx 10kW$. While this can in principle be provided by a 10W diode-bar pumped TFR laser (see Subsection 2, Section 1), it is a factor of ~ 5 times more than the power available with a conventionally pumped (e.g. 2x1W diode arrays) miniature laser system.

One way in which the tuning range could be extended without incurring the problem of walk-off would be through the exploitation of a nonlinear material that can be temperature tuned for noncritical phase-matching (NCPM). Two nonlinear materials of interest that can offer NCPM with a $0.532\mu m$ pump are $KNbO_3$ and MgO:$LiNbO_3$ (see Subsection 1, Section 1). Both of these materials can be tuned over—at least—the region $0.68\text{-}2.5\mu m$. MgO:$LiNbO_3$ has in its advantage the fact that it phase-matches for degeneracy at $\approx 110°C$ [28], as opposed to the higher temperature of $\approx 180°C$ [29] for $KNbO_3$. Even *MgO doped* $LiNbO_3$, however, is prone to optical damage, whereas $KNbO_3$ is unaffected by this process.

Angle tuning does, however, generally offer a wider range of accessible wavelengths. It also allows for the more rapid adjustment of the operating point of the OPO. Consequently, there is sufficient reason to develop a technique that will allow the exploitation of angle tuning with the pump powers that are currently available. This will necessitate a reduction in the level of peak pump power required to reach threshold (see Subsection 2). Though not strictly necessary in the case of the TFR laser systems, it would allow the OPO to be operated at powers of more than (the readily achievable) two times the threshold value (see Section 2). This is preferable, as it offers higher conversion efficiencies and amplitude stability.

Before going on to discuss possible ways of increasing the margin between threshold and available power, a brief note on the extension to wavelengths outside the near infrared. To achieve longer wavelengths, materials such as $AgGaS_2$ and $AgGaSe_2$ could be utilised with direct pumping by the output of the miniature solid state laser. These materials have been demonstrated to be capable of generating wavelengths of as long as $\approx 11\mu m$ in the case of Q-switched operation, but as they exhibit significant absorption ($\sim 0.1 cm^{-1}$, equivalent to a loss of $\sim 5\%$ over a propagation length of 5mm) are not suitable for use in a continuously operated OPO. This is one area of materials research where there is much scope for the development of new materials.

To achieve shorter wavelengths from a solid state laser pumped OPO, multiple frequency conversion processes will be necessary in addition to that of the parametric oscillator. With the exploitation of resonant doubling, the overall efficiency of the multiple process should be independent of the order in which the processes are performed. The argument for performing all up-conversion processes prior to pumping the OPO, is that the OPO would then be the only stage required to be tunable. If the OPO output is to be doubled, however, then a tunable frequency conversion stage would also be necessary.

8.3.2 Techniques to reduce the power requirement.

The first thing that must be done in order to reduce the power required for an OPO to reach threshold is to minimise the cavity losses. The cavity loss in the OPO described in Section 2, Chapter 7, was $\approx 5\%$ (round trip power loss). As the threshold in the case of the singly resonant OPO scales proportionally to the loss, a reduction of its value to $\approx 1\%$ (about the lowest practically feasible value) can offer a five-fold reduction in threshold. This is a reasonably significant amount. In the case of the TFR laser, it would then be able be possible to operate the OPO at about an order of magnitude above threshold. In the case of the 2x1W diode array pumped source, however, it is still not sufficient to allow threshold to be achieved.

One way to achieve oscillation at lower powers would be to exploit double resonance. This does offer a reduction in threshold of up to two orders of magnitude, but is undesirable from the point of view of stability. As mentioned in Section 1, Chapter 2, the instability of the doubly resonant OPO arises from the requirement to simultaneously resonate both signal and idler wavelengths. If the mode spacing is not identical for both signal and idler, oscillation can only be achieved at discrete clusters of frequencies that correspond to the pairs

of available signal and idler modes that are most nearly phase-matched. As the relative gain seen by each pair of signal and idler modes is sensitively dependent on the cavity length and pump frequency, even a slight variation in these quantities can lead to a significant frequency and amplitude excursions of the OPO output. If the cavity length at the signal and idler frequencies *could* be accurately matched, however, it would be possible to virtually eliminate clustering. In the case of a type II phase-matched OPO, this could potentially be achieved through the insertion of a variable wave-plate into the OPO resonator. With the synchronously pumped system, the length matching needs to be accurate enough that all modes across the acceptance bandwidth are accurately phase-matched. This would require interferometric stabilization of the relative lengths of the signal and idler cavity lengths, which while feasible, would result in a considerable complication in the design of the system.

Another way to reduce the threshold of a parametric oscillator is by the use of double-pass pumping. This can take two different forms. The first, and potentially most beneficial case, is when all three of the interacting field are totally reflected, and make a second pass through the crystal in synchronism. This is, however, only optimally efficient if the relative phase on re-entrance to the crystal is the same as on exit (which leads to a threshold of one quarter of that obtainable in the case of the equivalent single-pass pumped device)[30]. If the relative phase is not preserved, then the threshold is not significently different to that in the single pass case. The alternative case is when only the resonated wave and pump are reflected back through the crystal. In the case of total reflection, this provides a two fold reduction in the parametric threshold of the device, which is insensitive to the relative phase-lag between the pump and idler fields. This scheme also has the advantage that it can be readily adapted for use in a non-collinear pump scheme. In the case of a synchronously pumped parametric oscillator, the ability to adjust the round trip path-lengths travelled by the signal and pump independently allows for compensation of the group velocity mismatch in the crystal [28].

A third way to obtain the high intensities necessary for oscillation is via the utilization of intracavity pumping. Synchronous pumping—at ≈ 830nm—of an intracavity parametric oscillators has been demonstrated with a continuously mode-locked dye-laser [31]. At this time, however, all efficient solid state lasers operate in the near infra-red region of the spectrum, and consequently this technique is only applicable to parametric oscillators operating at wavelengths of $\sim 1.5\mu$m and longer. While possible in theory, the inclusion of a frequency doubling crystal and a parametric oscillator in the same cavity is not likely to be viable in practice. The gain competition between the various nonlinear effects would lead to

frequency and amplitude instabilities. It is possible, however, to frequency double the output of the intracavity pumped OPO to achieve shorter wavelength as required. If correctly optimised, the total tunable output power (signal and idler) available from an intracaviy OPO approaches the amount which is available from the same laser if optimally output coupled (note. signal and idler energies are partitioned according to frequency)[32].

The techniques developed for the resonant enhancement of the fundamental wavelength in resonant doubling [23][24] could potentially be exploited in a similar way for the pumping of a parametric oscillator. As neither the resonated pump or signal can afford the degree of loss that would be incurred by passage though a mirror, this would involve the use of a non-collinear pump geometry comprised of two interlocking cavities. It is consequently only practically applicable to singly-resonant devices; the exploitation of this technique in the case of the DRO would involve the synchronism of three separated cavities. In the case of resonant doubling, enhancements of ~ 20 times have been achieved using conventional cavity designs. Applied to the OPO this would lead to ~ 20 times the available small-signal parametric gain, and a corresponding effective reduction in threshold. Though not as significant as the reduction achieved in exploiting double-resonance, it does avoid the problem with clustering effects, as the idler is non-resonant.

8.3.3 Ultrashort pulse operation.

The inherently wide bandwidth of the parametric interaction allows operation of parametric devices using ultrashort pulse durations. The first demonstration of parametric oscillation in the femtosecond regime was reported by Edelstein *et al* [26], where 105fs pulses were generated by an OPO—based on KTP—pumped intracavity by a colliding-pulse dye laser. More recently, Laubereau *et al* [27], have achieved even shorter duration pulses of 85fs from a BBO parametric oscillator pumped by the amplified and frequency doubled output of a flash-lamp pumped Nd:Glass laser.

There are two advantages of utilising ultrashort duration ($\sim$ 1ps, and under). Firstly, for many materials, the damage threshold has been found to be dependent on energy—not power—density [33] in this situation. It is therefore possible to increase the peak intensity beyond the value that would cause damage in the case of a Q-switched pulse, as long as the total energy is kept low (The use of a low pulse repetition rate ensures that the average power corresponding to a given peak value is also kept low, which should minimise problems relating to average power). Secondly, the spectral aperturing of the crystal can be exploited

to limit the oscillation bandwidth, hence avoiding the need for additional linewidth control elements—and hence additional loss—in the cavity.

As mentioned before, the usable gain length for a given pulse duration is limited by dispersion. It can be shown that the acceptance bandwidth of a nonlinear crystal—for a given process—is inversely proportional to its length. Consequently, a reduction in pulse duration will necessitate a proportional reduction in crystal length to avoid a reduction in efficiency due to spectral aperturing. If the focusing, and hence intensity, is left unchanged, this would lead to a reduction in the available parametric gain. However, if the pump spotsize is reduced with the square-root of the pulse duration, then the parametric gain can be preserved. This does, however, ignore damage. The energy density can be shown to increase inversely to the pulse duration. Consequently, it is not possible to make the pulse duration, and therefore crystal, arbitrarily short and still maintain a given level of parametric gain.

References

[1]. C. Chen, Y. Wu, A. Jiang, B. Wu, G. You, R. Li, and S. Lin.
J. Opt. Soc. Am. B **6**, 616 (1989).

[2]. J.D. Bierlein, H. Vanherzeele, and A.A. Ballman.
Appl. Phys. Lett. **54**, 783 (1989).

[3]. C. Chen, B. Wu, A. Jiang, and G. You.
Sci. Sinica (Ser. B) **28**, 235 (1985).

[4]. J.T. Lin, J.L. Montgomery, J.R. DeSalvo, and A.M. Horner.
CLEO'90 Technical Digest, Abstract **CWF40** (1990).

[5]. E. Ebrahimzadeh, G. Robertson, M.H. Dunn, and A.J. Henderson.
CLEO'89 Technical Digest, Abstract **CDDP** (1990).

[6]. F.C. Zumsteg, J.D. Bierlein, and T.E. Gier.
J. Appl. Phys. **47**, 4980 (1976).

[7]. J. Zyss, I. Ledoux, D. Josse, R. Hierle, A. Perigaud, and J. Baden.
CLEO'90 Technical Digest, Abstract **CWJ1** (1990).

[8]. J.L. Oudar and R. Hierle.
J. Appl. Phys. **48**, 2699 (1977).

[9]. K. Kato.
IEEE J. Quantum Electron. **QE-16**, 1288 (1980).

[10]. C. Cassidy, J.M. Halbout, W. Donaldson, and C.L. Tang.
Opt. Commun. **29**, 243 (1979).

[11]. R.S. Craxton, S.D. Jacobs, J.E. Rizzo, and R. Boni.
IEEE J. Quantum Electron. **QE-17**, 1782 (1981).

[12]. G.D. Boyd, R.C. Miller, K. Nassau, W.L. Bond, and A. Savage.
Appl. Phys. Lett. **6**, 234 (1964).

[13]. D.A. Bryan, R. Gerson, and H.E. Tomaschke.
Appl. Phys. Lett. **44**, 847 (1984).

[14]. S.K. Kurtz and T.T. Perry.
J. Appl. Phys. **39**, 3798 (1969).

[15]. J.E. Geusic, H.J. Levinstein, J.J. Rubin, S. Singh, and L.G. Van Uitert.
Appl. Phys. Lett. **11**, 269 (1967).

[16]. J.E. Murray, R.J. Pressley, J.H. Boyden, and R.B. Webb.
IEEE J. Quantum Electron. **QE-10**, 263 (1974).

[17]. A. Piskarskas, V. Smil'gyavichyus, and A. Umbrasas.
Sov. J. Quantum Electron. **18**, 155 (1988).

[18]. J. Goodberlet, J. Jacobs, J.G. Fujimoto, P.A. Schulz, and T.Y. Fan.
CLEO'90 Technical Digest, Abstract **TuB6PD** (1990).

[19]. D.J. Kuizenga, D.W. Phillion, T. Lund, and A.E. Seigman.
Opt. Commun. **9**, 221 (1973).

[20]. D.J. Bradley and W. Sibbett.
Opt. Commun. **9**, 17 (1973).

[21]. H.W. Mocker and R.J. Collins.
Appl. Phys. Lett. **7**, 270 (1965).

[22]. A. Ashkin, G.D. Boyd, and J.M. Dziedzic.
IEEE J. Quantum Electron. **QE-2**, 109 (1966).

[23]. G.T. Maker and A.I. Ferguson.
Appl. Phys. Lett. **55**, 1158 (1989).

[24]. T.M. Baer, D.F. Head, and P. Gooding.
CLEO'90 Technical Digest, Abstract **CMF2** (1990).

[25]. G.T. Maker and A.I. Ferguson.
Appl. Phys. Lett. **54**, 403 (1989).

[26]. D.C. Edelstein, E.S. Wachman, and C.L. Tang.
Appl. Phys. Lett. **54**, 1728 (1989).

[27]. R. Laenen, H. Graener, and A. Laubereau.
Opt. Commun. **77**, 226 (1990).

[28]. M.V. Hobden and J. Warner.
Phys. Lett. **22**, 243 (1966).

[29]. Y. Uematsu.
Jap. J. Appl. Phys. **13**, 1362 (1974).

[30]. S.E. Harris
Appl. Phys. Lett. **14**, 335 (1969).

[31]. D.C. Edelstein, E.S. Wachman, and Tang.
Appl. Phys. Lett. **12**, 123 (1989).

[32]. M.K. Oshman and S.E. Harris.
IEEE J. Quantum Electron. **4**, 491 (1968).

[33]. E.S. Bliss.
Opto-Electronics **3**, 99 (1971).

Conclusion.

This work was aimed at the eventual development of a stable source of mode-locked pulses that could be tuned throughout the near infrared. The continuously operated, synchronously pumped, singly-resonant optical parametric oscillator offered the wide tunability [1], but for stable operation placed considerable demands on the frequency and amplitude stability of the pump source. The laser-diode pumped actively mode-locked miniature solid-state laser [2] possesses both of these properties, but at the time that this project commenced could not provide the high peak, output powers required for a parametric oscillator (based on one of the currently available nonlinear materials) to reach threshold.

It was therefore decided to first investigate the feasibility of achieving continuous operation of a singly-resonant optical parametric oscillator with the higher pump powers available from a c.w. lamp pumped mode-locked Nd:YAG laser. The experience gained from these investigations would be directly applicable to the planned work with the laser-diode based system. Consequently, when miniature lasers *could* offer the required powers, the majority of the necessary development of the OPO design would already have been completed.

To this end, three synchronously pumped optical parametric oscillators were investigated. The first, utilising the material barium borate ('BBO')[3], and the amplified and frequency doubled output of a Q-switched, mode-locked laser as the pump source, was found to provide a wide tunability (≈ 0.66–2.7μm). The high Poynting vector walk-off in BBO did severely limit the possible reduction in threshold, precluding the possible use of this material as the gain medium in a continuously mode-locked system. The experience gained with this system was valuable, however, as it provided an appreciation of the requirements of synchronously pumped parametric oscillators.

At the point that the initial investigation with BBO was coming to completion, it became possible to obtain the nonlinear material potassium titanyl phosphate ('KTP') [4]. While this material does not possess as high a damage threshold as BBO, its nonlinearity is somewhat larger. Of more importance, quasi-noncritical phase-matching of this material is possible for near degenerate operation of an OPO when pumped at 0.532μm. While this condition severely limits the tuning range, it does allow the use of a very tight pump focus. This material therefore offered a far better chance of achieving continuous operation than

BBO, as the intensity required for threshold would be available with a much lower pump power.

The second OPO investigated therefore utilised KTP - rather than BBO - as the gain medium. Instead of directly implementing a tight focus in an attempt to achieve operation at the power level that would be available from a c.w. pumped mode-locked laser, it was decided to first gain familiarity with KTP using a pump configuration that was similar to the one used with the BBO device; thus taking advantage of the experience already gained. This was to be a useful preliminary stage before moving to a configuration in which one could get a more direct measure of the power requirements for a continuously pumped system.

The final OPO investigated was also based on the gain medium KTP, but used the amplified and doubled output of the pulsed laser as pump source. In this case, threshold was obtained at an incident, peak power of $\approx$2kW, which in this case corresponded to an average 0.532μm power of 11.5W. Though this peak power was still in excess of that directly available from a c.w. lamp-pumped laser, it was potentially achievable through the exploitation of pulse compression [5]. An initial investigation of pulse compression was therefore made using a pulsed Nd:YAG laser; if the required degree of compression was found to be achievable, it was then planned to utilise this technique with a c.w. flash-lamp pumped laser to synchronously pump an OPO based on the material KTP. The pulse compressor *was* found to provide the necessary enhancement of peak power, but it was also found to cause gross fluctuations of the laser output. This was due to feedback from the ends of the optical fibre that was being used to frequency-broaden the mode-locked pulses. The fluctuations were large enough that, to avoid damage to the KTP crystal used to generate the 0.532μm pump, the degree of focusing usable was limited to such an extent that the efficiency necessary to provide the required pump power could not be achieved. The problem of feedback could in principle have been eliminated, by the utilisation of a low loss Faraday isolator. However, this step was not taken as, in the course of this work, it was reported that additive pulse mode-locking could provide pulses with a duration of under 2ps directly from a Nd:YAG laser [6]. This eliminated the necessity for pulse-compression, thereby avoiding the power loss inherent in that process. It was concluded that the exploitation of such a source offered the best possible route towards continuous parametric oscillation, and hence the work on compression was terminated.

The output pulse duration from an additively mode-locked laser is—unlike its actively mode-locked counterpart—solely determined by the gain bandwidth of the gain medium

utilised. This allows pulses of a short duration to be generated by a laser with a long resonator. In the actively mode-locked case, the pulse duration has been coupled to the cavity length, due to the sinusoidal nature of the loss-modulation used to achieve mode-locking. Consequently, in the additively mode-locked case, a higher peak power is available for the same average power. It is this technique that makes it possible for a laser-diode pumped miniature Nd:YAG laser to now offer the peak powers required for the operation of a synchronously pumped OPO.

The use of a short pulse duration pump source to pump an OPO has other advantages aside from the provision of an intensity sufficient to achieve oscillation. The damage threshold of many materials has been found to be dependent on the energy density when the incident pulse duration is of short enough duration ($\sim$ 1ps)[7]. This allows high peak power densities to be used—and hence high parametric gains to be achieved—without the occurrence of damage. Furthermore, if the crystal length is chosen such that the acceptance bandwidth of the parametric process is comparable with the pump pulse, the requirement for line-width control is eliminated.

The conclusion reached is that operation of a singly-resonant optical parametric oscillator *is* possible with the peak powers now available from laser-diode pumped Nd:YAG lasers; but only when the technique of additive pulse mode-locking [6] is used to provide short pump pulses from a long resonator. In the future, with the development of more powerful laser-diodes, and the use of side-pumped, multi-pass slab geometries [8], the necessary peak power will be available even in the case of longer mode-locked pulse durations. The use of short pulse durations does, however, offer better damage resistance and also eliminate the necessity for linewidth control, and is therefore likely to be the norm.

Finally, with the achievement of lower thresholds and improved efficiencies, the stability and reliability offered by the solid-state laser pumped optical parametric oscillators will find wide application in the research environment. Not only does the OPO offer wide tunability; it offers tunability in regions of the spectrum where none was available before. In particular, the ability to supply wavelengths within the mid-infrared makes these systems attractive to those working in the fields such as biochemistry and solid state physics, where there are currently few sources of radiation that can supply the ultrashort pulses necessary for the investigation of transient events. It is even possible that the synchronously pumped parametric oscillator will eventually become the most widely utilised source of mode-locked pulses.

References.

[1]. K. Burneika, M. Ignatavichyus, V. Kabelka, A. Piskarskas, and A. Stabinis. IEEE J. Quantum Electron. **QE-8**, 574 (1972).

[2]. G.T. Maker and A.I. Ferguson. Appl. Phys. **54**, 403 (1989).

[3]. C. Chen. B. Wu, A. Jiang, and G. You. Sci. Sinica (Ser. B) **54**, 403 (1989).

[4]. F.C. Zumsteg, G.D. Bierlein, and T.E. Gier. J. Appl. Phys. **47**, 4980 (1976).

[5]. D. Grischkwosky and A.C. Balant. Appl. Phys. Let. **41**, 1 (1981).

[6]. J. Goodberlet, J. Jacobson, J.G. Fujimoto, P.A. Schulz, and T.Y. Fan. CLEO'90 Technical Digest, Abstract **TuB6PD** (1990).

[7]. E.S. Bliss. Opto-Electronics **3**, 99 (1971).

[8]. T.M. Baer, D.F. Head, and P. Gooding. CLEO'90 Technical Digest, Abstract **CMF2** (1990).

A1 Nonlinear materials.

The purpose of this appendix is to give further information on the various nonlinear materials that were briefly mentioned in Section 4, Chapter 3 and Section 1, Chapter 8. The discussion is limited to those materials that are currently available, or should become so in the near future, which could potentially be of use as the gain medium in a widely tunable, continuously mode-locked, synchronously pumped optical parametric oscillator operating within the near infrared part of the spectrum. There is mention of neither the material potassium titanyl phosphate ('KTP')[1] nor barium borate ('BBO')[2] here, as these were discussed in some detail in Chapter 4 (Sections 4 and 5 respectively).

Another material that will not be further discussed is potassium di-deuterium phosphate ('KD*P')[3]. As mentioned in Section 4, Chapter 3, while it does possess a high damage threshold ($\sim 4 GWcm^{-2}$, for Q-switched pulses at $1.064\mu m$), and a low temporal walk-off ($\approx 0.08 ps \cdot mm^{-1}$), it can not provide the gain necessary for the operation of a continuously mode-locked OPO. Its small nonlinearity ($\sim 0.5 pmV^{-1}$), and high Poynting vector walk-off, limits its effective use to the cases where high powers are available (e.g. pulsed systems).

Attention will be drawn to the properties of the materials that pertain to operation with ultrashort pulses ($<5ps$). Under these operating conditions, the damage behaviour of many materials has been found to be solely dependent on the energy—not power—density [4]. It is also in this operating regime that bandwidth acceptance and temporal walk-off must be carefully considered, as they can severely limit the crystal length that can be efficiently utilised. If temperature tuning of the material is possible, it has been assumed that this would be used in preference to the alternative of angle tuning.

A1.1 Potassium titanyl arsenate ($KTiOAsO_4$).

Potassium titanyl arsenate ('KTA')[5] is a recently introduced material that is, as its name may suggest, isomorphic with the material potassium titanyl phosphate ('KTP') [6]. The majority of its properties including transparency ($0.35\text{-}4.5\mu m$ [5])—are comparable with those of the older material. An important exception is that of its nonlinearity, which has been found, from the measurement of the small-signal doubling efficiency ($1.053\mu m$ fundamental), to be $\approx 60\%$ larger than that of KTP [5].

The damage threshold for this material has not yet been determined, but it has been exposed to intensities of greater than $\approx 350 MWcm^{-2}$ without incurring damage [5]. As it has been found to exhibit lower bulk scattering losses, and a lower ionic conductivity, it is thought to have a lower number of crystal defects than KTP [5]. It has been suggested that this lower number of defects might result in KTA possessing a damage threshold that is somewhat higher than that of the older material [5].

The principle refractive indices of KTA have been measured at $1.064\mu m$ and $0.633\mu m$ [5], and were found to be all $\approx 2.5\%$ higher than the corresponding values for KTP. The fact that all are scaled by roughly the same ratio suggests that the fractional birefringence of KTA is close to that of KTP, and that it should therefore exhibit similar angular behaviour (i.e. tuning, angular acceptance, etc.). This has been confirmed by the determination of the locus of tuning angles (θ,ϕ) for type II doubling of $1.064\mu m$ [5], which was found to closely follow the behaviour of KTP [5], and of the angular acceptance, which—for propagation perpendicular to the z-axis—is $\approx 0.4°cm^{-2}$ [5]; somewhat smaller than, but comparable to, the value of $\approx 0.5°cm^{-2}$ for KTP [7]. A set of Sellmeier's equations is not yet available for this material, and consequently it was impossible to calculate the tuning behaviour for the case of a $0.532\mu m$ pumped parametric oscillator. It is likely, however, that this will also follow the behaviour shown by KTP.

As the refractive indices of KTA are comparable with those of KTP, the dispersive behaviour is also likely to be similar. Consequently, the shortest pulses usable with a given length of this material will be of a comparable duration to those usable with the same length of KTA. However, as KTA has a larger nonlinearity, the gain available at a given intensity will be significantly higher (about two times higher in the small signal case).

The absorption characteristics of KTA have not yet been determined, but are likely to be comparable to that of KTP. KTA has, however, been reported to exhibit a slight yellow colouring [5], and it is therefore likely that this material exhibits significant absorption in the blue.

A1.2 Lithium iodate ($LiIO_3$).

Lithium iodate ($LiIO_3$) is a negative uniaxial crystal of point group 6. It has a high nonlinearity ($d_{15}=5.5\pm 0.3 pmV^{-1}$ [8]), and is transparent from $0.3\text{-}5.5\mu m$ [9].

$LiIO_3$ phase-matches at 30° for the type I frequency doubling of a fundamental wavelength of 1.064μm. As the effective nonlinear coefficient for type I interactions in materials of point group 6 is given by $d_{eff}=d_{15}\sin\theta$ [10], the corresponding value at 30° is $\approx$2.8pmV^{-1}; comparable with the value of $\approx$3.2pmV^{-1} for KTP [11].

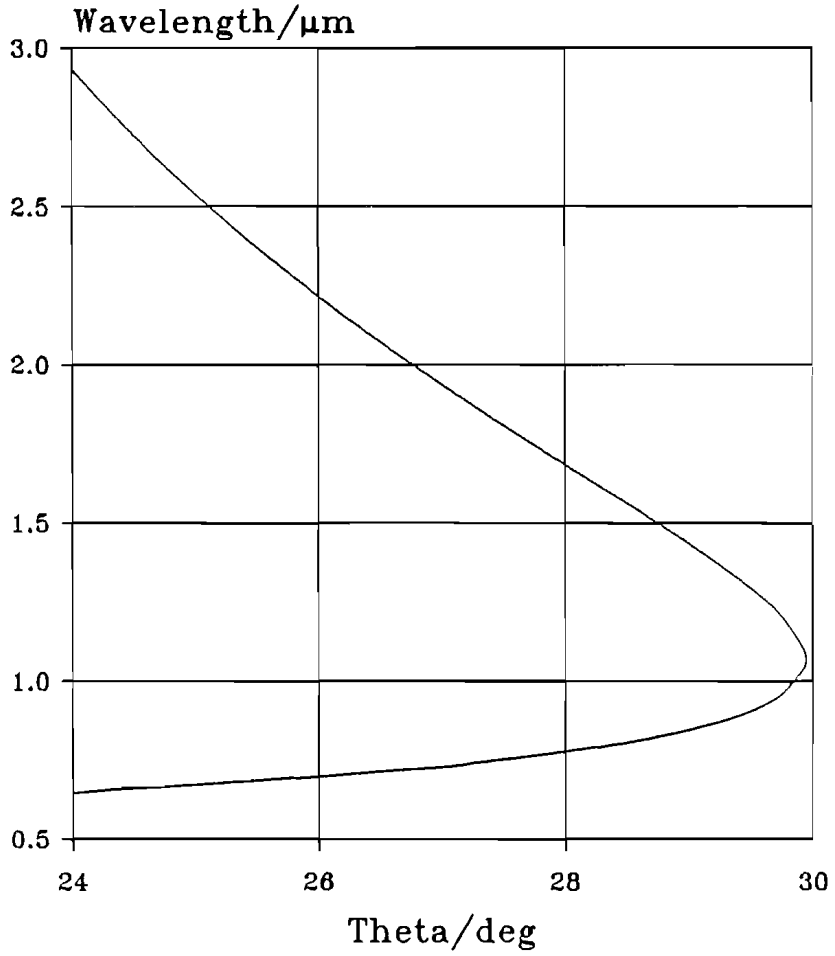

Fig. A1.1 Angle-tuning curve for a type I, $LiIO_3$ parametric oscillator pumped at 0.532μm.

Parametric generation has been demonstrated—with a 0.53μm pump—to tune over the range 0.68–2.4μm, for an angular variation of $\approx$5° [12]. The material has, however, been shown to be capable of tuning over twice this range of wavelengths ($\approx$0.6-5.5μm), by the measurement of spontaneous parametric scattering [13]. For illustrative purposes, the tuning curve (Fig. A1.1) for this interaction has been generated using the set of Sellmeier's equations after Kabelka *et al* [14].

There are three reasons why the high nonlinearity and tuning range of $LiIO_3$ can not be efficiently exploited. Firstly, $LiIO_3$ is a highly birefringent material ($\Delta n/n\approx 8.2\%$ at 0.532μm), and therefore exhibits a large degree of Poynting vector walk-off ($\approx$74mrad at 30°). This limits the degree of focusing that can be used, and hence the intensity achievable

with a given available pump power. Secondly, it has a prohibitively low damage threshold, of only $\approx 50 MWcm^{-2}$ (15ns pulses at $0.532\mu m$ [15], and so even when high powers are available a high intensity can not be utilised. Finally, this material can exhibit significant absorption: At $\approx 1\mu m$ the loss coefficient can be up to $\approx 0.06cm^{-1}$ [16], corresponding to a loss over 5mm of $\approx 3\%$. This is an unacceptably high amount in the case of a low gain parametric oscillator (in particular, all continuously operated systems). It must be noted here that it does not always exhibit such high absorption; values of as low as $\approx 0.003cm^{-1}$ (at $0.532\mu m$) and $\approx 0.001cm^{-1}$ (at $1.064\mu m$) have also been reported [17].

In the case of ultrashort pulses, at least one of these problems is probably absent. For $\approx 15ps$ mode-locked pulses (at $0.532\mu m$), the damage threshold of $LiIO_3$ has been demonstrated to be as high as $\approx 7GWcm^{-2}$ [18]. At these intensities, the gain provided by a short length of crystal ($\sim 1mm$) should be sufficient to achieve threshold of an OPO. The use of a short crystal length will also, to some degree, alleviate the problems of walk-off and of absorption (if present).

Finally, the dispersion in lithium iodate is about half that of KTP, and lithium niobate. As a result, the temporal walk-off is also about half the value. The shortest pulse duration that can be efficiently used to pump an OPO using a 5mm long $LiIO_3$ crystal is $\approx 1.3ps$, whereas it is $\approx 2.1ps$ and 2.7ps in the respective cases of KTP and $LiNbO_3$.

A1.3 Lithium niobate ($LiNbO_3$).

Lithium niobate, a ferroelectric crystal of point group 3m, was proposed for use as a nonlinear gain medium quite early on in the development of the OPO [19]. Its main advantages are a high nonlinearity ($\approx 6.3pmV^{-1}$ [20]) and the fact that, by temperature tuning, noncritical phase-matching of a $0.532\mu m$ pumped OPO can be achieved. Its main disadvantage is the fact that it is highly susceptible to photorefractive (or 'optical') damage by wavelengths in the visible part of the spectrum (damage threshold $< 50MWcm^{-2}$ [21]).

The photorefractive damage is known to result from the presence of impurity ions in the crystal (possibly Fe^{+3} [22]). As the impurity level is already low ($\approx 3ppmw$), a further improvement would lead to an unacceptably large increase of the fabrication costs. However, by varying the crystal stoichiometry, it has been found possible to increase the phase-matching temperature to above the self-annealing point, so that any optical damage that does occur in use is continuously annealed out [23]. More recently, some work has been done to lower the annealing point so that this operating condition may be reached at more readily

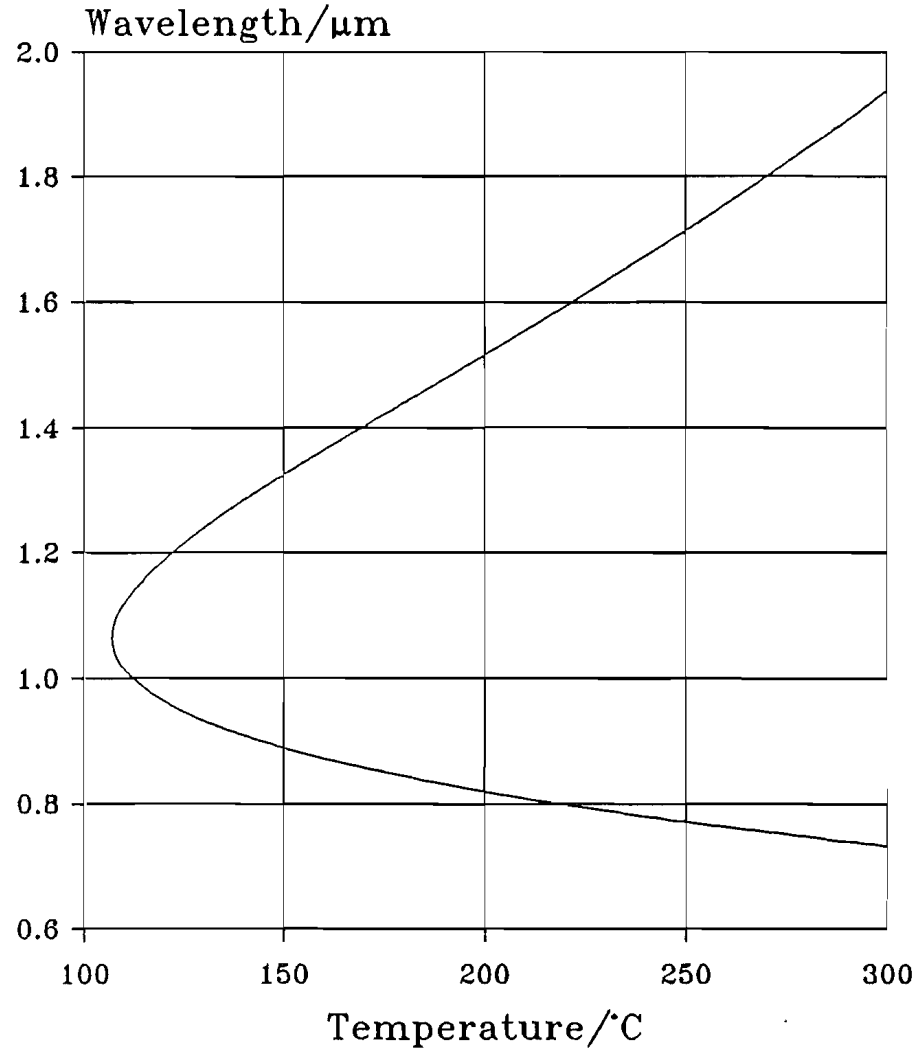

Fig. A1.2 Temperature phase-matching curve for a type I $MgO:LiNbO_3$ OPO pumped at $0.532\mu m$.

obtainable temperatures [24]. The most promising technique, however, has involved the addition of $\approx 5\%$ magnesium oxide (MgO) to the congruent crystal melt [25], which has been found to result in an increase of two orders of magnitude of the threshold for optical damage [26]. The problem with this technique is that the quantity of MgO added to the material is large enough to result in a significant reduction in the optical homogeneity of the crystal [27]. This problem should, however, be rectifiable with further improvements in the growth technique.

Fig. A1.2 shows the type I tuning curve for a $0.532\mu m$ pumped OPO based on the material MgO doped $LiNbO_3$ ('$MgO:LiNb_3$'). It was calculated using the set of Sellmeier's equations for congruent $LiNbO_3$ after Edwards and Lawrence [28], as modified by Kozlovsky *et al* [29] for use with $MgO:LiNbO_3$. From the graph, a variation in temperature of $\approx 200°C$ should tune the OPO over a range of $\approx 0.75\text{-}2.0\mu m$.

The absorption in lithium niobate [17] is low in the region of $\approx 1\mu m$ ($<0.003cm^{-1}$), while increasing significantly by the time the wavelength falls to $0.532\mu m$ ($<0.05cm^{-1}$). As the shortest wavelength $LiNbO_3$ transmits is $\approx 0.4\mu m$ [30], the use of this material, as the gain medium of an OPO, is restricted to the near infrared.

$LiNbO_3$ exhibits a high dispersion, and hence one of the largest values of temporal walk-off ($\approx 0.55ps \cdot mm^{-1}$). As it has a large nonlinearity and zero walk-off, this problem could be readily avoided through the use of a short crystal, if a high intensity was not precluded by optical damage. It is known that optical damage is the predominant damage mechanism. In the case of ultrashort mode-locked pulses ($\approx 6ps$), the damage threshold has been shown to be as high as $\approx 10GWcm^{-2}$ at $1.064\mu m$ [31]. Consequently, if $LiNbO_3$ did not suffer from optical damage, it would probably be one of the best suited crystals for use as the gain medium in a synchronously pumped OPO.

A1.4 Barium sodium niobate ($Ba_2NaNb_5Na_{15}$).

Barium sodium niobate ($Ba_2NaNb_5O_{15}$, 'BNN' or 'BSN')[32] was developed quite early on in the history of nonlinear optics. It was an attempt to produce a material with a nonlinearity as high as that of $LiNbO_3$, but which did not suffer from the problem of optical damage. The 'attempt' *was* successful: BNN does, in fact, have a nonlinearity ($\approx 13.2pmV^{-1}$ [33]) that is more than twice as large as that of lithium niobate ($\approx 6.3pmV^{-1}$ [18]). It is also virtually immune to the problem of optical damage [31], but it does have a surface-damage threshold of only $\approx$ 10-25$MWcm^{-2}$ (for 10ns pulses at $1.064\mu m$)[34]. The high nonlinearity, however, does allow high gains to be achieved at low intensities. Unfortunately, it did not prove possible to grow this material, on a routine basis, to a high enough optical quality for it to become a viable material for widespread use in parametric devices. Consequently, very little work has been done with this material. The few devices that have utilised this material have taken advantage of the high value of the high nonlinearity it offers. They include a single-longitudinal mode c.w. OPO [35] and a doubly resonant, continuously operated synchronously pumped OPO [36].

BNN is a positive biaxial, ferroelectric crystal of point group mm2. Like KTP, it is a nearly uniaxial crystal; unlike KTP, it can be temperature tuned to noncritically phase-match for parametric oscillation with a $0.532\mu m$ pump. The refractive indices of BNN have been fitted to sets of temperature dependent Sellmeier's equations by at least two parties [37][38]. The tuning curve shown in Fig. A1.4 was calculated using the set of

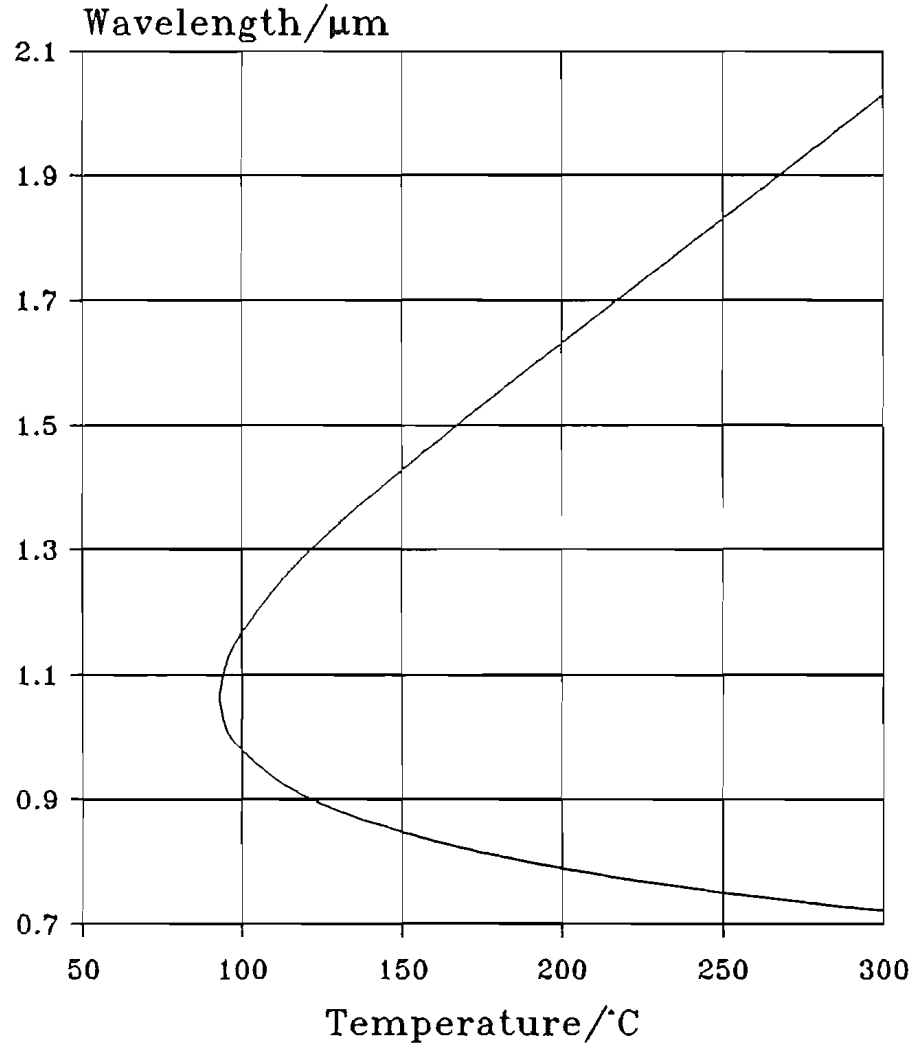

Fig. A1.3 Temperature phase-matching curve for a type II BNN OPO pumped at 0.532μm; propagation parallel to the x-axis.

Sellmeier's equations after Potopowicz [34], and is for a type I device, pumped at 0.532μm in the direction of the crystallographic y-axis. From the curve, a tuning range of 0.65–2.1μm should be possible for a temperature variation of $\approx$100–300°C. The lower temperature corresponds to degeneracy, so an extension of the tuning range would require an increase in temperature. It has been shown that above $\approx$350°C, the nonlinearity falls with increasing temperature [39]; the point at which half the 'low temperature' nonlinearity is available being $\approx$500°C.

Like KTP and $LiNbO_3$, BNN exhibits low absorption loss at 1.064μm ($<0.002cm^{-2}$ [40]), but a higher loss at 0.532μm ($0.04cm^{-2}$ [41]). Also like $LiNbO_3$, it possesses a large temporal walk-off ($\approx 0.55pm \cdot mm^{-1}$).

A1.5 Potassium niobate ($KNbO_3$).

Potassium niobate ($KNbO_3$) is a ferroelectric material of point symmetry 2mm that is closely related to lithium niobate (see Section A1.3) and barium sodium niobate (see Section A1.4). It has a nonlinearity comparable to BNN ($\approx 13 pmV^{-1}$ [42]), but a damage threshold of around an order of magnitude higher ($\approx 350 MWcm^{-2}$ [43]).

Noncritical phase-matching is possible for a wide range of wavelengths due to a strong temperature dependence of the birefringence. The refractive indices of potassium niobate has so far only been fitted to sets of constant temperature Sellmeier's equations (at room temperature), and so it was not possible to generate a temperature phase-matching curve for this material. A 0.532μm pumped parametric oscillation has, however, been demonstrated to tune over 0.86-1.4μm for a temperature variation of 184-220°C [44].

The absorption and temporal walk-off of this material are comparable to those of $LiNbO_3$ and BNN. The only disadvantage of this material, compared to the other niobates, is that a higher temperature is needed to phase-match a 0.532μm pumped OPO for degenerate operation, (≈ 184°C [44] c.f. ≈ 107°C for MgO:$LiNbO_3$ [28] and ≈ 100°C for BNN [34]).

A1.6 Lithium borate (LiB_3O_5).

Lithium borate [45] is a biaxial nonlinear crystal of point symmetry 2mm. It has properties that are close, but not identical, to BBO [2]. The transmission does not extend as far into the ultraviolet (≈ 200nm, c.f. 180nm for BBO), and the usable nonlinearity of LBO, $d_{32} \approx 1.24 pmV^{-1}$ [44], is only $\approx 60\%$ of that of BBO. It does, however, have an even higher damage threshold; $\approx 25 GWcm^{-2}$ [44] c.f. $\approx 13.5 GWcm^{-2}$ for BBO [46].

As with KTP, quasi-noncritical type I phase-matching, for the frequency doubling of 1.064μm, is possible for propagation in the xy-plane, (at $\theta = 90.00°$ and $\phi = 10.73°$). In this case, the effective nonlinearity for type I interactions is well approximated by $d_{eff} = d_{32}\cos\phi$, and takes the value of $\approx 1.2 pmV^{-1}$. A set of Sellmeier's equations have been fitted to the refractive index data by Chen *et al* [2]. Fig. A1.4 shows the phase-matching curve predicted for a 0.532μm pumped OPO angle-tuned about the z-axis to preserve the quasi-noncritical behaviour. In this case, Poynting vector walk-off is always < 6mrad. A feature of LBO that is not matched by KTP is noncritical phase-matching. It has been found possible to achieve noncritical phase-matching for the frequency doubling of 1.064μm by temperature tuning (≈ 150°C [47]). As no details of the temperature dependency of its birefringence

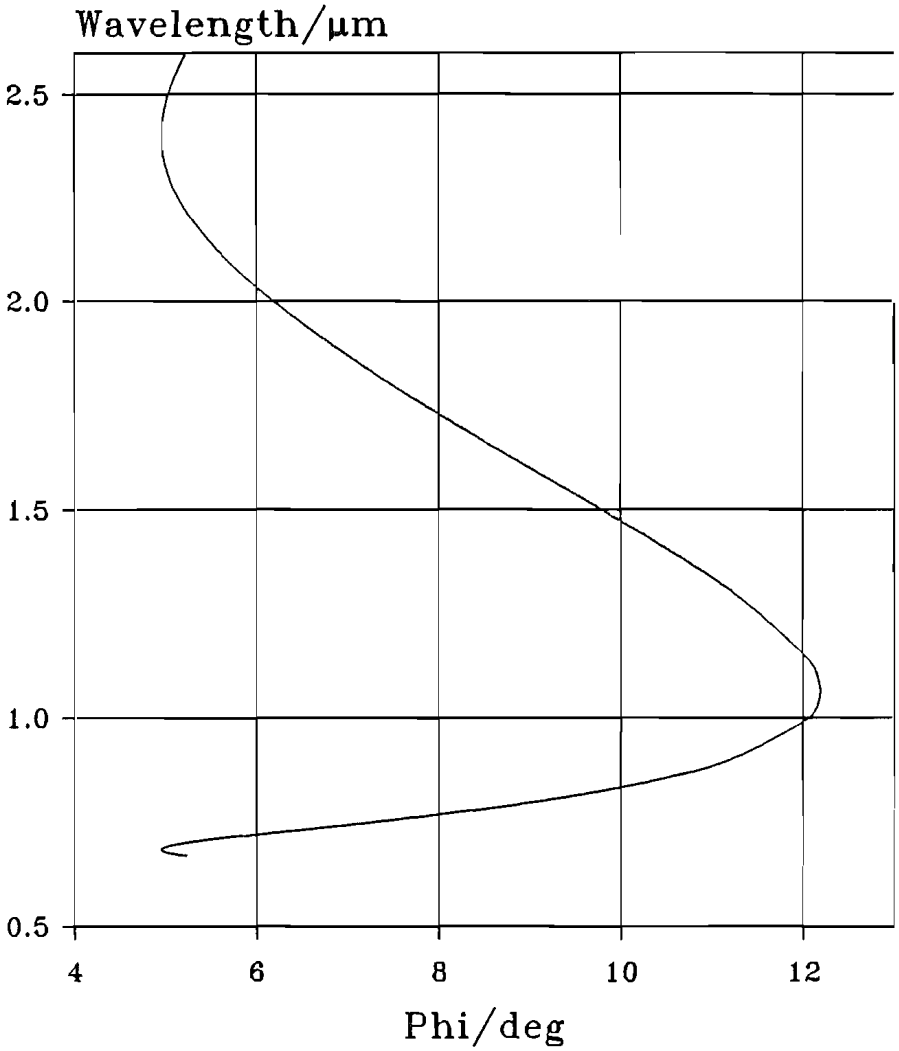

Fig. A1.4 Angle-tuning curve for type I LBO parametric oscillator pumped at 0.532μm. Propagation orthogonal to z-axis.

have been released, it is not yet known how wide an OPO tuning range will be possible using this technique.

The fact that the transmission of LBO extends into the ultraviolet has allowed optical parametric oscillators pumped at wavelengths of ~250nm to tune throughout the visible and into the near infrared [48]. It also leads to a low group velocity dispersion at 0.532μm and below. Consequently, the temporal walk-off between pulses at 1.064μm and 0.532μm is very low in this material ($\approx$0.06ps·mm).

A1.7 Organic nonlinear crystals.

There is currently a lot of interest in organic nonlinear materials. They offer high damage thresholds (e.g. $\approx$3GWcm^{-2} for MAP [49]) and high nonlinearities (e.g. $\approx$85pmV^{-1} for NNP [50]). Some of these materials also have their short wavelength absorption edge far into the ultraviolet, which is attracting a lot of attention from those working in this region of

the spectrum. Unfortunately, none of these materials can transmit wavelengths of longer than $\approx 2\mu$m, due to absorption due to the C-H and other molecular resonances, and so can not offer the wide tunability in the near infrared desired for an OPO working in the near infrared.

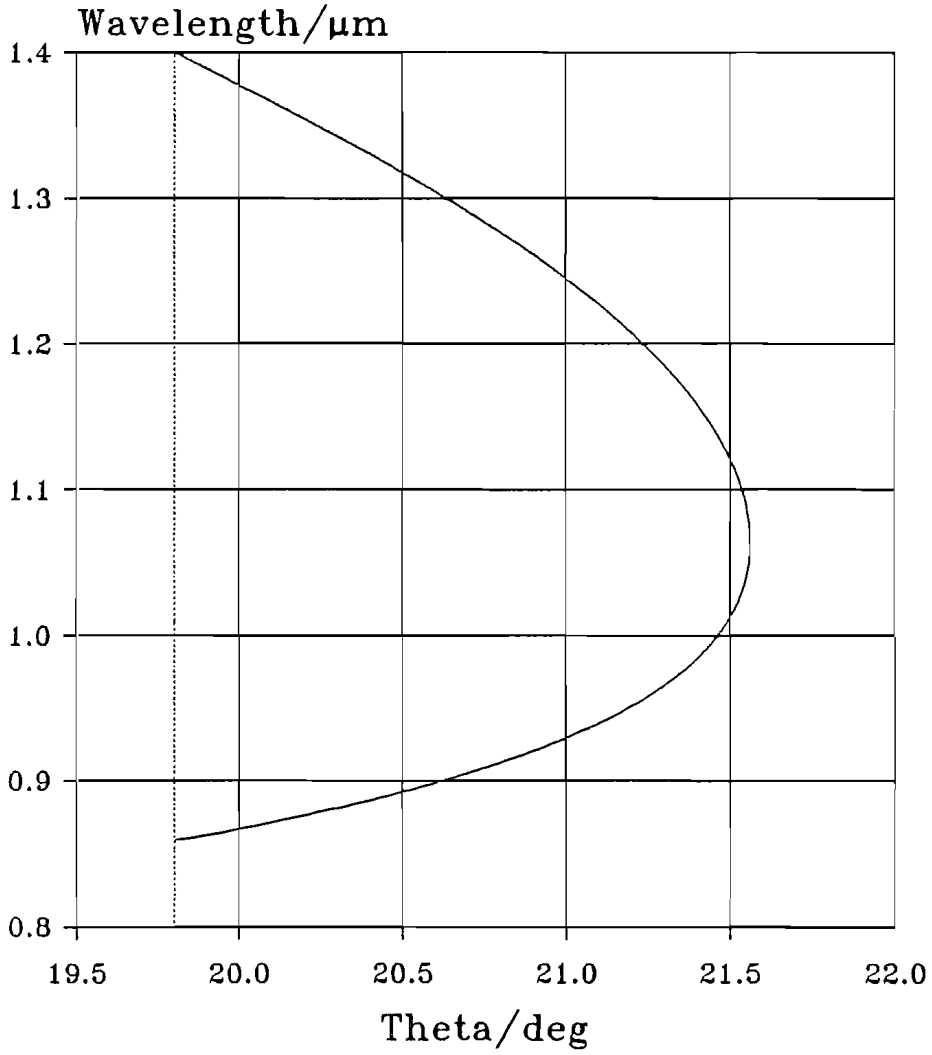

Fig. A1.5 Angle-tuning curve for a type I urea OPO pumped at 0.532μm.

At this time organic crystals are only now becoming commercially available of a usable size, with the exception of urea, which has been around for some time [51]. Urea ($(NH_2)_2CO$) is a positive uniaxial organic crystal with point symmetry $\bar{4}2m$. It has a nonlinearity of $\approx 1.4 pmV^{-1}$, and can be phase-matched for type I parametric oscillation with a 0.532μm pump over the range 0.86-1.4μm (transmission limited). Urea can, like LBO, transmit well into the ultraviolet ($\approx$200nm), and so it has also been exploited in parametric devices operating in the visible region of the spectrum [52]. It also exhibits a low temporal walk-off ($\approx 0.10 ps \cdot mm^{-1}$). It is, unfortunately, highly hygroscopic, which necessitates constant protection from atmospheric moisture.

A lot of the published information on organic nonlinear crystals up until now has been obtained from films or platelets of the material (i.e. lengths of $\sim 15\mu$m–1mm). Whilst the preliminary results do look very promising, it will probably be some time until these materials are as readily available as their inorganic counterparts. Materials that have been reported to date include MNA [53], MBA-NP [54], POM [49], and NPP [49]. The full names will not be given here for the sake of brevity, as the majority of organic nonlinear crystals have names like (—)2-(α-methylbenzylamino)-5-nitropyridine (for 'MBA-NP'). The latter two in the list above exhibit group velocity matching between the signal and idler waves [49], thus giving these materials very wide phase-matching bandwidths. This allows for the efficient doubling of subpicosecond pulses. MBA-NP is one of the few materials that has been grown up to an appreciable size (e.g. optically usable crystals of up to $5\times3\times3mm^3$)[52].

References.

[1]. F.C. Zumsteg, J.D. Bierlein, and T.E. Gier.
J. Appl. Phys. **47**, 4980 (1976).

[2]. C. Chen, B. Wu, A. Jiang, and G. You.
Sci. Sinica (Ser. B) **28**, 235 (1985).

[3]. R.S. Craxton, S.D. Jacobs, J.E. Rizzo, and R. Boni.
IEEE J. Quantum Electron. **QE-17**, 1782 (1981).

[4]. E.S. Bliss.
Opto-Electronics **3**, 99 (1971).

[5]. J.D. Bierlein, H. Vanherzeele, and A.A. Ballman.
Appl. Phys. Lett. **54**, 783 (1989).

[6]. F.C. Zumsteg, J.D. Bierlein, and T.E. Gier.
J. Appl. Phys **47**, 4980 (1976).

[7]. J.D. Bierlein and H. Vanherzeele.
J. Opt. Soc. B **6**, 622 (1989).

[8]. B.F. Levine and C.G. Bethea.
Appl. Phys. Lett. **20**, 272 (1972).

[9]. G. Nath, H. Mehmanesch, and M. Gsänger.
Appl. Phys. Lett. **17**, 286 (1975).

[10]. J.E. Midwinter and J. Warner.
Brit. J. Appl. Phys. **16**, 1135 (1965).

[11]. R.C. Eckardt, H. Masuda, Y.X. Fan, and R.L. Byer.
IEEE J. Quantum Electron. **26**, 922 (1990).

[12]. P.G. Kryukov, Yu.A. Matveets, D.N. Nikogosyan, A.V. Sharkov, E.M. Gordeev, and S.D. Fanchenko.
Sov. J. Quantum Electron. **4**, 979 (1975).

[13]. L.S. Goldberg.
Appl. Phys. Lett. **17**, 489 (1970).

[14]. V.I Kabelka, A.S. Piskarskas, A.Yu. Stabinis, and R.L. Sher.
Sov. J. Quantum Electron. **5**, 255 (1975).

[15]. A.P. Izrailenko, A.I. Kovrigin, and P.V. Nikles.
JETP Lett. **12**, 331 (1970).

[16]. F.R. Nash, J.G. Bergman, G.D. Boyd, and E.H. Turner.
J. Appl. Phys. **40**, 5201 (1969).

[17]. D.J. Gettemy, W.C. Harker, G. Lindholm, and N.P. Barnes.
IEEE J. Quantum Electron. **24**, 2231 (1988).

[18]. P.G. Kryokov, Yu.A. Matveets, D.N. Nikogosyan, A.V. Sharkov, E.M. Gordeev, and S.D.Fanchenko.
Sov. J. Quantum Electron. **6**, 127 (1977).

[19]. G.D. Boyd, R.C. Miller, K. Nassau, W.L. Bond, and A. Savage.
Appl. Phys. Lett. **6**, 234 (1964).

[20]. R.L. Byer and S.E. Harris.
Phys. Rev. **168**, 1064 (1968).

[21]. A. Ashkin, G.D. Boyd, J.M. Dziedzic, R.G. Smith, A.A. Ballman, J.J. Levenstein, and K. Nassau.
Appl. Phys. Lett. **9**, 72 (1966).

[22]. E. Krätzig.
Ferroelectrics **21**, 635 (1978).

[23]. J.G. Bergman, A. Ashkin, A.A. Ballman, J.M. Dziedzic, H.J. Levinstein, and R.G. Smith.
Appl. Phys. Lett. **12**, 92 (1968).

[24]. R.L. Byer, Y.K. Park, R.,S. Feigelson, and W.L. Kway.
Appl. Phys. Lett. **39**, 17 (1981).

[25]. D.A. Bryan, R. Gerson, and H.E. Tomaschke.
Appl. Phys. Lett. **44**, 847 (1984).

[26]. D.A. Bryan, R.R. Rice, R. Gerson, H.E. Tomaschke, K.L. Sweeney, and L.E. Halliburton.
Opt. Eng. **24**, 138 (1985).

[27]. E.O. Ammann and S. Guch, Jr.
Appl. Phys. Lett. **52**, 1374 (1988).

[28]. G.E. Edwards and M. Lawrence.
Opt. Quantum Electron. **16**, 373 (1984).

[29]. W.J. Kozlovsky, C.D. Nabors, R.C. Eckardt, and R.L. Byer.
Opt. Lett. **14**, 66 (1989).

[30]. K. Nassau, H.J. Levinstein, and G.M. Loiacoco.
J. Phys. Chem. Solids **27**, 989 (1966).

[31]. A. Laubereau, L. Gretier, and W. Kaiser.
Appl. Phys. Lett. **25**, 87 (1974).

[32]. J.E. Geusic, H.J. Levinstein, J.J. Rubin, S. Singh, and L.G. Van Uitert.
Appl. Phys. Lett. **11**, 269 (1967).

[33]. S. Singh, D.A. Draegert. and J.E. Geusic.
Phys. Rev. B **2**, 2709 (1970).

[34]. J.E. Murray, R.J. Pressley, J.H. Boyden, and R.B. Webb.
IEEE J. Quantum Electron. **QE-10**, 263 (1974).

[35]. R.G. Smith, J.E. Geusic, H.J. Levinstein, S. Singh, and L.G. Van Uitert.
J. Appl. Phys. **39**, 4030 (1968).

[36]. A. Piskarskas, V. Smil'gyavichyus, and A. Umbrasas.
Sov. J. Quantum Electron. **18**, 155 (1988).

[37]. J. R. Potopowicz.
CRC Handbook of Laser Science and Technology, Volume III, p134, (CRC Press 1986, M.J. Webb, Ed.).

[38]. W.R.M. Pomeroy.
Opto-Electronics **3**, 148 (1971).

[39]. R.L. Byer, S.E. Harris, D.J. Kuizenga, and J.F. Young.
J. Appl. Phys. **40**, 444 (1969).

[40]. J.D. Barry.
IEEE J. Quantum Electron. **QE-12**, 254 (1976).

[41]. J.D. Barry and C.J. Kennedy.
IEEE J. Quantum Electron. **QE-11**, 575 (1975).

[42]. Y. Uematsu.
Jap. J. Appl. Phys. **13**, 1362 (1974).

[43]. P. Günter.
Proc. SPIE **236**, 8 (1981).

[44]. K. Kato.
IEEE J. Quantum Electron. **QE-18**, 451 (1982).

[45]. C. Chen, Y. Wu, A. Jiang, B. Wu, G. You, R. Li, and S. Lin.
J. Opt. Soc. Am. B **6**, 616 (1989).

[46]. D. Eimerl, L. Davis, S. Velsko, E.K. Graham, and A. Zalkin.
J. Appl. Phys. **62**, 1968 (1987).

[47]. J.T. Lin, J.L. Montgomery, J.R. DeSalvo, and A.M. Horner.
CLEO'90 Technical Digest, Abstract **CWF40** (1990).

[48]. E. Ebrahimzadeh, G. Robertson, M.H. Dunn, and A.J. Henderson.
CLEO'90 Technical Digest, Abstract **CDDP26** (1990).

[49]. J.L Oudar and R. Hierle.
J. Appl. Phys. **48**, 2699 (1977),

[50]. J. Zyss, I. Ledoux, D. Josse, R. Hierle, A. Perigaud, and J. Badan.
CLEO'90 Technical Digest, Abstract **CWJ1** (1990).

[51]. C. Cassidy, J.M. Halbout, W. Donaldson, and C.L. Tang.
Opt. Commun. **29**, 243 (1979).

[52]. M.J. Rosker and C.L. Tang.
J. Opt. Soc. B **2**, 691 (1985).

[53]. K. Kato.
IEEE J. Quantum Electron. **QE-16**, 1288 (1980).

[54]. R.T. Bailey, F.R. Cruickshank, S.M.G. Guthrie, B.H. McArdle, H. Morrison, D. Pugh, E.A. Shepherd, J.N. Sherwood, C.S. Moon, R. Kashyap, B.K. Nayar, and K.I. White.
J. Mod. Opt. **35**, 511 (1988).

A2 Sellmeier's fits for BBO.

At least four different sets of Sellmeier's equations have been fitted to the refractive indices of barium borate (BBO) [1][2][3][4]. The earliest set was presented at IQEC'84 by Chen *et al* [1], but was never published. The first set to be published was also by Chen *et al* [2], and while not in exact agreement with their previous set, it does predict very similar tuning behaviour. Consequently, only the latter one will be considered further.

The third set of Sellmeier's equations currently available is after Kato [3]. This set was fitted to the refractive index data published by Chen *et al* [2], but in addition it was adjusted to give better agreement with the observed phase-matching behaviour. The final set of Sellmeier's equations is after Eimerl *et al* [4], who are the only party to have fitted to independently determined values of the refractive indices.

A2.1 Chen *et al* [2].

Chen *et al* experimentally determined the refractive indices of barium borate at thirteen wavelengths between 0.2138–1.079μm using the method of least angle deflection. This data was fitted to a pair of single-pole Sellmeier's equations of the form,

$$n^2 = A + \frac{B\lambda^2}{\lambda^2 - C} \qquad \text{(A2.1)}$$

where the coefficients are given in Table A2.1.

Table A2.1 Sellmeier's coefficients for BBO after Chen *et al*

Coefficient	A	B	C
n_o	1.9595	0.7892	0.02163
n_e	1.6932	0.6782	0.01816

A2.2 Kato [3].

Kato fitted a pair of single-pole Sellmeier's equations to the refractive index data after Chen *et al* [2], and also to the experimentally determined phase-matching angles for various second harmonic and sum frequency generation processes. This allowed the validity of the Sellmeier's equations to be extended below the minimum wavelength at which the refractive

indices had been experimentally determined (0.436μm). The form of the Sellmeier's equations was,

$$n^2 = A + \frac{B}{C - \lambda^2} - D\lambda^2 \qquad \textbf{(A2.2)}$$

where the coefficients are given in Table A2.2.

Table A2.2 Sellmeier's coefficients for BBO after Kato.

Coefficient	A	B	C	D
n_o	2.7359	0.01878	0.01822	0.01354
n_e	2.3753	0.01224	0.01667	0.01516

A2.3 Eimerl *et al* [4].

Eimerl *et al* measured the refractive indices of BBO in the region 400–1014nm directly by the method of minimum deviation. To improve the fit in the ultraviolet region, the phase-matching angles for the frequency doubling of various wavelengths were determined. The refractive index data, and the phase-matching behaviour, were fitted to a pair of single-pole Sellmeier's equations of the same form as used by Kato [3], but with the coefficients as given in Table A2.3.

Table A2.3 Sellmeier's coefficients for BBO after Eimerl *et al.*

Coefficient	A	B	D	C
n_o	2.7405	0.0184	0.0179	0.0155
n_e	2.3730	0.0128	0.0156	0.0044

The paper by Eimerl *et al* also presents results of calculations, based on the above set of Sellmeier's equations, of tuning behaviour for several different parametric processes. Among others, there are tuning curves for type I and type II parametric oscillation with 0.532μm, 0.355μm, and 0.266μm pumps.

A2.4 Comparison.

Fig. A2.1 shows the experimentally determined tuning behaviour of a 0.532μm pumped BBO parametric oscillator plotted as a function of angle from degeneracy. Also plotted is the

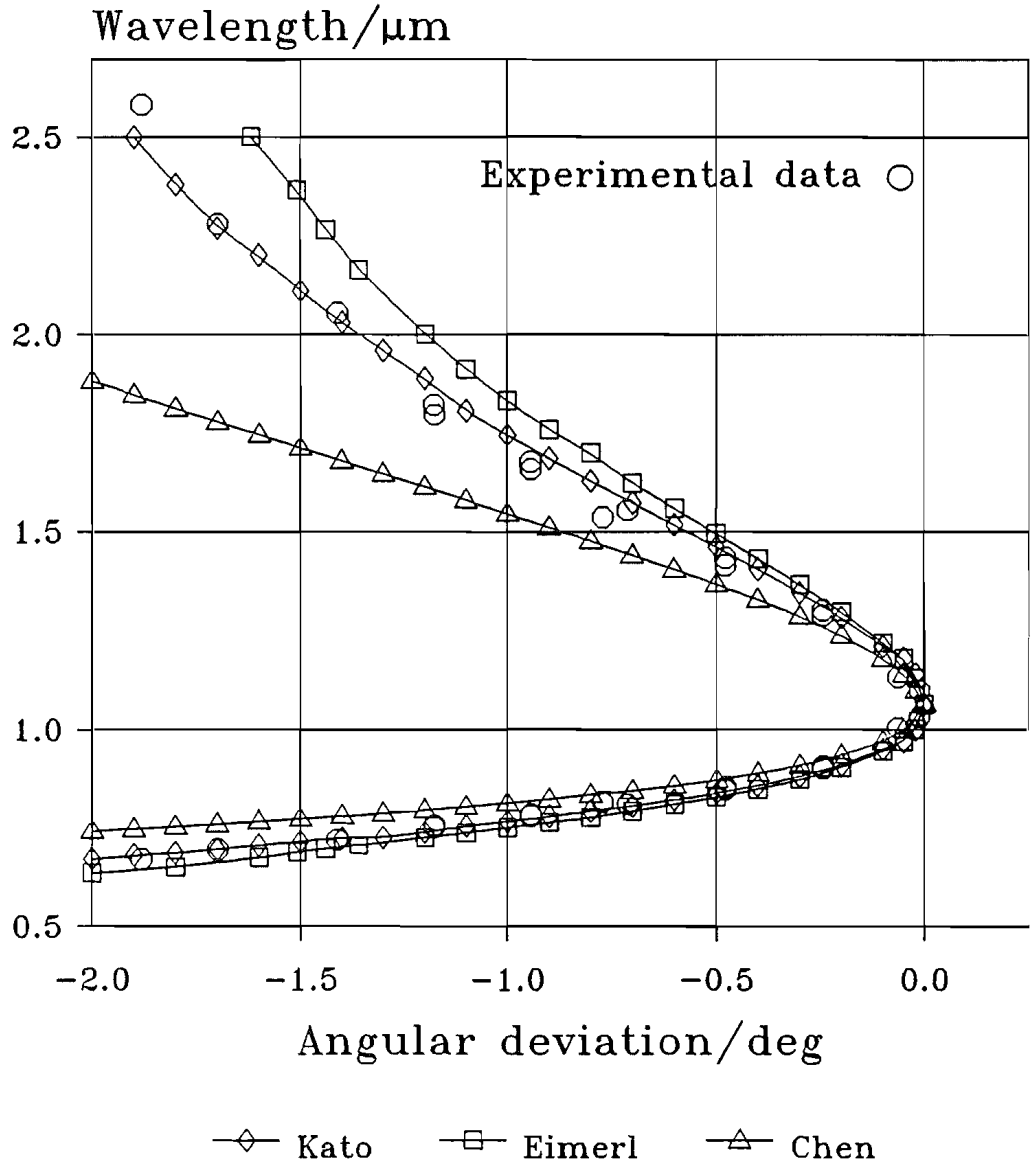

Fig. A2.1 Tuning behaviour of a 532μm pumped, type I BBO parametric oscillator. The points show the experimental data, whereas the lines show the fits calculated using various Sellmeier's (see text).

behaviour predicted by the sets of Sellmeier's equations after Chen *et al* [2], Kato [3], and Eimerl *et al* [4]. Absolute angular measurements were not possible as the angle at which the crystal had been cut at was not accurately known. It was therefore only possible to compare the rate of tuning with angle, and not the value of the angles themselves.

As can be seen, the experimental data most closely agrees with the curve generated using the set of Sellmeier's equations after Kato [3]. The fit obtained from the equations after Eimerl *et al* [4], though it does follow reasonably closely, is noticeably poorer. The tuning behaviour predicted by the pair of equations after Chen *et al* [2] shows much worse agreement with the experimental results.

A2.5 Conclusion.

It can be seen from Fig. A2.1 that the set of Sellmeier's equations after Kato [3] gives the best agreement for the tuning of a 0.532 pumped parametric oscillator. As none of the parties experimentally determined the refractive indices for wavelengths longer than $\sim 1\mu$m, predictions of phase-matching involving wavelengths beyond this value are less reliable. However, as the set of Sellmeier's equations after Kato has been shown to accurately predict the tuning behaviour all the way out to 2.7μm accurately, unless significant departure is found in future experiments, the determination of the refractive indices beyond 1μm by direct means does not seem to be necessary.

References.

[1]. C. Chen, B. Wu, G. You, and Y. Huang.
IQEC'84 Technical Digest, Abstract **MCC5** (1984).

[2]. C. Chen, B. Wu, A. Jiang, and G. You.
Scientia Sinica B **28**, 235 (1985).

[3]. K. Kato.
IEEE J. Quantum Electron. **22**, 1013 (1986).

[4]. D. Eimerl, L. Davis, S. Velsko, E.K. Graham, and A. Zalkin.
J. Appl. Phys. **62**, 1968 (1987).

A3 Sellmeier's fits for KTP.

At this time, five parties have fitted sets of Sellmeier's equations to the refractive indices of KTP [1][2][3][4][5]. At least three out of these five sets of Sellmeier's were only fitted to experimental values of refractive indices for wavelengths of $\sim 1\mu$m and under, and are consequently are only strictly valid within this range. In the case of parametric interactions involving only wavelengths of $\approx 1\mu$m and shorter, there is reasonable agreement between the phase-matching angles calculated using the different sets of Sellmeier's. For interactions involving only one or more longer wavelength, however, there is a significant departure. It is not yet clear if this disagreement is solely due to the fact that some of the Sellmeier's are being utilised outside their range of validity, or whether it may be—at least partially—attributed to the different growth techniques and melt-to-melt variations in crystal stoichiometry.

In this work, use has been made of the sets of Sellmeier's equations after both Fan *et al* [1], and Bierlein and Vanherzeele [2]. In the former case the Sellmeier's equations were fitted to refractive index data for wavelengths between 0.45–1.06μm, while in the latter case the longest wavelength used was 3.5μm. As the operating wavelength of the device investigated in this work (see Chapter 7) did not depart by more than $\approx$50nm from degeneracy, the values predicted by the two sets did not differ significantly.

Other sets of Sellmeier's equations have been published by Weber [3], Anthon and Crowder [4], and Kato [5]. The set of Sellmeier's equations after Weber [3] appears only in the book he edits, *C.R.C. Handbook of Laser Science and Engineering Vol. III.* (C.R.C. Press, 1985). It is, however, simply stated: there is no information given about how the coefficients were obtained. Anthon and Crowder [4] did not measure the refractive indices themselves, but optimised the coefficients in the Sellmeier's equations given by Weber to give best agreement between theoretically predicted and experimentally found phase-matching angles for second harmonic generation. This was also the approach Kato [5] used, except that he based his initial Sellmeier's equations on the index data taken by Zumsteg *et al* [6]. As the set of Sellmeier's equations after Anthon and Crowder [4] is an improved version of that after Weber [3], of these only the former will be further considered.

A3.1 Fan *et al* [1].

T.Y. Fan *et al* measured the principle indices of KTP at 16 wavelengths between 404.7nm and 1.064μm using the prism method. The resultant data, after correction for air, was fitted to a single pole Sellmeier's equation of the form,

$$n^2 = A + \frac{B}{1 - \frac{C}{\lambda^2}} - D\lambda^2 \qquad \text{(A3.1)}$$

where the final term in λ^2 is an infrared correction. The coefficients for the three principle indices are given below in Table A3.1,

Table A3.1 Sellmeier's coefficients for KTP after Fan *et al.*

Coefficient	A	B	C	D
n_x	2.16747	0.83733	0.04611	0.01713
n_y	2.19229	0.83547	0.04970	0.01621
n_z	2.25411	1.06543	0.05486	0.02140

A3.2 Bierlein and Vanherzeele [2].

Bierlein and Vanherzeele also used the prism method to determine the principle refractive indices. They did, however, use a larger number of data points (47 different wavelengths) over a wider spectral range (0.35–2.4μm). The form of the Sellmeier's equation used is virtually identical to that adopted by Fan *et al*, but with the coefficient 'C' of Fan *et al* being equal to the coefficient 'C^2' of Bierlein and Vanherzeele.

$$n^2 = A + \frac{B}{1 - \left(\frac{C}{\lambda}\right)^2} - D\lambda^2 \qquad \text{(A3.2)}$$

The coefficients as determined by Bierlein and Vanherzeele are given in Table A3.2,

Table A3.2 Sellmeier's coefficients for KTP after Bierlein and Vanherzeele.

Coefficient	A	B	C	D
n_x	2.1146	0.89188	0.20861	0.01320
n_y	2.1518	0.87862	0.21801	0.01327
n_z	2.3136	1.00012	0.23831	0.01679

3.3 Anthon and Crowder [4].

Like Kato, Anthon and Crowder determined their Sellmeier's coefficients from phase-matching data. They did, however, base them closely on those published in the *CRC Handbook of Laser Science and Engineering* [3]. The origin of these Sellmeier's coefficients is not given. The form of the Sellmeier's equation used has two poles, rather than the single pole and infrared correction used by the others.

$$n^2 = A + \frac{B\lambda^2}{\lambda^2 - C} + \frac{D\lambda^2}{\lambda^2 - 100.0} \qquad \textbf{(A3.3)}$$

where the coefficients are given in Table A3.3

Table A3.3 Sellmeier's coefficients for KTP after Anthon and Crowder.

Coefficient	A	B	C	D
n_x	2.029809	0.9737485	0.04093072	1.1048585
n_y	2.079195	0.9412874	0.04595899	0.9320789
n_z	2.006239	1.2965213	0.04807691	1.1329810

A3.4 Kato [5].

Kato generated his Sellmeier's coefficients, using some of the data points after Zumsteg *et al* [6] for an initial guess, by fitting it to the observed phase-matching angles for frequency doubling and sum frequency mixing. The form of equation used was

$$n^2 = A + \frac{B}{\lambda^2 - C} - D\lambda^2 \qquad \textbf{(A3.4)}$$

and the coefficients are given in Table A3.4

Table A3.4 Sellmeier's coefficient for KTP after Kato.

Coefficient	A	B	C	D
n_x	3.0129	0.03807	0.04283	0.01664
n_y	3.0333	0.04106	0.04946	0.01695
n_z	3.3209	0.05305	0.05960	0.01763

A3.5 Comparison.

To illustrate the relative behaviour of the four sets of Sellmeier's equations, two graphs of predicted tuning behaviour are given. The first case is for type II matching of a 0.532μm pump for propagation in the xy-plane (Fig. A3.1). This shows close agreement between the four curves, and it can be seen that it is not that important which equation is used.

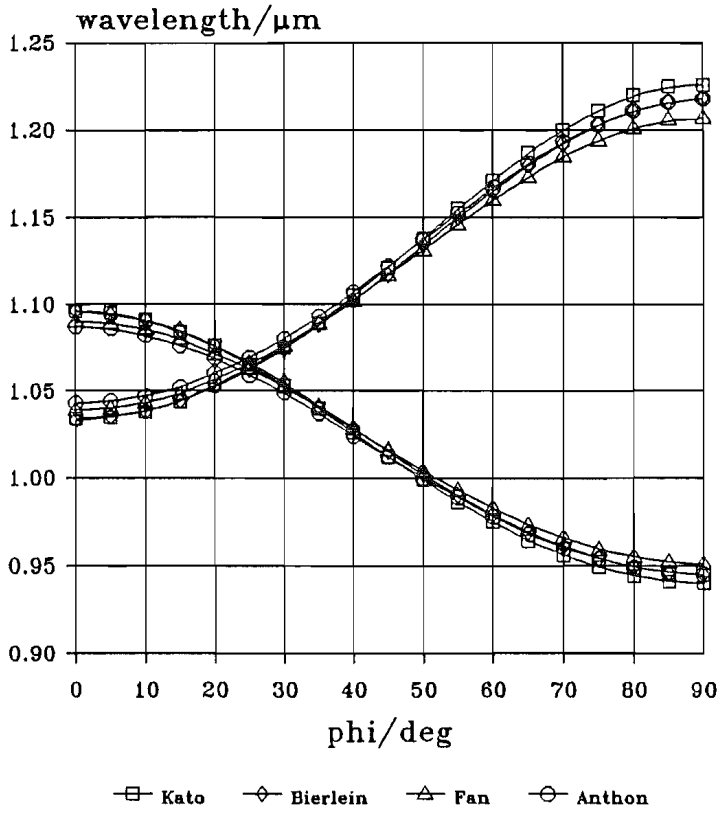

Fig. 3.1 Comparison of the tuning behaviour predicted using the different sets of Sellmeier's equations for a type II KTP OPO pumped at 0.532μm. Propagation is in the xy-plane and the pump is polarized perpendicularly to the z-axis.

The second set of curves shows the matched wavelengths for type II matching of a 1.064μm pump for propagation in the zx-plane (Fig. A3.2). In comparison to the previous case, this shows a significant scatter. As mentioned above, only Bierlein and Vanherzeele fitted their Sellmeier's to refractive index data for wavelengths above 1.064μm. It is, however, the set after Kato that has been found to give closest agreement with the experimentally found tuning behaviour in *this* case [7][8][9]. The Sellmeier's after Bierlein and Vanherzeele does not agree as closely, but is in better agreement than the other two.

To confuse matters, the Sellmeier's after Anthon and Crowder have been reported to give the best agreement with experiment when used to predict the matching behaviour for

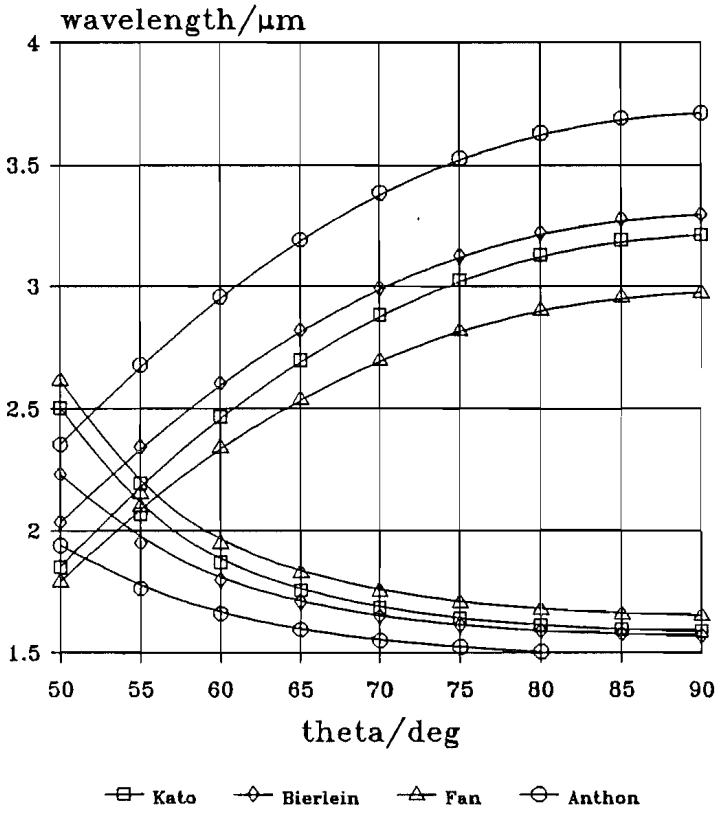

Fig. 3.2 Comparison of the tuning behaviour predicted by the four sets of Sellmeier's equations for a type II KTP OPO pumped at 1.064μm. Propagation is in the zx-plane, and the pump is y-polarized.

sum frequency generation of wavelengths around 1.33μm [10].

A3.6 Conclusion.

It is difficult to draw any real conclusion at this time. As mentioned above, the variation in tuning behaviour could result from a genuine variation in crystal stoichiometry. It is already known that the phase-matching angles for flux- and hydro-thermally grown KTP are significantly different (for phase-matching of 1.064μm in the xy-plane (i.e. θ=90°), ϕ is 25.2° and 24.0° respectively [4]), so it is quite possible that the scatter exhibited by the calculated tuning curves reflects a genuine variation.

References.

[1]. T.Y. Fan, E.E.Huang, B.Q. Hu, R.C. Eckardt, Y.X. Fan, R.L. Byer,and R.S. Feigelson.
Appl. Opt. **26**, 2390 (1987).

[2]. J.D. Bierlein and H. Vanherzeele.
J. Opt. Soc. Am. B **6**, 622 (1989).

[3]. M.J. Weber, Ed.
p152, *CRC Handbook of Laser Science and Technology Vol. III* (CRC Press 1985)

[4]. D.W. Anthon and C.D. Crowder.
Appl. Opt. **27**, 2650 (1988).

[5]. K. Kato.
IEEE J. Quantum Electron. **24**, 3 (1988).

[6]. F.C. Zumsteg, J.D. Bierlein and T.E. Gier.
J. Appl. Phys. **47**, 4980 (1976).

[7]. R. Burnham, R.A. Stolzenberger, and A. Pinto.
IEEE Photon. Tech. Lett. **1**, 27 (1989).

[8]. J.T. Lin and J.L. Montgomery.
Opt. Commun. **75**, 315 (1990).

[9]. L.R. Marshall, A. Hays, J. Kasinski, and R. Burnham.
CLEO'90 Technical Digest, Abstract **WC8PD** (1990).

[10]. R.A. Stolzenberger, C.C. Hsu, N. Peyghambarian, J.J.E. Reid, and R.A. Morgan.
IEEE Photon. Tech. Lett. **1**, 446 (1989).

A4 Oscillation threshold.

This appendix briefly outlines the theoretical model—after Brosnan and Byer [1]—that was used to predict the oscillation threshold of the three parametric oscillators that were investigated over the duration of this project (see Chapters 6 and 7). It specifically deals with the oscillation threshold of a singly resonant parametric oscillator when pumped by a Q-switched pulse (i.e. *not* a train of mode-locked pulses). Application to the case of a train of mode-locked pulses is possible, however, if it is *assumed* that the optical lengths of the OPO and pump laser resonators are perfectly matched. In this case, the Q-switched envelope described by the peaks of the mode-locked pulses can be treated as if it was actually the envelope of a Q-switched pulse.

A4.1 Outline of theory.

At threshold, as there is negligible pump depletion, the pump power can be taken to be constant over any given transit of the nonlinear crystal. In this case, the complex amplitudes of the generated fields at ω_1 and ω_2 (ω_3 being the frequency of the pump, such that $\omega_3=\omega_2+\omega_1$) are given by,

$$\begin{aligned} \frac{dE_1}{dz} + \alpha_1 E_1 &= i\kappa_1 E_3 E_2^* e^{i\Delta kz} \\ \frac{dE_2}{dz} + \alpha_2 E_2 &= i\kappa_2 E_3 E_1^* e^{i\Delta kz} \end{aligned} \qquad \text{(A4.1)}$$

where α_i are the field absorption coefficients, z is the spatial coordinate in the direction of propagation, $\Delta k=k_3-k_2-k_1$ is the phase-velocity mismatch, and the interaction coefficients, κ_i, are defined by

$$\kappa_i = \frac{\omega_i d}{n_i c} \qquad \text{(A4.2)}$$

where 'd' is the effective nonlinear coefficient for the interaction, and n_i is the appropriate refractive index.

In the case of the singly-resonant OPO, only one of the generated fields (the 'signal') is fed back. This means that the idler power at the beginning of each crystal transit will be virtually zero (i.e. at the level of quantum noise, and therefore insignificant compared to any sizeable input signal). With this assumption, and assigning '1' to the signal and '2' to the idler, the signal field at the exit of a crystal of length ℓ can be shown to be given by,

$$E_1(\ell) = E_1(0)\, e^{-\alpha \ell} \cosh \Gamma \mathfrak{L} \tag{A4.3}$$

where the parametric gain coefficient 'Γ' is given by,

$$\Gamma = \sqrt{\kappa_1 \kappa_2 g_1 |E_3|^2} \tag{A4.4}$$

in which κ_1, κ_2 are as defined by (A4.2), E_3 is the complex amplitude of the incident pump field, g_1 is the signal spatial mode coupling coefficient,

$$g_1 = \frac{w_3^2}{w_3^2 + w_1^2} \tag{A4.5}$$

which Brosnan and Byer [1] obtain using the mode-coupling formalism after Kogelnik [2], and '$\mathfrak{L}$' is the effective parametric gain length defined by,

$$\mathfrak{L} = \ell_w \operatorname{erf}\left(\frac{\sqrt{\pi}}{2} \frac{\ell}{\ell_w} \right) \tag{A4.6}$$

In (4.6), the quantity ℓ_w is the walk-off length [3]. It accounts for the eventual loss of spatial overlap between the pump and signal beams, resulting from Poynting vector walk-off, and is given by

$$\ell_w = \frac{\sqrt{\pi}}{2} \frac{w_3}{\rho} \sqrt{\frac{w_3^2 + w_1^2}{w_3^2 + \frac{1}{2} w_1^2}} \tag{A4.7}$$

where ρ is the Poynting vector walk-off angle, and the 'erf' function is defined as,

$$\operatorname{erf}(x) = \frac{1}{\sqrt{2\pi}} \int_0^x e^{-y^2} dy \tag{A4.8}$$

From (A4.3), the single-pass power gain can be shown to be given by,

$$\frac{P(\ell)}{P(0)} = e^{-2\alpha \ell} \cosh^2 \Gamma \mathfrak{L} \tag{A4.9}$$

If the pump pulse has a Gaussian temporal profile, the parametric gain coefficient may be rewritten, to show the time dependency explicitly, as,

$$\Gamma = \Gamma_0 e^{-(t/\tau)^2} \qquad \text{(A4.10)}$$

where τ is the $1/e^2$ intensity half-width of the pump pulse, and Γ_0 is the parametric gain coefficient evaluated at the peak of the pump pulse. From (A4.9) and (A4.10), it can be shown that the net change of power over the 'm^{th}' round-trip of the cavity is given by,

$$\frac{P_m}{P_{m-1}} = f_1 \cosh^2\left[\wp \Gamma_0 e^{-(t_m/\tau)^2}\right] \qquad \text{(A4.11)}$$

where t_m is the arrival time (at the input face) of the m^{th} mode-locked pulse, and f_1 is the fractional round-trip power feed-back of the resonator, at the signal frequency 'ω_1'. As written, the fractional feedback not only accounts for losses due to crystal absorption and scattering, but for those due to output coupling as well.

4.2 Example calculation.

In the case of a pulsed parametric oscillator, the oscillation threshold is taken by convention to be the incident pulse energy for which the gain accumulated over the duration of the pump pulse is sufficient for the signal power to build up, from noise, to a level comparable to the pump [4]. The level of gain required is commonly set as $\sim \exp(30)$ (i.e. $\sim 10^{13}$), which can be shown to be a reasonable assumption, from a consideration of the plane-wave parametric gain [4].

To determine the threshold pump intensity (and hence peak power and energy), the fractional change in resonated signal power given by equation (A4.11) can be iterated over the number of round-trips within the pump pulse train that see a net gain (i.e. those round-trips for which $P_m > P_{m-1}$). Repeating this process for a few trial values of the incident pump field, it is possible to find the threshold value that gives an overall gain of $\approx \exp(30)$.

In the case of the parametric oscillator described in Chapter 7, Section 1, which utilized potassium titanyl phosphate ('KTP')[5] as the nonlinear gain medium, and was pumped by the frequency-doubled output of a mode-locked, Q-switched, and amplified Nd:YAG laser, the relevant parameters for the threshold calculation are as follows.

Parametric oscillator: the length of the KTP crystal was $\approx$5mm; the refractive indices seen by all three electric field components were $n_0 \sim n_3 \sim 1.8$; when phase-matched for degenerate parametric oscillation with a 0.532μm pump, the nonlinearity is $\approx 3.2 pmV^{-1}$ [7], and the Poynting vector walk-off $\sim$4.5mrad [6]. The launched pump waist-size was $\approx$0.25mm, and

the resonator was designed such that the signal spot-size within the nonlinear crystal was ≈ 0.37mm. Finally, the fractional round-trip feedback was ≈ 0.53.

Pump source: the 0.532μm pump pulse train had a duration of ≈ 150nm (FWHM), and was comprised of mode-locked pulses of 85ps duration, which were temporally separated by around 7.5ns. There were consequently ~ 20 mode-locked pulses falling within the duration (FWHM) of the 'Q-switched train.

To simplify the threshold calculation somewhat, two additional assumptions were made about the behaviour of the parametric oscillator. Firstly, it was assumed that while the interaction in KTP was type II, it could be treated as if it was type I, since the fractional birefringence of KTP is a slowly varying function of wavelength. This means that there will always be one pair of fields between which the Poynting vector walk-off is virtually zero, as occurs in the type I case. Furthermore, as the walk-off in KTP—when phase-matched for degenerate operation of a 0.532μm pumped OPO—is very small (i.e. ~ 4.5mrad [6]), even if this assumption was not strictly valid, it would not affect the analysis particularly.

Secondly, it was taken to hold that in the case of a parametric oscillator cavity that supports stable Gaussian modes, the resonated signal would be constrained to be in the TEM_{00} mode defined by the passive cavity. This contrasts with the case of the plane-plane cavity considered by Brosnan and Byer [1], where it was assumed that the parametric gain profile acted to define the size of the signal mode [1].

Substituting the above parameters, describing the parametric oscillator and pump laser, into the relevant equation given in Section A4.1, it was found that the parametric oscillator was predicted to achieve threshold for an incident pump energy of ≈ 1.7mJ, corresponding to a peak power, of the most energetic pulse in the mode-locked train, of ≈ 880kW, and an on-axis peak intensity of ≈ 830MWcm^{-2}. The threshold was not found to be particularly sensitive to either the pulse duration or shape; approximately the same threshold energy (≈ 1.4-1.5mJ) was obtained for pulses which had a square temporal shape of durations in the range τ–2τ (where τ is defined as in (A4.10) above), and a Gaussian spatial profile.

Altering the analysis to calculate the gain seen by the peak on-axis intensity of the signal field—i.e. equivalent to plane wave situation—led to a predicted threshold of ≈ 250MWcm^{-2}, as opposed to ≈ 830MWcm^{-2} for the more general Gaussian case. This represents a 'reduction' in peak intensity of almost a factor of four. The analysis after Brosnan and Byer [1] was also found to predict that a further factor of three reduction in

threshold could be obtained by reducing the signal spotsize in the nonlinear crystal from $\approx$0.38mm down to $\approx$0.1mm, without changing the pump spotsize from 0.26mm. It is not apparent, however, that this provides the optimal coupling between signal and pump. In the case of a stable resonator, the signal spot-size of the TEM_{00} mode is not free to vary as the parametric gain changes. As only the fraction of the pump that overlaps the signal is coupled into the resonated mode, this would result in a lower conversion efficiency, or to the excitation of higher order transverse modes of the cavity. To avoid these potential problems, it was desired to work exclusively with pump and signal spotsizes which were 'confocally matched', vis. having the same confocal parameter in the crystal, and also the same focal plane. The somewhat subjective argument given above is borne out by the analysis of Sushchik and Freidman [8], who show for the singly-resonant oscillator that the optimal focusing corresponds to matched confocal parameters.

References.

[1]. S.J. Brosnan and R.L. Byer.
IEEE J. Quantum Electron. **QE-15**, 415 (1979).

[2]. H. Kogelnik.
p333, *Proc. Symp. on Quasi-Optics* (Polytechnic 1964. J. Fox, Ed.).

[3]. G.D. Boyd and A. Ashkin.
Phys. Rev. **146**, 198 (1968).

[4]. R.L. Byer.
Chap. 9, *Quantum Electronics: a treatise, Vol. 1* (Academic Press 1975).

[5]. F.C. Zumsteg, J.D. Bierlein, and T.E. Gier.
J. Appl. Phys. **47**, 4980 (1976).

[6]. J.Q. Yao and T.S. Fahlen.
J. Appl. Phys. **55**, 65 (1984).

[7]. R.C. Eckardt, H. Masuda, Y.X. Fan, and R.L. Byer.
IEEE J. Quantum Electron. **26** (1990).

[8]. M.M. Sushchik and G.I. Freidman.
Radiophys. and Quant. Elec. **92**, 689 (1973).